eman ta zabal zazu

Universidad del País Vasco
Euskal Herriko Unibertsitatea

UNDERSTANDING THE ROLE OF CAMKIIA IN ANGELMAN SYNDROME BY LOOKING AT ITS POTENTIAL INTERACTORS THROUGH PROXIMITY LABELLING

DOCTORAL THESIS

Cristina García Bárcena

2023

(c)2023 CRISTINA GARCIA BARCENA

INDEX

INDEX

ABSTRACT

Angelman syndrome (AS) is a rare disease (1:20,000 births) that affects the nervous system. Patients with this condition are characterised by delayed development, intellectual disability, severe speech problems and ataxia. The disease is caused by the lack of the protein UBE3A, an ubiquitin E3 ligase, in the nervous system.

Aiming to shed light on the molecular mechanisms underlying AS, our research group has focused on uncovering *in vivo* UBE3A substrates. Previous experiments performed in UBE3A overexpressing *Drosophila melanogaster* allowed us to identify differentially ubiquitinated proteins. Besides putative UBE3A substrates that are more ubiquitinated when UBE3A expression is enhanced, we detected proteins with decreased ubiquitination levels, such as CaMKII.

CaMKII is a serine-threonine kinase that plays a pivotal role, among others, in long-term potentiation (LTP) and memory, two processes that are unpaired in AS. Indeed, the phosphorylation status as well as the activation state of CaMKII is altered in AS model organisms. Consequently, in order to unveil, on one hand, the ubiquitin E3 ligase(s) and deubiquitinase(s) that act on CaMKII and, on the other hand, the possible link between CaMKII and UBE3A, we have studied the interactome of CaMKII in three distinct systems. We carried out a proximity labelling approach with BioID2 in HEK 293T cells and identified up to 155 potential CaMKII interactors, including three deubiquitinating enzymes (DUBs) and two ubiquitin E3 ligases. Further investigations revealed that the DUB MYSM1 has an indirect effect on CaMKIIa ubiquitination whereas the ubiquitin E3 ligase ITCH promotes CaMKIIa monoubiquitination. In both cases, an enhancement of CaMKIIa ubiquitination was

linked to an increase in CaMKIIa phosphorylation at T286. Similarly, we applied TurboID technology to search for CaMKII binding proteins in *Drosophila melanogaster* and discovered that biological processes like nervous system development and memory were enriched among putative CaMKII interactors. One of the CaMKII binding candidates detected was *rg*, the fly homolog for NBEA protein in humans and mice that is associated with autism spectrum disorders and we previously detected it as a putative UBE3A substrate in mice. We also studied the interactome of CaMKII in rat cortical slices and discovered that, among others, NCDN is likely to associate with CaMKII. Indeed, experiments performed in mice revealed that NCDN is a UBE3A substrate and that the E3 ligase forms K48-linked ubiquitin chains on NCDN to target it to proteasomal degradation. Moreover, we evaluated the relationship between CaMKII phosphorylation and UBE3A-dependent NCDN ubiquitination and set the bases for future experiments to elucidate this aspect.

ABBREVIATIONS

AMP	Adenosine monophosphate
AMPAR	α-amino-3-hydroxy-5-methyl-4-isoxazolepropionic acid receptor
AS	Angelman Syndrome
ASD	Autism spectrum disorder
ATP	Adenosine triphosphate
BAT	Biotin Acceptor Tag
BioID	Biotin Identification
BioID2	Biotin Identification 2
BirA	Biotin holoenzyme synthetase enzyme
BP	Breaking point
CaMKIIa	Calcium/calmodulin-dependent protein kinase type II subunit alpha
CaMKIIb	Calcium/calmodulin-dependent protein kinase type II subunit beta
CaMKIId	Calcium/calmodulin-dependent protein kinase type II subunit delta
CaMKIIg	Calcium/calmodulin-dependent protein kinase type II subunit gamma
CaMKII	Calcium/calmodulin-dependent protein kinase type II
diGly	Lys-ε-Gly-Gly
DLG	Discs large
DMEM	Dulbecco's modified Eagle medium
DMSO	Dimethyl sulfoxide
DNase	Deoxyribonuclease

dNTPs	Deoxynucleotide triphosphates
DTT	Dithiothreitol
DUB	Deubiquitinase
EDTA	Ethylenediamine tetraacetic acid
EL	Elution
EPSC	Excitatory postsynaptic current
FBS	Fetal Bovine Serum
hiFBS	Heat-inactivated Fetal bovine serum
FL	Full length
FT	Flow through
GFP	Green fluorescent protein
HBSS	Hank's balance salt solution
HECT	Homologous to the E6AP carboxyl terminus
HEK 293T	Human embryonic kidney 293 T
HEPES	4-(2-hydroxyethyl)-1-piperazineethanesulfonic acid
IBR	In-between-RING
IN	Input
LB	Luria-Bertani
LFQ	Label Free Quantitation
LTP	Long-term potentiation
mRNA	Messenger ribonucleic acid
MS	Mass spectrometry
NEM	N-Ethylmaleimide
NMDA	N-methyl- D.aspartate
NMJ	Neuromuscular junction

Nup43	Nucleoporin 43
PBS	Phosphate Buffer Saline
PBST	Phosphate Buffer Saline with Triton
PL	Proximity labelling
PPI	Protein-protein interaction
PSD	Postsynaptic density
PTM	Post-translational modification
PWS	Prader-Willi Syndrome
qPCR	Quantitative polymerase chain reaction
RBR	RING between RING
RING	Really-interesting new gene
RT	Room Temperature
RT-PCR	Reverse transcription polymerase chain reaction
SDS	Sodium Dodecyl Sulfate
TBS	Theta burst stimulation
TRIM	Tripartite motif
UAS	Upstream Activating Sequences
Ub	Ubiquitin
Ube3a	Ubiquitin Protein Ligase E3A
UBE3A	Ubiquitin-protein ligase E3A
UPD	Uniparental disomy
UV	Ultra Violet
WB	Washing Buffer
WT	Wild type
Zn	Zinc

INTRODUCTION

Ubiquitin-proteasome pathway

Ubiquitin is a 76-amino-acid protein highly conserved among organisms (Zuin, Isasa, and Crosas 2014), used –through the ubiquitin-proteasome system- to regulate many cellular processes. Proteins are covalently modified typically on their Lys residues with ubiquitin via amide isopeptide linkages (Laney and Hochstrasser 1999). Frequently, ubiquitinated proteins are targeted for degradation through the proteasomal system in an ATP hydrolysis-dependent manner (Hershko and Ciechanover 1998; Komander and Rape 2012). But protein ubiquitination participates in a plethora of additional cellular responses including regulation of gene expression, cell signalling, cell cycle, DNA repair and apoptosis (Pickart 2001; Gilberto and Peter 2017).

The ubiquitination reaction requires the coordinated action of three types of enzymes termed E1, E2 and E3. First, ubiquitin is activated with ATP in a process carried out by an activating E1 enzyme. Once ubiquitin is activated, it is transferred to the Cys on the active site of a conjugating E2 enzyme. Finally, ubiquitin is generally linked to a Lys of the target protein through an isopeptide bond, formed between the C-terminal carboxyl group of ubiquitin and the ε-amino group of the Lys. Substrate specificity in ubiquitination is attributed to E3 ligases, which are able to interact with both the ubiquitin-charged E2 and the substrates to be modified (Metzger et al. 2014). Like most post-translational modifications (PTMs), ubiquitination is reversible and deubiquitinating enzymes (DUBs) are responsible for hydrolysing the isopeptide bond between ubiquitin and substrate proteins or between ubiquitin molecules (**Figure 1**).

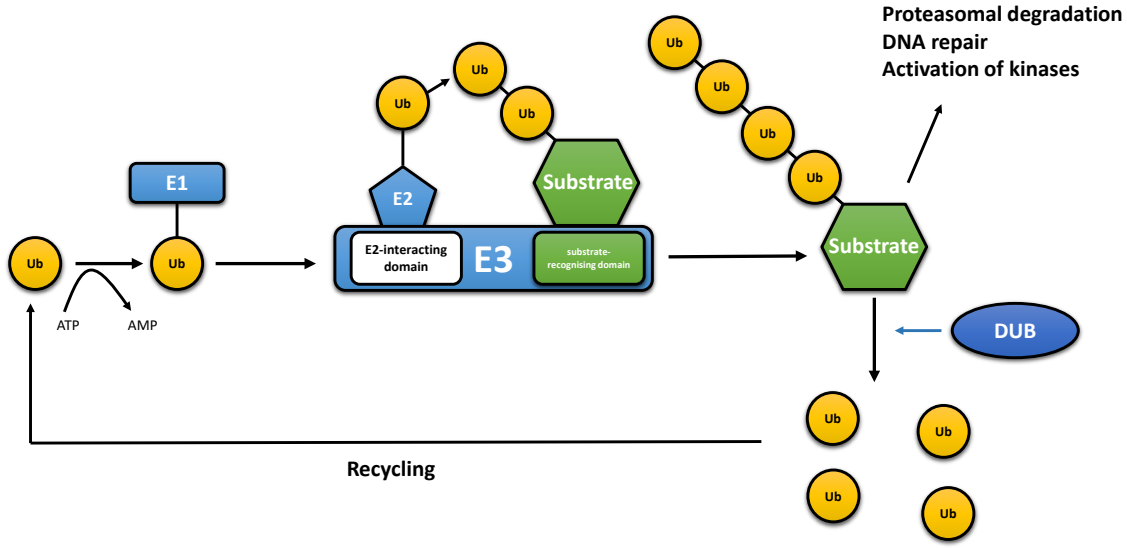

Figure 1. The ubiquitination reaction requires the coordinated action of three enzymes. First, ubiquitin is activated through the action of E1 enzymes and use of ATP. Second, activated ubiquitin interacts with an E2 enzyme. Third, ubiquitin is transferred to the substrate through the action of an E3 enzyme. Ubiquitinated substrates lead to different cellular responses. Ubiquitination reaction is reversible through the action of DUBs and it is recycled to start the process again. E1: E1 ubiquitin-activating enzyme; E2: E2 ubiquitin-conjugating enzyme; E3: E3 ubiquitin-ligase enzyme; Ub: ubiquitin; DUB: deubiquitinating enzyme.

Proteins can be modified by ubiquitin in a wide range of manners. For instance, in addition to Lys, ubiquitin can be conjugated via a peptide bond to the N-terminal amino group of the substrates (Ciechanover and Ben-Saadon 2004), as well as to Cys or Ser/Thr residues by thio- or oxy-ester bonds, respectively (X. Wang, Herr, and Hansen 2012). Substrates can be monoubiquitinated, meaning modified in a single residue by only one ubiquitin. Multi-monoubiquitination occurs when several residues of a given protein are simultaneously modified with one ubiquitin each. By contrast, polyubiquitination occurs when the C-terminus of a ubiquitin associates to one of the seven Lys (Lys6, Lys11, Lys27, Lys29, Lys33, Lys48 and Lys63) or the N-terminal Met (Met1) on the ubiquitin molecule already attached to

a given protein (**Figure 2A**). Consequently, a ubiquitin chain is formed on the target protein. Depending on how ubiquitin residues are bound together, different ubiquitin chain architectures can be formed: (i) homogenous, if the Lys used throughout the chain is the same (*e.g.* Lys48-linked chains), (ii) heterogeneous, if they alternate (*e.g.* Lys48-Lys11-linked chains) and (iii) branched, if multiple Lys of the same ubiquitin are modified at the same time. Altogether, ubiquitin can generate a huge number of different types of modifications on any given protein (**Figure 2B**) (Komander and Rape 2012). Consequently, ubiquitin-mediated cellular responses will depend not only on the specific residues of the substrate that are modified but also on the topology of the ubiquitin chains that are formed (Akutsu, Dikic, and Bremm 2016).

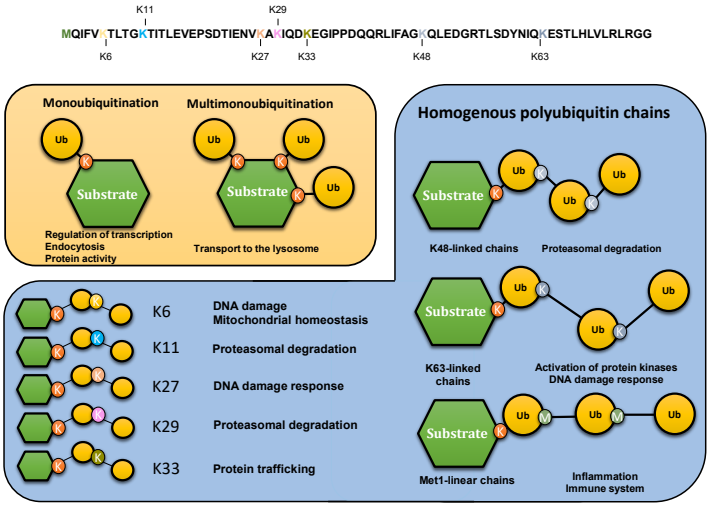

Figure 2. Ubiquitin can form different types of chains that will determine the faith of the ubiquitinated proteins. A) Amino acidic sequence of Ubiquitin. Ubiquitin itself has seven lysine residues that can be ubiquitinated to form longer chains. The first methionine can also be ubiquitinated at its amino end. B) Representation of the different chains that ubiquitin can generate and the cellular response they trigger. Depending on how ubiquitin residues are bound together, different ubiquitin chain architectures can be formed. Adapted from Akutsu et al., 2016.

E3 ligases

Eukaryotic cells express hundreds of ubiquitin E3 ligases, which can operate in different cellular contexts, respond to numerous cellular signals, and process diverse protein substrates (Ning Zheng and Shabek 2017). Ubiquitin E3 ligases have been classically classified into two different groups, based on conserved structural domains and the mechanism by which ubiquitin is transferred: RING (really interesting new gene)-type E3s and HECT (homologous to the E6AP carboxyl terminus)-type E3s. Whereas RING E3 ligases directly transfer the ubiquitin from the E2-ubiquitin complex to the substrate (**Figure 3A**), HECT-type E3s transfer ubiquitin to their own catalytic Cys before linking it to the substrate (**Figure 3B**) (Deshaies and Joazeiro 2009). More recently, a third group of E3s, that combines features from both RING- and HECT-type E3 families, has been established: the RING between RING (RBR) family (**Figure 3C**). RBR and RING E3s share RING binding domains, but RBR family members have the ability to generate a thioester intermediate with ubiquitin, as HECT-type E3s do (Morreale and Walden 2016).

Typically, one E3 ligase is able to modify several substrates, as well as to bind different E2s. The same protein can, therefore, be ubiquitinated by different E2/E3 combinations, which will lead to different ubiquitination patterns (Metzger et al. 2014). Substrate recognition by HECT-type E3 ligases depends on protein-protein interactions that are mediated by specific motifs typically located in the N-terminal of the HECT domain (Scheffner and Kumar 2014). Similarly, in monomeric RING-type E3s this is achieved through regions of the E3 other than the RING domain,

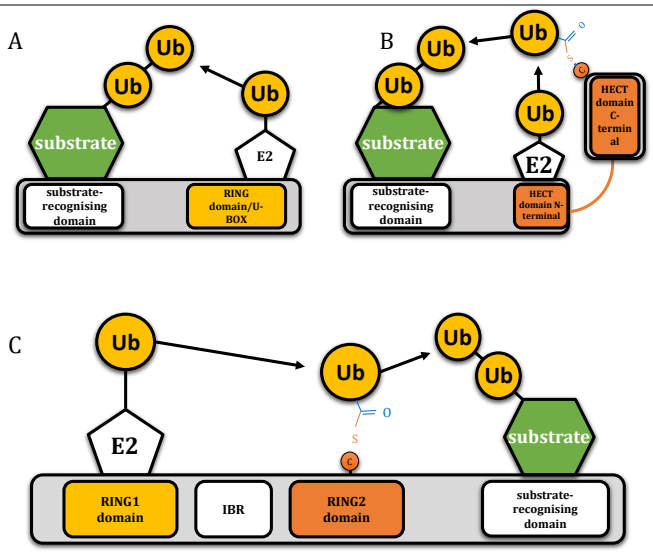

Figure 3. Mechanism of action of RING-, HECT- and RBR-type E3 ubiquitin ligases A) Schematic representation of a RING-type ubiquitin E3 ligase. RING E3s bind both the E2-ubiquitin and the substrate to be ubiquitinated, bringing them together which allows direct conjugation of ubiquitin on the substrate by the E2. A monomeric RING E3 ligase is shown for illustrative purposes. B) Schematic representation of a HECT-type ubiquitin E3 ligase. Ubiquitin is transferred first to a cysteine of the HECT domain through a thioester bond and then to the substrate. C) Schematic representation of an RBR-type ubiquitin E3 ligase. Two RING domains are separated by an in-between-RING domain. Ubiquitin is first transferred to a cysteine of the second RING domain through a thioester bond and then to the substrate.

whereas multi-subunit RING E3s bear substrate recognition elements for that purpose (Metzger et al. 2014). On the other hand, some studies have reported that ubiquitinated proteins have a short linear sequence, known as degron, to facilitate their recognition by the E3 ligases. Degrons can be also modified by kinases and other enzymes. These modifications appear to be crucial for timing the interaction between E3s and substrates, even though they are not always necessary and many substrates of HECT-type E3s are recognised in their native form (Rotin and Kumar 2009; Kamadurai et al. 2009; Muńoz-Escobar et al. 2015; Kanelis, Rotin, and Forman-Kay 2001).

The role mediated by E3 ligases is so crucial, that their activity must be tightly controlled in order to ensure they solely act when necessary. Oligomerisation is one of the mechanisms that modulate the activity of HECT- and RING-type E3s. For instance, structural studies suggest that the trimeric arrangement of E6AP (also called UBE3A) activates the ligase (Ronchi et al. 2014), whereas homodimerisation of the HECT domain of HUWE1 results in enzyme inactivity (Sander et al. 2017). RING-type E3s can act as independent enzymes, but most of them tend to form homo- or heterodimers, and even more complex multi-subunit assemblies in order to mediate ubiquitination (Metzger et al. 2014). For instance, RING E3 ligases cIAP, RNF4, BIRC7, IDOL, CHIP and Prp19 homodimerize, and RING domains of both units interact with E2 proteins. By contrast, RING-type E3 ligases BRCA1-BARD1, Mdm2-MdmX and RING1B-Bmi1 form heterodimers. While BRCA1 and Mdm2 have the ability to interact with E2 proteins, their partners do not. Nevertheless, they function as enhancers of ligase activity and interact with substrates (Brzovic et al. 2001; Cao, Tsukada, and Zhang 2005; Hengbin Wang et al. 2004; Joukov et al. 2001).

RING-type E3s

RING-type E3s are conserved from human to yeast, and it is estimated that the human genome encodes above 600 different RING-type E3s. The RING domain was first characterised by Freemont and colleagues (Freemont, Hanson, and Trowsdale 1991). The canonical sequence for this 40-60 amino acid long domain is Cys-X_2-Cys-$X_{(9-39)}$-Cys-$X_{(1-3)}$-His-$X_{(2-3)}$-Cys-X_2-Cys-$X_{(4-48)}$-Cys-X_2-Cys. The conserved Cys (7 in total) and His (a single one) are disposed in a “cross-brace” topology to coordinate two zinc ions and stabilise the structure (**Figure 4**) (Deshaies and Joazeiro 2009).

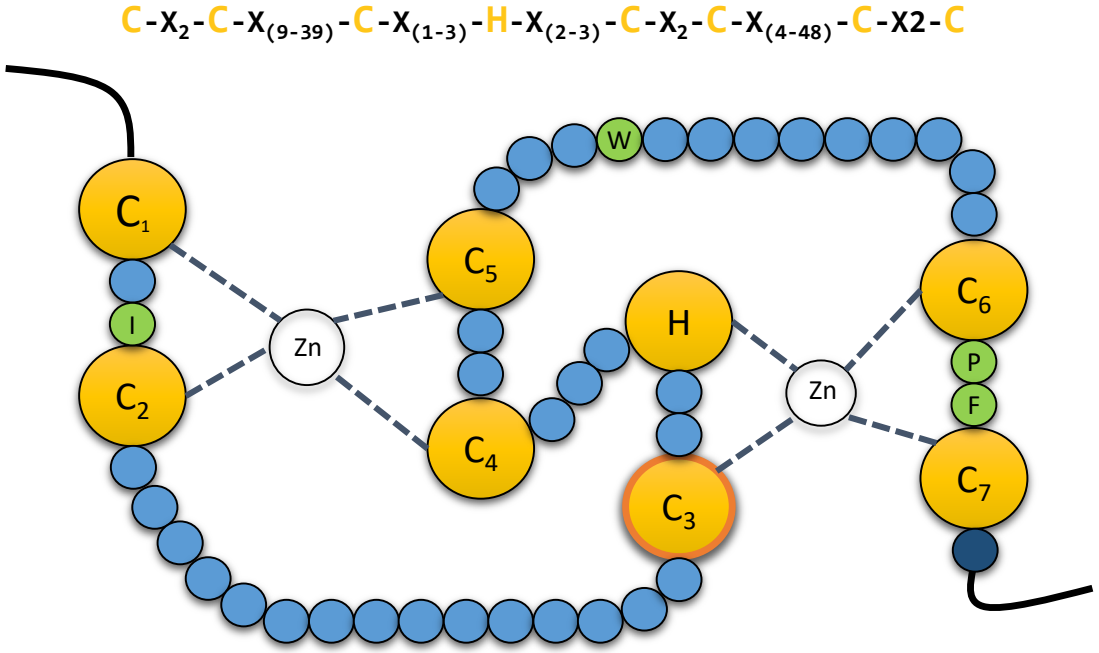

Figure 4. Schematic representation of the RING domain. The RING domain contains seven conserved cysteines and one histidine (yellow) which are involved in the coordination of two atoms of zinc. The third cysteine mediates the ubiquitin transfer in the second RING domain in RBR E3 ubiquitin ligases. Four conserved residues (green) guide the interaction with the E2 conjugating enzyme. Mutation of the last residue of the domain (dark blue), which is normally an arginine, compromises the stability of the adjacent cysteine, affecting the coordination of the zinc atom. Adapted from Deshaies and Joazeiro, 2009.

Initially, the role of RING domains was uncertain, although it was known they were involved in protein-protein interactions as well as in a wide range of cellular processes (Deshaies and Joazeiro 2009). However, it was not until 1997 that the function of RING domains was elucidated by Bailly and coworkers (Bailly et al. 1997). Moreover, in 1999, Joazeiro and coworkers observed that the adapter protein c-Cbl bears two domains that act coordinately to mediate ubiquitination and subsequent degradation of substrates. Whereas the SH2 domain of c-Cbl serves to recognize specific substrates, the RING domain is necessary to recruit and activate

a ubiquitin-conjugating E2 (Joazeiro et al. 1999). After that, a similar role was conferred to a number of RING domain-containing proteins (Lorick et al. 1999). At present, it is accepted that the RING domain present in all RING E3s associates and activates E2-Ub conjugates promoting the direct transfer of ubiquitin from the E2 to the target protein (**Figure 3A**).

The interaction between the RING domain of E3 ligases and E2s was first elucidated with the crystal structure of Cbl's RING domain bound to UbcH7 E2 (N Zheng et al. 2000). The combination of many structural studies allowed to characterise the four residues of each protein that play a crucial role in the interaction. A hydrophobic residue from the RING E3, generally an Ile or a Val, interacts with two Pro residues from the E2, which are localised in one of the two loops that compose the accessible surface of the enzyme. Additionally, another hydrophobic residue (typically Trp, His or Leu) from the E3 interacts with a Phe and a Pro present on the second loop of the E2. Simultaneously, this Pro interacts with a Pro of the E3, which is also connected to an Ala localised in the second loop of the E2. Moreover, the same Ala of the E2 interacts with a hydrophobic amino acid (typically Val, Phe or Ile) of the E3 (**Figure 5**) (Deshaies and Joazeiro 2009).

More recently, structural studies focused on RING-type E3:E2-Ub complexes have revealed the mechanism by which this class of ubiquitin ligases facilitates Ub transfer to substrate proteins. The E2-Ub complex has a flexible topology with multiple inter-domain configurations that are altered upon E3 binding (Pruneda et al. 2011). More precisely, the binding of RING E3 reduces the dynamics of E2-Ub and stabilizes in an ensemble of closed conformation. This modification facilitates the

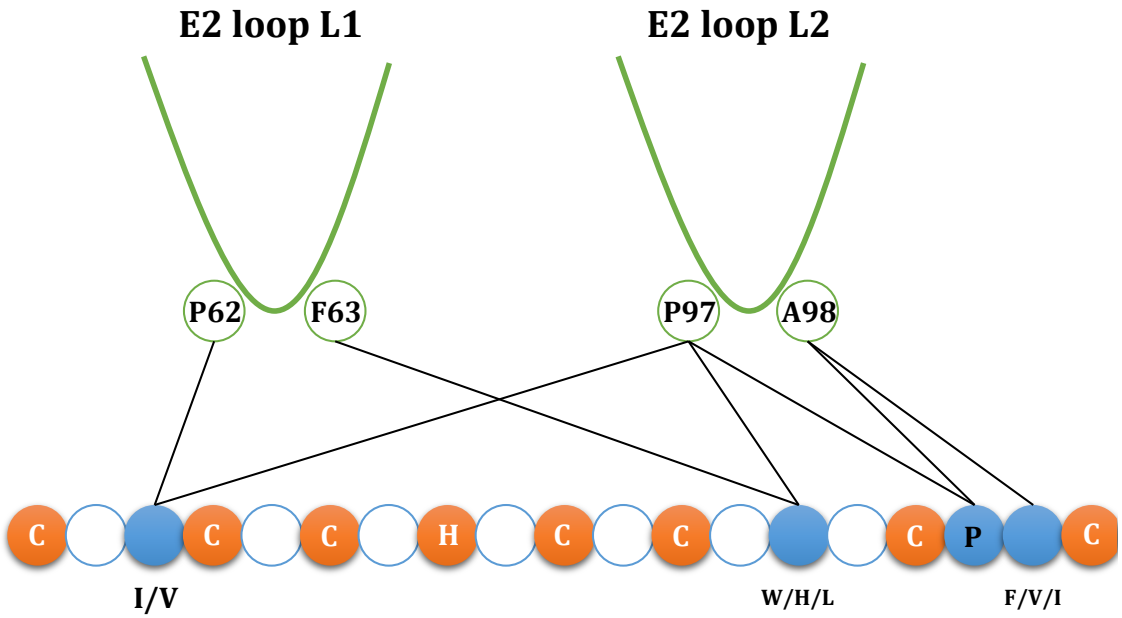

Figure 5. Schematic representation of the interaction of the E2 conjugating enzymes and the RING and U-BOX domains. The residues from the RING/U-BOX domain that form the most significant interactions determined by cocrystal structures are shown in blue and the conserved cysteines and histidine in orange. Adapted from Deshaies and Joazeiro, 2009.

reactivity for substrate Lys that can perform the corresponding nucleophilic attack (Soss, Klevit, and Chazin 2013; Pruneda et al. 2012). Studies carried out on dimeric E3s, such as RNF4 or BIRC7, also support the same mechanism by showing that an Arg residue conserved in many RING E3s supports the non-covalent interaction between E2-Ub (Dou et al. 2012; Plechanovov et al. 2012).

As mentioned above, although some RING-type E3s act independently, they have the tendency to form homo- and heterodimers. Most RING-type E3s dimerise through their RING domain, such as RNF4 homodimers or MDM2/MDMX and BRAC1/BARD1 heterodimers (Liew et al. 2010; Linke et al. 2008; Brzovic et al. 2001). Nevertheless, there are exceptions. For instance, MARCH9 E3 ligase can form active dimers with RING-less variants (Hoer, Smith, and Lehner 2007), whereas viral

RING-type E3s MIR1 and MIR2 are believed to homodimerise via their transmembrane domain (Lehner et al. 2005). The tripartite motif (TRIM) family members in metazoans contain an additional domain termed B-box. Like the above-mentioned RING domain, the B-box domain is a Zn-binding domain. However, whereas the RING domain is essential for E2 binding and E3 ligase activity, it has recently been shown that the B-box domain is involved in chain assembly rate modulation (Lazzari et al. 2019). Similarly, the U-box domain is also related to the RING domain, but unlike the B-box, it can interact with E2s. Additionally, U-box domain has no coordinating zinc, so in order to ensure the stability of the structure, zinc-binding residues present in RING are replaced by charged and polar residues (Vander Kooi et al. 2006; Aravind and Koonin 2000).

HECT type E3 ligases

The human HECT-type E3 family consists of 28 members that are divided into three different groups depending on their N-terminal domain architecture: (i) the *NEDD4* subfamily, characterized by containing a C2 domain, a HECT domain and two to four WW domains, which bind to the PY motifs of target proteins (Kanelis, Rotin, and Forman-Kay 2001; Staub et al. 1996); (ii) the *HERC* subfamily, which integrates at least one regulator chromosome condensation 1 (RCC1)-like domain (RLDs) and a reduced HECT domain; and (iii) the *other HECT* subfamily, that embrace HECT-type E3s not fitting the above mentioned two subfamilies.

All HECT-type E3s share a ~350 amino acid long HECT domain, which was first described in human papilloma virus E6 associated protein (E6AP), nowadays known as UBE3A. (Huibregtse et al. 1995). In the HECT domain, a conserved Cys

forms thioester-linked-intermediate complexes with ubiquitin (**Figure 3B**), before being transferred and attached to the substrate through a transthiolation reaction. This conserved Cys is located in the C-terminal region of the HECT domain, while the E2 interacting site is localised in the N-terminal site (Rotin and Kumar 2009).

RBR type E3 ligases

RBR family members contain two RING domains (RING1 and RING2) that are separated by an in-between-RING (IBR) zinc-binding domain. Morett and Bork first characterised these domains in 1999 in a sequence profile-based characterisation (Morett and Bork 1999). In the process of confirming that UbcH7 could also interact with RBR E3s, they discovered that RBR E3s act as RING/HECT hybrids. Whereas the first RING domain serves as an E2 binding platform, the C3 of the second RING serves as the active site that mediates ubiquitination in HECT E3 ligase fashion (Wenzel et al. 2011) (**Figure 3C**).

Sumoylation

SUMOylation is a posttranslational modification in which proteins are conjugated with a ubiquitin-like protein called SUMO that plays a key role in a plethora of cellular functions including DNA damage repair, telomere maintenance, mitosis and development (Flotho and Melchior 2013; Talamillo et al. 2020). SUMO proteins are related to the proteins involved in the ubiquitin pathway and the sequential action for SUMO association is very similar to the ubiquitin cascade: first, an E1 SUMO-activating enzyme activates SUMO which is then conjugated by an E2 SUMO-conjugating enzyme and finally, ligated to the substrate through the action of an E3 SUMO ligase (Capili and Lima 2007; Kerscher, Felberbaum, and Hochstrasser

2006). How substrate specificity is achieved in this pathway is unclear because the whole process relies on a single E2 SUMO-conjugating enzyme, UBC9, and a few E3 SUMO ligases (Capili and Lima 2007). Additionally, while in yeast and invertebrates there is a single SUMO-encoding gene, vertebrates have at least four different genes: SUMO1, SUMO2, SUMO3 and the less characterized SUMO4 (Owerbach et al. 2005; Guo et al. 2004).

Angelman Syndrome

Angelman Syndrome (AS) was first described by Harry Angelman in three patients in 1965. The patients presented a stiff, jerky gait, absence of speech, excessive laughter, and seizures. AS is a complex disease that affects primarily the nervous system, and affects approximately 1 of 15,000 births. The disease is characterised by motor dysfunction, severe intellectual disability, speech impairment, seizures, hyperactivity, and autism spectrum disorder (ASD) (Margolis et al. 2015; Buiting, Williams, and Horsthemke 2016). Most AS patients lack speech ability entirely but receptive language is less impaired. However, depending on the penetrance of the disease, in mild cases, a few words may be acquired. Seizures are also very common, occurring in more than 80% of cases. While seizures normally appear before the age of three, developmental delay is usually observed within the first year of life. Movement disorders include tremors, jerkiness, and ataxia. Among the characteristic behaviours, bringing objects to the mouth, a happy demeanour with easily provoked laughter, attraction to water, hyperactivity, short attention span, and decreased sleeping are included (**Figure 6**) (Bird 2014; Dagli, Buiting, and Williams 2012; C. A. Williams, Driscoll, and Dagli 2010).

AS is caused by the lack of a ubiquitin E3 ligase: UBE3A. *UBE3A* locus is located in 15q11-q13, an approximately 120 kb long region with 21 genes, and its expression in neurons is controlled by genomic imprinting. Genomic imprinting is an epigenetic phenomenon in which the expression of a gene or group of genes is silenced in either the maternal or the paternal chromosome through methylation of the region. The imprinting can be complete, partial and even tissue-dependent (Bajrami and Spiroski 2016) (**Figure 7A**). Specifically, in neural tissue, the paternal copy of *UBE3A* is silenced. Consequently, AS is developed when *UBE3A*, which is paternally imprinted, is not expressed from the maternal copy. By contrast, Prader-Willi syndrome (PWS), another rare neurodevelopmental disorder, is caused by paternal loss of maternally imprinted 15q11-q13 chromosomal identical region (Butler and Thompson 2000).

Lack of UBE3A may be triggered by different causes (**Figure 7B**): (i) deletion of the maternal 15q11-q13 region (70%), (ii) paternal uniparental disomy (UPD) for chromosome 15 (2%), (iii) imprinting defects that lead to a deficient expression of maternal *UBE3A* (2-3%), or (iv) point mutations in the *UBE3A* coding gene (25%) (Kishino, Lalande, and Wagstaff 1997). Depending on the cause of AS, the penetrance of the disease may be more or less severe (previous causes have been ordered depending on the severity, starting with the most severe).

Figure 6. Individuals with Angelman Syndrome. a-d 15q11.2–q13 microdeletion. e | Ubiquitin–protein ligase E3A gene (*UBE3A*) mutation. f | Paternal uniparental disomy. g | Non-deletion, mosaic imprinting defect. h | Deletion-type imprinting defect. Characteristic features of Angelman syndrome include excessive laughter and apparently happy personality, along with stiff gait and uplifted arms (shown in a and b). Relatively large mouth and short philtral height occurs in some adults (shown in c), but most adults and children do not have distinctive facial dysmorphism (shown in d, e, g and h). Malocclusion — for example, an open bite — can be seen after prolonged tongue protrusion in childhood (shown in d); mild tongue protrusion is common (shown in f). Microcephaly is observed in many cases (shown in a, b, e and f), but is rarely severe. Individuals with mosaic imprinting defects show higher adaptive functioning than do those with other defects, and are less likely to exhibit a classic behavioural or physical phenotype (shown in g) (Buiting, Williams, and Horsthemke 2016).

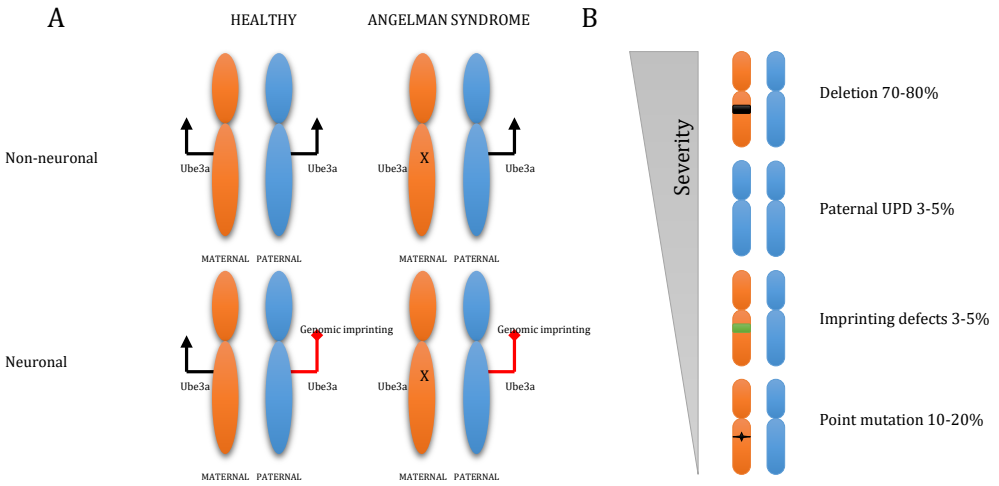

Figure 7. Genomic imprinting of 15q11-q13 in healthy and AS situations. A) Methylation of the region in neuronal tissue triggers the silencing of the genes within that region. Lack of maternal copy of Ube3a leads to AS. B) Principal causes of AS by severity and frequency of ocurrance. UPD: uniparental disomy.

As indicated above, the most frequent mechanism that triggers the disruption of UBE3A is the deletion of 15q11-q13. Within this region, there are three chromosomal breakpoints involved in most AS-causing deletion events (90%) (**Figure 8A**): BP1, BP2 and BP3. These regions are characterised by having low-copy repeat regions. The originated deletions span approximately 5-7 Mb. There are different classes of deletions: class I involve deletions from BP1 and BP3 and occur in 40% of the cases; class II deletions affect the region from BP2 to BP3, corresponding to 50% of the cases; finally, deletions from BP1/BP2 to more distal breakpoints (BP4, BP4A, BP5, or BP6) are less frequent (fewer than 10%). Paternal uniparental disomy**,** most probably caused by somatic segregation errors, leads to a milder disease compared to deletions, with fewer seizures (**Figure 8B**). The probability for an individual to develop AS if the parents have paternal UPD and no Robertsonian translocation is less than 1%. In AS patients with biparental

inheritance, disease-causing imprinting defects (**Figure 8C**) arise when the maternal 15q11-q13 region presents a paternal epigenotype and, therefore, is silenced through genomic imprinting in neurons. More precisely, small deletions (8-15% of the cases) and abnormal DNA methylation patterns (>90%) within the imprinting centre (IC) in 15q11.2-q13 can cause changes in DNA methylation, and consequently, in gene expression patterns. Finally, mutations in the UBE3A coding gene frequently lead to protein truncation (**Figure 8D**). 60-70% of the reported mutations (more than 60) are small deletions and duplications that result in frameshift mutations. Missense and nonsense mutations have also been described (25%), in addition to splicing defects, gross deletions and complex rearrangements. Interestingly, most described mutations disrupt the HECT ligase domain of UBE3A. Less frequently, complete or partial overlapping deletions of UBE3A and intragenic deletions have also been described (C. A. Williams, Driscoll, and Dagli 2010; Dagli, Buiting, and Williams 2012).

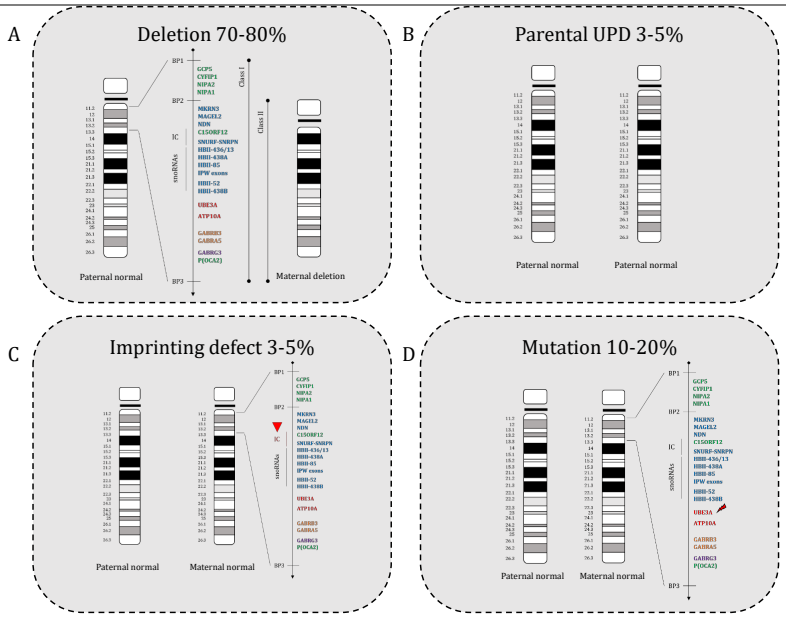

Figure 8. Lack of UBE3A is caused through four mechanisms. A) Deletion of the maternal 15q11.2-q13 region is the cause of lack of UBE3A in 70-80% of AS cases. Three breakpoints are usually involved: BP1, BP2 and BP3. Class I deletions (from BP1 to BP3) occur in 40% of the cases and class II deletions (from BP2 to BP3) in 50%. B) Paternal UPD (3-5%) is normally caused by a somatic segregation error and less frequently, the origin is meiotic. C) Imprinting defects (3-5%) may be caused because the maternal 15q11-q13 regions presents a paternal epigenotype. Small deletions (about 8-15% of the cases) and abnormal DNA methylation pattern (>90%) within the IC in 15q11.2-q13 can cause changes in the DNA methylation and expression patterns. D) Mutations in the UBE3A codifying gene (10-20%) frequently lead to protein truncation. IC: imprinting centre.

Human UBE3A coding region has 60 kb and codes three different mRNAs. All of them comprise 10 different exons, with 5 kb in size, that encode three different protein isoforms: I (canonical), II and III (Kishino, Lalande, and Wagstaff 1997). Isoform I corresponds to the open reading frame for UBE3A and is 852 amino acids long. Compared to it, isoforms II and III contain 23 and 20 extra aminoacids at their amino terminal part, respectively. All isoforms share the AZUL, HERC2 binding, E6 binding and HECT domains (**Figure 9**) (Sirois et al. 2020). Recently, it has been established that whereas the most abundantly expressed UBE3A isoforms I and III are nuclear, isoform II is localized in the cytoplasm (Zampeta et al. 2020). Interestingly, knocking out of the nuclear isoform I in mice results in a similar phenotype to mice lacking the maternal copy of Ube3a (Ube3a$^{m-/p+}$ AS mice models) (Avagliano Trezza et al. 2019).

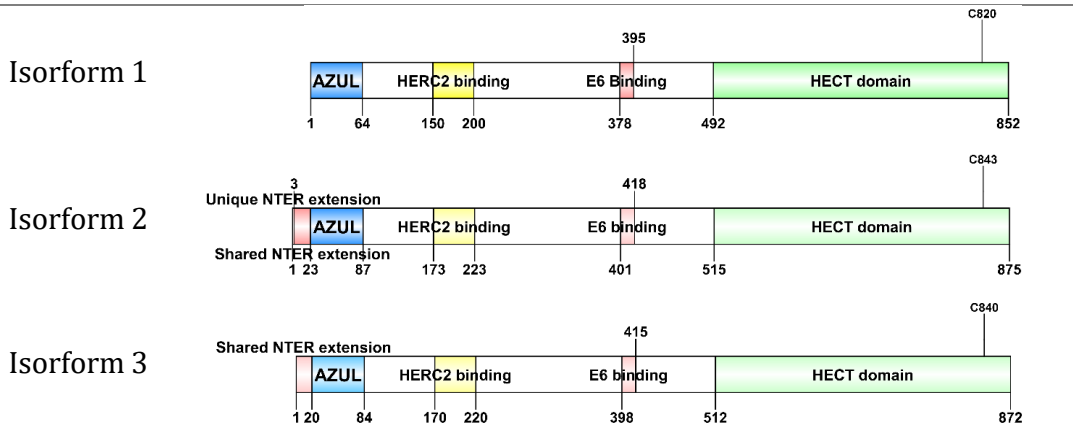

Figure 9. Schematic representation of the domains of the human UBE3A isoforms. All isoforms share the AZUL (blue), HERC2 binding (yellow), E6 binding (pink) and the HECT (green) domains. The catalytic cysteine of each isoform is showed. Isoform 2 is the longest one and shares with isoform 3 a 20 amino acid sequence (red) at the amino terminal region, but it also has 3 unique amino acids just at the beginning of the protein.

Methodologies to study protein-protein interaction

In general, proteins do not act individually in living cells and they tend to form complexes in order to exert their function (Yanagida 2002). Therefore, the study of protein-protein interactions (PPIs) is crucial to uncover the molecular mechanisms underlying cellular functions including metabolism, proliferation and apoptosis (Braun and Gingras 2012). A number of strategies have been developed to study protein interactions. The different PPI detection methods can be classified into (i) *in silico*, (ii) *in vitro* and (iii) *in vivo* approaches (Rao et al. 2014).

In silico techniques used for PPI detection are computer simulations based on protein structure, chromosome proximity or gene fusion, among others.

Additionally, there are many *in vitro* strategies to study PPIs. For example, TAP-tagging consists of the fusion of two tags to the protein of interest. Afterwards, a tandem affinity purification is performed and the proteins that remain attached to the protein of interest are typically analysed by SDS-PAGE followed by mass spectrometry (Rigaut et al. 1999; Pitre et al. 2008; Rohila et al. 2004). The main advantage of this technique is that affinity purification enables the detection of weak interactions. However, proteins that are not truly involved in the cellular environment might come up as interactors arising as false positives. Coimmunoprecipitation can also be employed to study PPIs *in vitro*. In this approach, protein interactions are tested using a whole-cell extract where proteins are present in their native form. By contrast, in protein microarrays, which allow for high-throughput detection of PPIs, proteins are immobilized separately in the array allowing to study interaction with different proteins at the same time (MacBeath and Schreiber 2000). Sometimes, the size of the protein can be a problem when studying PPIs. As an alternative, protein-fragmentation complementation assays (PFCAs) have been developed. In PFCAs, two proteins of interest are fused to a complementary fragment of a reported protein. If the proteins of interest interact with each other, the reported protein is reconstituted and generates a detectable signal (e.g., fluorescence or luminescence). Indeed, due to its high sensitivity, it is a powerful approach to study PPIs between proteins expressed at endogenous levels either *in vivo* or *in vitro* (Michnick et al. 2011). Finally, thanks to nuclear magnetic resonance (NMR), the binding interface, a crucial aspect of PPIs, can be also studied, as it is capable of identifying contacts between individual atoms of a protein and its partner, but also the kinetics of ligand binding (O'Connell, Gamsjaeger, and Mackay

2009; Gao, Williams, and Campbell 2004). The basis of NMR is that nuclei that are magnetically active are oriented by a strong magnetic field and the absorbed electromagnetic radiation at known frequencies. Chemical bonds, molecular conformations and dynamic processes alter the absorbance producing different spectral lines of the same nuclei (Roberts 1993).

In vivo techniques are performed in whole living organisms so that the host organism in which the PPI takes place is alive when the analysis is performed. The yeast-two hybrid (Y2H) is one of the most frequently used methods to study PPIs *in vivo*. Y2H methods are a type of PFCA as the DNA-binding domain (DBD) and activating domain (AD) of a transcription factor are split and separately fused to two putative interactors. If they interact, the transcription factor is reconstituted and promotes the transcription of a reporter gene. Although Y2H screens have successfully been applied to study numerous PPIs (X. Zhang et al. 2022; Q. Yang et al. 2022; Lv et al. 2022), they are prone to both false positives and false negatives given that the interactor is studied on a host organism that might provide a different environment (Uetz et al. 2000; Ito et al. 2001).

A major limitation of the above-mentioned methods is that they are not sensitive or efficient enough to detect transient or weak interactions. To cope with it and to provide a complementary approach to the traditional methods, the Proximity Labelling (PL) strategy was introduced in the field of proteomics.

PL methods consist of tagging the endogenous interaction partners of a specific protein of interest (bait). For that purpose, the bait protein is genetically fused to a promiscuous enzyme that catalyses the generation of reactive species in

living cells that can be further enriched and analysed either by mass spectrometry or western blot (Shkel et al. 2022). Distinct PL strategies rely on specific labelling enzymes that differentially label proteins in close proximity to the bait. For example, in the peroxidase-based approach, in which proteins are labelled with free radical species generated from the substrates, HRP or APEX enzymes are used. Both enzymes employ biotin-phenol as their substrate and through peroxidation with H_2O_2 release biotin that is subsequently attached to the surrounding proteins. Ultimately, biotinylated proteins can be purified due to the high affinity between biotin and avidin (Nguyen et al. 2020). As APEX was developed after HRP, it has some advantages. In addition to being smaller than HRP, it works in a monomeric state and does not form disulphide bonds (Martell et al. 2012). By contrast, PUP-IT approach and transpeptidase sortase A (SrtA) method rely on the bacterial PufA ligase and *S. aureus* SrtA enzyme, respectively, to label proteins interacting with the protein of interest. In the PUP-IT strategy, the PufA ligase is fused to the bait. Then, the Pup protein, which is a PufA substrate, is activated by the ligase and similar to ubiquitin, Pup is conjugated to any surrounding lysine (Deane 2018). On the contrary, SrtA requires the presence of a specific sequence to ligate two proteins by a transpeptidase reaction (H. H. Wang and Tsourkas 2019). It has been demonstrated the PUP-IT is efficient to study membrane protein interactions (Q. Liu et al. 2018) whereas SrtA method is suitable for receptor-ligand interaction studies (Pasqual et al. 2018). Additionally, biotin ligases including BioID, BASU, AirID, BioID2, TurboID and miniTurbo have efficiently been employed to tag endogenous interactors with biotin (D. I. Kim et al. 2016; Roux et al. 2012; Yunfei Li et al. 2021; Branon et al. 2018).

PL offers several advantages compared to the traditional methods applied to delineate PPIs (Qin et al. 2021). First, PL strategy allows the identification of interactors of insoluble protein complexes. For example, the interactome of the nuclear envelope protein lamin-A as well as interactors of TDP43 aggregates were unveiled by PL fusing the bait to BioID (Roux et al. 2012; Chou et al. 2018). Second, PL approaches are able to capture transient interactions. Indeed, interactors along different signalling pathways such as Hippo, Ras, MAPK or NF-κB pathways have been discovered by PL methods (Couzens et al. 2013; Phelan et al. 2018; Cui et al. 2019; Dumont et al. 2019). Third, studying dynamic processes like enzyme-substrate interactions is easier with PL. For instance, dynamic processes found in Wnt and GPCR signalling were analysed thanks to the short time frame of APEX labelling (Paek et al. 2017; Grainger et al. 2019). Similarly, BioID fused to the CSF E3 ubiquitin ligases β-TrCP1 and β-TrCP2 has allowed to detect 12 new substrates of the enzymes (Coyaud et al. 2015). Another powerful use of PL is the capability of splitting the PL enzyme and forming two inactive fragments. These fragments are fused to two different baits that when they interact, the enzyme becomes active and proceeds to label (Cho et al. 2020; Y. Han et al. 2019; Kwak et al. 2020; Schopp et al. 2017; De Munter et al. 2017; Martell et al. 2016). Finally, most PL methods are suitable for analysing interactomes in living organisms. Peroxidase-based approaches are not used to study plant interactomes as they require hydrogen peroxide and, in plants, endogenous peroxidases trigger high background activity. Nevertheless, biotin-based approaches (e.g., BioID, BioID2, TurboID, miniTurboID) to study individual baits in flies (Shinoda et al. 2019; Carnesecchi et al. 2020) and mice (Uezu et al. 2016; Caforio et al. 2018), among others. It is worth noting that

biotin-based approaches rely on the strong interaction between biotin and avidin to purify the labelled products. Avidin-biotin interaction is one of the most specific and stable non-covalent interaction, as it is about 10^3 and 10^6 times higher than any antigen-antibody interaction (Diamandis and Christopoulos 1991). Thanks to the high affinity between biotin and avidin, harsh lysis conditions and subsequent stringent washes in denaturing conditions can be applied (e.g. 8 M urea, 6 M guanidine hydrochloride, 2 % SDS), which significantly reduces contamination by non-specific bound targets.

BioID and BioID2 systems

BirA is a 35 kD protein present in *E. coli* that catalyses the biotinylation of substrates containing a biotin acceptor tag (BAT) sequence. BirA-mediated biotinylation is performed in two steps: first, biotin is activated by ATP generating biotinoyl-5'-AMP, which remains at the active site of BirA. Then, when BirA recognizes a BAT sequence, it transfers the biotin to a specific lysine of the target protein (O'Callaghan et al. 1999). Consequently, BirA is an extremely specific enzyme solely modifying BAT sequence containing substrates.

In 2012, Roux and colleagues generated the first genetically engineered mutant of BirA (BirA R118G, BioID), which is promiscuous, meaning substrate unspecific. They demonstrated that expression of this construct in *E. coli* resulted in the biotinylation of any given protein at a radius of approximately 10 nm from the enzyme as free biotioyl-5'-AMP readily react with primary amines (Roux et al. 2012). So far, BioID strategy has been successfully applied to uncover the interactome of lamin-A protein in mammalian cells (Roux et al. 2012), the nuclear

pore complex architecture in human cells (Dae In Kim et al. 2014), centriole composition (Comartin et al. 2013) and the Herpesvirus PPI networks (Cheerathodi and Meckes 2020), among others.

The main disadvantage of the BioID tool is that the promiscuous biotin ligase is slightly bigger than GFP and could interfere with the normal functioning of the protein of interest, triggering abnormal targeting or assembly. Indeed, it has been observed that the presence of BioID occasionally prevents efficient localisation of certain fusion proteins. Upon searching for smalls biotin ligases across different genomes, the biotin ligase of the thermophilic bacterium *Aquifex aeolicus* was identified, hence forward termed BioID2, as a very small alternative that lacks the DNA-binding domain not needed for biotinylation (D. I. Kim et al. 2016).

The optimal working temperature of BioID2 is 50ºC, but it also works efficiently at 37ºC. Additionally, in comparison to BioID, BioID2 requires less supplementation of biotin. Whereas BioID-mediated biotinylation is dramatically reduced when biotin concentration drops below 50 µM, BioID2 can efficiently biotinylate even with 3.2 µM biotin. Additionally, and due to its small size, BioID2 has barely any impact on the localization of the proteins is fused to (Antonin, Ungricht, and Kutay 2011; Ungricht et al. 2015).

The practical labelling radius for protein biotinylation is critical since a larger radius means a higher risk of biotinylating non-specific proteins or interactors, whereas a very small radius would only allow tagging of proteins very close to the bait. Moreover, it has to bear in mind that some proteins are quite rigid, so if the radius of action is too small it may result that proteins interacting with the opposite

region in which the ubiquitin ligase is fused are not tagged, and hence, not detected. Consequently, it is important to find the right balance so that only proteins associating with the bait are tagged. Indeed, in order to enlarge the practical labelling radius of the biotin ligase, a flexible linker is often inserted between the enzyme and the protein of interest. Among the linkers that have been used, in the present doctoral thesis, we used the one consisting of 3 GSGS repeats. The insertion of the linker does not trigger any abnormal proteolytic processing and enables the biotinylation of endogenous proteins in live cells (D. I. Kim et al. 2016).

TurboID and miniTurbo systems

BioID and BioID2 methods require long-term labelling (around 18 hours). This precludes the use of BioID or BioID2 for studying processes that occur in a timescale of a few hours or even minutes. Moreover, due to the low catalytic activity of both BioID and BioID2, it is extremely difficult to use them to study PPIs in whole organisms such as worms or flies.

Alternatively, Brandon and coworkers developed two new promiscuous biotin ligases from BirA-R118S through directed evolution: TurboID (35 kD), with 15 mutations relative to wild-type BirA, and miniTurbo (28 kD), with the N-terminal domain deleted and 13 mutations relative to wild-type BirA (Branon et al. 2018). Biotinylation speed of TurboID and miniTurbo is 3-6 and 15-23 times faster than BioID at early and later time points, respectively. Overall, TurboID is about two-fold more active than miniTurbo, but exhibits more labelling before adding biotin as it may use endogenous biotin. Consequently, miniTurbo seems to be better for experiments in which precise time control is critical (Branon et al. 2018).

In **Table 1** the main characteristics of BioID, miniTubo and TurboID are summarized and in **Figure 10** is represented a simplified scheme of the typical workflow applied when using BioID2 or TurboID.

Table 1. Main characteristics of BioID, miniTurbo and TurboID (Branon et al. 2018).

	BioID	miniTurbo	TurboID
Biotinylation speed (for the same biotinylated material)	18 hours	10 minutes	10 minutes
Biotinylation rate (in flies)	1x	10x	22x
Consumes endogenous biotin	NO	NO	YES
Protein instability	NO	NO	YES
Persistent biotinylation (even with no biotin added)	NO	NO	YES
Increase in practical radius	NO	NO	YES
in vivo behaviour	Similar to negative controls	Suitable for short-term reactions. Low background	Convenient for experiments in which protein amount is critical
Toxicity in flies	NO	NO	Decrease in survival and fly size

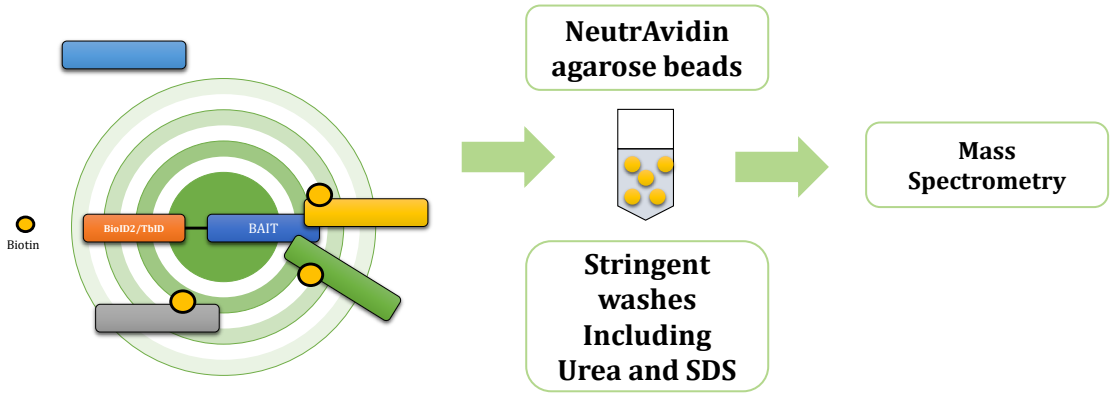

Figure 10. Schematic representation of the BioID2/TurboID system. BioID2/TurboID is fused to a protein of interest either with a linker or not. When biotin is added to the medium, proteins near to the practical labelling radius will be biotinylated by BioID2/TurboID. Purification with avidin/streptavidin beads will allow to enrich and thoroughly clean the samples and analyse them with mass spectrometry to identify the potential interactors of the bait.

Strategies to isolate ubiquitinated material

The analysis of the ubiquitinated proteins present in the cells is challenging mainly due to the low stoichiometry of ubiquitin conjugates. Nevertheless, during the last years, the development of novel strategies to enrich ubiquitinated proteins and more sensitive mass spectrometers have greatly improved the detection and quantification of ubiquitinated peptides/proteins. The first studies developed in yeast used His-tagged ubiquitin to enrich ubiquitinated material (Peng et al. 2003). However, the presence of endogenous histidine-rich proteins in mammals leads to the detection of false positives when performing these analyses in mammalian models. More recently, diGly-specific antibodies, which recognize the Lys-ε-Gly-Gly (diGly) remnant that is generated upon trypsin digestion of ubiquitinated proteins, have been used to isolate ubiquitinated conjugates. Consequently, enrichment strategies based on antibodies targeting diGly remnants combined with mass

spectrometry (MS) have enabled the detection of thousands of ubiquitination sites (Hansen et al. 2021; van der Wal et al. 2018; G. Xu, Paige, and Jaffrey 2010). However, diGly signature is not unique for ubiquitin as ubiquitin-like proteins such as Nedd8 also present it (Leidecker et al. 2012). Moreover, as ubiquitinated proteins must be digested with trypsin in order to be enriched with diGly antibodies, neither the ubiquitin chains formed *in vivo* nor the whole protein can be further analysed (Shi, Xu, and Qin 2011).

BioUb approach

To cope with the above-mentioned difficulties, our lab developed a new strategy to enrich ubiquitinated proteins *in vivo* termed BioUb. In BioUb approach, six copies of ubiquitin, each of them containing a 14 amino acid long biotinylable (BAT) sequence, and the biotin ligase BirA are coexpressed either in cells or whole living organisms (Ramirez et al. 2016; Franco et al. 2011). Once the construct is expressed, endogenous DUBs digest the precursor and free BirA biotinylates released ubiquitin moieties, which can then be used by the UPS machinery to conjugate target proteins Therefore, as ubiquitinated proteins become biotinylated, they can be efficiently purified with neutravidin beads and further analysed by mass spectrometry (**Figure 11**). Indeed, the combination of BioUb strategy and mass spectrometry has allowed us to identify many ubiquitinated substrates in flies and mice (Lectez et al. 2014; Martinez et al. 2017; Ramirez et al. 2018; Elu et al. 2019).

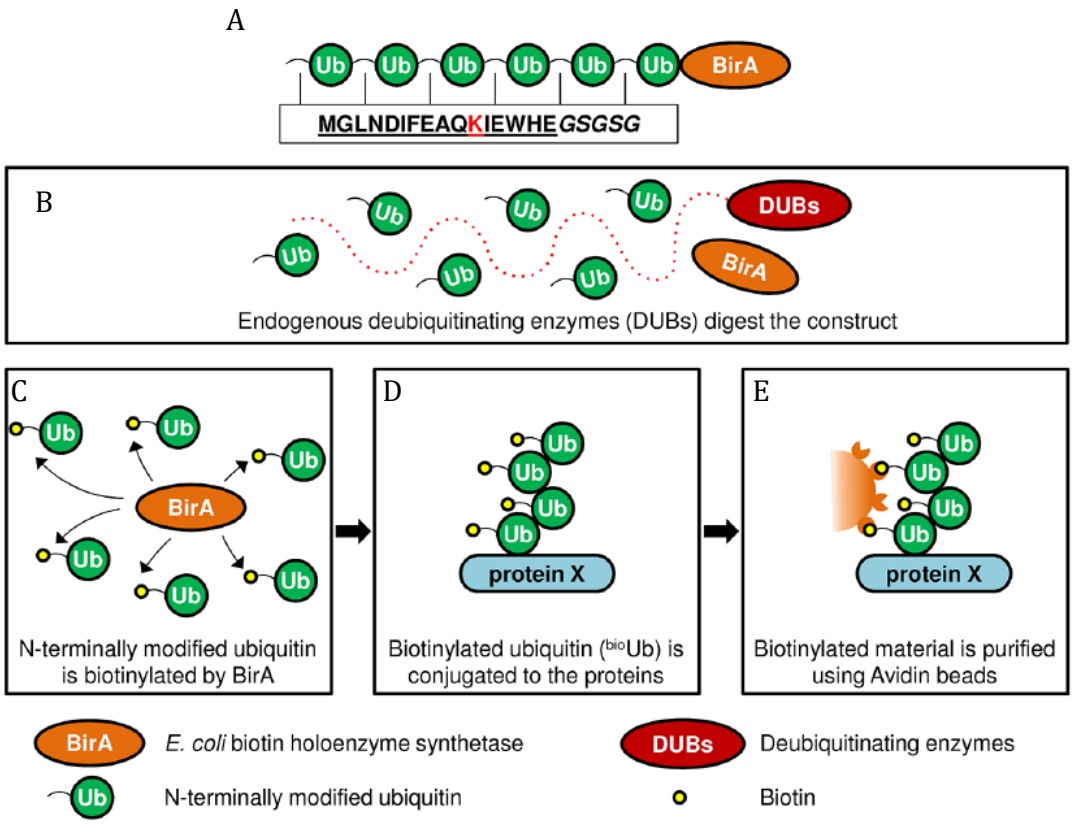

Figure 11. The BioUb strategy. A) Six copies of ubiquitin are fused in tandem to BirA. N-terminal to each ubiquitin copy, a BAT sequence is placed. B) The construct is expressed in the cells and the endogenous action of the DUBs will detach the ubiquitin copies from BirA. C) Free ubiquitin is labelled with biotin on the BAT sequence by BirA. D) Biotin-tagged ubiquitin is employed by the ubiquitin E3 ligases and it is conjugated to its physiological substrates. E) Biotinylated material is purified with Avidin beads.

GFP pulldown in denaturing conditions

Often the main scope is not analysing the whole ubiquitome landscape but studying the ubiquitination status or even the ubiquitination sites on a specific given protein. For instance, once the BioUb strategy has been applied to search for the putative substrates of a specific E3 ubiquitin ligase, these results must be individually validated. For that purpose, the ubiquitinated version of the substrate

candidate must be detected. Antibodies can be used, but it may happen that they are not very specific or that they are simply not commercially available. Moreover, traditional coprecipitation methods are performed in non-denaturing conditions, and consequently, many contaminants or false positives arise.

To overcome all the above-mentioned obstacles, our lab has developed a GFP pulldown strategy that is performed in denaturing conditions so that contaminants and false positive identifications are avoided. In this approach, the protein of interest, which is fused to GFP tag, is coexpressed with FLAG-tagged ubiquitin either in cells or whole living organisms. Then, it is enriched with anti-GFP beads, as mentioned before subjected to stringent washes to discard contaminant proteins, and finally analysed by western blot. Whereas anti-GFP antibody detects the non-modified version of the protein, anti-FLAG antibody is used to detect the ubiquitinated form(s) of the same protein (**Figure 12**). Moreover, material from GFP pulldown can be analysed by mass spectrometry to identify site-specific ubiquitination sites, as well as the type of ubiquitin chains that are formed in the protein of interest (Ramirez et al. 2016).

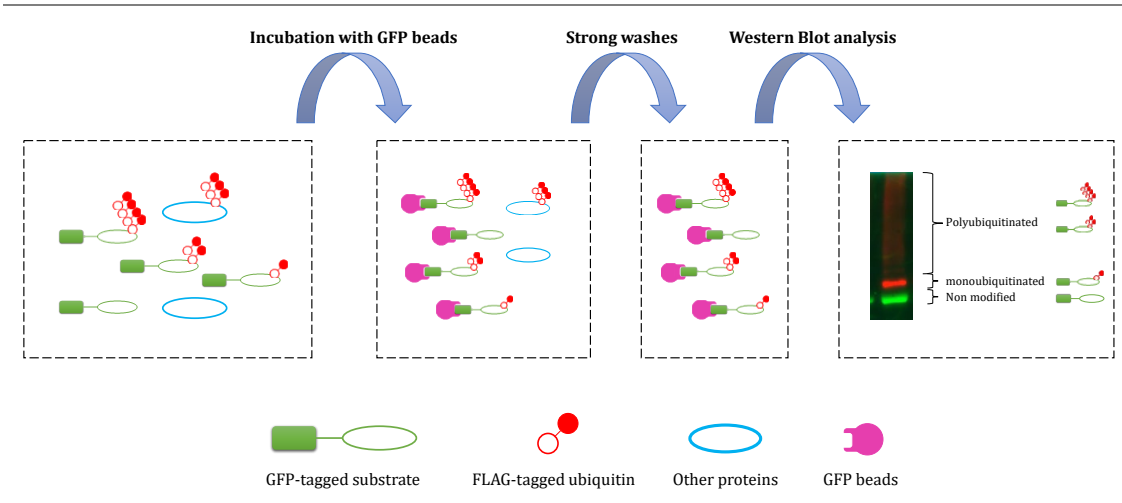

Figure 12. GFP pulldown in denaturing conditions. The substrate of interest is fused to GFP and cotransfected with FLAG-tagged ubiquitin. The lysed material is incubated with beads with anti-GFP antibodies and, therefore, the GFP-tagged substrate is purified. Through harsh washes, the material that was not attached to the GFP beads is removed. Since ubiquitination is a covalent modification, FLAG-tagged ubiquitin remains bond to the substrate and both are purified. Finally, western blot analysis by incubation with anti-GFP and anti-FLAG antibody allows to identify the polyubiquitinated material, the monoubiquitinated fraction and the non-modified protein.

CaMKII

CaMKII structure and regulation

The Ca2+/calmodulin-stimulated protein kinase II (CaMKII) family is encoded by four genes: CAMK2A, CAMK2B, CAMK2G, CAMK2D which produce CaMKIIa, CaMKIIb, CaMKIId and CaMKIIg, respectively. CaMKII proteins contain three structural domains: a regulatory domain, an association domain and a catalytic domain bearing the ATP- and substrate-binding (S site) sites as well as sites for interaction with other proteins (Gaertner et al. 2004; Brocke, Srinivasan, and Schulman 1995; Srinivasan, Edman, and Schulman 1994). All isoforms form dodecameric holoenzymes that are composed of diverse subunit types.

The regulation mechanism is common for all the holoenzymes: under basal conditions, CaMKII is largely inactive as it is subjected to autoinhibition through the autoinhibitory domain that interacts with the substrate-binding site in the catalytic domain and blocks the kinase activity (**Figure 13**). When intracellular calcium, and consequently, Ca^{2+}/Calmodulin concentration increases, Ca^{2+}/Calmodulin binds to the regulatory domain disrupting the interaction between the regulatory and

catalytic domains. This results in a conformational change that releases the autoinhibition, exposes the catalytic domain for substrate binding and induces the kinase activity of CaMKII. Then, T286 of the autoinhibitory domain can be phosphorylated by a neighbouring subunit of the oligoenzyme. Once T286 is phosphorylated (pT286), the autoinhibitory domain cannot block again the enzyme, even if Ca^{2+} levels fall. Thus, CaMKII can also function in a Ca^{2+}-independent manner (Hudmon and Schulman 2002). For the enzyme to be autonomous, the autoinhibitory domain binds to the catalytic domain through the S and the T site. The surroundings of the T286 that binds to the T site block T286 phosphorylation. Binding to the T site is necessary to position the pseudosubstrate sequence and block the S site. However, when T286 is phosphorylated, interaction with the T site cannot occur and, consequently, the S site is not blocked and the kinase remains active (E. Yang and Schulman 1999).

CaMKIIa and CaMKIIb are the most abundant proteins in the brain (1-2% of the total protein). The protein is enriched at the synapses and it is the main protein at the postsynaptic density (PSD). Indeed, shortly after being phosphorylated on T286, CaMKII T305 and T306 can be phosphorylated, which results in a reduction in the autonomous kinase activity of CaMKII (Coultrap et al. 2010). Long-term potentiation (LTP), a process involved in learning and memory, is triggered by the increase in Ca^{2+} levels. Moreover, in LTP, NMDA and AMPA receptors trafficking plays a crucial role (Yasuda et al. 2003; Malinow 2003). CaMKII is able to detect changes in Ca^{2+} levels, and, consequently, initiate the signalling cascade that leads to the potentiation of synaptic transmission. CaMKII seems to be involved in additional processes as well. Since CaMKII remains activated for at least one hour after LTP

induction, it might be involved in LTP maintenance and, consequently, in memory events. T286 autophosphorylation is necessary for CaMKII persistent activation as mutation of this residue blocks LTP (Lou, Lloyd, and Schulman 1986)

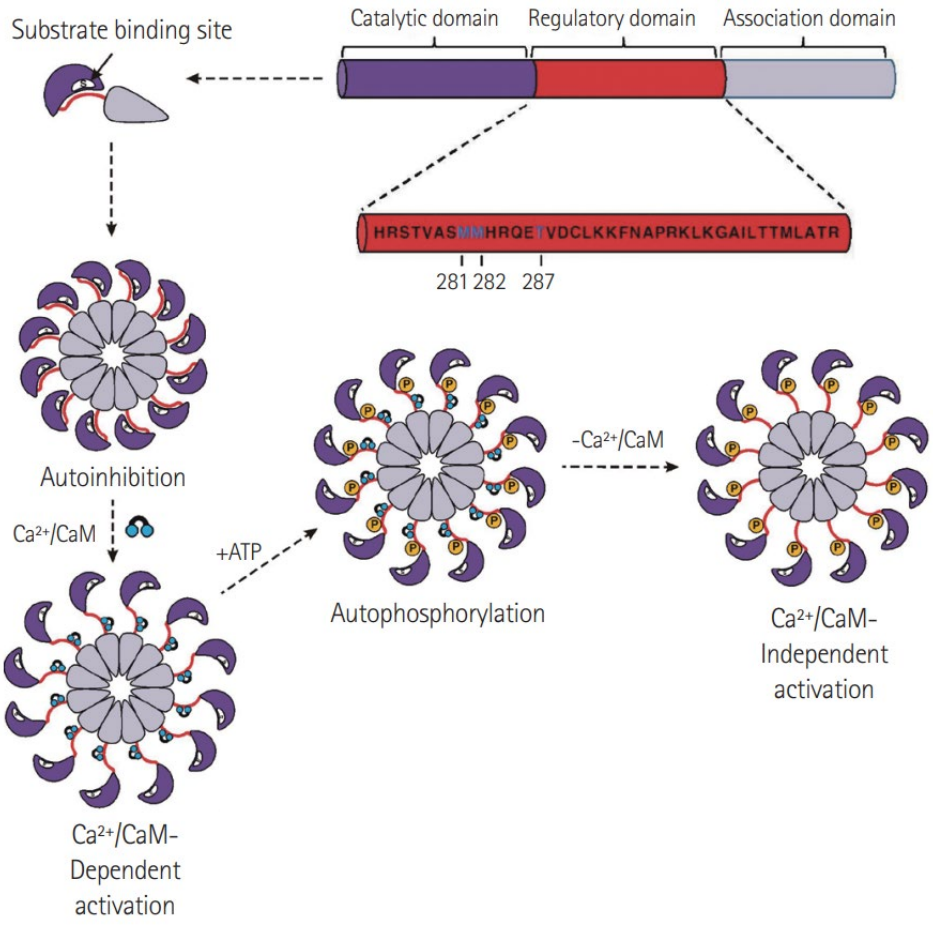

Figure 13. Ca2+ dependent and independent activation of CamKII. In basal conditions, the autoinhibitory domain of CaMKII inhibits the enzyme blocking the catalytic domain. When Ca2+/Calmodulin concentration increases, a conformational change exposes T286 of the autoinhibitory domain, which becomes phosphorylated and consequently cannot block the enzyme, not even if Ca2+ levels fall (Song, 2013).

Depending on the magnitude of Ca^{2+} signalling, CaMKII can be activated at different levels. Weak Ca^{2+} signals activate the kinase but autophosphorylation of T286 does not occur. Thus, higher Ca^{2+} levels are necessary for T286 to

autophosphorylate. To make it possible, two Ca^{2+}/Calmodulin molecules have to bind to two subunits on the same holoenzyme. Whereas one Ca^{2+}/Calmodulin will activate one CaMKII subunit, the other will trigger the conformational change in another CaMKII subunit, making T286 accessible. Once a CaMKII subunit is phosphorylated in T286, all subunits forming the holoenzyme can easily be phosphorylated, probably in a directional process. Propagation of phosphorylation does not need high Ca^{2+} levels because only one Ca^{2+}/Calmodulin is necessary. Activation will last even with no Ca^{2+} until the kinase is dephosphorylated (Lisman 1985; Miller and Kennedy 1986).

After the induction of LTP, the enzyme is long-term persistent activated. This event may be possible due to the special chemical environment of the postsynaptic density (PSD), allowing CaMKII to act as a bistable switch. When a threshold number of kinase sites are phosphorylated, the switch turns on. Because CaMKII functions faster than the PSD phosphatase, the "on" mode can last for long periods. The "on/off" switch explains the all-or-nothing nature of LTP induction (Fukunaga, Muller, and Miyamoto 1995).

NMDA receptors detect released glutamate from the presynaptic terminal and the postsynaptic membrane is depolarised triggering the opening of Ca^{2+} channels, and the consequent rise of Ca^{2+} levels. Several studies have demonstrated that Ca^{2+} elevation through NMDA receptor activation triggers the induction of CaMKII activity. Furthermore, recent studies show that CaMKII translocates to synapses, where it binds directly to NMDA (N-methyl- D-aspartate) receptors. This

translocation places the kinase in an ideal site to control synaptic strength (Strack et al. 2000).

Role of CaMKII in Drosophila melanogaster

CaMKII was first isolated in *Drosophila melanogaster* in 1993, when four cDNA sequences were purified (Ohsako et al. 1993). Through *in situ* hybridization, it was established that, in older stages of embryonic development CaMKII was mostly concentrated in the central and peripheral nervous system. Subsequent functional studies of flies with CaMKII deficit showed that these transgenic flies failed to learn normally in two behavioural plasticity paradigms (acoustic priming and courtship conditioning) that are typically used to study memory and learning in *Drosophila melanogaster* (Griffith et al. 1993).

CaMKII is also involved in the development of proper synapse structure and function through the regulation of the localisation of Disc Large (DLG) proteins at the synapses (Koh et al. 1999). Indeed, the expression of a constitutively active form of CaMKII (CaMKII T287D) dramatically altered the synaptic structure at both pre- and postsynaptic sites (Saitoh and Schwartz 1985; Miller and Kennedy 1986).

Moreover, CaMKII activity seems to be involved in dendritic growth (G. Y. Wu and Cline 1998). In young neurons, dendritic arbour elaboration is faster than in mature neurons. High CaMKII activity in young neurons triggers the slowdown of dendritic growth to levels seen in mature neurons. Furthermore, it has been shown that CaMKII increases the dynamic nature and formation of dendritic filopodia throughout larval development (R. Andersen 2005).

CaMKII and the proteasome

Apart from its role in synaptic function and structure, the four mammalian CaMKII proteins have been related to the proteasome. For instance, CaMKIIa and CaMKIIb expression promotes the accumulation of Rpt1 – a subunit of the 19S proteasome – in spines after NMDA stimulation. Moreover, a constitutively active form of CaMKIIa (CaMKIIa T286D) coimmunoprecipitates with the proteasome subunit Rpt6 5-fold more than WT CaMKIIa. Additionally, CaMKIIa translocation to the spines has been shown to be necessary to promote the degradation of proteasomal substrates (Bingol et al. 2010). And besides that, CaMKII has been associated with the regulation of proteasome phosphorylation and activation after the retrieval of contextual fear memory (Jarome et al. 2016).

High throughput analyses have revealed that CaMKII can be ubiquitinated (Udeshi et al. 2013; Povlsen et al. 2012; W. Kim et al. 2011; Ramirez et al. 2018), but no functional analyses have been performed. As a result, to date, the E3 ubiquitin ligase responsible for CaMKII ubiquitination remains unknown.

CaMKII and Angelman syndrome

The AS mouse model (maternally inherited *Ube3a* mutation) shows seizures as well as motor and cognitive abnormalities. These mutant animals show increased CaMKII phosphorylation levels, specifically at T305, despite having the same total amount of CaMKIIa. Consequently, the activity and autophosphorylation capacity of CaMKII is reduced, and the total amount of CaMKII associated with postsynaptic density is lower (Weeber et al. 2003).

The above-mentioned AS mouse model has been employed to study the levels of phosphorylated CaMKIIa in AS. When this mouse model was crossed with mice expressing CaMKIIa-T305V/T306A, a truncated version of CaMKII that cannot be inhibited through phosphorylation of those sites, the kinase activity of the double mutant mice was restored and comparable to the kinase activity of wild-type mice. Additionally, despite AS mice exhibiting several LTP defects, CaMKII and UBE3A double mutant mice showed LTP levels similar to wild-type mice. Altogether, it was concluded that the inhibitory phosphorylation of CaMKII might be responsible for the plasticity deficits observed in AS mice (Van Woerden et al. 2007).

Furthermore, when the AS mouse model was treated with a drug that modulates AMPA receptors in a positive manner, LTP was restored to WT levels and response to fear conditioning was restored too (Baudry et al. 2012).

CaMKIIa and UBE3A

To date, there is no clear link between CaMKII and UBE3A. As it was mentioned before, in AS mouse models that do not express UBE3A in neurons, the activity of CaMKII is decreased most probably due to an enhancement of CaMKII phosphorylation (Weeber et al. 2003). Recent studies have revealed a possible crosstalk between the HUN (HERC2, UBE3A and NEURL4) protein complex and CaMKII, which may explain the mouse phenotype of AS mouse model. Moreover, it has been shown that ASPP2 (Apoptosis- Stimulating of p53 Protein 2) is degraded upon UBE3A-mediated ubiquitination. ASPP2 inhibits the phosphorylase PP1, which dephosphorylates CaMKII. Therefore, it is hypothesized that in the absence of

UBE3A, ASPP2 is not degraded but accumulated, and, thereby, PP1 is less active and CaMKII remains phosphorylated (Martínez-Noël et al. 2018).

Drosophila melanogaster

The fruit fly (*Drosophila melanogaster*) is suitable as an experimental organism due to several reasons. On one hand, its small size and short cell cycle make it very easy to work with and obtain various generations within a short period of time. On the other hand, it has a small genome (1/20 the size of an average mammalian genome), facilitating molecular genetic analysis. Although other organisms also share these features, *Drosophila melanogaster* is one of the first choices thanks to the hard work carried out by researchers in the past, starting with T. H. Morgan's laboratory at the end of the XXth century (Morgan 1910). *Drosophila melanogaster* was employed as a model in the discovery of *Notch*, a very important gene in development (Bridges and Morgan 1916), or *Toll*, a gene involved in the immune response (Anderson, Bokla, and Nüsslein-Volhard 1985; Anderson, Jürgens, and Nüsslein-Volhard 1985).

Life cycle

The common media in which flies are raised is composed of corn meal, brewer's yeast, sugar, agar, and a small amount of mould inhibitor. Breeding in that medium at 25ºC enabled the flies to complete their life cycle from fertilization to the emergence of the adult fly within 10 days. The embryo completes its development in just under 24 hours, making it possible to see in real-time some key developmental events. Embryogenesis is complete with the first instar larva, which

grows dramatically fast and needs to moult 24 and 48 hours after hatching to produce second and third instar larvae. After three days from the production of the third instar larva, the larva exits the food and pupates. Moulting and pupation are controlled by the ecdysone hormone. Once inside the pupa, the larvae undergo metamorphosis, a reorganisation of the fly body plan that takes about four days. Most larval tissues are disintegrated and replaced through the proliferation and differentiation of cells that produce adult structures. Most adult structures, such as the wings, legs, eyes, and genitalia, are formed from imaginal discs. Imaginal discs are flattened epithelial sacs that develop from small groups of cells set aside in the early embryo. Once metamorphosis is complete, the adult emerges from the pupal case, the wings are expanded and the entire exoskeleton hardens and becomes pigmented (**Figure 14**) (Hartwell et al. 2003).

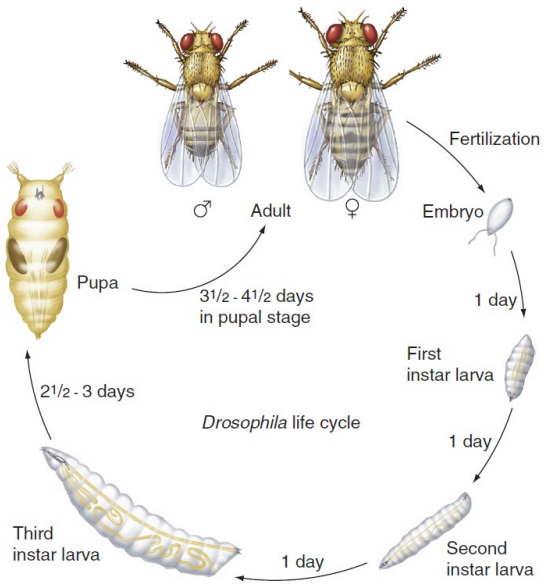

Figure 14. *Drosophila melanogaster* life cycle. Hatching is the transition from embryo to larva. Through molting second and third instar larva are generated. Pupariation converts third instar larva to a pupa. Adults emerge from the pupal case in a process called eclosion (Hartwell 2013).

Genetics

The *D. melanogaster* genome contains four chromosomes, designated numerically as 1-4. Chromosome 1 corresponds to chromosomes X and Y, and chromosomes 2, 3 and 4 are the autosomes. Sex is determined by the ratio of X chromosomes to the number of copies of each autosome (X:A ratio). Thus, a ratio of 1 will give a female and a 0.5 ratio results in the development of a sterile male. Chromosome Y is not involved in sex determination but is involved in the conference of fertility (Hartwell et al. 2003).

Through the employment of X-rays, special chromosomes, such as balancer chromosomes, have been developed by geneticists. Balancer chromosomes have multiple overlapping inversions and, normally, result in a dominant marker that enables tracking through crosses and a recessive lethal mutation to prevent homozygotes survival. Like all inversion-containing chromosomes, they prevent the recovery of crossovers between normal chromosomes and themselves. Thereby, balancer chromosomes and their homologues are inherited as intact units, and no recombinant chromosomes are passed on to the next generation (Hartwell et al. 2003).

The P elements transposon is another critical tool in *Drosophila* molecular genetics. P elements trigger hybrid dysgenesis, a phenomenon that occurs when males from strains with P elements are crossed with females that lack P elements. They become highly mobile in the germ line resulting in chromosome breakage and reduced fertility in the hybrids. Thus, those that survive come with many new mutations induced by the insertion of P elements at new sites in the genome. The

high mobility makes it possible to exploit these elements for the transformation of new vectors and as genetic tags. The gene of interest is cloned in a vector that contains a tracking gene, *white*$^{+}$ for example, flanked with P-element inverted ends. The vector lacks the gene that encodes for the transposase, thus, a helper vector that carries the gene is coinfected. As a consequence, the gene of interest will be introduced into the fly genome, and eventually to the progeny. Because the gene of interest is inherited as a unit with the tracking gene, positive flies will be selected by looking at the phenotype. For example, if the tracking gene is *white*$^{+}$, positive flies will have red eyes, while negative flies will have white eyes (Hartwell et al. 2003).

Drosophila's nervous system

Unlike many of the larva tissues that are disintegrated during metamorphosis, the brain remains from larva to adult fly with some restructuration of the neurons. Despite not being structurally analogous to mammalian brains, the myriad of developed tools makes the fly brain accessible and rapid to work with.

The fly brain has between 100,000-200,000 neurons, distributed equally in the central brain, the paired optic lobes and the segmentally organised ventral nerve cord. Although fly neuron structure presents some structural differences compared to vertebrates, the dendrites appear to share organisational and functional characteristics with vertebrate dendrites (Simpson 2009). Acetyl-choline, glutamate and biogenic amines neurotransmitters are found in *Drosophila*, while epinephrine and norepinephrine are not produced. However, biogenic amines in *Drosophila* function similarly to norepinephrine and epinephrine in vertebrates (Monastirioti 1999). Glia cells represent 90% of the cells of the human brain;

however, in fly brain comprise 10-25% of the cells (Freeman and Doherty 2006). Flies employ a highly branched tracheal system that works as an analogue to the vascular system of the vertebrates' brain, which is involved in meeting oxygen demands. The fly neuromuscular junction (NMJ) in its larva period is basically a glutamatergic synapse that innervates each muscle segment ending in round synaptic boutons (Ghabrial et al. 2003).

GAL4/UAS system

The GAL4, which was first identified in *Saccharomyces cerevisiae,* is a galactose-induced transcription factor that once it is induced by the galactose regulatory system, its transcription is enhanced by 1000-fold. Then, GAL4 is capable of binding to Upstream Activating Sequences (UAS), triggering the expression of genes required for the galactose metabolism.

GAL4 system is frequently employed in the targeting of gene expression of binary systems by placing the genes of interest in *Drosophila* under the control of a UAS element. However, as GAL4 is not expressed in *Drosophila,* a separate transgenic "driver" line has to be generated. In these lines, GAL4 is placed under the control of tissue-or temporally-specific regulatory sequences. As the fly genome lacks UAS elements, Gal4 will not be functional in these lines. Nevertheless, when both lines are crossed, within the progeny flies with GAL4 and the gene of interest under the control of UAS will be found. This strategy allows to express either a gene of interest, reporter genes or RNAi sequences (**Figure 15**) (Brand and Perrimon 1993).

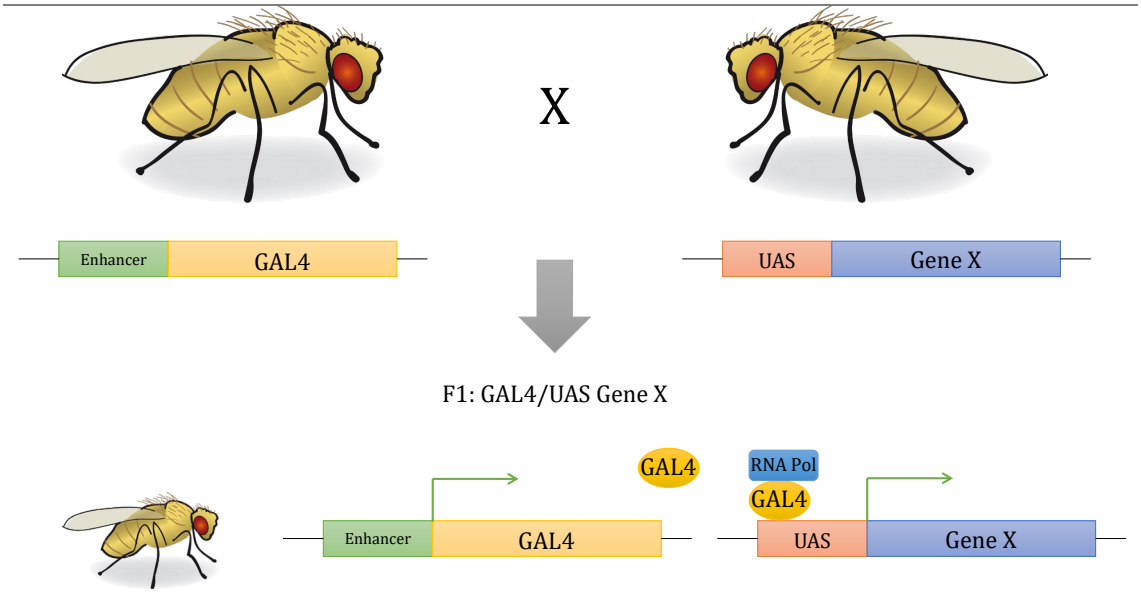

Figure 15. The GAL4/UAS system. The GAL4/UAS system is widely employ to express a protein of interest in *Drosophila melanogaster*. Flies that express GAL4 are crossed with flies that have the gene of interest under the UAS promoter. The progeny will have both constructions, GAL4 will be expressed and the protein will recruit RNA polymerase to the UAS promoter. Therefore, the protein of interest will be produced.

HYPOTHESIS AND OBJECTIVES

CHAPTER I: Deciphering the interactome of CaMKII in HEK 293T cells by proximity labelling with BioID2

There is indirect evidence linking the brain kinase CaMKIIa with Angelman syndrome-causing E3 ligase UBE3A. Moreover, it is known that CaMKIIa can be ubiquitinated, although the ubiquitin ligase responsible remains undiscovered. We hypothesize that CaMKIIa might interact with UBE3A or other proteins involved in the ubiquitin-proteasome pathway, therefore, studying the interactome of CaMKIIa in HEK 293T cells could allow us to have a better understanding of the role of CaMKIIa in AS.

The particular objectives for the 1st chapter of this PhD Thesis are:

1. Determine the best conditions and reproducibility of the BioID2 system for future studies of CaMKII in neuronal tissue
2. Identify potential CaMKIIa interactors in HEK 293T cells.
3. Validate candidates through coimmunoprecipitation experiments.
4. Identify the DUB enzyme responsible for CaMKII's deubiquitination.
5. Identify the E3 ubiquitin ligase responsible for CaMKII's ubiquitination.

CHAPTER II: Uncovering CaMKII interactors in Drosophila melanogaster through TurboID

We believe that uncovering CaMKII interactors in neurons will help us have a better understanding of the role of this kinase in neurophysiology. We considered that a TurboID-based approach would allow us to better resolve the interactome of

CaMKIIa in flies, and hypothesized that those CaMKII fly interactors would have human homologues.

Therefore, for this second chapter of this thesis we have established the following objectives:

1. Validate the TurboID system in *Drosophila melanogaster*.
2. Uncover CaMKII interactors in *Drosophila melanogaster* neurons.
3. Analyse the interaction between CaMKIIa and the human homologues of the identified interactors.

CHAPTER III: Neurochondrin: the possible link between CaMKII and UBE3A

Recently, our group discovered that NCDN, a well-known negative regulator of CaMKIIa pT286, is a substrate of the ubiquitin E3 ligase UBE3A. Therefore, we suggest that these three proteins may interact, either physically and/or functionally. Indeed, CaMKIIa can be ubiquitinated (Udeshi et al. 2013; Povlsen et al. 2012; W. Kim et al. 2011; Ramirez et al. 2018) but, to date, the E3 ubiquitin ligase responsible for it remains unknown. Therefore, we wanted to assay the ubiquitination of CaMKIIa by UBE3A. As we have confirmed that NCDN becomes ubiquitinated by UBE3A, we hypothesize that UBE3A-mediated ubiquitination of NCDN might be involved in changes in CaMKIIa phosphorylation, and try to understand how CaMKIIa and UBE3A functionally interact.

The particular objectives for the third chapter of this PhD Thesis are:

1. Study the interaction between CaMKIIa, NCDN and UBE3A.
2. Determine whether CaMKIIa is ubiquitinated by UBE3A or not
3. Identify the ubiquitin chains that UBE3A forms on NCDN.
4. Evaluate the link between UBE3A-dependent NCDN ubiquitination and CaMKIIa phosphorylation on T286.

CHAPTER IV: How to inactivate E3 ubiquitin ligases

Inactive mutants of E3 ubiquitin ligases are widely employed to determine the ligase's interactors and substrates. However, the generation of these mutants depends on the type of E3 ubiquitin ligase.

In order to characterise the inactivating mutations we propose the following objective:

1. Review the available information about the inactivation of E3 ubiquitin ligases.

MATERIALS AND METHODS

Molecular Biology

Oligonucleotides

Designed primers were at least 15 nucleotides long complementary to the template sequence. To improve primer annealing, primers finished in G or C at the 3' end. New restriction sites, Kozak sequence or extra nucleotides necessary for proper frame reading were added at the 5' end. All primers were ordered from Invitrogen and they are compiled in **Table 2**.

Table 2. Primer names and sequences of the oligonucleotides employed for the PCR reactions for the different constructs. F: Forward; R: Reverse

Primer name	Primer sequence
BioID2 in pCAG	
BioID2 NTER AgeI F	GCCACCGGTCCACCATGTTCAAGAACCTGATCTGG
BioID2 NTER NotI R	GGCGCGGCCGCGCTTCTTCTCAGGCTG
LinkerI_BioID2 NTER NotI R	AATGCGGCCGCGCTGCCGCTACCGCTTCTTCTCAGGC
LinkerII_BioID2 NTER NotI R	AATGCGGCCGCGCTGCCGCTACCGCTGCCGCTACCGCTTCTTCTCAGGC
LinkerIII_BioID2 NTER NotI R	AATGCGGCCGCGCTGCCGCTACCGCTGCCGCTACCGCTGCCGCTACCGCTTCTTCTCAGGC
BioID2 CTER NotI F	AAAGCGGCCGCGGTGGCGGCGGCAGCGGTGGCGGCGGCAGCGGTGGCGGCGGCAGCATGTTCAAGAACCTGATCTGG
BioID2 CTER SacI R	GGGGAGCTCTTAGCTTCTTCTCAGGCTGAAC
Rat CaMKIIa in pCAG	
CaMKIIa FL NotI F	TTAGCGGCCGCCATGGCTACCATCACC
CaMKIIa FL/CTER SacI R	TTTGAGCTCTCAATGGGGCAGGACGG
CaMKIIa CTER NotI F	AAAGCGGCCGCCCAGCACCCCTGGATCTCGCACCG
CaMKIIa NTER AgeI F	GGCACCGGTATGGCTACCATCACCTGC
CaMKIIa NTER NotI R	TTAGCGGCCGCTGAGAGCCTCAGCGGCC
TurboID in pUAS	
TurboID NTER XhoI F	CCCCTCGAGATGGACTACAAAGACGATGACGACAAG
TurboID NTER KpnI R	AAAGGTACCGCTGCCGCTACCGCTGCCGCTACCGCTGCCGCTACCCTTTTCGGCAGACCG
TurboID CTER KpnI F	AAAGGTACCGGTAGCGGCAGCGGTAGCGGCAGCGGTAGCGGCAGCATGGACTACAAAGACGATGACGACAAG
TurboID CTER XbaI R	CCCTCTAGATTACTTTTCGGCAGACCG
Drosophila CaMKII in pUAS	
CaMKII FL XbaI R	GGGTCTAGACTATTTTTGGGGTATAAAATCG
CaMKII FL/CTER KpnI F	TTTGGTACCATGGCTGCACCAGCAGCC
CaMKII CTER KpnI F	TTTGGTACCATGGCTGCACCAGCAGCC
CaMKII NTER XhoI F	TTACTCGAGATGGCTGCACCAGCAGCC
CaMKII NTER KpnI R	TTTGGTACCCGAGTTTCCTATATTTTGC

DNA plasmids

pEGFP-C1-CaMKIIa and pEGFP-C1-CaMKIIb were a kind gift by professor Hayashi (Okamoto et al. 2007).

The pCAG-IRES-EGFP plasmid was kindly provided by Dr. Zhi-Qi Xiong (Miao et al., 2013), contains the CAG mammalian promoter, and was employed to generate the BioID2 construct. The EGFP insert was removed and BioID2 with the different linkers was introduced between *AgeI* and *NotI* restriction sites for the C-terminal constructs (pCAG-BioID2-C; pCAG-BioID2L1-C; pCAG-BioID2L2-C; pCAG-BioID2L3-C) and between *NotI* and *SacI* restriction sites for the N-terminal constructs (pCAG-N-BioID2). Then, CaMKIIa FL, CaMKIIa I206K and CaMKIIa C-TER (267-479) sequences were introduced between the *NotI* and *SacI* restriction sites. CaMKIIa N-TER (1-266) was introduced between the *AgeI* and *NotI* restriction sites.

The pUASTattB expression vector from Flybase (FBmc0003002), which contains the UAS promoter from yeast, was used to generate the constructs that were employed in *Drosophila melanogaster*. First, TurboID sequence was introduced between the *KpnI* and *XbaI* restriction sites for the N-terminal constructs (pUASattb-N-TuboID) or between the *XhoI* and *KpnI* restriction sites for the C-terminal ones (pUASattb-TurboID-C). Then, CaMKII FL and CaMKII CTER (389-530) were introduced in the pUASattb-TurboID-C plasmid between the *KpnI* and *XbaI* restriction sites. CaMKII NTER (1-388) was introduced in pUASattb-N-TurboID between the *XhoI* and *KpnI* restriction sites.

pCMV-CaMKIIa_N-TER-GFP and pCMV-GFP-CaMKIIa_C-TER were ordered from VectorBuilder as controls. VectorBuilder has a complete library of genes and

allows one to select the desired promoter, the gene of interest and if needed, a tag. No starting material was needed to be sent as they can generate the custom plasmids with their own library.

For the validation of CaMKIIa interactors and ubiquitylation assays, the following plasmids were used: pCMV2-FLAG-ITCH WT and LD (C830A) were kindly gifted by professor Angers (Angers, Ramjaun, and McPherson 2004). The pcDNA3.0-6xmyc-RC3H2 WT and LD (C33S) were kindly gifted by (Maruyama et al. 2014). PME18S-FLAG-TXNL1 plasmid was a gift from professor Gruenberg (Felberbaum-Corti et al. 2007). The pLentilox-FLAG-SART3 plasmid was a gift from professor Garner (Sherman, Mitchell, and Garner 2019). pcDNA3.1-FLAG-ARS2 was a gift from professor Ohno (Machitani, Taniguchi, and Ohno 2020). The pEF-HA-RANBP2 plasmid was a gift from professor Flotho (Ritterhoff et al. 2016).

For the coimmunoprecipitation studies, pEGFP-NCDN (NCDN-GFP) construct was a gift from professor Sleeman (Thompson et al. 2018) and pCMV-FLAG-UBE3A WT and LD were kindly gifted by professor Tomaić (Tomaić and Banks 2015).

siRNA

To silence the different DUBs we employed specific siRNAs targeting their genes: siRNA SilencerSelect for MYSM1 (s41639), siRNA SilencerSelect for OTUD4 (s224312) and siRNA SilencerSelect for USP16 (s20808), all ordered from (Invitrogen). A negative control siRNA was also purchased from Invitrogen (AM4611).

Cloning Procedures

For PCR amplification, around 1 ng of template DNA was incubated with 200 µM of each dNTP, 0.5 µM of each primer and 0.02 U/µL of Phusion-High Fidelity DNA Polymerase (Invitrogen) in 1X Phusion HF Buffer (Invitrogen). Moreover, BioID2 amplification required the addition of 3% DMSO to the reaction mix. Initial denaturation was carried out at 98 ºC for 30''. Then, 35 cycles of (i) denaturation at 98ºC for 10 seconds, (ii) annealing at the appropriate temperature was calculated with Thermo Fisher Scientific Tm Calculator for 20'', and (iii) extension at 72 ºC for 15'' per kb were programmed using a BioRad C1000 Touch thermal cycler. The final extension step was performed at 72 ºC for 5' and, finally, samples were cooled down to 4 ºC.

Amplicons were run in 1% agarose gels, and DNA was extracted from the appropriate band using E.Z.N.A Gel Extraction Kit (Omega). Digestions were performed sequentially: first, one enzyme was added, incubated and inactivated and, afterwards, the second enzyme was introduced following the same steps. Digestion of the inserts and the plasmids was carried out at 37ºC for 1h and 30' with each enzyme. Restriction enzymes (Invitrogen) were inactivated at 65ºC or 80ºC (depending on the enzyme) for 20'. After digestion with both enzymes, plasmids were dephosphorylated with alkaline phosphatase (Roche) for 1h at 37ºC to avoid re-circularization. Ligation was performed with T4 DNA Ligase (Invitrogen) for 10' at 22ºC in 1X T4 DNA Ligase Buffer (Invitrogen). The ratio between insert and vector for the ligations was 10:1 as default, and it was increased if the transformation was not successful.

DH5α competent cells were transformed with the ligation product. Cells and plasmids were incubated 30' on ice, then 45'' at 42ºC and again 2' on ice to perform the heat shock. Immediately after, 1mL of LB medium was added, and they were incubated 1h at 37ºC with shacking. The sample was then plated on LB-agar plates (Conda-Pronadisa) with the appropriate antibiotic (kanamycin or ampicillin, both from Sigma) and incubated at 37ºC overnight. To prepare the plates, 14 g of LB-agar (Conda-Pronadisa) was diluted in 400 mL of Mili-Q water. Then, it was autoclave for around 45' at araound 130 ºC. Once the mixture was cooled down, ampicillin or kanamycin (Sigma) was added in a 1:1000 dilution. The mixture was then poured into the Petri plates. Once polymerised, the plates were kept at 4ºC until usage.

The presence of plasmids with the correct construct was analysed by PCR. Positive colonies were then grown in LB broth (Conda-Ponadisa) overnight at 37ºC, and plasmid DNA was extracted from cells and purified with E.Z.N.A Plasmid DNA Mini Kit (Omega). Sequences were verified by sequencing by Eurofins GATC Biotech Company (Köln, Germany).

RNA extraction

E.Z.N.A. MicroElute Total RNA Kit (OMEGA Bio-Tek) was employed to extract RNA from HEK 293T cell cultures First, 350 µl of TRK Lysis buffer supplemented with 2% of 2-mercaptoethanol was added to a 2-ml Eppendorf tube. The samples were homogenised and mixed with the pipette and transferred into the TRK Lysis buffer-containing tube and vortexed for 30''. Afterwards, the samples were centrifuged for 2' at maximum speed (13,000 x g). The supernatant was transferred to a new tube and 350 µl of 70 ethanol was added. The samples were vortexed, a precipitate was formed and it was transferred into the MicroElute LE RNA Column.

The columns were centrifuged at maximum speed for 15'', and the collecting tube was discarded and replaced with a new one. 500 µl of RWF Wash buffer was added and the samples were centrifuged at maximum speed for 30'' and the filtrate was discarded. 500 µl of RNA Wash Buffer II diluted with 100% ethanol were added and the samples were centrifuged at maximum speed for 30'' and the filtrate was discarded (this step was performed twice). To completely dry the columns, they were centrifuged for 2' at maximum speed. The columns were transferred into 1.5-ml Eppendorf tubes and 15 µl of nuclease-free water was added directly onto the columns. Finally, they were centrifuged at maximum speed for 1' and the obtained material was stored at -70 ºC. All the centrifugations were carried out at room temperature.

RT-PCR

The High Capacity cDNA Reverse Transcription kit (Applied Biosystems) was employed. First, the 2X RT master mix was prepared: 2X RT buffer, 2X dNTP mix, 2X RT Random Primers, 1 µl of RNase inhibitor, 50 U MultiScribe Reverse transcriptase and nuclease-free water to obtain a final volume of 10 µl. 10 µl of RNA was added to the tube and mixed by pipetting up and down. The thermal cycler was set up with the following conditions: 25 ºC for 10', 37ºC for 120' and 85ºC for 5'. Finally, the samples were cooled to 4ºC.

Q-PCR

For the quantitative PCR, the Power SYBR Green PCR master mix was used. (Life Technologies). The employed primers are compiled in **Table 3**.

Table 3. Primer names and sequences of the oligonucleotides employed for the qPCR reactions for the different genes. q: primer for qPCR; F: Forward; R: Reverse

Primer name	Primer sequence
USP16 qF	CTCTGTCGCCGTGGATTG
USP16 qR	GTCCGTTTCTTTCCCATGTTGG
MYSM1 qF	TGTTTGAACAAGGGCTGGC
MYSM1 qR	GGCCGGTCTTCTGATTTGG
Actin qF	CCGCGAGCACAGAGCC
Actin qR	ATCATCCATGGTGAGCTGGC
Tubulin qF	CCCACCGGCACCTACCAC
Tubulin qR	CTGCCCCAGACTGACCAAATAC

For 50-µl reactions, 1X Power SYBR Green PCR master mix, 300 nM of forward primer, 300 nM of reverse primer, 100 ng of template RNA and nuclease-free water were added. The following thermal cycling parameters were employed in the Pharmaceutical Analytics QuantStudio™ 5 Real-Time PCR System: first, a single step at 95ºC for 10' was set for the AmpliTaq Gold Polymerase activation. Second, 40 cycles of 15'' at 95ºC and 1' at 60ºC were performed. A melt curve was generated using the Pharmaceutical Analytics QuantStudio™ 5 Real-Time PCR System software.

Cell Cultures

HEK 293T

Human Embryonic Kidney cells (HEK 293T) are a highly transfectable cell line that contains the SV40 T-antigen. HEK 293T were cultured under standard conditions (37ºC, 5% CO2) using Dulbecco's modified Eagle medium/nutrient mixture F-12 (DMEM/F-12) with GlutaMAX (Thermo Scientific) and supplemented with 10% fetal bovine serum (Thermo Scientific), 100 U/ml of penicillin (Invitrogen) and 100 mg of streptomycin (Invitrogen).

Fly crosses

All *Drosophila* fly lines were grown and mated at 25 ºC in 12-hours light-dark cycles in wheat flour and yeast medium (1% agar (Industrias Roko), 5.5% of dextrose (VWR Chemicals), 3.5% of wheat flour (Carrefour) and 5% of yeast flakes (Ynsadiet) in distilled H_2O. To prevent mould and bacterial growth, 0.25% of Nipagin (Lemmel), 0.4 % of propionic acid (Sigma) and 0.02% of benzalkonium chloride (Sigma) were added to the food mixture when it had cooled down below 60 ºC and before aliquoting into the corresponding plastic bottles (Scientific Laboratory Supplies) and vials (Genesee Scientific).

The eye-specific Glass Multimer Reporter-GAL4 (GMR^{GAL4}; Hay et al., 1994) was used for crossing with the transgenic lines expressing TurboID fused to the protein of interest downstream of the UAS sequence.

GMR^{GAL4};^{UAS}TurboID-Bait/*CyO* stable lines were generated by crossing GMR^{GAL4}/*CyO*; TM4/TM6 flies with ^{UAS}TurboID-Bait/*Cyo* flies. First, the expression of the construct was tested in order to select the best clone. Afterwards, GMR^{GAL4}/^{UAS}TurboID-bait females were crossed with *Bl/CyO* balancer males and flies in which a recombination event had occurred were obtained. Recombinant flies were independently crossed one more time with *Bl/CyO* and flies in the offspring carrying both constructs over the *CyO* chromosome were selected.

Drosophila heads were collected from flies grown at 25 ºC in wheat flour and yeast medium. One to three days-old adult flies were frozen in liquid nitrogen and heads were collected by shaking the frozen flies and using a combination of sieves

with nominal cut-off passages of 710 and 425 µm tie separate their heads from the body. Heads were stored at -80 ºC.

Biotin pulldown

HEK 293T cells and fly heads were homogenized in 2.5 mL of Lysis buffer (8 M urea and 1% SDS in PBS) supplemented with 50 mM N-ethylmaleimide (Sigma) and 400 µL of Lysis Buffer complemented with Complete protease inhibitor cocktail (Roche Applied Science). Whereas HEK 293T cell lysates were obtained by centrifugation at 16,000 x g for 10´at 4ºC, fly heads samples were homogenised with Precellys Evolution (Bertin Instruments) applying 3 cycles of 6,500 rpm for 30''.

In both cases, the supernatants were applied to a PD10 desalting column (GE Healthcare) previously equilibrated with 25 ml of Binding buffer (3 M urea, 1 M NaCl, 0.25% SDS and 50 mM N-ethylmaleimide). Eluates, except 50 µl that were kept for monitoring the inputs, were then incubated with 150 µl of NeutrAvidin agarose beads suspension (Thermo Scientific) for 40' at RT and for 2h and 20' at 4ºC in a roller. Unbound material (flow through) was separated by spinning the beads at 230g for 2'. Beads were then subjected to stringent washes with six different washing buffers (WB): twice with WB1 (8 M urea, 0.25% SDS), thrice with WB2 (6 M guanidine-HCl), once with WB3 (6.4 M urea, 1 M NaCl, 0.2% SDS), thrice with WB4 (4 M urea, 1 M NaCl, 10% isopropanol, 10% ethanol, 0.2%SDS), once with WB1, once with WB5 (8 M urea, 1% SDS) and thrice with WB6 (2% SDS). All buffers, including binding buffer, were prepared in 1X PBS. Beads were then heated at 95ºC for 5' in 80 µl of elution buffer (250 mM Tris–HCl pH 7.5, 40% glycerol, 4% SDS, 0.2% BPB,

100 mM DTT) and centrifuged for 2' at 16,000 x g in a Vivaclear Mini 0.8 mm PES micro-centrifuge filter unit (Sartorius) to recover the eluted proteins.

GFP stringent pulldown

25 µL per sample of GFP-Trap-A beads (Chromotek GmbH) were pre-washed by resuspending in Dilution Buffer (10 mM Tris/Cl pH 7.5, 150 mM NaCl, 0.5 mM EDTA) and centrifugation for 2' at 2,700 x g. This step was repeated 3 times. Cells were washed with 1X PBS and harvested using ice-cold Lysis Buffer (50 mM Tris-HCl pH 7.5, 150 mM NaCl, 1 mM EDTA, 0.5% Triton-X100, 1x Protease inhibitor cocktail (Riche Applied Science), 50 mM NEM). Collected cells were centrifuged for 10' at maximum speed (16,000 x g). 30 µL of the supernatant was kept as "input" fraction for western blot analysis. Then, 450 µL of Dilution Buffer (10 mM Tris-HCl pH 7.5, 150 mM NaCl, 0.5 mM EDTA, 1x Protease inhibitor cocktail, 50 mM NEM) were added to the lysates. The mixture was combined with the previously prewashed GFP beads and incubated for 2h and 30' at room temperature with gentle rolling. After incubation, samples were centrifuged for 2' at 2,700 x g and 30 µL of the supernatant was kept as "flow-through" fraction. Samples were then washed for 5' with 1 ml of the following buffers: once with ice-cold Dilution Buffer, three times with Washing Buffer (8 M urea, 1% SDS in 1x PBS) and once with 1% SDS in 1X PBS. Each washing step required centrifugation of the samples at 2,700 x g for 2' and the supernatant was discarded. After the last centrifugation, samples were centrifuged for an extra time to discard all the supernatant. Beads were then resuspended in 25 µL of Elution Buffer (200 mM Tris HCl, pH 6.8, 8% SDS, 40% glycerol, 0.8 mg/ml bromophenol blue, with the addition of 100 mM dithiothreitol (DTT) prior to use) and heated at 95 ºC for 10'. Afterwards, beads were centrifuged at maximum speed

(16,000 x g) for 2' and the supernatant was transferred into a clean tube ("elution" fraction) (Ramirez et al. 2017).

GFP mild pulldown

25 µL per sample of GFP-Trap-A beads (Chromotek GmbH) were prewashed by resuspending in Dilution Buffer, followed by centrifugation for 5' at 2,500 x g. Cells were washed with 1X PBS and harvested using ice-cold soft Lysis Buffer (10 mM Tris-HCl pH 7.5, 150 mM NaCl, 0.5 mM EDTA, 0.5% Igepal CA-630 (Sigma-Aldrich), 1x Protease inhibitor cocktail (Roche Applied Science), 50 mM NEM). The cell suspension on the lysis buffer was incubated on ice for 30', pipetting every 10'. Collected cells were centrifuged for 10' at maximum speed (16,000 x g). 50 µL of the supernatant was kept as "input" fraction for western blot analysis. Then, 300 µL of Dilution Buffer (10 mM Tris-HCl pH 7.5, 150 mM NaCl, 0.5 mM EDTA, 1x Protease inhibitor cocktail, 50 mM NEM) was added to the lysates. The mixture was combined with previously prewashed GFP beads and incubated for 1h at 4ºC with gentle rolling. After incubation, samples were centrifuged for 5' at 2,500 x g and 50 µL of the supernatant was kept as "flow-through" fraction. Samples were then washed three times with Washing buffer (10 mM Tris/Cl pH 7.5, 150 mM NaCl, 0.5 mM EDTA, 0.05% Nonidet P40 substitute), centrifuged for 5' at 2,500 x g and the supernatant discarded. Beads were resuspended in 30 µL of Elution Buffer (120 mM Tris HCl, pH 6.8, 4% SDS, 20% glycerol, 0.04 % bromophenol blue, with the addition of 10% β-mercaptoethanol prior to use) and heated at 95 ºC for 10'. Afterwards, beads were centrifuged at 2,500 x g for 5' and the supernatant was transferred into a clean tube ("elution" fraction). All the steps were performed at 4ºC.

Western blot and silver staining

Both 4–12% Bolt Bis–Tris Plus pre-cast gels (Invitrogen) and 4–12% NuPAGE Bis–Tris gels (Invitrogen) were used to fractionate proteins by SDS-PAGE. Then, proteins were transferred to PVDF membranes using the iBlot system (Invitrogen). Following primary and secondary antibody incubation, membranes were developed with an ECL kit (Biorad Clarity).

The antibodies that were employed for western blot analyses are summarised in **Table 4** and **Table 5.**

Table 4. Primary antibodies employed for western blot and immunocytochemistry. The employed dilution for the different assays is represented and the commercial house with the correspondent reference too. WB: Western Blot.

Antibody Name	Dilution for WB	Commercial House (reference)
Goat anti-biotin-HRP-conjugated	1:1000	Cell Signalling (#7075)
Chicken anti-BioID2	1:1000	BioFront Technologies (BID2-CP-100)
Mouse anti-myc tag	1:1000	Cell Signalling (2276)
Rabbit anti-NCDN	1:1000	Sigma (HPA023676)
Mouse anti-E6AP/UBE3A	1:1000	Sigma (E8655)
Mouse anti-Flag-M2-HRP conjugated	1:1000	Sigma (A8592)
Mouse anti-tubulin-beta-E7-c	1:1000	Developmental Studies Hybridoma Bank (# AB_2315513)
Mouse anti-GFP	1:1000	Roche Applied Science (# 11814460001)
Rabbit anti-GFP	1:1000	Santa Cruz Biotechnology (# sc 8334)
Mouse anti-HA tag	1:1000	Sigma (H3663)
Rabbit anti-phospho-CaMKII (T286)	1:1000	Cell Siganalling (12716)

For silver staining, gels were fixed for 1h at room temperature with 40% methanol and 10% acetic acid-containing solution, and then, stained using the SilverQuest kit from Invitrogen according to the manufacturer's instructions.

Table 5. Secondary antibodies employed for western blot and immunocytochemistry. The employed dilution for the different assays is represented and the commercial house with the correspondent reference too. WB: Western Blot.

Antibody	Dilution for WB	Commercial House
Donkey anti-chicken-HRP labelled	1:4000	Jackson ImmunoResearch (703-035-155)
Goat anti-rabbit HRP conjugated	1:4000	Jackson ImmunoResearch (111-035-144)
Alexa Fluor 488 goat anti-chicken	1:4000	ThermoFisher Scientific (A11039)
Alexa Fluor 488 Goat anti-rabbit	1:4000	ThermoFisher Scientific (A21441)
Rabbit anti-mouse HRP conjugated	1:4000	ThermoFisher Scientific (A27025)
Alexa Fluor plus 488 Goat anti-mouse	1:4000	ThermoFisher Scientific (A32723)
Alexa Fluor plus 647 Goat anti-mouse	1:4000	ThermoFisher Scientific (A32728)
Alexa Fluor plus 647 Chicken anti-mouse	1:4000	ThermoFisher Scientific (A21463)
IRDye 800 CW Goat anti-mouse	1:4000	Li-cor (926-32210)

Sample preparation and LC-MS/MS

40% and 50% of the eluates obtained from HEK 293T cells and *D. melanogaster* respectively, were run in 4-12% NuPAGE Bis-Tris gels (Invitrogen) and visualised with Coomassie blue staining following manufacturers' instructions. Then, each gel lane was cut into 3 slices (HEK 293T experiments) or 2 slices (fly experiments) which were further chopped before proteins of interest were subjected to in-gel digestion using trypsin as described before (Osinalde et al., 2015). Briefly, gel pieces, previously dehydrated with acetonitrile (ACN), were reduced with 10 mM dithiothreitol (DTT) at RT, alkylated with 55 mM chloroacetamide at 56 ºC, and finally rehydrated in 12.5 ng/ml trypsin and incubated overnight at 37 ºC. The following day, the resulting tryptic peptides were extracted from the gel by serial incubation with 100% ACN and 1% trifluoroacetic acid in 30% ACN. Finally, prior to MS analysis, peptide solutions were dried down in a SpeedVac centrifuge (Thermo Scientific).

Mass spectrometric analyses were performed on an EASY-nLC 1200 liquid chromatography system interfaced with a Q Exactive HF-X mass spectrometer

(Thermo Scientific) via a nanospray flex ion source. Peptides were loaded onto an Acclaim PepMap100 pre-column (75 µm x 2 cm, Thermo Scientific) connected to an Acclaim PepMap RSLC (50 µm x 25 cm, Thermo Scientific) analytical column. Peptides were eluted from the column using a linear gradient of 2% to 32% acetonitrile in 0.1% formic acid at a flow rate of 300 nL min-1 over 120 minutes. The mass spectrometer was operated in positive ion mode. Full MS scans were acquired from m/z 375 to 1800 with a resolution of 60.000 (m/z 200). The 10 most intense ions were fragmented by higher energy C-trap dissociation with a normalized collision energy of 28 and MS/MS spectra were recorded with a resolution of 15000 (m/z 200). The maximum ion injection time was 50 ms for survey scan and 100 ms for MS/MS scans, whereas AGC target values of 3×10^6 and 3×10^5 were used. In order to avoid repeat sequencing of peptides, dynamic exclusion was applied for 20''. Singly charged ions or ions with unassigned charge states were also excluded from MS/MS. Data were acquired using Xcalibur software (Thermo Scientific).

Data processing and bioinformatics analysis

All mass spectrometric raw data have been processed with the MaxQuant software (version 1.6.0.16) using the internal search engine Andromeda. The raw files acquired in the BioID2 and NCDN experiments were searched against the UniProtKB *Homo sapiens* database (released 2017_11; 42257 entries and released 2021_08; 42392 entries, respectively) in which BioID2 and avidin sequences were manually added, whereas TurboID experiment data was searched against the UniProtKB *Drosophila melanogaster* database (released 2021_07; 44230 entries) where TurboID and avidin sequences were manually added.

In all experiments, spectra originated from the different slices corresponding to the same biological sample were combined. Carbamidomethylation (C) was set as fixed modification, whereas Met oxidation and protein N-terminal acetylation were defined as variable modifications. For the NCDN experiment, the variable modifications GlyGly (K), GlyGly (N-term), LRGG (K) and LRGG (N-term) were selected as well.

Mass tolerance was set to 8 and 20 ppm at the MS and MS/MS level, respectively. Enzyme specificity was set to trypsin, allowing for a maximum of two missed cleavages. Match between runs option was enabled with a 1.5 min match time window and a 20 min alignment window to match identification across samples. The minimum peptide length was set to seven amino acids. The false discovery rate for peptides and proteins was set to 1%. Normalized spectral protein label-free quantification (LFQ) intensities were calculated using the MaxLFQ algorithm.

MaxQuant output data was analysed with the Perseus module (version 1.6.6.0) (Tyanova et al. 2016). Initially, proteins only identified by site, contaminants, reverse hits and proteins with no unique peptides and/or no intensity were discarded. Missing LFQ intensity values were replaced with values from a normal distribution (width 0.3 and downshift 1.8), meant to simulate expression below the detection limit (Tyanova et al. 2016). To determine statistically significant changes in protein abundance, as well as in ubiquitin diGly peptides, a two-tailed Student's t-test was used.

A volcano plot is a type of scatterplot that represents the p-value against the fold change (W. Li et al. 2014). Thus, on the right side of the volcano will appear those proteins that are more enriched in a given sample. Moreover, the statistical significance is given by the p-value. All of the volcanos were generated with Prism (Graphpad software). Box plots and frequency histograms were also generated with Prism. The Venn diagrams were generated with eulerAPE v3 (Micallef and Rodgers 2014) and BioVenn (https://www.biovenn.nl/index.php) (Hulsen, de Vlieg, and Alkema 2008).

The bioinformatic tool DAVID was employed for the gene ontology analysis (https://david.ncifcrf.gov/tools.jsp). DAVID performs functional annotation of large lists of genes. We have used the GO_Fat category in all cases as it allows us to use a subset of the more specific terms represented. Moreover, the minimum number of hits was modified for the different analyses to get rid of non-specific results (Huang, Sherman, and Lempicki 2008, 2009).

The bioinformatic database STRING v11 was employed to generate a map of the known interactions between our proteins (Szklarczyk et al. 2019). The aim of this database is to collect, score and integrate all the publicly available information about protein-protein interactions. Moreover, the data is complemented with computational predictions. String extracts experimental data from BIND, DUP, GRIP, HPRD, IntAct, MINT and PID; and extracts curated data from Biocarta, BioCyc, GO, KEGG, and Reactome. The analysis provides different stats: the *average node degree* indicates the number of interactions that the proteins have on average in the network. The *clustering coefficient* measures the level of connection of the nodes in the network. Thus, highly connected networks have high values. The *expected*

number of edges indicates the expected edges in a random selection of nodes. The *PPI enrichment p-value* measures the significance of the number of edges. A small PPI enrichment p-value indicates that the nodes are not random and that the observed number of edges is significant. A random list of proteins was generated with the Random Gene Set Generator (http://molbiotools.com/randomgenesetgenerator.html).

Statistical Analyses

Results are expressed as the SEM mean of the number of independent experiments. The number of replicas performed in each case is specified. Differences were analysed using a two-tailed Student's t-test with a level of significance set at $p<0.05$.

The symbols used are: "*" for $p<0.05$; "**" for $p<0.01$; and "***" for $p<0.001$. No symbol was employed for no significant results.

CHAPTER I

Deciphering the interactome of CaMKII in HEK 293T cells by proximity labelling with BioID2

Summary

A number of evidence suggest there is a link between UBE3A, the E3 ubiquitin ligase absent in brains of Angelman syndrome patients, and CaMKII which is known to be ubiquitinated but neither the E3 ligase nor the DUB responsible for its ubiquitination and deubiquitination respectively, are known. Consequently, we have followed a cell-culture-based strategy in order to identify the best conditions to apply the BioID2 system and search for potential CaMKIIa interactors in HEK 293T cells. Rat CaMKIIa full length (wild type and I206K), C terminal and N terminal sections were fused to BioID2 and overexpressed in HEK 293T cells. Biotinylated proteins were purified by biotin pulldown employing streptavidin beads and subsequently analysed by mass spectrometry. Discovered interactions were validated through coimmunoprecipitation followed by western blot analysis. Moreover, identified E3 ubiquitin ligases and DUBs were tested as possible enzymes involved in CaMKIIa ubiquitination and deubiquitination, respectively. Additionally, changes in CaMKIIa phosphorylation were studied. We uncover that silencing the DUB MYSM1 reduces CaMKIIa ubiquitination levels and enhances phosphorylation at T286. By contrast, the E3 ubiquitin ligase ITCH promotes CaMKIIa monoubiquitination and decreases CaMKIIa pT286 levels.

Introduction

Angelman syndrome (AS) is a complex and rare (1/20,000) genetic disorder that primarily affects the nervous system. Characteristic features of this condition include delayed development, intellectual disability, severe speech impairment, and problems with movement and balance (ataxia). Patients with AS show mutations at

the 15q11-13 affecting the UBE3A gene and diminishing the amount of the protein (Kishino, Lalande, and Wagstaff 1997; Matsuura et al. 1997). The UBE3A gene encodes an E3 ubiquitin ligase, an enzyme that functions during the ubiquitination pathway attaching ubiquitin to its substrates (Pickart and Eddins 2004). UBE3A is localised in the nucleus and the pre- and post-synaptic compartments (Dindot et al. 2008).

Calmodulin-dependent kinase II subunit alpha (CaMKIIa) plays a crucial role in the molecular mechanisms of memory formation including long-term potentiation (LTP). Indeed, when LTP is induced, CaMKIIa translocates to the spine head of dendrites and phosphorylates AMPA receptors and the protein stargazin, which are directly involved in LTP regulation (Y.-P. Zhang, Holbro, and Oertner 2008; Poncer, Esteban, and Malinow 2002; Tomita et al. 2005). Moreover, CaMKIIa is associated with proteasomes in the brain; whereas CaMKII autophosphorylation promotes proteasome recruitment to spines, CaMKIIa-mediated phosphorylation of Rpt6 on Ser120 stimulates proteasome activity (Bingol et al. 2010). Many studies link the function of CaMKIIa with AS. Mice models for AS that lack UBE3A (Ube3a $^{m-/p+}$) show a deficit in LTP, whereas AS models expressing a truncated version of CaMKIIa that cannot be phosphorylated at T305/306 exhibit a normal LTP (Van Woerden et al., 2007). Besides, this AS mouse model exhibits enhanced CaMKIIa phosphorylation (Weeber et al. 2003). Recent studies have revealed a possible crosstalk between the HUN complex (HERC2, UBE3A and NEURL4) and CaMKII (Martínez-Noël et al. 2018). Moreover, it was shown that ASPP2, an inhibitor of the CaMKII phosphatase PP1, is degraded as a consequence of UBE3A-mediated ubiquitination. Thereby, it was hypothesised that lack of UBE3A triggers the

accumulation of ASPP2, and, thereby, PP1 is inhibited and does not dephosphorylate CaMKII. Consequently, the levels of phosphorylated CaMKII are increased (Martínez-Noël et al. 2018). Finally, CaMKII is subjected to ubiquitination (Udeshi et al. 2013; Povlsen et al. 2012; W. Kim et al. 2011; Ramirez et al. 2018); however, the E3 responsible for its ubiquitination remains unknown. Therefore, taking into account all the information above, we considered that CaMKIIa might be a substrate of UBE3A or that there is an intermediate pathway that links the two proteins. To test our hypothesis, we aimed to identify potential CaMKIIa interactors using the BioID2 system.

Hypothesis and objectives

There is indirect evidence that links CaMKIIa with UBE3A. Moreover, it is known that CaMKIIa can be ubiquitinated, although the E3 ubiquitin ligase responsible remains elusive. We hypothesize that CaMKIIa might interact with UBE3A or other proteins involved in the ubiquitin-proteasome pathway which would allow us to have a better understanding of its role in AS. For that purpose, we have studied the interactome of CaMKIIa in HEK 293T cells.

In order to shed light on the relationship between CaMKII and UBE3A, five main objectives are defined in this section of the thesis:

- Determine the best conditions and reproducibility of the BioID2 system for future studies of CaMKII in neuronal tissue
- Identify potential CaMKIIa interactors in HEK 293T cells.

- Validate detected CaMKII binding candidates through coimmunoprecipitation experiments.
- Identify the DUB enzyme(s) responsible for CaMKII's deubiquitination.
- Identify the E3 ubiquitin ligase(s) responsible for CaMKII's ubiquitination.

Results

BioID2 combined with LC-MS/MS to uncover CaMKII binding proteins

BioID2 is a promiscuous biotin ligase that can biotinylate any protein that is in close proximity to the protein of interest that is fused to. It is possible to ensure the biotinylation range of BioID2 towards any interactor of its fused protein by adding a flexible linker (D. I. Kim et al. 2016; Roux et al. 2012). Therefore, BioID2 was fused to CaMKIIa through a $(GSGS)_n$ (where n went from 0 to 3) linker to increase the flexibility of the fusion protein and allow the biotinylation of all its potential interactors. We observed $(GSGS)_3$ linker showed higher biotinylation levels and, thereby, we selected it for the following studies. (**Figure S1**)

In order to investigate the interactome of CaMKII four different constructs were created: BioID2-CaMKIIa FL (full length, FL), BioID2-CaMKIIa I206K (mutant, MUT), BioID2-CaMKIIa 266-479 (C terminal, CTER) and CaMKIIa 1-266-BioID2 (N terminal, NTER). CTER and NTER were used as controls that should allow us to differentiate between contaminants and real interactors of CaMKIIa. Moreover, they would serve to determine whether a potential interactor associates with the N- or the C-terminal region of CaMKIIa. Therefore, screening the interactome of FL, NTER and CTER CaMKII enables us not only to discern between contaminants and putative

interactors but also to determine if the interactor associates with the N terminal region, the C terminal region or the whole protein. In brief, if a protein is more enriched in the FL sample than in both controls, it will be considered a FL interactor, meaning that it needs the whole protein to interact with the kinase. By contrast, if a protein is more enriched, for example, in the FL and in the CTER with respect to the NTER sample, it will be considered an interactor of C-terminal CaMKIIa. Similarly, a protein associating with N-terminal CaMKIIa should be more enriched in FL and NTER samples in comparison to CTER. Finally, proteins detected with similar abundance in the three samples would be considered contaminants or BioID2 interactors (**Figure 16**).

The interactome of CaMKIIa I206K mutant was also investigated. I206 is located at the T-site of CaMKIIa and is crucial for the translocation of the kinase into the post-synaptic density. In this context, as we are using HEK 293T cells, this mutant would have little impact; however, we wanted to test it for future experiments. Once we ensured that the four constructs were expressed correctly and that they promote biotinylation in our conditions, HEK 293T cells were transfected separately with each of the four constructs mentioned above (3 replicas each) and the medium was supplemented with 50 µM biotin. 24 hours after transfection, cells were harvested and biotinylated proteins were isolated using avidin.

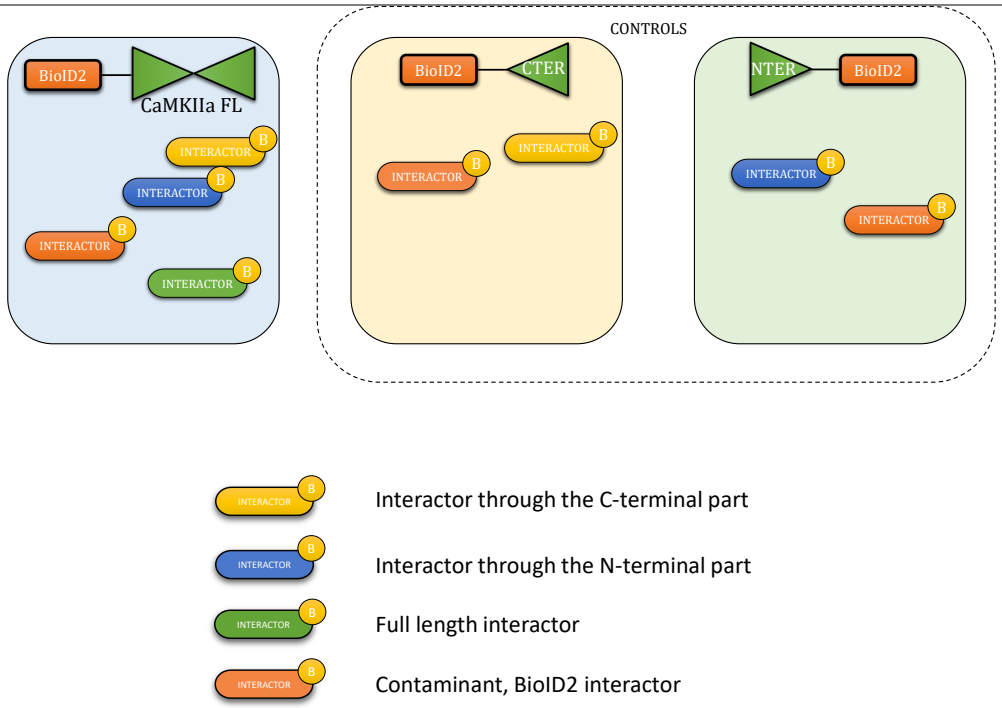

Figure 16. Representation of the expected BioID2 results. Three constructs have been employed to look for CaMKIIa interactors: BioID2-CaMKIIa FL, BioID2-CaMKIIa C-TER and CaMKIIa N-TER-BioID2. Interactors will be biotinylated and enriched through biotin pull-down. This strategy will allow to distinguish full-length interactors, one-side interactors and contaminants.

The elution and the input fraction were analysed by western blot (**Figure 17A**). The BioID2 signal was comparable in all conditions when monitored either by autobiotinylation (most intense bands in the upper panel in **Figure 17A**) or by anti-BioID2 antibody (lower panel in **Figure 17A**). Additionally, we observed that FL, MUT and CTER samples exhibited similar levels of biotinylated material in the inputs. However, the NTER sample showed a lower biotin signal indicating that fewer proteins were being biotinylated by the NTER construct. Similar results were observed in the eluted fractions: whereas all samples displayed similar autobiotinylation levels of the overexpressed constructs, the remaining biotin signal was much weaker in the NTER sample indicating it was less biotinylated.

Since western blot signals are not necessarily quantitative, to better assess the total amount of protein present in each sample and ensure there is enough material for subsequent mass spectrometry analysis, a small portion of the elution (around 7% of each sample) was also analysed by silver staining (**Figure 17B**).

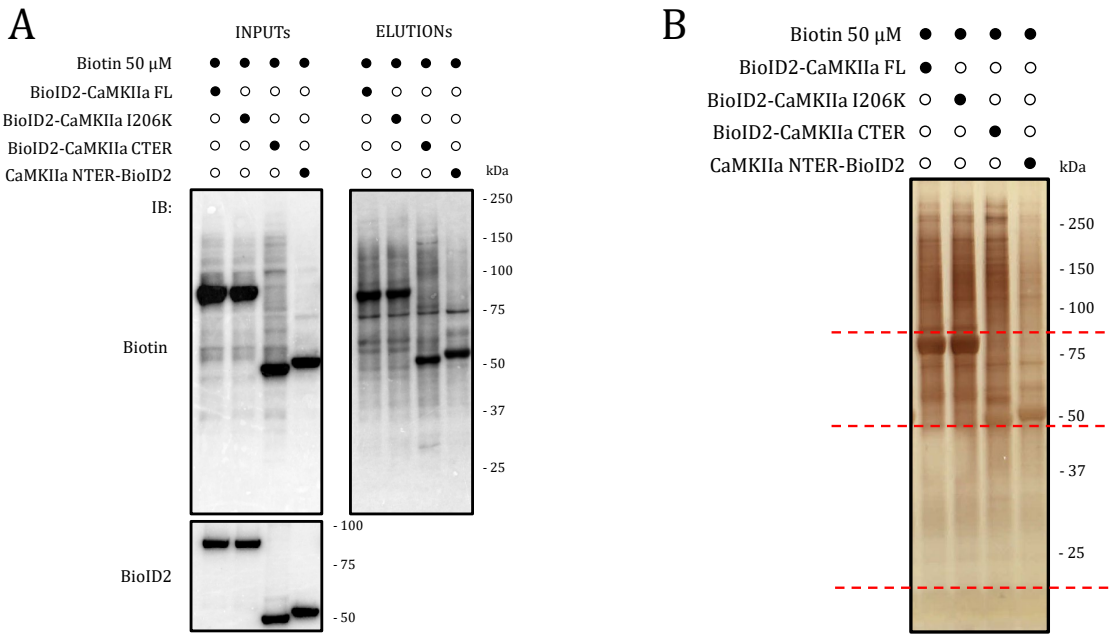

Figure 17. Efficient biotinylation by BioID2 fused to the different versions of CaMKIIa. We expressed BioID2-CaMKIIa FL, BioID2-CaMKIIa I206K, BioID2-CaMKIIa CTER and CaMKIIa NTER-BioID2 in HEK 293T and we supplemented the media with biotin (50 µM). The biotinylated material was enriched with purification with neutravidin beads. A) Input and eluted fraction were tested by western blot for biotin. Construct expression was tested with BioID2 (left bottom). B) Silver staining of 7% of the eluted fraction to ensure enough material is available for subsequent mass spectrometry analysis. The red discontinuous lines indicate the sites were the commassie gel was cut afterwards.

Fractionation and processing of enriched biotinylated proteins prior to LC-MS/MS analysis

Once verified there was enough material for mass spectrometry-based protein detection, 50% of the elutions were loaded in a gel and stained with coomassie blue. Each lane was cut into three slices: one slice contained the section from the avidin monomer to CTER and NTER band height (around 25 kDa - 40 kDa). The second slice included the section of the four constructs (40 kDa – 80 kDa) and the third slice contained the material localised above the 80 kDa band (**Figure 17B** showed with red lines). All gel pieces were subjected to in-gel protein digestion by Jabier Beaskoetxea. In brief, proteins were reduced with DTT, alkylated with chloroacetamide and digested with trypsin. Finally, the resulting peptides were extracted from the gel and mass spectrometric analyses were performed on an EASY-nLC 1200 liquid chromatography system interfaced with a Q Exactive HF-X mass spectrometer (Thermo Scientific) via a nanospray flex ion source in the Proteomics Core Facility of the UPV/EHU (SGIker).

Protein identification and label-free quantitation by LC-MS/MS

The mass spectrometric raw data were processed with the MaxQuant software using a label-free intensity-based approach. First, contaminants and reverse hits were removed. Additionally, proteins only identified by site and displaying no intensity were also discarded. Besides that, we only considered proteins detected with at least two peptides, including at least one unique peptide. Following these criteria, we detected hundreds of proteins in the distinct replicas of FL, CTER, NTER and MUT samples.

We checked the reproducibility of the experiment by measuring the overlapping of the proteins detected in distinct replicas of the same experimental condition and concluded that, in general terms, the reproducibility was very high (**Figure 18A**). We also analysed the average Log_2 LFQ intensity of the proteins identified in 1, 2 or the 3 replicas of each experimental condition. As shown in **Figure 18B**, proteins detected in all the replicas tend to be more abundant, and hence, have higher Log_2 LFQ intensities than those appearing in only 1 or 2 replicas.

We also compared the proteins detected in the different experimental conditions. For that purpose, we considered all proteins detected in all the replicas of each sample. As shown in **Figure 19A**, FL and MUT samples share more than 97% of the proteins detected, suggesting that CaMKII I260K mutant does not greatly alter CaMKII's structure but only affects some specific interactions. Similarly, the overlapping between proteins detected in FL, CTER and NTER samples is very high (**Figure 19B**), which was quite surprising as western blot and silver staining results suggested the amount of biotinylated material for the NTER sample was lower compared to the other samples (**Figure 17A and B**). In brief, 2850 proteins were detected in the three conditions. Additionally, 287 proteins were exclusively shared by FL and CTER, 181 by CTER and NTER, and 35 by FL and NTER. Finally, 44, 193 and 30 unique proteins were detected in FL, CTER and NTER samples, respectively.

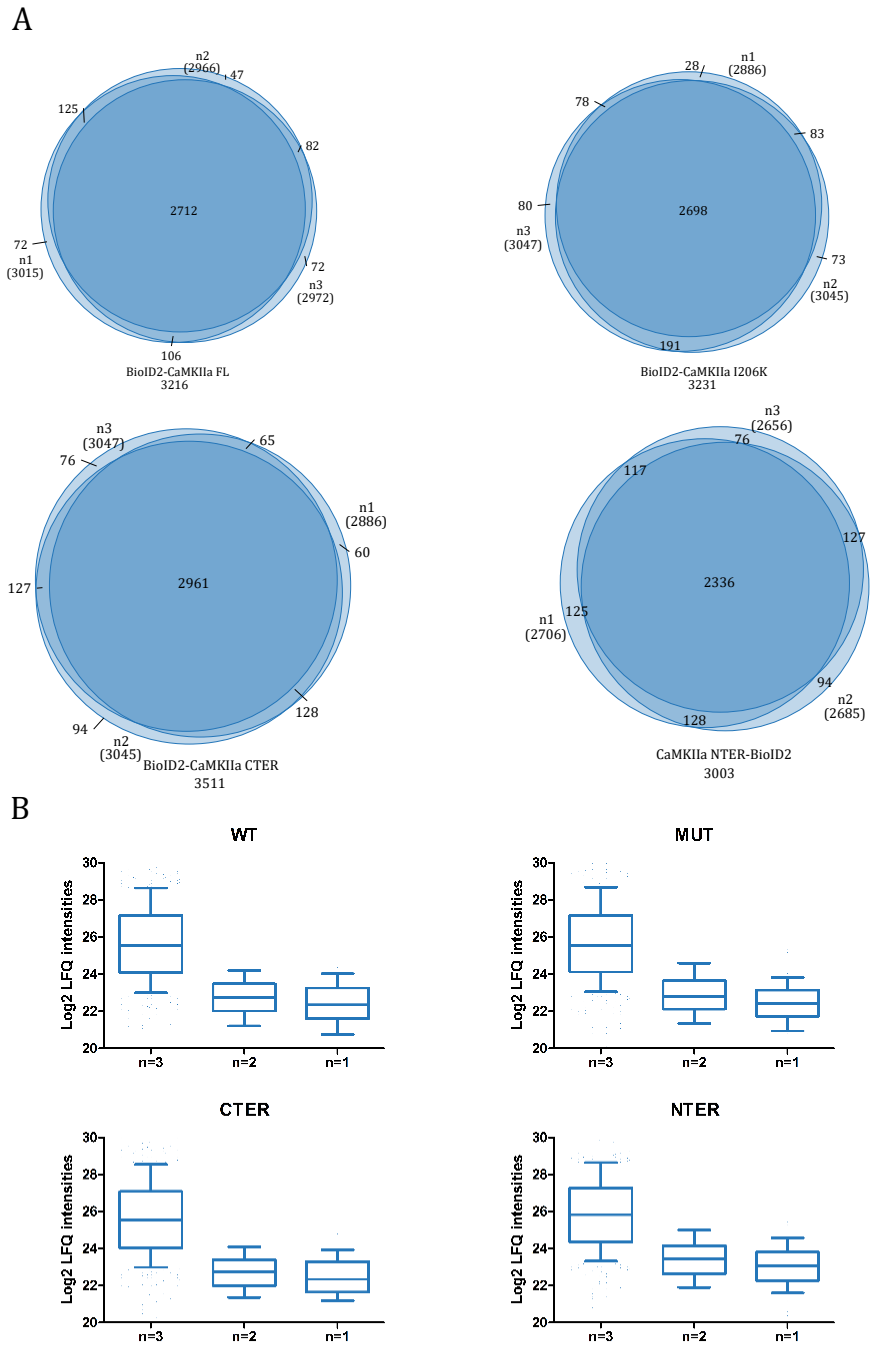

Figure 18. High reproducibility between distinct replicas of the same BioID2 experiment.

A) Venn diagrams showing the overlapping of the identified proteins in the three replicas of the same experimental condition. Between brackets the total number of identified proteins is shown.

B) Box plots showing the LFQ intensities of proteins that appeared either in 1, 2 or 3 of the replicas.

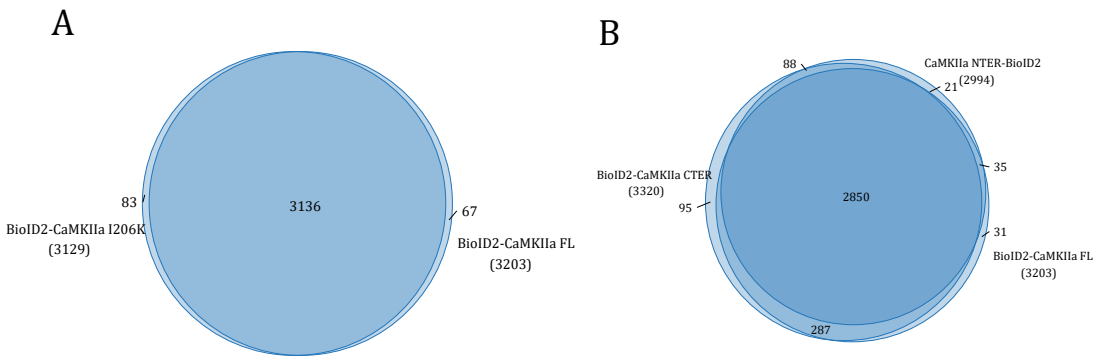

Figure 19. Overlapping between distinct BIoID2 experimental conditions. A) Venn diagram showing the common and unique proteins between WT and I206K constructs. Between brackets the total number of identified proteins is shown. B) Venn diagram showing the common and unique proteins between WT, N-TER and C-TER constructs. Between brackets the total number of identified proteins is shown.

We also assessed the reproducibility of the experiment by comparing the LFQ intensity of the proteins present in the different replicas using Perseus (**Figure 20A**). On average, the Pearson correlation within the replicas of NTER, CTER, FL and MUT samples is 0.933, 0.956, 0.959 and 0.961 respectively, indicating the reproducibility between replicas is high. Moreover, the similarity between FL and MUT is also high (0.959 on average), whereas the similarity between NTER and CTER samples is much lower (0.827 on average).

Afterwards, data was imputed following a normal distribution so that an intensity value was assigned to the proteins that were not detected or quantified in a given sample. As shown in **Figure 20B**, recorded mass spectrometric data follow a normal distribution (in green) and missing values were replaced by LFQ values at the lowest detection range (in red). Overall, the amount of imputed values is rather small. Nevertheless, and in line with western blot and silver staining results, as protein biotinylation in the NTER sample was not as abundant as in the rest of the

conditions, comparatively NTER sample contains a larger number of imputed values (**Figure 20B**).

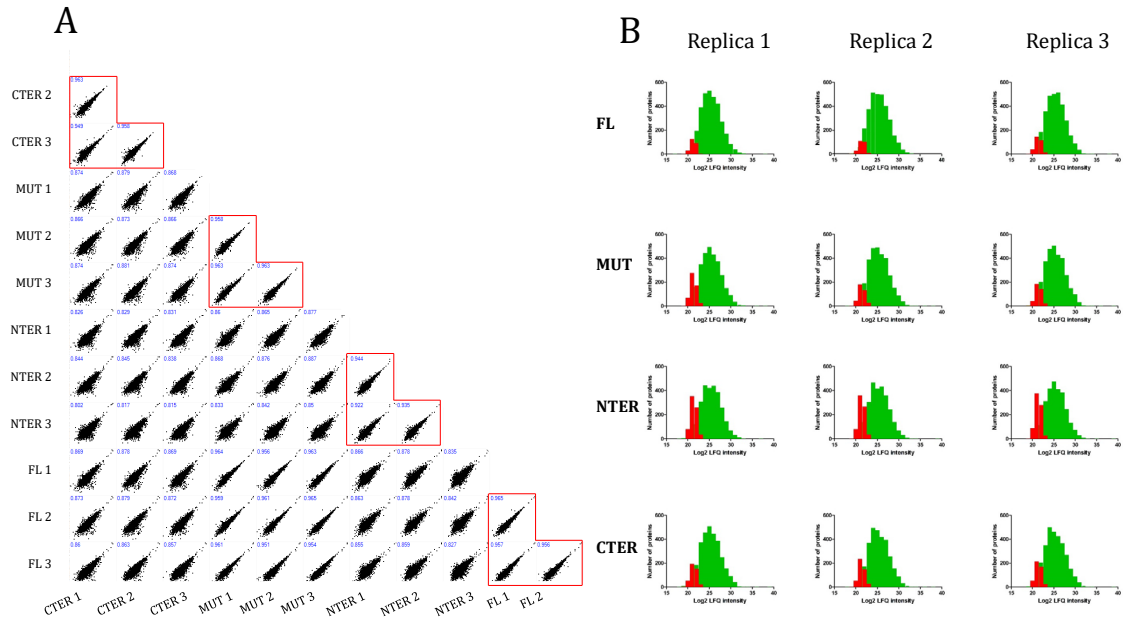

Figure 20. Correlation between replicas and distribution of the LFQs. A) Multi-scatter plot showing the correlation between replicas. The red squares define the correlation between replicas of the same sample. B) Frequency histograms showing the number of proteins with a given LFQ intensity (green). In red, imputed LFQ intensities.

Finally, we searched for statistically significant quantitative changes between the FL, CTER and NTER samples to look for potential CaMKII interactors. We performed several two-sample t-test analyses and represented the results in a volcano plot, a type of scatterplot that shows statistical significance (p-value) against the magnitude of change (fold change) (W. Li et al. 2014). As internal controls of the experiment, we checked the ratio of BioID2, avidin, and endogenously biotinylated carboxylases (Acetyl-CoA carboxylase, pyruvate carboxylase and methylcrotonoyl-CoA carboxylase) which should be around 1 (log2

ratio 0) if overexpression, purification efficiency and amount of biological material, respectively, were kept constant across experimental conditions.

With three comparisons (FL vs CTER; FL vs NTER; CTER vs NTER) we were able to discern between contaminants, N-terminal and C-terminal CaMKII interactors as well as proteins interacting with the whole protein kinase (**Figure 21**).

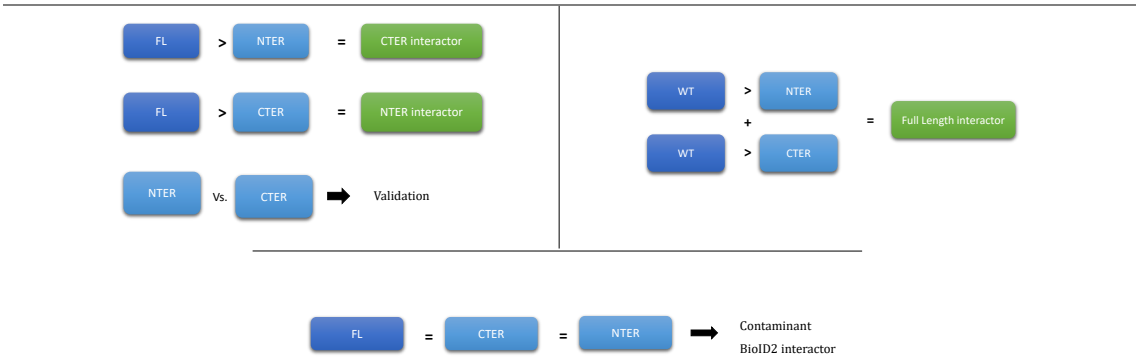

Figure 21. Scheme of the conditions for the proteins to be considered as either a CTER, NTER or FL interactor. Comparing the protein ratios obtained in the different comparisons (FL vs CTER; FL vs NTER; CTER vs NTER) we can discern between contaminants or BioID2 interactors as well as FL, NTER and CTER CaMKII interactors.

In brief, we compared the FL sample against the CTER to search for N-terminal CaMKII interactors (**Figure 22A**). Similarly, the FL sample was compared against NTER to uncover proteins binding to C-terminal CaMKII (**Figure 22B**). Moreover, N-terminal, as well as C-terminal CaMKII interactors, were validated by comparing the NTER against the CTER sample (**Figure S2**). As mentioned before, proteins that were enriched in the FL sample in both comparisons (vs. NTER and vs. CTER) were considered proteins that require the whole kinase in order to interact with it. Finally, proteins that were equally enriched in all samples were considered contaminants or BioID2 binding proteins.

A

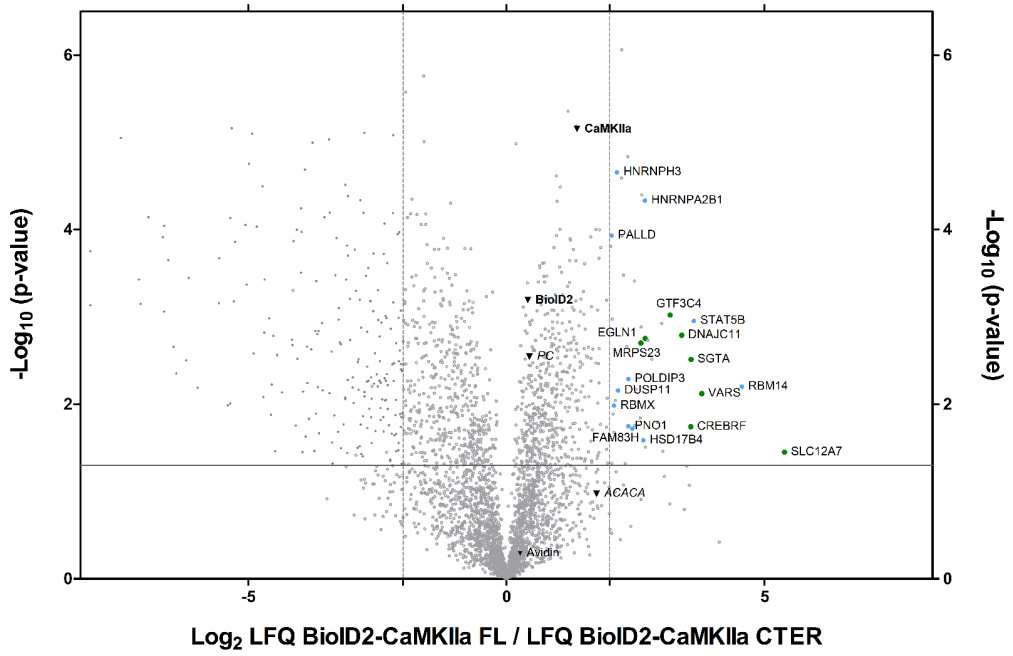
-Log10 (p-value)
-Log10 (p-value)
CaMKIIa
HNRNPH3
HNRNPA2B1
PALLD
BioID2
GTF3C4
STAT5B
EGLN1
DNAJC11
PC
MRPS23
SGTA
POLDIP3
DUSP11
VARS
RBM14
RBMX
PNO1
CREBRF
FAM83H
HSD17B4
SLC12A7
ACACA
Avidin
Log2 LFQ BioID2-CaMKIIa FL / LFQ BioID2-CaMKIIa CTER

B

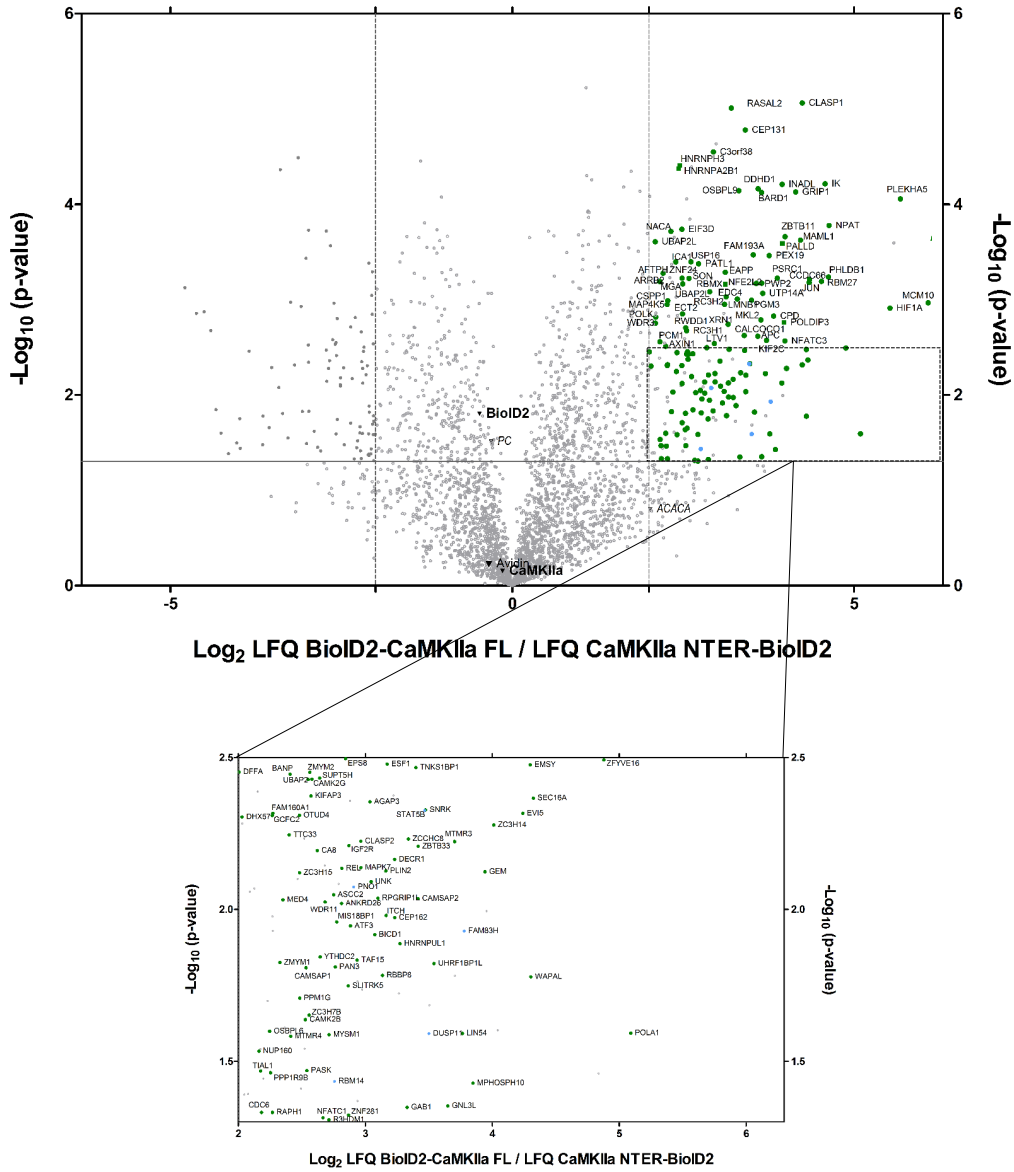
-Log10 (p-value)
-Log10 (p-value)
BioID2
PC
ACACA
Avidin
CaMKIIa
Log2 LFQ BioID2-CaMKIIa FL / LFQ CaMKIIa NTER-BioID2
-Log10 (p-value)
-Log10 (p-value)
Log2 LFQ BioID2-CaMKIIa FL / LFQ CaMKIIa NTER-BioID2

Figure 22. Interactome of full length, C terminal and N terminal CaMKII. A volcano plot in which the Log_{10} of the p-value is represented against fold change between samples. BioID2, avidin and endogenously biotinylated carboxylases (PC: Pyruvate carboxylase, ACACA: Acetyl-CoA Carboxylase) that are considered as controls are also highlighted. A) Proteins on the right square are more enriched in the FL-CaMKII expressing sample in respect to the CTER-CaMKII expressing sample. Only proteins displaying a LFQ fold change bigger than 4 with a P-value smaller than 0.05 were considered as candidate binding proteins. Putative N-terminal CaMKII interactors are shown with a green circle and full-length interactors with a blue circle. B) Proteins on the right square are more enriched in the FL-CaMKII expressing sample in respect to the NTER-CaMKII expressing sample. Only proteins displaying a LFQ fold change bigger than 4 with a P-value smaller than 0.05 were considered as candidate binding proteins. Putative C-terminal CaMKII interactors are shown with a green circle and full-length interactors with a blue circle.

Proteins should fulfill the following criteria to be considered as CaMKII interactors: (i) be identified in all replicas of one of the conditions or at least in 2 replicas of both conditions, (ii) display a statistical significance p-value<0,05 ($-\log_{10}$ p-value>1,3) and (iii) display a fold change greater than 4 ($-2 > \log_2$ fold change >2).

Following the criteria mentioned above, we detected 19 and 144 proteins that were significantly enriched in the FL sample with respect to the CTER and NTER samples, respectively. Of those, 12 proteins were enriched in both comparisons, and hence, were considered as putative CaMKII binding proteins that associate with the whole protein kinase (**Table 6**). Consequently, the remaining 7 (**Table 7**) and 132 (**Table 8**) proteins could be considered candidate binding proteins for N-terminal and C-terminal CaMKII, respectively.

Table 6. Putative N-terminal CaMKIIa binding proteins. The protein name in UniProt and their full name. LFQ ratio: fold change between samples. P-value: statistical significance.

		FL vs CTER		FL vs NTER		CTER vs NTER		
Protein	**Full name**	**LFQ ratio**	**p-value**	**LFQ ratio**	**p-value**	**LFQ ratio**	**p-value**	**Peptide (unique**
SLC12A7	Solute carrier family 12 member 7	5,38	1,45	-2,34	0,82	-7,73	2,63	5 (5)
VARS	Valine--tRNA ligase	3,78	2,12	-0,39	1,07	-4,17	2,31	13 (13)
SGTA	Small glutamine-rich tetratricopeptide repeat-containing protein alpha	3,57	2,51	-0,65	0,34	-4,22	2,58	3 (3)
DNAJC11	DnaJ homolog subfamily C member 11	3,39	2,79	0,97	0,98	-2,43	2,51	2 (2)
GTF3C4	General transcription factor 3C polypeptide 4	3,17	3,02	0,22	0,43	-2,94	2,68	8 (8)
MRPS23	28S ribosomal protein S23, mitochondrial	2,69	2,75	0,04	0,04	-2,65	5,26	8 (8)
EGLN1	Egl nine homolog 1	2,60	2,70	-1,4	0,81	-4	2,25	9 (9)

Table 7. Putative C-terminal CaMKIIa binding proteins. The protein name in UniProt and their full name. LFQ ratio: fold change calculated between samples. P-value: statistical significance.

		FL vs NTER		FL vs CTER		CTER vs NTER		
Protein	**Full name**	**LFQ ratio**	**p-value**	**LFQ ratio**	**p-value**	**LFQ ratio**	**p-value**	**Peptides (Unique)**
MCM10	Protein MCM10 homolog	6,08	2,97	-0,80	2,45	6,88	3,19	21 (21)
PLEKHA5	Pleckstrin homology domain-containing family A member 5	5,68	4,06	1,28	2,13	4,40	3,27	30 (30)
HIF1A	Hypoxia-inducible factor 1-alpha	5,52	2,91	0,42	0,95	5,10	2,85	15 (15)
POLA1	DNA polymerase alpha catalytic subunit	5,09	1,59	0,48	1,12	4,61	1,46	13 (13)
ZFYVE16	Zinc finger FYVE domain-containing protein 16	4,88	2,49	-0,30	0,37	5,18	2,59	18 (18)
NPAT	Protein NPAT	4,63	3,78	-0,44	1,66	5,08	3,89	16 (16)
CCDC66	Coiled-coil domain-containing protein 66	4,63	3,24	-0,26	0,59	4,88	3,37	11 (11)
IK	Protein Red	4,57	4,22	0,51	0,80	4,06	4,97	5 (5)
RBM27	RNA-binding protein 27	4,52	3,19	-0,53	0,35	5,05	2,82	22 (20)
PHLDB1	Pleckstrin homology-like domain family B member 1	4,35	3,21	-0,60	1,35	4,95	3,53	9 (9)
JUN	Transcription factor AP-1	4,34	3,18	-0,61	1,46	4,95	3,34	6 (6)
SEC16A	Protein transport protein Sec16A	4,32	2,37	1,18	0,96	3,15	1,90	47 (47)
WAPAL	Wings apart-like protein homolog	4,30	1,78	-0,06	0,11	4,37	1,80	12 (12)
EMSY	Protein EMSY	4,30	2,48	-0,78	2,17	5,07	2,74	27 (27)
EVI5	Ecotropic viral integration site 5 protein homolog	4,24	2,32	-1,03	2,37	5,27	2,65	24 (23)
CLASP1	CLIP-associating protein 1	4,24	5,06	1,80	4,00	2,44	3,97	25 (23)
MAML1	Mastermind-like protein 1	4,22	3,62	1,78	2,47	2,44	3,09	12 (12)
GRIP1	Glutamate receptor-interacting protein 1	4,14	4,13	0,69	0,86	3,46	3,31	19 (19)
ZC3H14	Zinc finger CCCH domain-containing protein 14	4,01	2,28	-0,52	1,06	4,53	2,46	22 (22)
ZBTB11	Zinc finger and BTB domain-containing protein 11	3,99	3,66	-0,77	1,15	4,76	5,53	11 (11)
NFATC3	Nuclear factor of activated T-cells, cytoplasmic 3	3,99	2,57	0,18	0,22	3,81	2,31	10 (10)
INADL	InaD-like protein	3,95	4,21	-0,15	0,24	4,10	5,41	29 (29)
GEM	GTP-binding protein GEM	3,94	2,12	-0,36	1,05	4,31	2,24	4 (4)
PSRC1	Proline/serine-rich coiled-coil protein 1	3,88	3,23	-1,67	1,55	5,54	3,83	4 (4)
MPHOSPH10	U3 small nucleolar ribonucleoprotein protein MPP10	3,85	1,43	-0,41	0,96	4,26	1,58	14 (14)
CPD	Carboxypeptidase D	3,82	2,83	-5,34	4,13	9,17	4,44	41 (41)
LIN54	Protein lin-54 homolog	3,77	1,59	0,17	0,31	3,60	1,52	16 (16)
PEX19	Peroxisomal biogenesis factor 19	3,76	3,46	-1,07	1,29	4,83	4,03	7 (7)
KIF2C	Kinesin-like protein KIF2C	3,72	2,57	1,31	2,74	2,41	1,91	9 (9)
MTMR3	Myotubularin-related protein 3	3,70	2,22	0,37	0,91	3,33	2,06	21 (19)
UTP14A	U3 small nucleolar RNA-associated protein 14 homolog A	3,66	3,07	-0,96	1,28	4,62	4,16	20 (15)
PWP2	Periodic tryptophan protein 2 homolog	3,65	3,17	0,35	1,08	3,30	3,04	8 (8)
GNL3L	Guanine nucleotide-binding protein-like 3-like protein	3,65	1,35	-0,03	0,05	3,68	1,37	11 (11)
BARD1	BRCA1-associated RING domain protein 1	3,65	4,12	-0,98	1,33	4,63	3,87	9 (9)
MKL2	MKL/myocardin-like protein 2	3,64	2,79	-0,60	0,77	4,24	3,61	10 (10)
DDHD1	Phospholipase DDHD1	3,60	4,16	0,22	0,46	3,38	4,33	14 (14)
APC	Adenomatous polyposis coli protein	3,59	2,62	-0,95	1,16	4,54	3,46	32 (32)
NFE2L2	Nuclear factor erythroid 2-related factor 2	3,57	3,17	0,30	0,24	3,27	2,79	4 (4)
UHRF1BP1L	UHRF1-binding protein 1-like	3,54	1,82	0,91	2,18	2,63	1,44	20 (20)
FAM193A	Protein FAM193A	3,52	3,47	-1,00	2,77	4,52	4,03	15 (15)
PGM3	Phosphoacetylglucosamine mutase	3,50	3,00	-0,52	0,38	4,02	3,04	4 (4)
SNRK	SNF-related serine/threonine-protein kinase	3,47	2,33	0,91	0,74	2,56	2,07	8 (8)
ZBTB33	Transcriptional regulator Kaiso	3,42	2,21	0,99	2,61	2,43	1,73	16 (16)
CAMSAP2	Calmodulin-regulated spectrin-associated protein 2	3,41	2,04	-0,32	0,58	3,74	2,22	18 (18)
CEP131	Centrosomal protein of 131 kDa	3,41	4,78	0,60	3,07	2,81	4,29	54 (54)
TNKS1BP1	182 kDa tankyrase-1-binding protein	3,40	2,47	0,82	1,16	2,58	1,91	22 (22)
CALCOCO1	Calcium-binding and coiled-coil domain-containing protein 1	3,39	2,62	0,15	0,15	3,25	2,46	9 (9)
ZCCHC8	Zinc finger CCHC domain-containing protein 8	3,34	2,23	-0,78	2,58	4,12	2,56	7 (7)

Table 7. Continuation

		FL vs NTER		FL vs CTER		CTER vs NTER		
Protein	**Protein names**	**LFQ ratio**	**p-value**	**LFQ ratio**	**p-value**	**LFQ ratio**	**p-value**	**Peptides (Unique)**
GAB1	GRB2-associated-binding protein 1	3,33	1,35	-1,07	1,98	4,40	1,70	13 (13)
OSBPL9	Oxysterol-binding protein-related protein 9	3,31	4,14	0,93	0,48	2,38	1,35	6 (6)
HNRNPUL1	Heterogeneous nuclear ribonucleoprotein U-like protein 1	3,27	1,89	1,05	2,02	2,22	1,34	10 (10)
CEP162	Centrosomal protein of 162 kDa	3,23	1,97	0,10	0,14	3,13	1,89	11 (11)
DECR1	2,4-dienoyl-CoA reductase, mitochondrial	3,23	2,16	0,06	0,03	3,17	1,57	2 (2)
RASAL2	Ras GTPase-activating protein nGAP	3,20	5,01	-0,84	3,08	4,05	5,05	11 (10)
ESF1	ESF1 homolog	3,17	2,48	-1,85	1,83	5,03	3,98	14 (14)
ITCH	E3 ubiquitin-protein ligase Itchy homolog	3,16	1,98	-0,25	0,38	3,41	2,20	10 (9)
PLIN2	Perilipin-2	3,16	2,13	0,62	3,21	2,54	1,80	3 (3)
XRN1	5-3 exoribonuclease 1	3,16	2,74	0,32	0,33	2,83	3,25	24 (24)
RBBP8	DNA endonuclease RBBP8	3,14	1,78	-0,28	0,90	3,41	1,92	17 (17)
EDC4	Enhancer of mRNA-decapping protein 4	3,13	3,03	0,17	0,73	2,96	2,88	46 (46)
EAPP	E2F-associated phosphoprotein	3,12	3,29	-1,21	1,58	4,33	3,67	5 (5)
RC3H2	Roquin-2	3,10	2,95	-1,02	2,59	4,13	3,39	13 (7)
RPGRIP1L	Protein fantom	3,10	2,04	0,05	0,06	3,05	1,91	24 (24)
BICD1	Protein bicaudal D homolog 1	3,08	1,92	0,00	0,00	3,08	2,33	5 (5)
UNK	RING finger protein unkempt homolog	3,05	2,09	-1,46	2,19	4,50	2,84	10 (10)
AGAP3	Arf-GAP with GTPase, ANK repeat and PH domain-containing protein 3	3,04	2,35	-1,94	2,46	4,98	3,28	10 (10)
MAPK7	Mitogen-activated protein kinase 7	2,97	2,14	-0,06	0,11	3,03	2,13	12 (12)
CLASP2	CLIP-associating protein 2	2,96	2,22	0,96	1,90	2,00	1,71	10 (3)
LTV1	Protein LTV1 homolog	2,96	2,54	-0,95	2,88	3,91	2,97	20 (20)
C3orf38	Uncharacterized protein C3orf38	2,94	4,55	0,48	1,49	2,46	4,74	4 (4)
TAF15	TATA-binding protein-associated factor 2N;RNA-binding protein FUS	2,94	1,83	-0,23	0,22	3,17	1,73	3 (3)
ATF3	Cyclic AMP-dependent transcription factor ATF-3	2,88	1,95	-1,35	1,20	4,23	2,89	6 (6)
IGF2R	Cation-independent mannose-6-phosphate receptor	2,87	2,21	-2,98	2,31	5,85	4,61	49 (49)
ZNF281	Zinc finger protein 281	2,87	1,32	-0,97	2,58	3,83	1,72	13 (13)
SLITRK5	SLIT and NTRK-like protein 5	2,87	1,75	-2,04	2,46	4,91	2,65	15 (15)
EPS8	Epidermal growth factor receptor kinase substrate 8	2,85	2,50	0,23	0,47	2,61	2,53	19 (19)
REL	Proto-oncogene c-Rel	2,81	2,14	0,62	0,58	2,19	2,58	3 (3)
ANKRD26	Ankyrin repeat domain-containing protein 26	2,81	2,02	-0,71	1,62	3,52	2,33	16 (16)
MIS18BP1	Mis18-binding protein 1	2,77	1,96	0,53	1,00	2,24	1,67	7 (7)
PAN3	PAB-dependent poly(A)-specific ribonuclease subunit PAN3	2,76	1,81	0,48	0,62	2,29	1,45	11 (11)
ASCC2	Activating signal cointegrator 1 complex subunit 2	2,75	2,05	-1,71	2,28	4,46	2,99	14 (14)
PATL1	Protein PAT1 homolog 1	2,73	3,38	-0,16	0,59	2,88	3,44	14 (14)
MYSM1	Histone H2A deubiquitinase MYSM1	2,71	1,59	-0,81	1,22	3,52	2,07	7 (7)
R3HDM1	R3H domain-containing protein 1	2,71	1,31	-1,49	1,86	4,20	2,01	8 (8)
WDR11	WD repeat-containing protein 11	2,68	2,02	-0,09	0,13	2,78	2,11	8 (8)
NFATC1	Nuclear factor of activated T-cells, cytoplasmic 1	2,67	1,31	0,17	0,14	2,50	1,36	3 (3)
YTHDC2	Probable ATP-dependent RNA helicase YTHDC2	2,64	1,84	-2,62	2,31	5,26	3,27	18 (18)
SUPT5H	Transcription elongation factor SPT5	2,64	2,43	-1,01	1,95	3,65	2,96	7 (7)
CA8	Carbonic anhydrase-related protein	2,62	2,19	-0,44	1,44	3,06	2,47	3 (3)
ATG101	Autophagy-related protein 101	2,62	3,31	-0,83	1,98	3,45	3,64	4 (4)
USP16	Ubiquitin carboxyl-terminal hydrolase 16	2,61	3,40	-0,46	0,87	3,08	3,15	9 (9)
SON	Protein SON	2,59	3,22	0,53	0,64	2,06	2,34	15 (15)
CAMK2G	Calcium/calmodulin-dependent protein kinase type II subunit gamma	2,58	2,43	0,52	1,83	2,06	2,08	3 (3)
KIFAP3	Kinesin-associated protein 3	2,57	2,37	-0,24	0,75	2,81	2,58	6 (6)
ZMYM2	Zinc finger MYM-type protein 2	2,56	2,45	-0,66	1,52	3,23	2,74	7 (7)
ZC3H7B	Zinc finger CCCH domain-containing protein 7B	2,56	1,65	-0,39	1,09	2,95	1,82	8 (8)
RC3H1	Roquin-1	2,55	2,67	-0,64	1,21	3,19	3,23	6 (6)
UBAP2	Ubiquitin-associated protein 2	2,55	2,43	-0,92	1,73	3,47	2,89	16 (16)
PASK	PAS domain-containing serine/threonine-protein kinase	2,54	1,47	0,17	0,75	2,37	1,39	20 (20)
RWDD1	RWD domain-containing protein 1	2,54	2,70	-0,82	1,18	3,36	3,79	2 (2)
CAMSAP1	Calmodulin-regulated spectrin-associated protein 1	2,53	1,81	0,48	0,58	2,05	1,65	7 (7)
MGA	MAX gene-associated protein	2,49	3,17	0,14	0,28	2,35	2,80	5 (5)
ECT2	Protein ECT2	2,49	2,85	-0,40	0,85	2,89	2,83	11 (11)
PPM1G	Protein phosphatase 1G	2,48	1,71	-2,33	2,05	4,82	2,48	8 (8)
ZNF24	Zinc finger protein 24	2,48	3,23	-1,96	3,31	4,44	4,41	10 (10)
ZC3H15	Zinc finger CCCH domain-containing protein 15	2,48	2,12	-2,20	4,19	4,68	3,20	10 (10)
OTUD4	OTU domain-containing protein 4	2,48	2,31	0,29	0,17	2,19	1,74	5 (5)
EIF3D	Eukaryotic translation initiation factor 3 subunit D	2,48	3,74	0,41	0,88	2,07	2,99	11 (11)
MTMR4	Myotubularin-related protein 4	2,41	1,58	0,14	0,19	2,27	1,54	6 (6)
BANP	Protein BANP	2,41	2,45	0,31	0,29	2,09	3,15	3 (3)
TTC33	Tetratricopeptide repeat protein 33	2,40	2,25	-0,02	0,03	2,42	2,34	5 (5)
ICA1	Islet cell autoantigen 1	2,39	3,40	-0,12	0,13	2,51	2,82	2 (2)
MED4	Mediator of RNA polymerase II transcription subunit 4	2,35	2,03	-0,49	0,92	2,84	2,26	7 (7)
ZMYM1	Zinc finger MYM-type protein 1	2,33	1,83	-0,05	0,11	2,37	1,82	19 (19)
NACA	Nascent polypeptide-associated complex subunit alpha;Nascent polypeptide-associated complex subunit alpha, muscle-specific form	2,32	3,71	0,11	0,35	2,21	3,30	5 (4)
MAP4K5	Mitogen-activated protein kinase kinase kinase kinase 5	2,27	2,99	-0,05	0,17	2,32	2,91	6 (6)
FAM160A1	Protein FAM160A1	2,27	2,32	0,09	0,07	2,18	2,29	3 (3)
RAPH1	Ras-associated and pleckstrin homology domains-containing protein 1	2,27	1,33	-0,39	0,42	2,66	1,44	6 (6)
GCFC2	GC-rich sequence DNA-binding factor 2	2,27	2,31	0,02	0,02	2,24	3,37	10 (10)
CSPP1	Centrosome and spindle pole-associated protein 1	2,26	2,95	-0,01	0,10	2,28	2,97	26 (26)
PPP1R9B	Neurabin-2	2,25	1,46	-1,75	3,48	4,01	2,33	17 (16)
OSBPL6	Oxysterol-binding protein-related protein 6	2,25	1,60	-1,79	2,89	4,03	2,55	11 (11)
AXIN1	Axin-1	2,24	2,51	-0,04	0,07	2,29	2,80	10 (10)
AFTPH	Aftiphilin	2,20	3,28	0,02	0,08	2,18	3,19	11 (11)
CDC6	Cell division control protein 6 homolog	2,18	1,33	0,04	0,83	2,14	1,31	6 (6)
TIAL1	Nucleolysin TIAR	2,18	1,47	-0,94	1,86	3,11	2,04	6 (6)
NUP160	Nuclear pore complex protein Nup160	2,16	1,53	-0,99	2,12	3,16	2,02	16 (16)
ARRB2	Beta-arrestin-2	2,16	3,19	-0,18	0,20	2,34	2,49	2 (2)
POLK	DNA polymerase kappa	2,10	2,82	0,06	0,04	2,04	1,78	5 (5)
WDR3	WD repeat-containing protein 3	2,09	2,75	-0,34	1,20	2,43	3,09	10 (10)
DHX57	Putative ATP-dependent RNA helicase DHX57	2,03	2,30	-2,63	3,18	4,66	4,40	15 (14)
DFFA	DNA fragmentation factor subunit alpha	2,00	2,45	-0,73	1,39	2,74	3,04	7 (7)

Table 8. Putative CaMKIIa full-length interactors. The protein name in UniProt and their full name. LFQ ratio: fold change calculated between samples. P-value: statistical significance.

		FL vs NTER		FL vs CTER		CTER vs NTER		
Protein	**Full name**	**LFQ ratio**	**p-value**	**LFQ ratio**	**p-value**	**LFQ ratio**	**p-value**	**Peptides (unique)**
POLDIP3	Polymerase delta-interacting protein 3	3,97	2,76	2,36	2,29	1,20	1,61	2 (2)
HSD17B4	Peroxisomal multifunctional enzyme type 2	3,95	1,99	2,65	1,59	1,31	0,53	5 (5)
PALLD	Palladin	3,95	3,59	2,03	3,93	1,92	2,27	17 (17)
FAM83H	Protein FAM83H	3,78	1,93	2,44	1,72	1,34	0,55	9 (9)
DUSP11	RNA/RNP complex-1-interacting phosphatase	3,50	1,59	2,16	2,16	1,34	0,56	10 (10)
STAT5A/B	Signal transducer and activator of transcription 5A/B	3,47	2,33	3,63	2,96	-0,16	0,08	15 (15)
RBMX	RNA-binding motif protein, X chromosome	3,12	3,16	2,08	1,98	1,04	0,94	10 (10)
PNO1	RNA-binding protein PNO1	2,91	2,07	2,36	1,75	0,00	NaN	3 (3)
RBM14	RNA-binding protein 14	2,76	1,43	4,56	2,20	-1,80	0,67	14 (13)
HNRNPH3	Heterogeneous nuclear ribonucleoprotein H3	2,45	4,41	2,14	4,66	0,31	1,05	12 (12)
HNRNPA2B1	Heterogeneous nuclear ribonucleoproteins A2/B1	2,43	4,38	2,68	4,33	-0,25	1,06	21 (20)

Validation of the potential CaMKIIa interactors through coimmunoprecipitation

From our list of putative CaMKIIa interactors, we selected a number of full-length, N-terminal and C-terminal CaMKII binding proteins in order to validate them through coimmunoprecipitation followed by Western blot. To do so, we generated the following plasmids: pCMV_EGFP-CaMKIIa FL, pCMV_EGFP_CaMKIIa CTER, pCMV_CaMKIIa NTER_EGFP and FLAG-GFP, which was used as a control to ensure that candidate proteins were not interacting with GFP. Distinct versions of GFP-CaMKIIa as well as control GFP were overexpressed in HEK 293T cells, protein extracts were precipitated by GFP pulldown, and the presence of the putative CaMKII interactor was detected by western blot.

DUSP11 is a phosphatase involved in nuclear mRNA metabolism that according to our MS results may associate with full-length CaMKIIa (**Table 8**). As shown in **Figure 23A**, FLAG-DUSP11 coimmunoprecipitated with FL and CTER CaMKIIa but not with NTER (**Figure 23A**), suggesting DUSP11 interacts with CaMKIIa and most probably, through the C-terminal region of the kinase.

Among putative C-terminal interactors of CaMKIIa detected by MS (**Table 7**), we focused on validating E3 ubiquitin ligases, BARD1 and ITCH. Both HA-BARD1 and FLAG-ITCH coprecipitated with the three CaMKII constructs (**Figure 23B and C**), appearing, therefore, to be non-specific interactors.

Finally, the hydroxylase EGLN1 and the potassium-chloride cotransporter SLC12A7 were selected from the candidate list of N-terminal CaMKIIa binding proteins (**Table 6**). HA-EGLN1 coimmunoprecipitated with all CaMKIIa constructs (**Figure 23D**), whereas FLAG-SLC12A7 (**Figure 23E**) with none of them. Consequently, we could not validate MS results suggesting these proteins associate with CaMKII's N-terminal region.

The DUB MYSM1 regulates CaMKIIa ubiquitination in an indirect negative manner in HEK 293T cells

One of the objectives of this section of the thesis was to understand the molecular machinery underlying the ubiquitination of CaMKIIa. In previous studies, we have observed that *D. melanogaster's* CaMKII can be ubiquitinated (Ramirez et al. 2018), but neither the E3 ubiquitin ligase(s) nor the DUB(s) involved are known. To study the DUBs involved in CaMKIIa ubiquitination, we silenced them separately and assessed the ubiquitination status of the kinase. For that purpose, 24 hours after HEK 293T cells were transfected with the corresponding DUB silencing RNA, cells were cotransfected with FLAG-Ub and GFP-CaMKIIa. Then, GFP-CaMKIIa was pulled down using GFP-trap agarose beads and after performing stringent washes to get

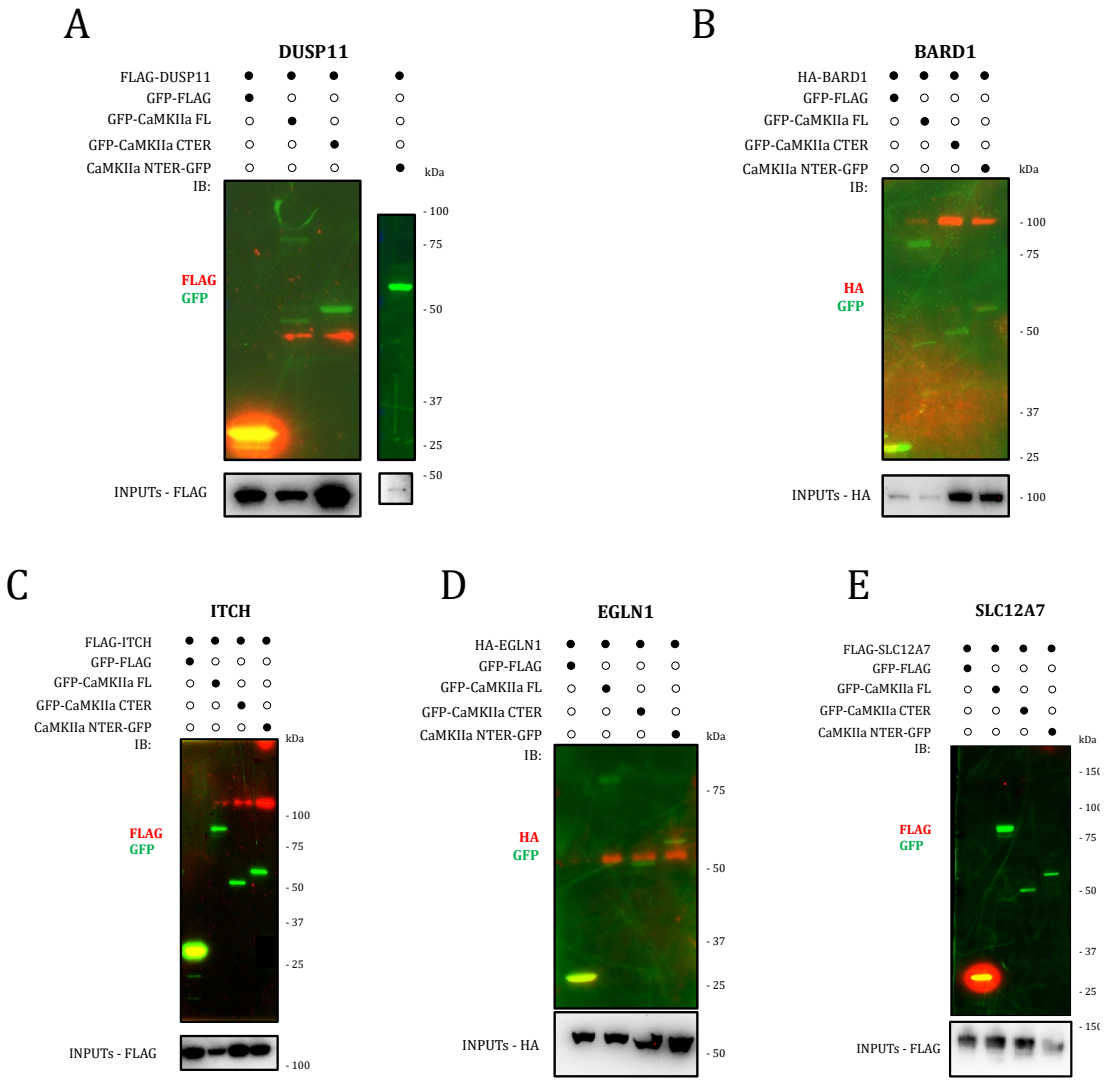

Figure 23. Validation of CaMKIIa interacting proteins. We coexpressed GFP-FLAG, GFP-CaMKIIa FL, GFP-CaMKIIa CTER and CaMKIIa NTER-GFP together with one of the five potential CaMKIIa interactors selected for validation: (A) FLAG-DUPS11, (B) HA-BARD1, (C) FLAG-ITCH, (D) HA-EGLN1 and (E) FLAG-SLC12A7. In green the version of CaMKII expressed is visualized whereas in red the Flag tagged biotin. The candidate interactor is monitored through its tag (either Flag or HA).

rid of any non-covalent binding proteins, the eluted material was analysed by western blot to visualize the unmodified version of CaMKIIa (using anti-GFP to detect GFP-CaMKIIa) and the ubiquitinated fraction of the kinase (using antiFLAG to detect FLAG-Ub). Finally, we compared the signal of FLAG-Ub relative to GFP-

CaMKIIa of samples silenced with a control siRNA or with a given DUB. If CaMKIIa was a substrate of the DUB, we would expect higher levels of CaMKII ubiquitination when the DUB is depleted.

In the mass spectrometry-based approach, we detected three DUBs (OTUD4, MYSM1 and USP16) as putative C-terminal CaMKIIa interactors (**Table 7**) and therefore, we aimed to functionally validate them. To analyse the effect of these in the absence of efficient antibodies to detect the DUBs, efficient silencing of the deubiquitinating enzymes was verified through qPCR (**Figure 24A**). Of the three DUBs mentioned above, OTUD4 was the only one we could not properly study as its silencing triggered abnormal expression of the FLAG-Ub construct. Upon USP16 silencing, we observed no change in GFP-CaMKIIa ubiquitination with respect to the control (**Figure 24B**). Upon silencing of MYSM1 (**Figure 24C**), however, the ubiquitination of CaMKIIa decreased significantly, precisely the opposite effect to that expected in case the kinase was a substrate of the DUB.

Given that phosphorylation of T286 blocks the autoinhibitory domain of CaMKIIa and it is persistently active even in a calcium-independent manner, we checked whether MYSM1 silencing had any effect on the phosphorylation status of the kinase. Interestingly, we detected an increase in T286 phosphorylation when MYSM1 was silenced and CaMKIIa was less ubiquitinated (**Figure 24D**). Altogether, these results suggest that MYSM1 depletion constitutively activates CaMKIIa by enhancing phosphorylation on T286.

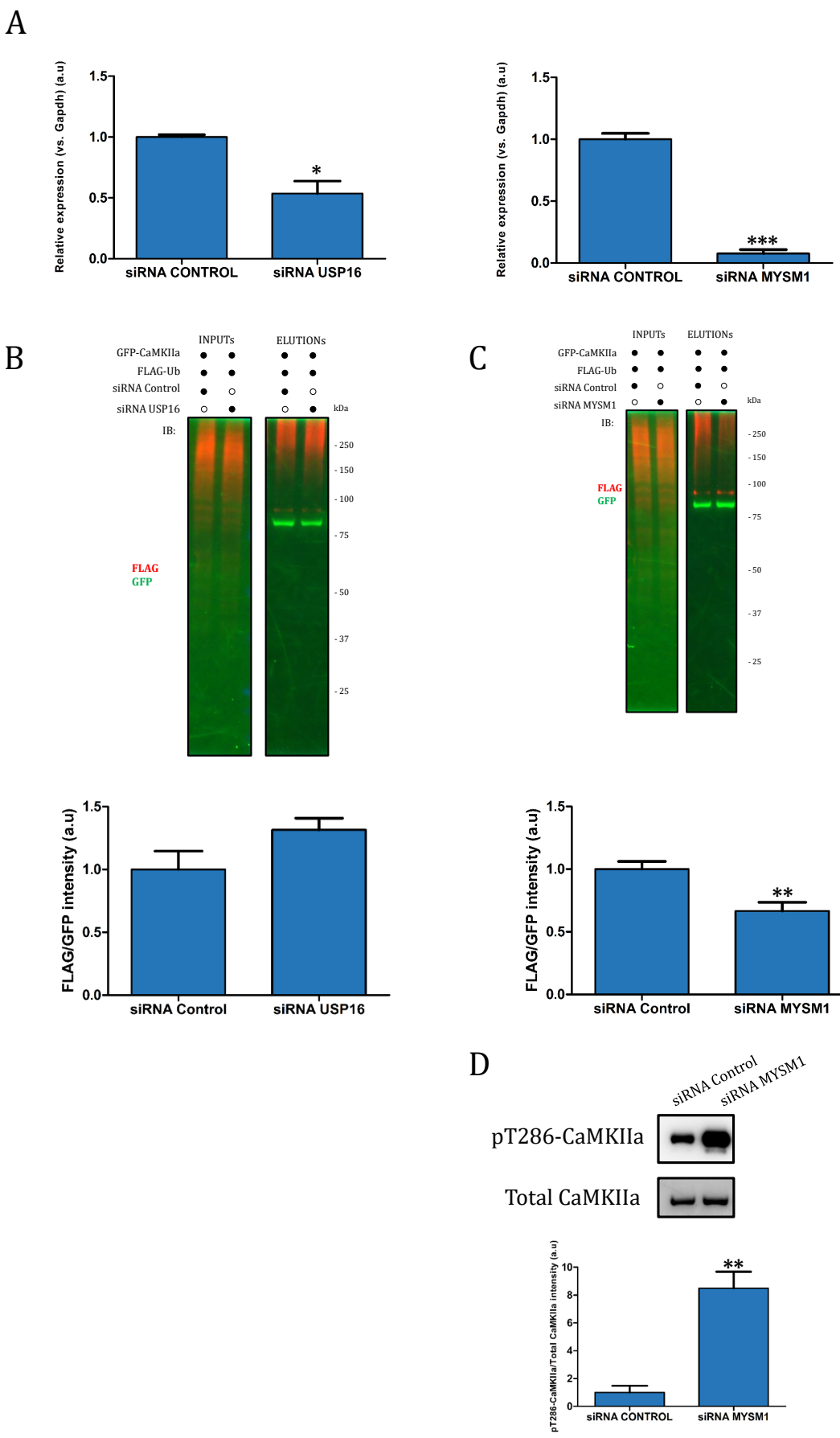
A
Relative expression (vs. Gapdh) (a.u)
1.5
1.0
0.5
0.0
*
siRNA CONTROL
siRNA USP16
Relative expression (vs. Gapdh) (a.u)
1.5
1.0
0.5
0.0
***
siRNA CONTROL
siRNA MYSM1
B
INPUTs
ELUTIONs
GFP-CaMKIIa
FLAG-Ub
siRNA Control
siRNA USP16
IB:
kDa
- 250
- 150
- 100
- 75
- 50
- 37
- 25
FLAG
GFP
C
INPUTs
ELUTIONs
GFP-CaMKIIa
FLAG-Ub
siRNA Control
siRNA MYSM1
IB:
kDa
- 250
- 150
- 100
- 75
- 50
- 37
- 25
FLAG
GFP
FLAG/GFP intensity (a.u)
1.5
1.0
0.5
0.0
siRNA Control
siRNA USP16
FLAG/GFP intensity (a.u)
1.5
1.0
0.5
0.0
**
siRNA Control
siRNA MYSM1
D
siRNA Control
siRNA MYSM1
pT286-CaMKIIa
Total CaMKIIa
pT286-CaMKIIa/Total CaMKIIa intensity (a.u)
10
8
6
4
2
0
**
siRNA CONTROL
siRNA MYSM1

Figure 24. Deubiquitination of GFP-CaMKIIa by USP16 and MYSM1. We silenced USP16 and MYSM1 genes and 24 hours later coexpressed FLAG-Ub and GFP-CaMKIIa. GFP-CaMKIIa was enriched by a GFP pulldown A) After 24 hours from transfecting with siRNA control or siRNA targeting USP16 or MYSM1, RNA was extracted and transform to cDNA which was analysed by qPCR as described in *materials and* methods. Relative expression levels of the USP16 or MYSM1 gene normalised to Gapdh expression levels. Intensity was normalised to the siRNA control (USP16: * p-value < 0.05; n=3; two-tailed p-value; error bars denote SEM MYSM1: *** p-value < 0.001; n=3; two-tailed p-value; error bars denote SEM). B) Western blot of the input and elution fraction of the three different conditions when USP16 was silenced. Ubiquitinated forms of GFP-CaMKIIa are shown in red (anti-FLAG) and no-ubiquitinated GFP-CaMKIIa is shown in green (anti-GFP). C) The Column bar graph represents the FLAG/GFP ratio obtained by measuring the signal for the whole smear in the elution membrane. Intensity was normalised to the siRNA control (p-value > 0.05; n= 5; two-tailed p-value; error bars denote SEM). C) Western blot of the input and elution fraction of the three different conditions when MYSM1 was silenced. Ubiquitinated forms of GFP-CaMKIIa are shown in red (anti-FLAG) and no-ubiquitinated GFP-CaMKIIa is shown in green (anti-GFP). C) The Column bar graph represents the FLAG/GFP ratio obtained by measuring the signal for the whole smear in the elution membrane. Intensity was normalised to the siRNA control (p-value < 0.01; n= 5; two-tailed p-value; error bars denote SEM). D) Western blot showing the levels of pT286-CaMKIIa and total CaMKIIa levels. The Column bar graph shows the difference of expression of pT286-CaMKIIa between control and MYSM1 silencing. Intensisty was normalised to the siRNA control (**p-value < 0.01; n=3; two-tailed p-value; error bars denote SEM).

The E3 ubiquitin ligase ITCH is responsible for CaMKIIa monoubiquitination in HEK 293T cells

As mentioned above, the E3 ubiquitin ligase(s) mediating CaMKIIa ubiquitination remain(s) elusive. Interestingly, using the BioID2 system we identified 155 potential interactors for CaMKIIa including three ubiquitin E3 ligases: ITCH, RC3H2 and BARD1 (**Table 7**).

ITCH is a HECT-type E3 ubiquitin ligase that has been described to mediate the ubiquitination of Endophilin-A1 (Angers, Ramjaun, and McPherson 2004). Mutations of ITCH are associated with syndromic multisystem autoimmune disease that triggers developmental delay among other symptoms (Lohr et al. 2010). RC3H2 is involved in the regulation of stress responses through ASK1 kinase ubiquitination (Maruyama et al. 2014) whereas BARD1 is an E3 ubiquitin ligase with no ligase activity by itself as it has to form heterodimers with BRCA1 to be active (Morris and Solomon 2004).

We initially planned to study the functional interaction between CaMKIIa and the three E3 ligases detected in our proteomics study. Nevertheless, attempts with BARD1 were unsuccessful probably because, as mentioned above, BARD1 must associate with BRCA1 to be active. Consequently, we focused on investigating whether ITCH and/or RC3H2 had an effect on the ubiquitination of CaMKII. For that purpose, we carried out a cell-culture-based GFP pull-down strategy. Shortly, HEK 293T cells were cotransfected with GFP-CaMKIIa, FLAG-Ub and either the active (wild type; WT) or inactive (ligase dead; LD) version of the E3 ubiquitin ligases. GFP-CaMKIIa and its ubiquitinated forms were purified with GFP-trap agarose beads and analysed by western blot.

In both experiments, where the effect of RC3H2 and ITCH on the ubiquitination of CaMKIIa was under investigation, control samples containing an empty pCDNA3 plasmid tended to express less FLAG-Ub. However, we could compare the ubiquitination levels of CaMKIIa in the presence of WT and LD versions of the E3 ligases. As shown in **Figure 25**, CaMKIIa ubiquitination levels were similar in the presence of WT and LD RC3H2, suggesting RC3H2 does not mediate CaMKIIa

ubiquitination. On the contrary, although overall ubiquitination levels of CaMKIIa were comparable in the presence of WT and LD ITCH, we detected a significant reduction in the monoubiquitination of CaMKIIa when the inactive version of ITCH was expressed (**Figure 26A**). Therefore, ITCH seems to promote the monoubiquitination of CaMKIIa in HEK 293T cells.

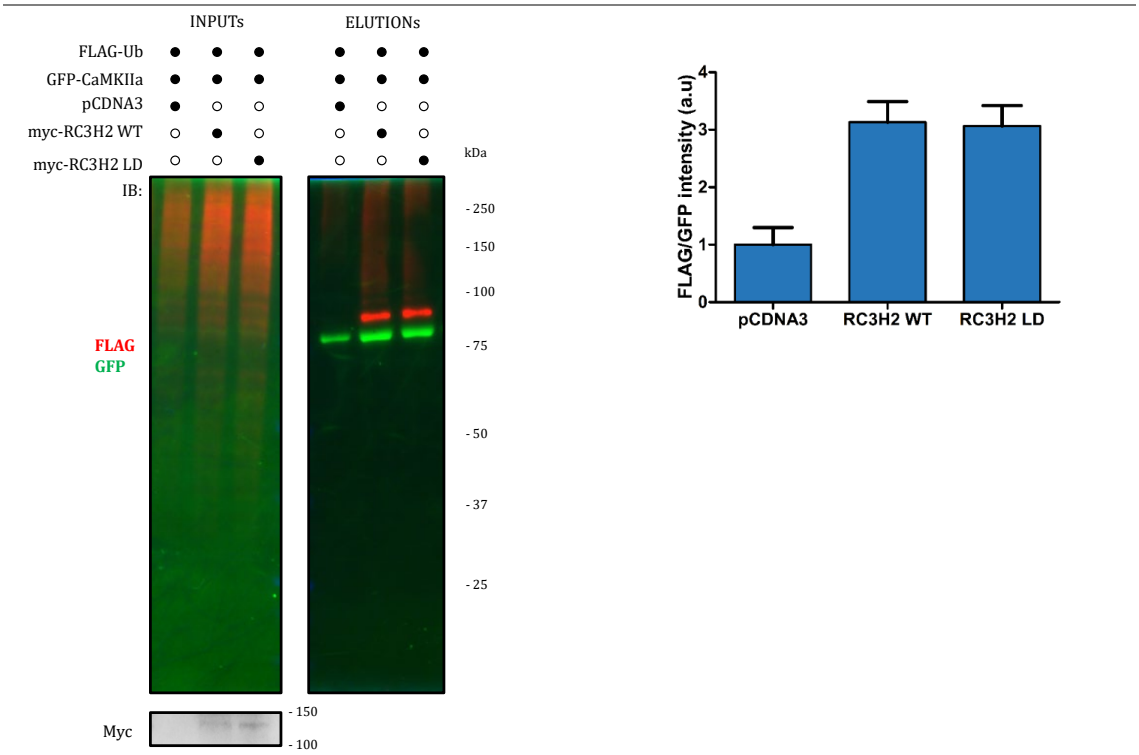

Figure 25. Ubiquitination of GFP-CaMKIIa by RC3H2. We coexpressed FLAG-Ub and GFP-CaMKIIa with either myc-RC3H2 WT or LD. GFP-CaMKIIa was enriched by a GFP pulldown. Western blot of the input (left) and eluted (right) fraction of the three different conditions. Anti-FLAG is show in red and anti-GFP in green. On the Column bar graph it is represented the FLAG/GFP ratio obtained by measuring the signal for the whole smear in the elution membrane. Intensity was normalised to the pCDNA3 control (p-value > 0.05; n= 5; two-tailed p-value; error bars denote SEM).

Besides that, we analysed the levels of CaMKIIa activating-phosphorylation at T286 when active and inactive ITCH were expressed, and therefore, CaMKIIa was differentially monoubiquitinated (**Figure 26B**). As observed in the MYSM1-silencing experiment, in the presence of ITCH LD, when CaMKIIa was less ubiquitinated, there is an increase in T286 phosphorylation. Altogether, the data presented above suggest that ITCH monoubiquitinates CaMKIIa and might modulate the activity of the kinase by compromising phosphorylation at T286.

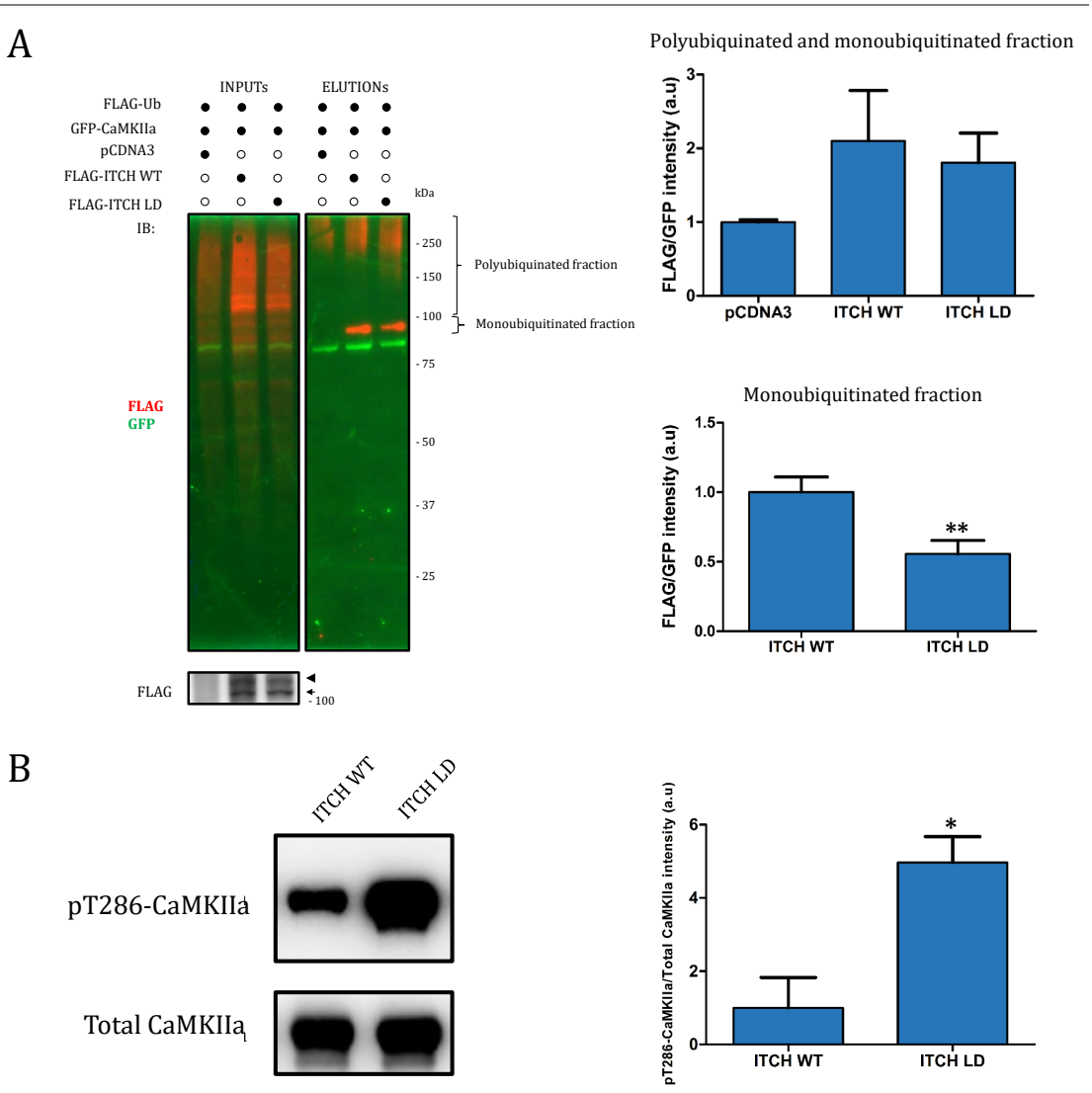

Figure 26. Ubiquitination of GFP-CaMKIIa by ITCH. We coexpressed FLAG-Ub and GFP-CaMKIIa with either FLAG-ITCH WT or LD. GFP-CaMKIIa was enriched by a GFP pulldown. A) Western blot of the input (left) and eluted (right) fraction of the three different conditions. Anti-FLAG is show in red and anti-GFP in green. The upper column bar graph represents the FLAG/GFP ratio obtained by measuring the signal for the whole smear in the elution membrane. Intensity was normalised to the pCDNA3 control (p-value > 0.05; n= 5; ; two-tailed p-value; error bars denote SEM). The lower column bar graph represents the FLAG/GFP ratio obtained by measuring the signal for the monoubiquitination band in the elution membrane. Intensity was normalised to the ITCH WT sample (p-value < 0.01; n = 5; two-tailed p-value; error bars denote SEM). B) Western blot showing CaMKIIa phosphorylation at T286 and total CaMKIIa. The column bar graph represents the phosphorylated CaMKIIa/Total CaMKIIa ratio. Intensity was normalised to the ITCH WT sample (p-value < 0.05; n=3; two-tailed p-value; error bars denote SEM).

Discussion

BioID2 is a relatively new system and a number of studies are now starting to be published with different design strategies. Most of the investigations have applied the BioID2 system in combination with western blot analysis to look for specific interactors (Anczurowski et al., 2019; Mazina, Ziganshin, Magnitov, Golovnin, & Vorobyeva, 2020; Nessel et al., 2020; Prikas, Poljak, & Ittner, 2020; Zheng et al., 2019). However, some studies have also combined the BioID2 system with mass spectrometry analyses to uncover, in an unbiased manner, interactors of a given protein. For instance, a similar approach to the one we carried out was applied to decipher the interactome of MAP kinase p38α and MK in HEK 293T (Prikas, Poljak, & Ittner, 2020) and SH-SY5Y cell, respectively (Komata et al. 2021). Similarly, the mitochondrial interactome of Src was studied (Guedouari et al. 2021) and spindle assembly checkpoint proteins' interactors were found with proximity labelling with BioID2 (Garcia et al. 2021). This system has also helped to identify

BVES as an ANO5 interactor (H. Li et al. 2021) or the activation of the hippo pathway via LIMD1 by SKI to inhibit cardiac fibroblast activation (Landry et al. 2021). Besides that, a BioID2 knock-in strategy was developed to look for the cardiac dyad proteome (Feng et al. 2020).

Good quality controls are always needed to achieve the set objectives and, therefore, selecting the proper negative controls is crucial. Traditionally, BioID2 alone has been used as a negative control to look for those proteins that might interact with BioID2 (Garcia et al., 2021; Green & Levine, 2014; Komata et al., 2021; Landry et al., 2021; Pitzen, Sander, Baumann, Gräf, & Meyer, 2021; Prikas, Poljak, & Ittner, 2020). However, BioID2 alone is capable of biotinylating more efficiently than when it is attached to the bait due to a matter of flexibility, diffusion rate, mobility to the nucleus and biotinylation speed. Consequently, employing this strategy as the only control can underestimate the number of potential interactors. A good solution is to attach BioID2 to a signal that localises to the organelle of interest (H. Li et al. 2021). Another robust approach is to employ different mutants of the bait as negative control (Guedouari et al. 2021). We decided to split the bait into C- and N-terminal regions and compare them to each other, as has been done in distinct recently published research studies (Abbasi and Schild-Poulter 2021; Roboti, Lawless, and High 2022).

To our knowledge, so far there is a single study that employed mass spectrometry to search for CaMKIIa interactors (Baucum et al. 2015). Fewer proteins were detected, but whereas our approach was carried out in HEK 293T cells, they performed it in the mouse forebrain. Furthermore, they analysed immunoprecipitates with no signal increase like the one observed with BioID2.

Nevertheless, dissecting CaMKIIa interactome in the mouse forebrain is for certain physiologically more relevant than studying in HEK 293T cells. Thus, no common proteins were identified between both investigations. But now that we have tested the suitability of the BioID2 system to search for CaMKIIa interacting proteins in HEK 293T cells, future experiments should focus on applying the same approach to dissect the CaMKIIa interactome in systems that include brain or neuronal structures, such as neuron-like cells, mouse brain slices, or *in vivo* labelling using whole organisms like *Drosophila melanogaster* or mice.

Despite being aware that our system is not the most suitable one to search for CaMKIIa interacting proteins, we uncovered several novel CaMKIIa binding partners. One of them is the dual-specificity phosphatase DUSP11. DUSP11 preferentially binds to RNA displaying 5'-triphosphatase and diphosphatase activities to modulate nuclear mRNA metabolism (Burke and Sullivan 2017). In vitro, GST-tagged DUSP11 also has intrinsic tyrosine phosphatase activity (Patterson et al. 2009) but the phosphatase exhibits higher specificity for RNA molecules than for phosphoproteins (T. Deshpande et al. 1999). By yeast-two-hybrid system, it has been proved that DUSP11 can also associate with some splicing factors, but these interactions have not been verified in mammalian cells. Our proteomics data suggested that DUSP11 might associate only with full-length CaMKIIa. Nevertheless, according to western blot-based validation experiment, DUSP11 could also interact with the C-terminal domain of the kinase. Therefore, we conclude that DUSP11 interacts with CaMKIIa. Further experiments are needed to determine the extent to which the C-terminal region of the kinase is involved in this interaction.

We aimed to validate by coimmunoprecipitation and western blot four additional putative CaMKIIa interacting proteins that were detected by mass spectrometry (BARD1, ITCH1, EGLN1 and SLC12A7) but did not succeed. According to our proteomics screen, they were either C-terminal (BARD1 and ITCH) or N-terminal (EGLN1 and SLC12A7) CaMKIIa binding proteins. However, in the validation experiment, they coimmunoprecipitated with all or none of the CaMKIIa constructs (FL, NTER and CTERM). Consequently, we could not confirm they specifically interact with the kinase.

We could not prove the physical interaction between those proteins and CaMKII, but we managed to uncover a functional interaction between the E3 ubiquitin ligase ITCH and the kinase. We have observed that the E3 ubiquitin ligase ITCH promotes CaMKIIa monoubiquitination in HEK 293T cells. Indeed, it has previously been reported that ITCH monoubiquitinates and hence, plays a pivotal role in regulating the cellular localization of the survival motor neuron (SMN) protein, which is involved in spinal muscular atrophy (K. J. Han et al. 2016). The role of monoubiquitination in cells is less clear than polyubiquitination. However, proteomics analyses have revealed that monoubiquitination is more represented in cells than polyubiquitination (Kaiser et al. 2011). Moreover, when the proteasome is blocked, polyubiquitinated proteins are accumulated. However, monoubiquitinated proteins are reduced, suggesting that monoubiquitination is reversible in a manner that is sensitive to changes in the cellular state (Mimnaugh et al. 1997; W. Kim et al. 2011). Monoubiquitination is also involved in additional key cellular processes such as transcriptional repression (Bhatnagar et al. 2014), protein activation (Pavlopoulos et al. 2011), and proteasomal degradation (Liani et

al. 2004; Boutet et al. 2007). Nevertheless, since we did not detect a significant decrease in CaMKIIa total levels, we suggest that ITCH-mediated monoubiquitination does not target the kinase to proteasomal degradation, but has another role that remains elusive.

We also discovered that the deubiquitinase MYSM1 affects CaMKIIa ubiquitination, but contrary to what might be expected if the interaction was direct, silencing of the DUB causes a decrease in CaMKII ubiquitination. Consequently, we suggest that MYSM1 indirectly regulates CaMKII ubiquitination status by either activating an E3 ubiquitin ligase or inactivating a DUB that targets kinase. MYSM1 deficiency is associated with bone marrow failure syndrome 4, characterised by hematopoietic defects and patients present anaemia, leukaemia and other developmental aberrations including neurodevelopmental delay, which is a characteristic feature of Angelman syndrome. Besides that, it should be noted that MYSM1 is a metalloprotease that promotes histone H2A deubiquitination. As histone H2A monoubiquitination triggers epigenetic transcriptional repression and chromatin inaccessibility (Jiang et al., 2011; Nandakumar, Chou, Zang, Huang, & Chen, 2013; Robzyk, Recht, & Osley, 2000; Wang et al., 2013), it is also plausible that MYSM1 modulates the expression of an E3 ubiquitin ligase that mediates CaMKII ubiquitination. Nevertheless, further studies should be performed to elucidate the intermediate steps that link the two proteins.

Protein post-translational modifications (PTMs) are known to crosstalk among each other creating a PTM code that brings a new layer of complexity in a widespread aspect of biology (Hunter 2007). For instance, there is evidence for the regulation of ubiquitination by phosphorylation either through the regulation of E3

ubiquitin ligase activity, the formation of phosphodegrons or the regulation of subcellular localisation and subsequent substrate-ligase interaction. However, little is known about the effect of ubiquitination on protein phosphorylation (Hunter 2007). We have discovered an inverse relation between CaMKII T286 phosphorylation and ubiquitination. More precisely, we found out that when CaMKIIa is less ubiquitinated, either upon MYSM1 or ITCH depletion, T286 is more phosphorylated and, thus, more active as the autoinhibitory domain is blocked. On one hand, it is possible that ubiquitinated CaMKIIa adopts a conformation that keeps T286 hidden and inaccessible to be phosphorylated. On the other hand, it is also plausible that ubiquitinated CaMKIIa recruits a phosphatase that dephosphorylates CaMKIIa pT286. Future experiments are necessary to shed light on such inverse relation. Furthermore, it would be interesting to evaluate whether MYSM1 and ITCH have any effect on the inhibitory phosphorylation at T305/306 of CaMKII.

CHAPTER II

Uncovering CaMKII interactors in Drosophila melanogaster through TurboID

Summary

An *in vivo* strategy was carried out to look for CaMKII interactors in *Drosophila melanogaster* combining a proximity labelling strategy based on TurboID with label-free quantitative mass spectrometry. For that purpose, we developed three *Drosophila melanogaster* lines expressing FLAG-TurboID-CaMKII FL, CTER and NTER under the GMR/UAS promoter. The biotinylated material obtained from the heads of the flies was purified with streptavidin beads and then analysed by mass spectrometry to search for CaMKII interactors in flies. Results were highly reproducible and uncovered several proteins of interest related to synapses, neuronal events, neurodegenerative disease and behaviour that may associate with CaMKII. Additionally, we demonstrated that human homologs of two of those CaMKII binding candidates actually interact with human CaMKIIa/b. We also tried to validate the functional interaction between a putative CaMKII interacting protein detected but did not succeed.

Introduction

Mice models for AS show a deficit in long-term potentiation (LTP) (Van Woerden et al. 2007), a process in which CaMKIIa plays a crucial role. Indeed, CaMKIIa translocates to the spine head of dendrites and by phosphorylating the AMPA receptor and the protein stargazin produces potentiation (Y.-P. Zhang, Holbro, and Oertner 2008; Poncer, Esteban, and Malinow 2002; Tomita et al. 2005).

CaMKIIa is reduced in the synapses of AS mice, whereas CaMKIIa phosphorylated at T286 and T305 seems to be increased (Weeber et al. 2003). In line with this, AS models mutated at the inhibitory autophosphorylation residues T305 and/or T306 (TT305/6VA) exhibit normal LTP and behaviour, suggesting AS deficits are a direct consequence of enhanced inhibitory phosphorylation of CaMKIIa (Van Woerden et al. 2007). Moreover, it has been shown that autophosphorylation of CaMKIIa on T286 enhances its association with proteasomes, promotes proteasome accumulation in spines and stimulates proteasome activity by phosphorylation of proteasome subunit Rpt6 on S120. Therefore, CaMKII interacts with Rpt6 and specifically complexes with proteosomes in mice brains (Bingol et al. 2010).

There are many different approaches, such as proximity labelling, to look for the interactors of a given protein. As thoroughly explained in the introduction of this thesis, various proximity labelling strategies have been developed including the BioID2 that was applied in the first chapter of this thesis, as well as the so-called TurboID that has been applied in the present section (Shkel et al. 2022).

Due to the low catalytic activity of BioID2, it is extremely difficult to use it to study protein-protein interactions in whole organisms such as worms or flies. TurboID consists of the fusion of the protein of interest with BirA, a promiscuous biotin protein ligase from *A. aeolicus* with 15 mutations relative to wild-type BirA. These mutations confer TurboID a higher biotinylation capacity compared to the wild-type version of BirA and allow to obtain sufficient material in a living organism such as flies for mass spectrometry analyses (Branon et al. 2018). When the fusion

protein is expressed in cells, TurboID biotinylates all proteins that are in close proximity to the protein of interest. Then, biotinylated proteins, including the interactors of interest, can be isolated using streptavidin, and finally, analysed either by western blot or mass spectrometry.

Hypothesis & objectives

We believe that uncovering CaMKII interactors in neurons will help us have a better understanding of the role of this kinase in neuron physiology. Having first tested the suitability of applying the BioID2 strategy using the linker $(GSGS)_3$ to search for CaMKIIa binding proteins in HEK 293T cells (chapter 1), we considered that a similar approach based on TurboID and using the same linker would allow us to decipher the interactome of CaMKIIa in flies. Finally, we hypothesize that those CaMKII fly interactors might have human homologues.

In order to study the interactome of CaMKIIa in flies, three main objectives are defined in this section of the thesis:

- Validate the TurboID system in *Drosophila melanogaster*.
- Identify CaMKII interactors in *Drosophila melanogaster*.
- Extrapolate to human homolog the identified interactors.

Results

Generation of GMR:UAS TurboID-CaMKII/Cyo fly lines

To obtain recombinant flies expressing the fusion protein containing full length (FL, 1-530), C-terminal (CTER, Δ1-388) and N-terminal (NTER, Δ389-530) CaMKII under the GMR/GAL4 promotor. First, UAS TurboID-CaMKII FL/Cyo; TM2/TM6, UAS TurboID-CaMKII CTER/Cyo; TM2/TM6 or CaMKII NTER-TurboID/Cyo; TM2/TM6 clones were crossed with GMR/GMR; TM2/TM6 flies, respectively. UAS FLAG-TurboID-CaMKII FL/GMR, UAS FLAG-TurboID-CaMKII CTER/GMR and UAS CaMKII NTER-FLAG-TurboID/GMR flies were selected by phenotype (red eyes and normal wings). In the different clones selected, the expression and biotinylation capability of the corresponding construct were tested, and the one with higher expression and higher biotinylation was selected.

Once a clone for each construct was selected, females were crossed with Sco/Cyo; TM2/TM6 flies. The appearance of white-eyed flies points out that recombination has occurred. Females with darker eyes and curvy wings were selected and were crossed again with Sco/Cyo; TM2/TM6 males. Finally, GMR: UAS FLAG-TurboID-CaMKII FL/Cyo, GMR: UAS FLAG-TurboID-CaMKII CTER/Cyo and GMR: UAS CaMKII NTER-FLAG-TurboID/Cyo both male and female flies were obtained and crossed with each other to maintain each of the lines.

Validation of TurboID system in Drosophila melanogaster fly lines

Recombinant fly lines were grown in big bottles and around 15 mL of flies were collected per replica. 1- and 3-day-old flies were harvested, heads crushed and biotinylated material was purified with streptavidin beads as explained in the material and methods section.

The expression of FL-, CTER- and NTER-CaMKII was visualised in the inputs by western blot using an anti-FLAG antibody. As shown in **Figure 27A** (lower panel), both CTER and especially FL constructs were efficiently expressed, whereas NTER was not detected, not even revealing the membrane with SuperSignal™ West Femto Maximum Sensitivity Substrate (Thermo Scientific). In line with that, flies expressing FLAG-TurboID-CaMKII FL construct exhibit the highest biotinylation efficiency, whereas flies expressing CaMKII NTER-FLAG-TurboID showed the lowest, comparable to the GMR/GMR negative control (**Figure 27A**, upper panel). Nevertheless, as differences could be detected between GMR negative control and CaMKII NTER-FLAG-TurboID samples, we decided to proceed with the experiment. Endogenously biotinylated carboxylates (Pcb, Mccc1 and Acc) are considered control proteins as they report on the amount of biological material used for the pulldowns independently of the transfected constructs. It should be noted that using an anti-biotin antibody, among others, endogenous carboxylases such as pyruvate carboxylase (*pcb*) and methylcrotonoyl-CoA carboxylase 1 (*mccc1*) were visible at around 130 kDa and 75 kDa, respectively.

Deciphering the interactome of CaMKIIa in *D. melanogaster*

Next, we aimed to make sure that the procedure applied above resulted in the enrichment of sufficient biotinylated and hence, ubiquitinated material to be further analyzed by mass spectrometry. Since western blot signals are not quantitative, we loaded 7% of the elutions straight into a gel and we performed silver staining to assess the total amount of protein present in each sample. As shown in **Figure 27B**, silver staining results correlated with western blot signals described above and verified there was enough material for mass spectrometry-based protein detection. Consequently, 50% of the elutions were loaded in a gel and stained with coomassie blue. Each lane was cut into two slices: slice B contained all the proteins between the avidin monomer (16 kDa) and the carboxylase Pcb (130 kDa), and slice A proteins above 130 kDa.

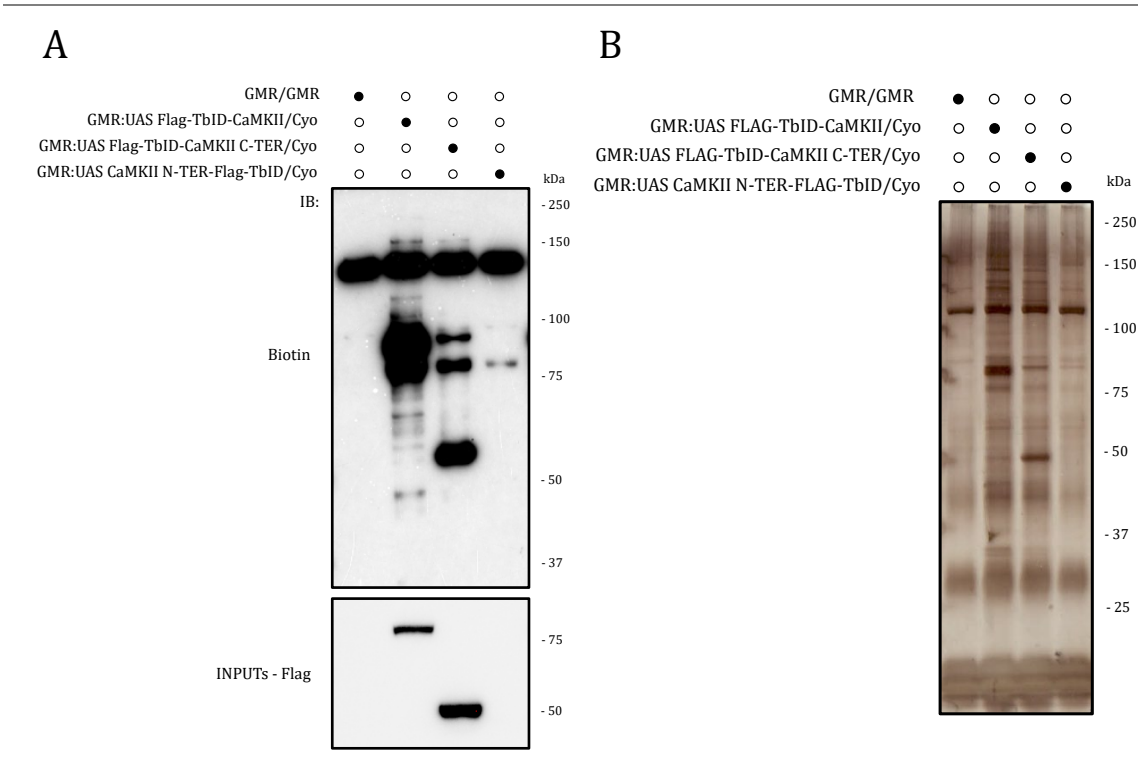

Figure 27. Biotinylation efficienty by TurboID fused to the different versions of CaMKII. Biotinylated material from head homogeneates of transgenic flies expressing TurboID-CaMKII FL, TurboID-CaMKII CTER and CaMKII NTER-TurboID under the GMRUAS promotor was enriched through a biotin pulldown. A) Biotinylation efficiency was assessed by western blot using anti-biotin antibody, whereas construct expression was checked in the input fraction with anti-Flag antibody. B) Silver staining of 10% of the eluted fraction to ensure enough material is available for mass spectrometry.

Gel pieces were chopped and subjected to in-gel protein digestion as explained before (Material and methods: Sample preparation and LC-MS/MS). In brief, proteins were reduced with DTT, alkylated with chloroacetamide and digested with trypsin. Finally, mass spectrometric analyses were performed on an EASY-nLC 1200 liquid chromatography system interfaced with a Q Exactive HF-X mass spectrometer (Thermo Scientific) via a nanospray flex ion source in the Proteomics Core Facility at the UPV/EHU (SGIker).

The mass spectrometric raw data was analysed by MaxQuant using a label-free intensity-based approach. In order to obtain a table of proteins confidently identified and quantified we filtered the data as described before (chapter I: Results: Protein identification and label-free quantitation by LC-MS/MS). As a result, we detected hundreds of proteins in the distinct replicas of FLAG-TurboID-CaMKII-FL, CaMKII NTER-FLAG-TurboID and FLAG-TurboID -CaMKII-CTER.

We checked the reproducibility of the experiment by measuring the overlapping of the proteins detected in distinct replicas of the same experimental condition and concluded that, in general terms, the overlapping is high (**Figure**

28A). In line with western blot data suggesting that FL- and NTER-CaMKIIa were the most and less efficiently biotinylated samples, we detected a total of 713, 552 and 235 proteins in FL, CTER and NTER-CaMKIIa interactome experiments, respectively. We also analysed the average Log_2 LFQ intensity of the proteins identified in 1, 2 or the 3 replicas of each experimental condition. As shown in **Figure 28B**, proteins detected in all the replicas tend to have higher Log_2 LFQ intensities than those appearing in only 1 or 2 replicas.

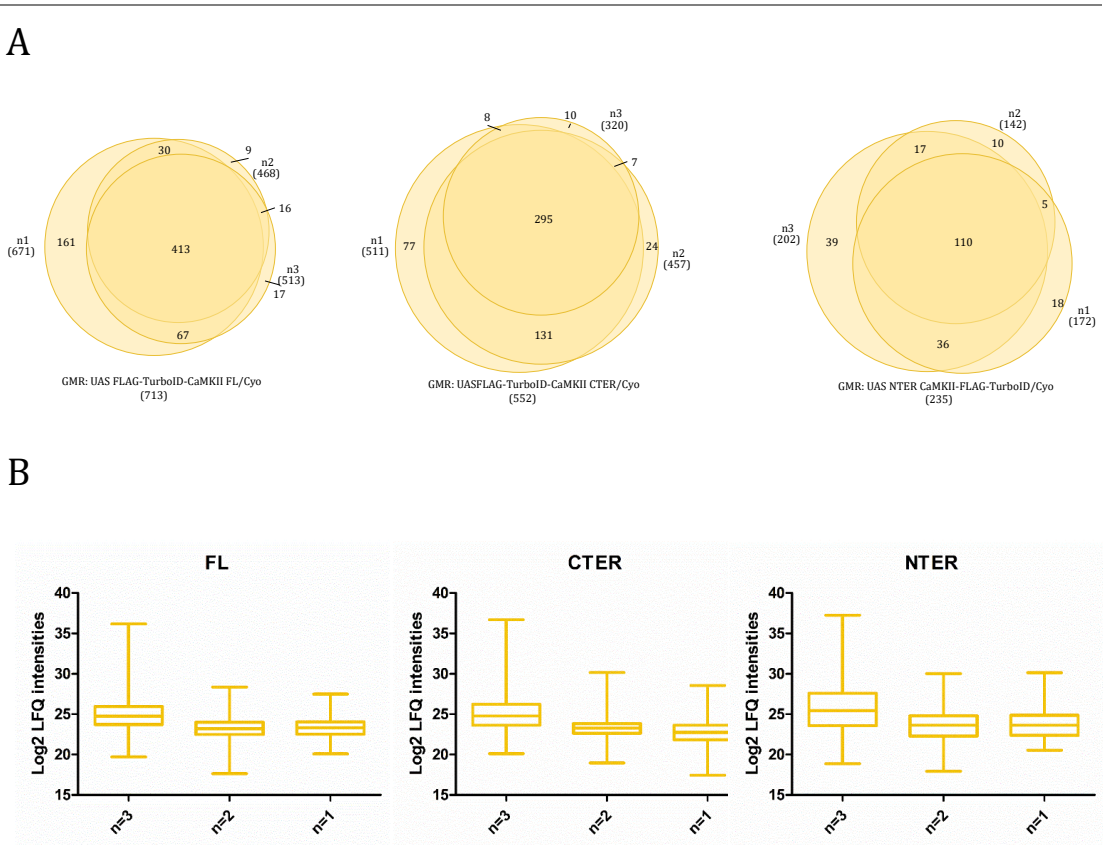

Figure 28. Overlapping between proteins detected and quantified by LC-MS/MS. A) Venn diagrams showing the overlap between the three replicas of the different samples. Between brackets the total number of identified proteins is shown. B) Box plots showing the LFQ intensities of proteins that appeared either in 1, 2 or 3 of the replicas

In addition, we analysed the overlapping between the different experimental conditions by comparing all the proteins detected in each of the experiments (**Figure 29A**). Not surprisingly, a lot of the proteins present in the FL sample were not detected in the other two conditions, but most of the proteins detected in NTER and CTER conditions were also identified in the FL. Nevertheless, few proteins, specifically 6 and 15, were exclusively detected in the NTER and CTER experiments, respectively.

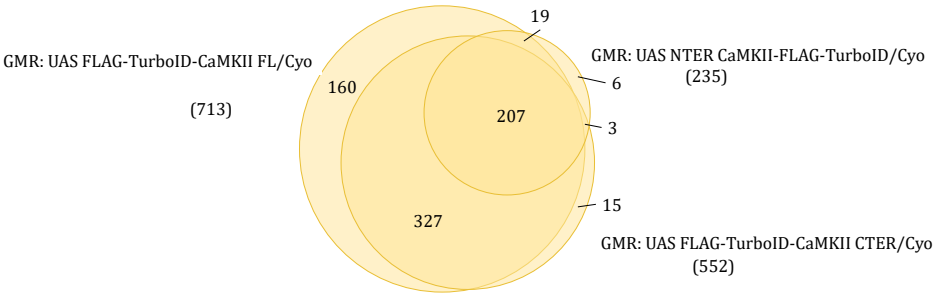

Figure 29. Similarity between samples. A) Venn diagram showing the common and unique proteins between the three conditions. Between brackets the total identified proteins is shown.

We also assessed the reproducibility of the experiment comparing the LFQ intensity of the proteins present in the different samples using Perseus (version 1.6.0.16) (**Figure 30**). On average, the correlation between the replicas of NTER, CTER and FL samples is quite high as average Pearson coefficient values are 0.911, 0.932 and 0.869, respectively. Moreover, the correlation between FL and CTER is also relatively high, whereas the correlation between NTER samples and the other two conditions is much lower.

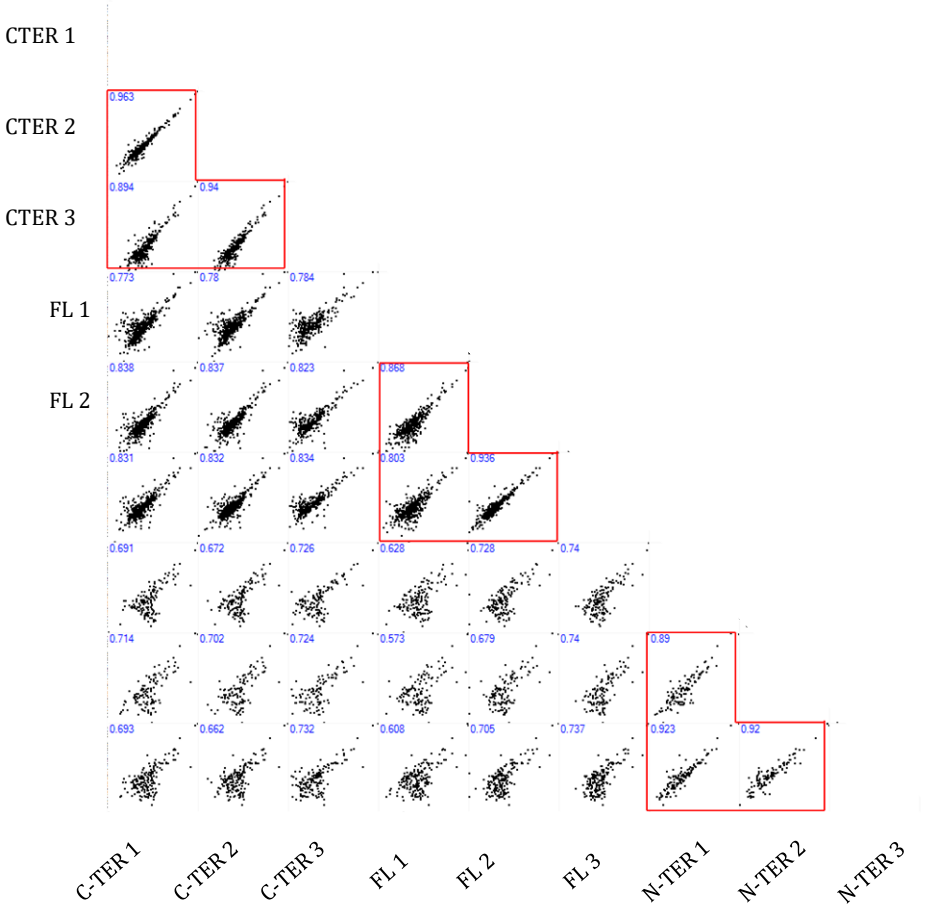

Figure 30. Reproducibility between samples. Multi-scatter plot showing the correlation between replicas. The red squares define the correlation between replicas of the same sample.

TurboID was one of the proteins detected in all samples. Nevertheless, and in line with western blot results described above, the enrichment abundance of TurboID is considerably lower in the CaMKII NTER-FLAG-TurboID sample as evidenced by the number of peptides detected, as well as the raw intensity and MS/MS counts recorded (**Table 9**).

Once having filtered the data and confirmed that all constructs, despite at different levels, were expressed in flies, data was imputed following a normal distribution in

order to assign an intensity value to the proteins that were not detected in a given sample. As shown in **Figure 31**, recorded mass spectrometric data follow a normal distribution (in green) and missing values are replaced by low LFQ values (in red). As the CaMKII NTER-FLAG-TurboID sample had fewer identifications, contained more imputed data.

Table 9. TurboID detection by LC-MS/MS. The number of TurboID-associated peptides detected on the different replicas of each sample, normalized TurboID intensity and MS/MS counts is shown.

	FLAG-TurboID-CaMKII FL	FLAG-TurboID-CaMKII C-TER	CaMKII N-TER-FLAG-TurboID
# peptides detected (replica 1, 2 and 3)	29, 26 and 25	31, 31 and 26	16, 9 and 12
Normalized Raw intensity	179	300	1
MS/MS counts (replica 1, 2 and 3)	621, 380 and 380	683, 586 and 375	52, 25 and 43

Aiming to uncover CaMKII N-terminal, C-terminal and full-length interactors, we searched for statistically significant changes between different experimental conditions. For that purpose, we performed several two-sample t-test analyses and represented the results in a volcano plot.

Endogenously biotinylated carboxylates (Pcb, Mccc1 and Acc) are considered control proteins as they report on the amount of biological material used for the pulldowns independently of the transfected constructs. By contrast, TurboID

abundance is a control of transfection efficiency across constructs. Both types of control should display a ratio of around 1 (log2 ratio ~0) and hence, should appear in the middle section of the volcano. When we compared FL and NTER experiments, TurboID was highly enriched in the FL condition indicating that the transfection efficiency was much higher in FL samples. Due to that huge difference, we decided to exclude the NTER data (**Figure 32**). On the contrary, when comparing FLAG-TurboID-CaMKII FL and FLAG-TurboID-CaMKII CTER conditions all controls mentioned above displayed a similar abundance indicating both samples were comparable (**Figure 33**).

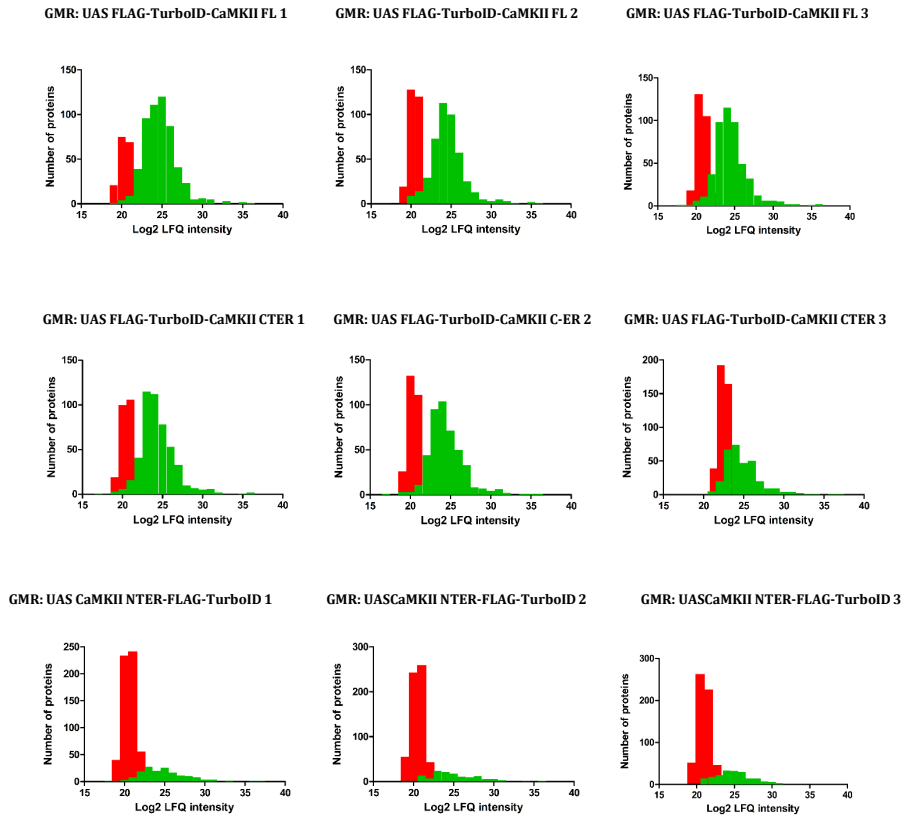

Figure 31. Distribution of LFQ values. Frequency histograms showing that LFQ follow a normal distribution. In green, number of proteins with a given LFQ intensity; In red, number of proteins with imputed LFQ intensities.

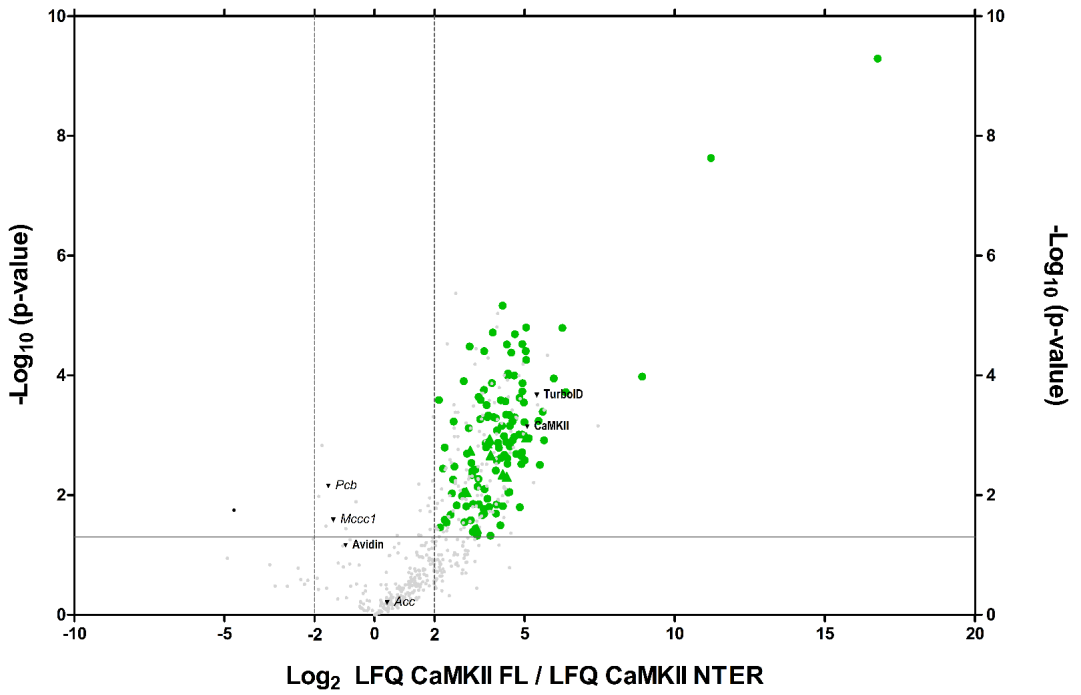

Figure 32. Volcano plot of the comparison of the FL against the NTER sample. A volcano plot in which the Log_{10} of the p-value is represented against fold change between samples. Proteins on the right are more enriched compared to the other sample and vice versa. It is remarkable the enrichment of TurboID in the FL sample compared to the NTER. TurboID, avidin, CaMKII and the carboxylases that are endogenously biotinylated are marked as controls: Pcb: Pyruvate carboxylase; Acc: Acetyl-CoA Carboxylase; and Mccc1: methylcrotonoyl-CoA carboxylase 1. Proteins displaying a LFQ fold change bigger than 4 with a p-value smaller than 0.05 are marked in green

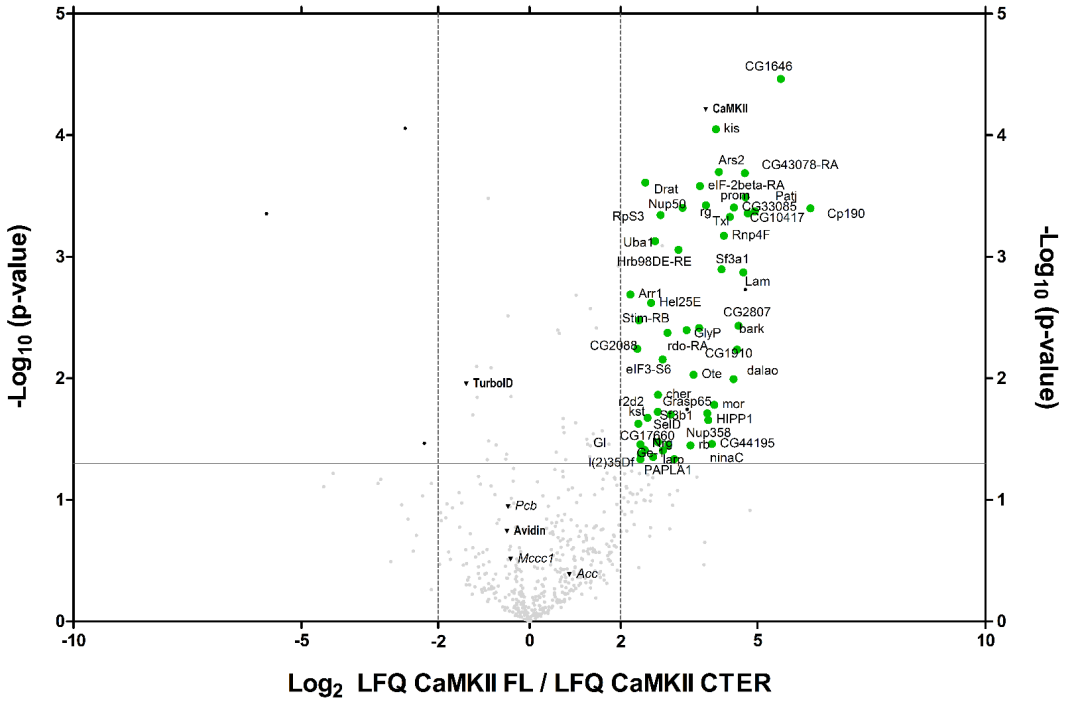

Figure 33. Proteins that potentially interact with CaMKII in *Drosophila melanogaster*. A volcano plot in which the Log_{10} of the p-value is represented against fold change between samples. Proteins on the right are more enriched compared to the other sample and vice versa. TurboID, avidin, CaMKII and the carboxylases that are endogenously biotinylated are marked as controls: Pcb: Pyruvate carboxylase; Acc: Acetyl-CoA Carboxylase; and Mccc1: methylcrotonoyl-CoA carboxylase 1. Proteins displaying a LFQ fold change above 4 with a p-value < 0.05 were considered as putative CaMKII FL binding proteins (marked in green).

From all the proteins detected in FL and CTER samples, a stringent list of potential CaMKII interactors was generated containing proteins fulfilling the following criteria: (i) be identified in all replicas of one of the conditions or at least in 2 replicas of both, (ii) display statistically significance p-value<0,05 ($-\log_{10}$ p-value>1,3), and (iii) a minimum fold change of 4 ($-2 > \log_2$ and FL/C <2). A total of 49 proteins followed these criteria and hence, were considered putative CaMKII binding partners (**Table 10**).

Table 10 Enriched proteins in the comparison of FL against CTER sample. Proteins whose abundance in the biotin pulldown is significantly enriched in the FL sample compared to the CTER sample. The human homolog genes and proteins are displayed and their localisation. CC: cellular compartment

Fly gene	Fold Change	P-value	peptides (unique)	Human homolog gene	Human homolog protein	CC
Cp190	6,2	3,4	25 (25)	SAMD15	sterile alpha motif domain containing 15	Unknown
Prp39	5,5	4,5	11 (11)	PRPF39	Pre-mRNA-processing factor 39	Nuclear
Patj	4,9	3,4	11 (11)	PATJ	InaD-like protein	Apical cell membrane
CG10417	4,8	3,4	6 (6)			
prom	4,7	3,5	16 (16)			
CG43078-RA	4,7	3,7	32 (32)			
Lam	4,7	2,9	19 (19)	LMNA	Prelamin-A/C	Nuclear
bark	4,6	2,4	32 (32)			
CG1910	4,6	2,2	11 (11)			
Bap111	4,5	3,4	6 (6)	SMARCE1	SWI/SNF-related matrix-associated actin-dependent regulator of chromatin subfamily E member 1	Nuclear
Txl	4,4	3,3	4 (4)	TXNL1	thioredoxin like 1	Cytoplasm, Nucleus, Proteasome
Rnp4F	4,3	3,2	27 (27)	SART3	Squamous cell carcinoma antigen recognized by T-cells 3	Cytoplasm; Nucleus
Sf3a1	4,2	2,9	15 (15)	SF3A1	splicing factor 3a subunit 1	Nuclear
Ars2	4,2	3,7	8 (8)	SRRT	serrate, RNA effector molecule	Nuclear
kis	4,1	4,0	7 (7)			
mor	4,1	1,8	14 (14)	SMARCC2	SWI/SNF complex subunit SMARCC2	Nuclear
CG44195	4,0	1,5	6 (6)			
HIPP1	3,9	1,7	17 (17)			
Sf3b1	3,9	1,7	39 (4)	SF3B1	splicing factor 3b subunit 1	Nuclear
rg	3,9	3,4	7 (7)	NBEA	Neurobeachin	Cytoplasm
eIF2β	3,7	3,6	4 (4)	EIF2S2	Eukaryotic translation initiation factor 2 subunit 2	Cytoplasm
Ote	3,6	2,0	8 (8)			
rb	3,5	1,4	13 (13)	AP2B1	adaptor related protein complex 2 subunit beta 1	Cell membrane
GlyP	3,4	2,4	15 (15)	PYGM	glycogen phosphorylase, muscle associated	Cytoplasm Extracellular
Nup50	3,4	3,4	6 (6)	NUP50	nucleoporin 50	Nuclear
Hrb98DE-RE	3,3	3,1	3 (3)	HNRNPA2B1	Heterogeneous nuclear ribonucleoproteins A2/B1	Cytoplasm
Mtr4	3,2	1,3	28 (28)	MTREX	Exosome RNA helicase MTR4	Nuclear
Grasp65	3,1	1,7	4 (4)	GORASP1	golgi reassembly stacking protein 1	Golgi
ninaC	3,0	1,5	11 (11)	MYO3A	Myosin-IIIa	Cytoskeleton
rdo-RA	3,0	2,4	9 (9)			
larp	2,9	1,4	16 (16)	LARP4B	La ribonucleoprotein 4B	Nuclear
eIF3e	2,9	2,2	11 (11)	EIF3E	eukaryotic translation initiation factor 3 subunit E	Cytoplasm
RpS3	2,9	3,3	10 (10)	RPS3	ribosomal protein S3	Cytoplasm, Cytoskeleton, Membrane, Mitochondrion, Mitochondrion inner membrane, Nucleus
Nup358	2,8	1,5	16 (16)	RANBP2	E3 SUMO-protein ligase RanBP2	Nuclear
cher	2,8	1,9	14 (14)	FLNA	Filamin-A	Cytoskeleton
r2d2	2,8	1,7	9 (9)			
Uba1	2,8	3,1	8 (8)	UBA1	Ubiquitin-like modifier-activating enzyme 1	Cytoplasm, Mitochondrion, Nucleus
Ge-1	2,7	1,4	10 (10)	EDC4	enhancer of mRNA decapping 4	Nuclear
Hel25E	2,7	2,6	3 (3)	DDX39A	DExD-box helicase 39A	Nuclear; Cytoplasm
kst	2,6	1,7	31 (17)	SPTBN5	spectrin beta, non-erythrocytic 5	Cytoskeleton
Drat	2,5	3,6	2 (2)	VAT1	vesicle amine transport 1	Cytoplasm
Nrg	2,5	1,4	14 (14)	NRCAM	Neuronal cell adhesion molecule	Cell membrane
Gl	2,4	1,4	22 (22)			
PAPLA1	2,4	1,3	5 (5)	DDHD2	DDHD domain containing 2	Cytosol
CG17660	2,4	1,5	4 (4)	TMEM87A	transmembrane protein 87A	Golgi apparatus membrane
Stim	2,4	2,5	8 (8)	STIM1	Stromal interaction molecule 1	Cytoskeleton
SelD	2,4	1,6	3 (3)	SEPHS1	Selenide, water dikinase 1	Cell membrane, Cytoplasm, Membrane, Nucleus
CG2088	2,4	2,2	13 (8)			
Arr1	2,2	2,7	10 (10)			

Of the mentioned 49 proteins, 47 were enriched in the FL sample. One of those proteins was CaMKII itself. This result makes sense considering that the FLAG-TurboID-CaMKII FL construct expresses full-length CaMKII and therefore, has more peptides than the CaMKII CTER expressed by the FLAG-TurboID-CaMKII CTER construct. Reassuringly, Grasp65, a known CaMKII interacting protein (Rajan et al. 2017) was also present in our final list of putative CaMKII binding proteins. Consequently, we confirmed that combining TurboID-based proximity labelling with LC-MS/MS analysis is suitable to uncover CaMKII interactors in flies.

In order to look for the processes and functions that were enriched among putative CaMKII binding partners, a gene ontology analysis was performed using DAVID functional annotation tool (Huang, Sherman, and Lempicki 2008, 2009). We detected within our putative CaMKII interactors the overrepresented gene ontology (GO) terms related to "biological process" (BP) and "molecular function" (MF) using as background the whole list of identified proteins. Among terms that were highly similar, we just kept the one with the highest fold enrichment. The only significant molecular function detected was "binding" including nucleotide binding, heterocyclic compounds binding or RNA binding, among others.

Interestingly, we found enriched biological processes such as nervous system development, memory, post-embryonic animal organ development and defence response (**Figure 34A**). Amongst these, of particular interest, the protein *rugose* is involved in both memory and central nervous system development (Shamloula et al. 2002; Wech and Nagel 2005), making it interesting for further study. Moreover, the E1 activating enzyme *Uba1* is also known to be involved in the development of

the central nervous system, as expected from being a master regulator of the ubiquitination pathway (H. Y. Liu and Pfleger 2013).

When analysing the localisation of the proteins with g:profiler, we analysed first the localisation of all the proteins that were quantified and, second, the localisation of the enriched proteins in FL-CaMKIIa condition in respect to CTER-CaMKII (**Figure 34B**). In the total and the enriched fraction, the representation of membrane proteins was similar: 38% and 40%, respectively. Interestingly, proteins that localised in the nucleus in the enriched fraction represented 48%, while in the total fraction they represented 30%, meaning that there was a 1.6-fold enrichment. Surprisingly, only 10% of the identified proteins localised to the cytosol when the representation in the whole sample was around 28%. The least represented localisation is the extracellular region (2%) which was also lowly represented in the total fraction (4%) (**Figure 34B**).

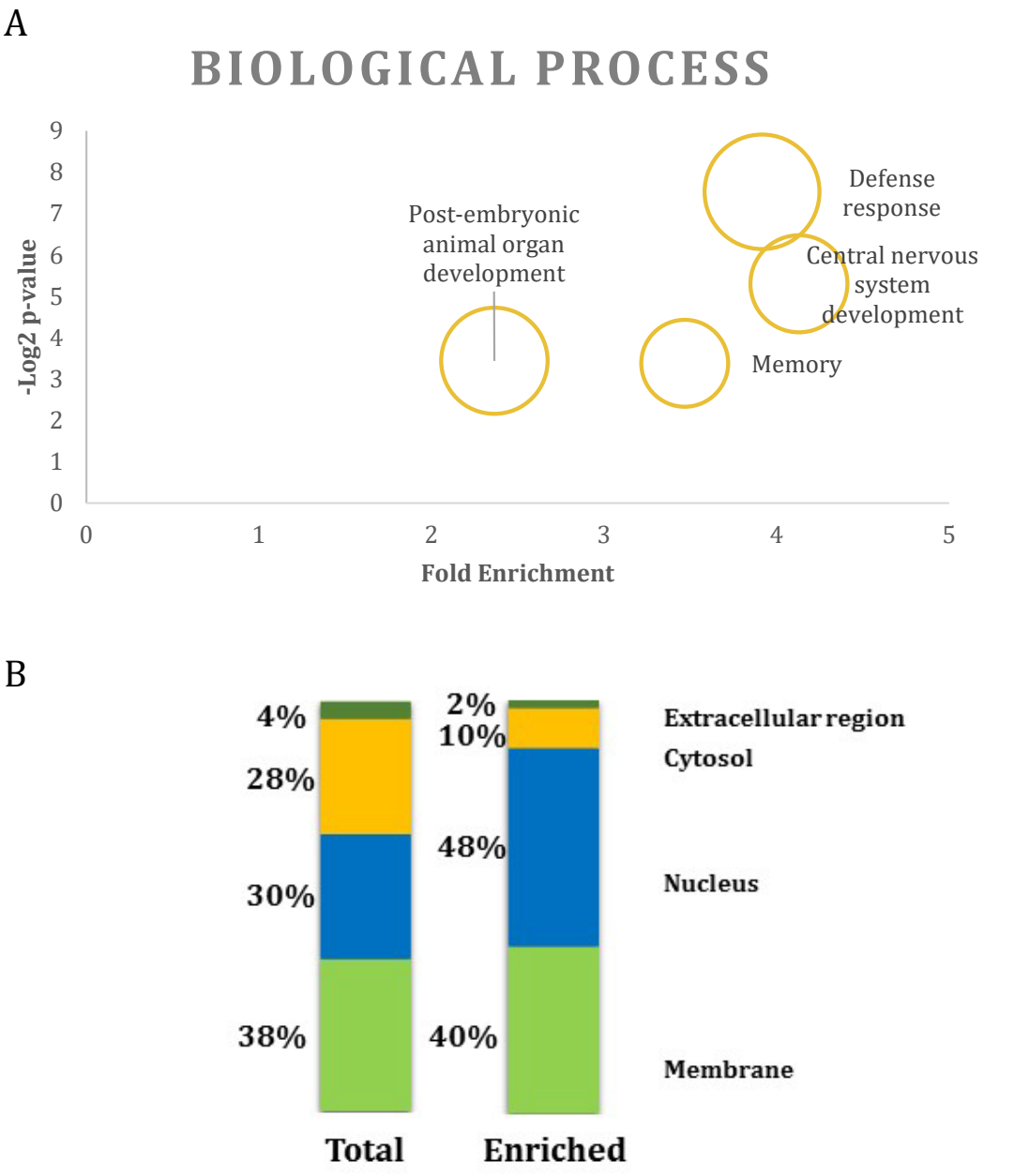

Figure 34. Functional interpretation of potential CaMKII interactors with DAVID. Potential CaMKII interactors found in *Drosophila melanogaster* were analysed with DAVID tool. As background, the complete list of the proteins detected by mass spectrometry was used. A) Representation of some of the enriched biological processes. The size of the bubbles is determined by the amount of proteins associated with that term. B) Representation of the localization of all the proteins detected in the MS analysis (left panel) and of the proteins that were enriched (right panel). Total bar represents 100% (Huang, Sherman, and Lempicki 2008; 2009).

Validation of human homologs of detected CaMKIIa binding candidates in HEK 293T cells

In *D. melanogaster* there is a single gene for CaMKII while in humans there are four different genes that encode CaMKIIa, CaMKIIb, CaMKIId and CaMKIIg. In terms of sequence, *Drosophila's* CaMKII is close to human CaMKIId, however, its functionality resembles more to CaMKIIa and CaMKIIb (Griffith et al. 1993; Saitoh and Schwartz 1985; Miller and Kennedy 1986; G. Y. Wu and Cline 1998). Therefore, our next aim was to evaluate whether putative CaMKII interactors detected in our proteomics screen performed in flies had human homologs and if they could interact with human CaMKIIa and CaMKIIb.

For that purpose, we focused our attention on fly genes that had human homolog(s) and that were functionally relevant. We found that among the 15 proteins most highly enriched in FL condition with respect to CTER there were three proteins (Txl, Rnp4f and Ars) containing human homologs (TXNL1, SART3 and ARS2, respectively) that were worth investigating. TXNL1 is involved in reducing oxidative stress during seizures in mice as it is expressed 2 or 3 times higher in the cortex of acute and chronic seizure model mice (J. T. Yu et al. 2019). ARS2 is an essential neural regulator and in its absence, mice exhibit behavioural defects (Y. Yu et al. 2020). Finally, SART3 is known to be indirectly involved in neuronal survival and dendrite growth through its interaction with APBB1, a substrate of the E3 ubiquitin ligase RNF157 (Matz et al. 2015).

To validate if the three human homologs mentioned above interact with human CaMKIIa and/or CaMKIIb, we first coexpressed the flag-tagged version of

each of them together with either GFP, GFP-CaMKIIa or GFP-CaMKIIb and performed several GFP pulldowns in mild conditions.

Importantly, none of the three putative CaMKII binding proteins coimmunoprecipitated with GFP control which was highly expressed (**Figure 35A-C**). As shown in **Figure 35A**, SART3 coimmunoprecipitates more efficiently with GFP-CaMKIIa than with GFP-CaMKIIb. This difference could be attributed to a lower expression of CaMKIIb detected by WB, but by immunofluorescence, it can be observed that both kinase isoforms are similarly expressed (**Figure 35D**). ARS2 coimmunoprecipitated similarly with both GFP-CaMKIIa and GFP-CaMKIIb suggesting it has no preference for one of the isoforms. Finally, we could not properly investigate the relationship between TXNL1 and human CaMKIIa/b as none of the kinases was expressed as evident from western blot (**Figure 35B**) and fluorescence microscopy results (**Figure 35C**).

Altogether, we found that human homologs of putative CaMKII binding fly proteins SART3 and ARS2 interact with CaMKIIa and CaMKIIa/b, respectively.

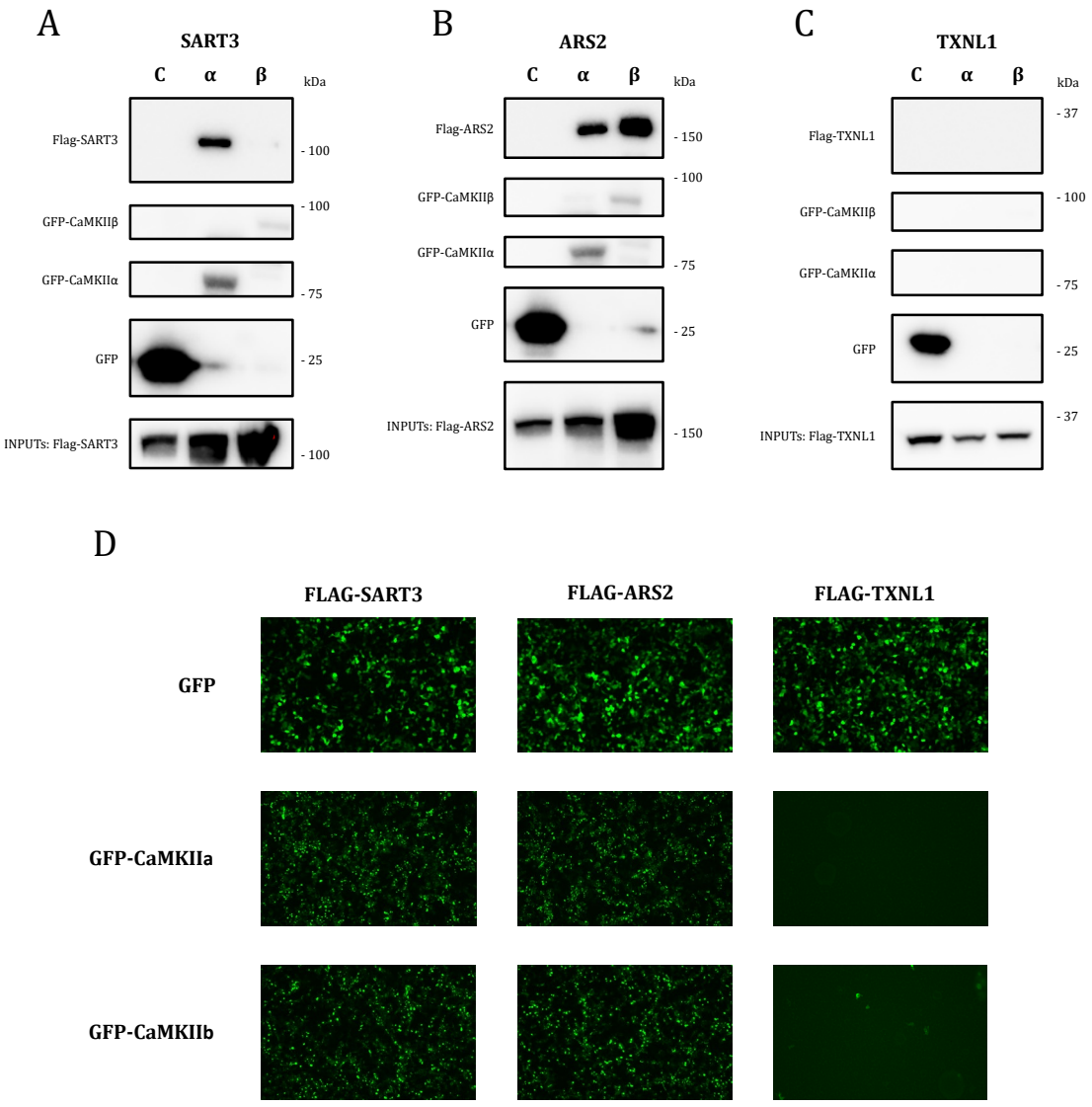

Figure 35. Validation of human TXNL1, SART3 and ARS2 with CaMKIIa and CaMKIIb. We coexpressed three potential interactors with wither GFP, GFP-CaMKIIa or GFP-CaMKIIb in HEK 293T. A) Western blot analysis of coimmunoprecipitation of SART3 with GFP, GFP-CaMKIIa and GFP-CaMKIIb. B) Western blot analysis of coimmunoprecipitation of ARS2 with GFP, GFP-CaMKIIa and GFP-CaMKIIb. C) Western blot analysis of coimmunoprecipitation of TXNL1 with GFP, GFP-CaMKIIa and GFP-CaMKIIb. D) Fluorescent microscopy images for GFP.

CaMKIIa sumoylation by the SUMO1 E3 ligase RANBP2 in HEK 293T cells

Our proteomics screen also allowed us to identify Nup358 as a potential interactor of CaMKII (**Table 10**). The human homolog for Nup358 is RANBP2, a SUMO1 E3 ligase which facilitates SUMO1 and SUMO2 conjugation on target proteins (Sakin et al. 2015; D. H. Kim et al. 2016; J. Yang et al. 2017). As it is reported that fly CaMKII is conjugated to SUMO1 *in vivo* (Long and Griffith 2000), we wondered whether RANBP2 could be involved in CaMKIIa sumoylation. To test our hypothesis, we coexpressed HA-SUMO1 together GFP-CaMKIIa and RANBP2 or UBE3A (negative control). Then, sumoylated proteins were enriched by strong GFP pulldown protocol and finally, eluted material, as well as initial inputs, were analysed by western blot.

Analysis of the inputs revealed that in both experimental conditions all constructs were properly expressed (**Figure 36** left panel). By analysing the eluted fraction with an anti-GFP antibody it was evident that GFP-CaMKIIa levels were similar in both experimental conditions, whereas the absence of an anti-HA signal indicated HA-SUMO1 was not present in none of the samples (**Figure 36** right panel). This result suggests that CaMKIIa is not sumoylated by RANBP2.

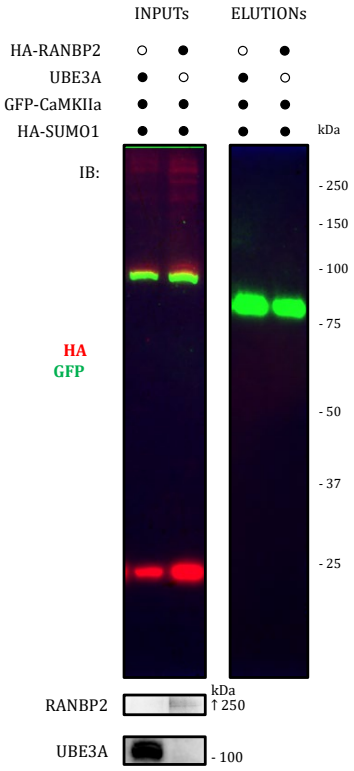

Figure 36. SUMOylation assay of CaMKIIa by RANBP2 SUMO E3 ligase. We coexpressed HA-Sumo1, and GFP-CaMKIIa with either UBE3A or HA-RANBP2. GFP-CaMKIIa was enriched by GFP pulldown. Western blot analysis showing the input fraction (left) and eluted fraction (right). HA-SUMO1 and HA-RANBP2 expression was tested with anti-HA. GFP-CaMKIIa expression was checked with anti-GFP and UBE3A expression with anti-UBE3A.

Discussion

TurboID system is a new alternative for the identification of protein interactors by proximity labelling in living organisms, in which BioID2 is not strong enough to biotinylate sufficient material (Branon et al. 2018). Indeed, TurboID has been recently successfully employed for the identification of interactors in living organisms including *A. thaliana* (Mair et al. 2019), *D. rerio* (Rosenthal et al. 2021) and *D. melanogaster* (B. Zhang, Zhang, and Liu 2019). Indeed, in the present chapter

of the thesis, we have combined the TurboID system with LC-MS/MS analysis to uncover candidate proteins interacting with CaMKII kinase in flies.

Our results corroborate that combining TurboID with mass spectrometry analysis is suitable to uncover protein-protein interactions in living organisms. Indeed, we have discovered proteins that have not been established as CaMKII interactors to date. Our results could also be employed as a basis for future groups interested in finding interactors in *Drosophila melanogaster*.

Good quality controls are always needed to achieve the set objectives and, therefore, selecting the proper negative control(s) is crucial. When working with TurboID, different strategies can be carried out. Some studies compare the interactome of the protein of interest with the proteome of a mutant version of the same protein (Hu et al. 2022). Others use as negative control another protein different to TurboID, like Cherry, fused to the bait (B. Zhang, Zhang, and Liu 2021). When using TurboID alone as a negative control, in general, researchers tend to add a signal peptide to mimic the localisation of the protein of interest (Y. Zhang et al. 2019; Teplova et al. 2021). There is an alternative in which TurboID is split into two inactive fragments that are fused to different baits that if associated together TurboID becomes active (Cho et al. 2020). For example, when studying sumoylation, split-TurboID can be fused to the substrate and to SUMO. As a consequence, if the protein gets sumoylated it will get biotinylated too. In this case, it is recommendable to employ as negative control a dead version of the substrate that cannot be sumoylated (Barroso-Gomila et al. 2021). Another option is to employ as control a part of the protein of interest (Y. Zhang et al. 2019), similar to what we have

performed in this study. We studied the interactome of FL, CTERM and NTERM CaMKII in flies but could not use the data regarding NTER CaMKII-TurboID as the expression levels of the construct were extremely low in comparison to the FL and CTER conditions. In future experiments, we should consider employing controls that have similar expression levels to avoid losing potential interactors. In case this option is not feasible, TurboID could be fused with a different protein that has a similar localisation pattern to CaMKII. In any case, even if it has been used in some investigations (Y. Zhang et al. 2019; Teplova et al. 2021), we consider employing TurboID alone as a control is not a good option. Due to the small size and high flexibility of TurboID, the construct can move very fast and localise in any compartment biotinylating a huge amount of material.

We have combined TurboID technology with label-free quantitative mass spectrometry to compare the interactome of FL and CTER CaMKII and we managed to identify 49 potential CaMKII interactors in *D. Melanogaster*. We have identified eIF3e, which mediates the internalization of the L-type calcium channel $Ca_V1.2$ in a calcium dependent-manner (E. M. Green et al. 2007) and, thus, has an indirect association with CaMKII. Additionally, among our list of putative CaMKII binding proteins is *rugose (rg)*, whose human homolog is the Autistic Spectrum Disorder (ASD)-associated protein NBEA (neurobeachin) (D. Castermans et al. 2003). Interestingly, NBEA was also detected in a crosslinking mass spectrometry-based study in synapses as a CaMKIIa interactor in one of the three hippocampal synaptosome replicas (Gonzalez-Lozano et al. 2020). NBEA shows functions that could be linked to CaMKII. On one hand, NBEA interacts with SAP102 which is

involved in AMPA and NMDA receptors trafficking during synaptogenesis (Lauks et al. 2012). Moreover, it regulates neurotransmitter receptor trafficking to synapses (Nair et al. 2013) and heterozygous mice for NBEA showed alteration in protein kinase A (PKA) activity (Nuytens, Tuand, et al. 2013). Furthermore, NBEA and its fly homolog *rg* have been associated with learning, memory and behaviour, characteristics also found in AS. Studies performed in *D. melanogaster rg* homozygous mutants exhibited aberrant associative odour learning, changes in gross brain morphology, altered locomotion, impaired adult social behaviour and synaptic architecture (Volders et al. 2012; Wise et al. 2015). Similarly, patients with NBEA variants present epilepsy and often generalized seizures (Mulhern et al. 2018). Behavioural studies of heterozygous mice for NBEA showed induction of autism-like behaviours and affection for molecular and cellular processes of synaptic plasticity (Nuytens, Gantois, et al. 2013). Additionally, NBEA has been identified as an inhibitor of the secretory of large dense-core vesicles which may be involved in the pathogenesis of autism (Dries Castermans et al. 2010). It has also been described that NBEA is upregulated in the hippocampal synapses immediately after fear memory retrieval and that the induction of the expression could be blocked by inhibiting the mTOR-dependent signalling pathway (B. Lee et al. 2018). Moreover, recent studies have identified NBEA as a possible substrate of UBE3A in mice (Lectez et al., unpublished). Altogether, it seems plausible that there is a physical and functional interaction between NBEA,

Many of the human homologs of the proteins identified as fly CaMKIIa binding partners have been associated with ASD, behavioural defects and memory. For

instance, knocking out ARS2, which we have proved interacts with human CaMKIIa and CaMKIIb, triggers specific behavioural defects in mice (Y. Yu et al. 2020). SPTBN1 loss-of-function has been associated with global developmental delay, intellectual disability, and behavioural disturbance and a subset of the studied patients showed autistic features and epilepsy (Rosenfeld et al. 2021). NrCAM is involved in neural development, axon growth and synapse formation and alterations of this protein are associated with psychiatric disorders such as autism (Sakurai 2012). TXNL1 has been shown to be involved in reducing oxidative stress during seizures in mice as it is expressed 2 or 3 times higher in the cortex of acute and chronic seizure model mice (J. T. Yu et al. 2019). Uncovering that the above-mentioned proteins are putative CaMKII interactors increase the evidence of the involvement of the kinase in ASD, behaviour and memory.

Furthermore, some of the proteins detected as potential CaMKII interactors are already known to be involved in distinct neurodegenerative diseases. For example, a rat model for Parkinson's disease has decreased levels of phosphorylated EIF2S2 -the human homolog of the *eiF2β* gene- (P. Deshpande et al. 2020), whereas patients with Alzheimer's disease exhibit aberrant AP2B1 expression levels (Sjödin et al. 2019). Additionally, the E1 ubiquitin-activating enzyme UBA1, which is also within our list of putative CaMKII interacting proteins, is impaired in several neurodegenerative conditions like Alzheimer’s disease, Parkinson’s disease, Huntington’s disease or spinal muscular atrophy (Lambert-Smith, Saunders, and Yerbury 2020; Groen and Gillingwater 2015).

Besides UBA1, there are additional potential CaMKII interactors that are somehow related to components of the UPS machinery. For instance, SART3, the human homolog of fly *Rnp4F* that we confirmed interacts with human CaMKIIa, associates with APBB1, a substrate of the E3 ubiquitin ligase RNF157 that is involved in neuronal survival and dendrite growth and maintenance (Matz et al. 2015). Our proteomics screen also uncovered fly *txl* as a putative CaMKII binding protein. We tried to validate the interaction between its human homolog TXNL1 and CaMKIIa/b and we observed that overexpression TXNL1 resulted in a reduction CaMKIIa/b levels. TXNL1 is a redox-active cofactor of the 26 S proteasome, and when it is knocked down, the ubiquitinated proteins are stabilised (K. M. Andersen et al. 2009). Therefore, we suggest that TXNL1 may be promoting CaMKIIa and CaMKIIb proteolytic degradation. Moreover, we have identified the Sumo1 E3 ligase *Nup358* as a putative CaMKII binding protein in flies, and it is documented that its human homolog RANBP2 mediates sumoylation together with Ubc9 E2-enzyme (Pichler et al. 2002). Sumoylation is a posttranslational modification in which proteins are conjugated with a ubiquitin-like protein called SUMO that plays a key role in a plethora of cellular functions including DNA damage repair, telomere maintenance, mitosis and development (Flotho and Melchior 2013; Talamillo et al. 2020). It has been reported that CaMKII sumoylation with SUMO1 is crucial in the differentiated central nervous system of *D. melanogaster but* the SUMO E3 ligase that promotes CaMKII sumoylation remains unknown (Long and Griffith, 2000). We tested whether RANBP2 could sumoylate CaMKII and concluded that it does not conjugate SUMO1 to the kinase. However, it cannot be discarded that RANBP2 mediates SUMO2-3 sumoylation as proteins can be differentially sumoylated

(Becker et al. 2013; L. C. Chen et al. 2021). In summary, we believe the results we have obtained by studying the interactome of CaMKII in flies open new research avenues. First, we have detected novel putative CaMKII interactors in *D. melanogaster*, giving the possibility of increasing the knowledge of the interaction network of CaMKII. Second, we consider that the comparison of TurboID-CaMKII flies against TurboID-Ube3a flies could allow us to identify common and unique interactors of CaMKII and Ube3a. Knowing the common interactors could shed light on the link between the two proteins and their involvement in AS. Third, further studies with NBEA should be performed as it looks like a good candidate to understand the link between CaMKIIa and UBE3A. Moreover, the role of NBEA in memory and central nervous system development makes it very interesting as it may be involved in the phenotype observed in AS patients. Fourth, once corroborated the physical interaction between human CaMKII with SART3 and ARS, their functional relationship should be elucidated.

CHAPTER III

Neurochondrin: the possible link between CaMKII and UBE3A

Summary

Recent studies identified NCDN as a putative substrate of UBE3A. Moreover, NCDN has already been described as a negative regulator of CaMKIIa phosphorylation and activity. However, whether there is a link between the three proteins remains to be assessed. A cell culture-based strategy was carried out to assay the interaction between UBE3A, CaMKIIa, and NCDN. We discovered that UBE3A can ubiquitinate NCDN but not CaMKIIa. Besides, it was found that K48-linked chains were formed in NCDN, resulting in proteasome-mediated degradation, and a subsequent reduction of NCDN protein levels. Finally, we observed that UBE3A-dependent NCDN ubiquitination is not sufficient to trigger changes in CaMKIIa phosphorylation on T286.

Introduction

To date, there is no clear link between CaMKII and UBE3A, but there is evidence that points towards a possible relationship between both proteins. Twenty years ago, it was observed that an AS mouse model with a maternal null mutation in the Ube3a gene exhibited enhanced phosphorylation on T286 and T305 of hippocampal CaMKIIa (Weeber et al. 2003). More recently, it has been shown that UBE3A associates with ASPP2, an inhibitor of CaMKII phosphatase PP1. As ASPP2 is degraded as a consequence of UBE3A-mediated ubiquitination, in the absence of UBE3A ASPP2 is accumulated, and, thereby, PP1 is inhibited and does not dephosphorylate CaMKII. Consequently, it was postulated that the levels of phosphorylated CaMKII are indirectly regulated by UBE3A (Martínez-Noël et al. 2018).

Maternal loss of Ube3a ($Ube3a^{m-/p+}$) increased PTPA levels, promoted PP2A holoenzyme assembly, and elevated PP2A activity, while maternal 15q11–13 duplication (including Ube3a) downregulated PTPA levels and lowered PP2A activity. Reducing PTPA levels *in vivo* restored the defects in dendritic spine maturation in $Ube3a^{m-/p+}$ mice (J. Wang et al. 2019).

CaMKII autophosphorylation at T286, which results in calcium-calmodulin-independent activity, is necessary for long-term potentiation (LTP) (Giese et al. 1998). It has recently been shown that CaMKII pT286 has distinct key roles in three forms of LTP (NMDAR-dependent LTP and LTD, and mGluR-dependent LTD) (Cook, Rumian, and Bayer 2022). In line with that, impaired CaMKII kinase function is involved in intellectual disabilities, developmental delay and seizure activity (Küry et al. 2017; Rhein et al. 2020; Chia et al. 2018; Akita et al. 2018)

Interestingly, mice models for AS show deficient LTP (Van Woerden et al. 2007), a process in which CaMKIIa plays a crucial role, as it translocates to the spine head of dendrites to phosphorylate AMPA receptor and stargazin when LTP is induced (Y.-P. Zhang, Holbro, and Oertner 2008; Poncer, Esteban, and Malinow 2002; Tomita et al. 2005). AMPA receptors are involved in the control of the majority of fast excitatory transmission in the brain, being LTP the most important one. LTP relies on the accumulation of AMPA receptors at the postsynapse (Díaz-Alonso and Nicoll 2021). Moreover, dephosphorylation of stargazing by calcineurin triggers long-term depression in the hippocampus as it needs to be phosphorylated to positively regulate AMPA receptor trafficking (Matsuda et al. 2013). As mentioned before, AS mouse models exhibit increased phosphorylation of the activating T286 and of the inhibitory CaMKII T305 and T306 without any alteration of total protein

levels. Persistent activation of the kinase makes it insensitive to Ca^{2+}-CaM levels and reduces its activity after the induction with Ca^{2+}-CaM. Moreover, the phosphorylation of the protein in T305 and T306 reduces its overall activity (Coultrap et al. 2010) and reduces its translocation to the postsynaptic density (PSD) (Elgersma et al. 2002). The accumulation of pT305/pT306 results in a reduction of the kinase activity and the reduction of CaMKII in the PSD (Weeber et al. 2003). Interestingly, AS models expressing T305/306 CaMKII mutants that cannot be phosphorylated recover normal LTP (Van Woerden et al. 2007). Therefore, it is accepted that inhibitory phosphorylation of CaMKIIa is important in setting the threshold for the induction of LTP, memory and other neuronal events (Elgersma et al. 2002; Elgersma, Sweatt, and Giese 2004; L. Zhang et al. 2005)

Although it is evident the interrelation between CaMKII and UBE3A and CaMKII's role in AS, to date we have not been able to unravel the cascade that connects both proteins. However, recent work from our lab has shed some light on this issue: combining a BioID2-based proximity labelling approach with label-free quantitative mass spectrometry, our research group identified Neurochondrin (NCDN) as a UBE3A substrate in mouse brains, confirming that UBE3A ubiquitinates NCDN *in vivo* (Lectez et al., under revision). NCDN is a cytoplasmic protein that is mainly expressed in the whole adult brain. Interestingly, NCDN negatively regulates CaMKII phosphorylation of T286, reducing its activity independently of PP1 or PP2A, the main CaMKII phosphatases (Dateki et al. 2005). Mutations in NCDN are associated with neurodevelopmental delay, intellectual disability and epilepsy (Fatima et al. 2021). NCDN expression is increased when LTP is induced in cultured hippocampal slices, and its overexpression triggers neurite outgrowth (Shinozaki et

al. 1997). Besides, NCDN is involved in hippocampal synaptic plasticity through the regulation of mGluR5 signalling at the dendritic spine (Hong Wang et al. 2009), and it associates with PKA at the postsynaptic density in hippocampal neurons (Ojha, Pal, and Bhattacharyya 2022).

Summarising, AS mice have a hippocampal learning deficit and the mutant phenotype can be rescued by decreasing CaMKII inhibitory phosphorylation. Altogether, NCDN seems to be a promising candidate to elucidate the relation between CaMKIIa and UBE3A that could explain the changes observed in the AS mouse model.

Hypothesis & objectives

Recently, our group discovered that NCDN, a well-known negative regulator of CaMKIIa pT286, is a substrate of the ubiquitin E3 ligase UBE3A. Therefore, we suggest that these three proteins may interact, either physically and/or functionally. Indeed, CaMKIIa can be ubiquitinated (Udeshi et al. 2013; Povlsen et al. 2012; W. Kim et al. 2011; Ramirez et al. 2018) but, to date, the E3 ubiquitin ligase responsible for it remains unknown. We speculated that UBE3A could be involved in CaMKIIa ubiquitination. As we have confirmed that NCDN becomes ubiquitinated by UBE3A, we hypothesize that UBE3A-mediated ubiquitination of NCDN might be involved in changes in CaMKIIa phosphorylation. To test the hypothesis described above, four main objectives have been defined in this section of the thesis:

- Study the interaction between CaMKIIa, NCDN and UBE3A.
- Determine whether CaMKIIa is ubiquitinated by UBE3A or not.

- Identify the ubiquitin chains that UBE3A forms on NCDN.
- Evaluate the link between UBE3A-dependent NCDN ubiquitination and CaMKIIa phosphorylation on T286.

Results

UBE3A, NCDN and CaMKIIa interact with each other

Our group recently established that NCDN is a UBE3A substrate and consequently, becomes ubiquitinated by the action of the E3 ubiquitin ligase (Letcez et al., under revision). As explained in the introduction of this chapter, there is increasing evidence that UBE3A and CaMKII are related, but the actual linkage remains elusive. We performed a preliminary experiment infecting rat cortical slices with viruses carrying BioID2-CaMKIIa expressing vectors. As control, rat cortical slices infected with an empty vector were employed. After the purification of biotinylated material through a pulldown with streptavidin, the enriched material was analysed by mass spectrometry. Preliminary results showed an enrichment of NCDN (6.1-fold enrichment compared to control slices with no infection with BioID2-CaMKIIa). This suggests CaMKIIa and NCDN to be direct interactors. Aiming to elucidate the connection between NCDN, CaMKII and UBE3A, we first aimed to analyse if the three proteins coimmunoprecipitate together in HEK 293T cells.

NCDN, CaMKII and UBE3A, either the wild type or ligase dead version, were coexpressed in pairs and altogether using the following constructs: NCDN-GFP (isoform II), GFP-CaMKII, UBE3A WT, UBE3A LD and BioID2-CaMKIIa. As control

and to discard that tags might actually induce the interactions, each of these constructs was coexpressed together with BioID2 or GFP alone.

NCDN-GFP, GFP-CaMKII and control GFP were pulled down using GFP-trap agarose beads and washed with mild conditions to purify covalent and non-covalent interactions. Enriched samples were run in a gel and analysed by western blot. As seen in **Figure 37 (inputs)**, all the constructs were expressed correctly and no big differences were detected except for the sample that coexpressed NCDN-GFP, UBE3A WT and BioID2-CaMKIIa, in which the presence of UBE3A was barely detectable. UBE3A LD appears with a single band while UBE3A WT appears with a double band, as a consequence of UBE3A autoubiquitination that is absent in the inactive enzyme. All the GFP-containing constructs were successfully pulled down (**Figure 37, elutions**). Whereas control GFP did not coimmunoprecipitate with any of the above-mentioned proteins, NCDN-GFP precipitated together with BioID2-CaMKII in all three conditions. Moreover, it seems that UBE3A WT and LD can interact with NCDN-GFP in both the presence and absence of BioID2-CaMKIIa, with UBE3A WT associating with GFP-CaMKIIa even in the absence of NCDN.

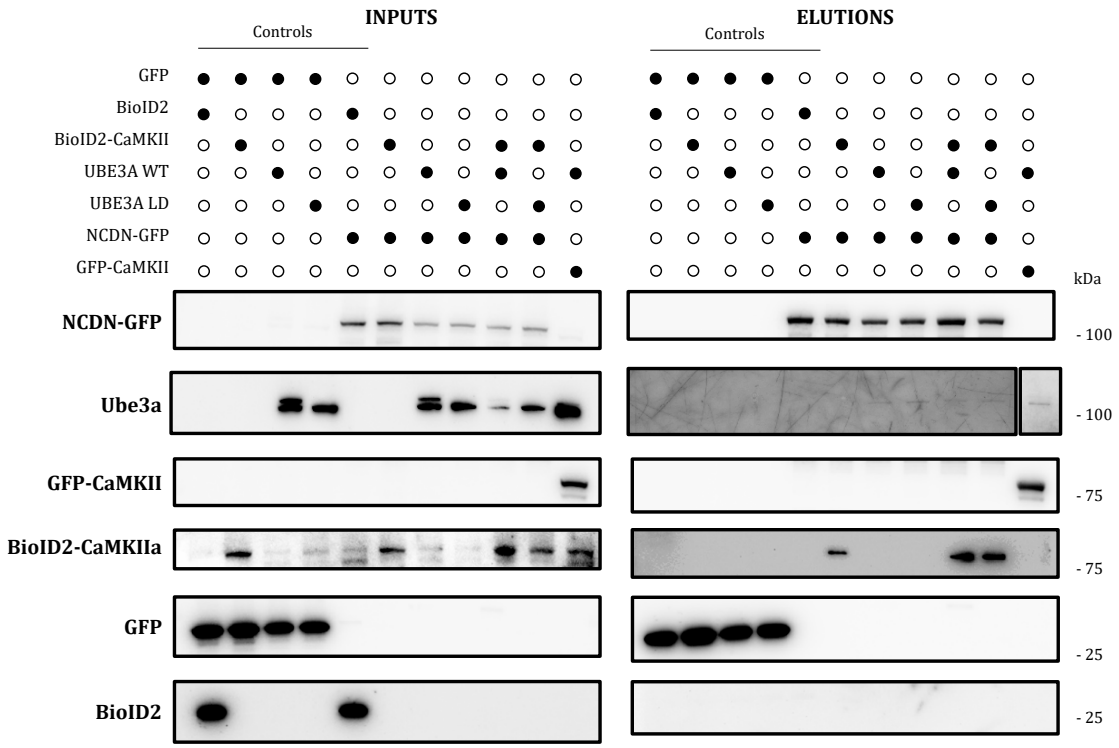

Figure 37. UBE3A interacts with NCDN and CaMKIIa, and NCDN interacts with CaMKIIa too. The inputs and the eluted fractions obtained from HEK 293T cell cultures were analysed by western blot to detect the presence of NCDN-GFP, UBE3A, GFP-CaMKIIa, BioID2-CaMKIIa, GFP and BioID2. We performed a mild GFP pulldown to enrich the GFP-tag proteins and detect the possible interactions with the other proteins. To discard the interaction between GFP with BioID2-CaMKIIa or UBE3A and BioID2 with NCDN, we cotransfected a plasmid that expressed GFP untagged with the different constructs and BioID2 untagged with NCDN-GFP (controls).

CaMKIIa is not a substrate for UBE3A

We next performed a cell-cultured-based analysis to check whether CaMKIIa is a substrate of UBE3A. We coexpressed in HEK 293T cells FLAG-Ub and GFP-CaMKIIa with either pmCherry fused to FLAG (negative control), UBE3A WT or UBE3A LD. GFP-CaMKIIa was then pulled down with GFP-trap agarose beads and stringent washes performed in order to just preserve covalent interactions such as

ubiquitination. Enriched samples were run in a gel and the presence of CaMKII and ubiquitin were monitored by western blot.

As previously observed (Chapter 1: The E3 ubiquitin ligase ITCH is responsible for CaMKIIa monoubiquitination in HEK 293T cells), coexpression with the control plasmid triggered a lower signal for FLAG-Ub in the inputs (**Figure 38A**). Moreover, no significant differences between UBE3A WT and LD levels were detected. We did not find obvious changes in GFP-CaMKIIa levels in the inputs nor in the elutions (the weaker band in the elutions for the LD sample seems to be due to transferring issues as it was not a tendency). We measured the intensity of FLAG-Ub relative to GFP intensity both in UBE3A WT- and LD-expressing samples and, as no significant differences were detected (**Figure 38B**), we determined that UBE3A does not ubiquitinate CaMKIIa.

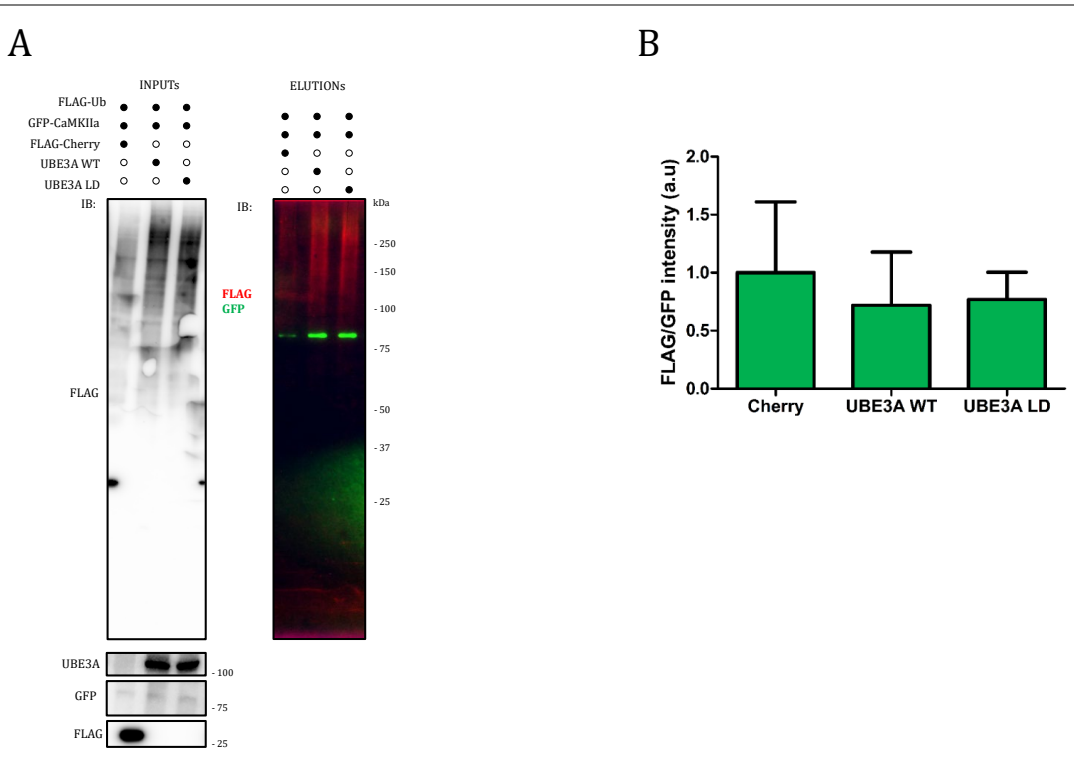

Figure 38. CaMKIIa is not a substrate of UBE3A. We coexpressed FLAG-Ub and GFP-CaMKIIa with either FLAG-Cherry, UBE3A WT or UBE3A LD. GFP-CaMKIIa was purified through a GFP pulldown. A) Western blot of the input and the eluted fraction of the GFP pull down. In the inputs (left), the expression of Flag-Ub and Cherry-Flag were detected with mouse anti-Flag-M2-HRP conjugated antibody, whereas UBE3A and GFP-CaMKII were detected with mouse anti-UBE3A and anti-GFP antibodies, respectively. In the elutions (right), the ubiquitinated versions of GFP-CaMKIIA were detected with mouse anti-Flag-M2-HRP conjugated antibody and non-ubiquitinated GFP-CaMKIIa was observed with mouse anti-GFP antibody. **B)** Bar graph showing the Flag/GFP intensity of the five different samples. Intensity was normalised to the Cherry control (n=4; two-tailed p-value; error bars denote SEM)

UBE3A targets NCDN with K48 polyubiquitin chains presumably to be degraded

Our lab has recently uncovered that UBE3A ubiquitinates NCDN (Benoit et al., under revision) but the ubiquitin chain types that were formed could not be detected. Thereby, we performed an *in vitro* assay in HEK 293T cells to identify the type of ubiquitin linkage(s) UBE3A builds on NCDN.

For that purpose, NCDN-GFP and UBE3A WT were cotransfected with five different versions of HA-Ub: HA-Ub WT, HA-Ub K0, HA-Ub K48R, HA-Ub K63 and HA-Ub K48. The HA-Ub K0 construct has all lysines capable of generating chains mutated to arginine, whereas HA-Ub K63 and HA-Ub K48 constructs only conserve the specified lysine and hence, can only build K63 and K48 linkages, respectively. By contrast, HA-Ub K48R expresses a mutant version of ubiquitin that can form any type of ubiquitin linkage but K48 chains. NCDN-GFP was pulled down using GFP-trap agarose beads and stringent washes were performed to purify only covalent

interactions. As before, enriched samples were run in a gel and analysed by western blot.

As observed in the left panel in **Figure 39A**, in all the inputs the intensity of NCDN-GFP and the 9-kDa band corresponding to HA-Ub was quite similar. However, the intensity of HA-Ub K0 polyubiquitin chains (smear) was, obviously, very low because this construct prevents the extension of ubiquitin chains. The HA-Ub WT and the HA-Ub K48R samples did show more intensity that could be triggered due to the higher expression levels we saw in the single ubiquitin band. The remaining three constructs did not show big differences in HA-Ub expression at a chain-forming level. Interestingly, in the eluted fractions, the smear corresponding to ubiquitinated NCDN observed in the control sample (HA-Ub WT) was dramatically reduced in HA-Ub K0, K48R and K63 expressing samples, and recovered to higher than WT levels when HA-Ub K48 was expressed (**Figure 39A**). A prominent monoubiquitination band was observed for NCDN in all three constructs capping K48-chain linkages. This band being weaker in the two constructs allowed further K48-chain extension. We quantified the smear of all samples, normalized them to the corresponding GFP signal, and compared them by a student t-test analysis to conclude that the reduction of NCDN ubiquitination detected in HA-Ub K0, K48R and K63 samples, as well as the ubiquitination increase observed in HA-Ub K48 expressing cells were statistically significant (**Figure 39B**). Besides, we were able to detect a decrease in NCDN-GFP intensity in the eluted fraction of HA-Ub WT and HA-Ub K48 samples compared to the other three (**Figure 39C**). These results suggest that UBE3A forms K48-ubiquitin chains on NCDN and triggers NCDN degradation.

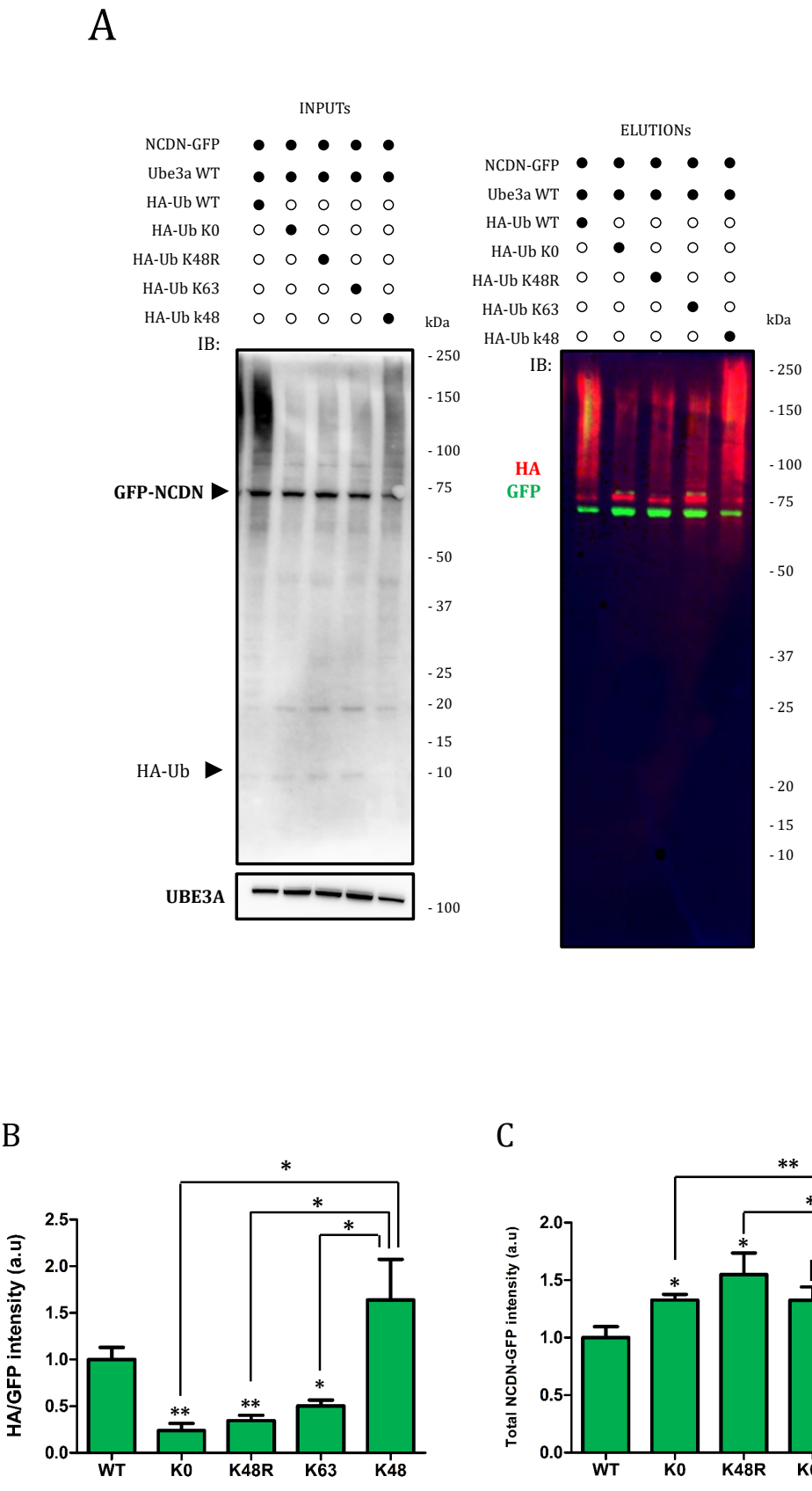
A
INPUTs
NCDN-GFP
Ube3a WT
HA-Ub WT
HA-Ub K0
HA-Ub K48R
HA-Ub K63
HA-Ub k48
kDa
IB:
- 250
- 150
- 100
- 75
- 50
- 37
- 25
- 20
- 15
- 10
GFP-NCDN
HA-Ub
UBE3A
- 100
ELUTIONs
NCDN-GFP
Ube3a WT
HA-Ub WT
HA-Ub K0
HA-Ub K48R
HA-Ub K63
HA-Ub k48
kDa
IB:
HA
GFP
- 250
- 150
- 100
- 75
- 50
- 37
- 25
- 20
- 15
- 10
B
HA/GFP intensity (a.u)
2.5
2.0
1.5
1.0
0.5
0.0
WT
K0
K48R
K63
K48
C
Total NCDN-GFP intensity (a.u)
2.0
1.5
1.0
0.5
0.0
WT
K0
K48R
K63
K48

Figure 39. UBE3A triggers de formation of K48-ubiquitin chains on NCDN. We coexpressed NCDN-GFP and UBE3A WT with either HA-Ub WT, K0, K48R, K63 or K48. NCDN-GFP was purified through a GFP pulldown. A) Western blot of the input and the eluted fraction of the GFP pull down. In the inputs (left), the free-ubiquitin monomer (10 kDa) and the formed chains (smear) were detected with mouse anti-HA antibody. NCDN-GFP expression was observed with mouse anti-GFP antibody. Apparently, no changes in NCDN-GFP expression was detected in the inputs. In the elutions (right), the ubiquitinated forms of NCDN-GFP were identified with mouse anti-HA antibody and non-ubiquitinated NCDN-GFP was observed with mouse anti-GFP antibody, detecting lower intensity in the WT and K48 samples. B) Bar graph showing the HA/GFP intensity of the five different samples. Intensity was normalised to the WT sample (n=4; * p-value < 0.05; ** p-value < 0.01; two-tailed p-value; error bars denote SEM) C) Bar graph showing the total levels of non-ubiquitinated NCDN normalised to the WT sample. (n=3; *p-value < 0.05; **p-value < 0.01; two-tailed p-value; error bars denote SEM).

Analysis of the ubiquitination sites of NCDN by UBE3A

Once having proved that UBE3A promotes the formation of K48-linked chains on NCDN, we aimed to define the lysine(s) on which ubiquitins are conjugated. To determine which of the 25 lysines of NCDN are modified by ubiquitin, we expressed in HEK 293T cells NCDN-GFP together with either WT or LD UBE3A. Then, NCDN-GFP was purified employing GFP-trap agarose beads, washed using stringent conditions (Material and methods: GFP stringent pulldown) and eluted fractions were run in a gel that was stained with coomassie blue. The gel was cut so that the monoubiquitinated and the polyubiquitinated versions of NCDN-GFP were separated. Subsequently, each gel piece was subjected to in-gel digestion and extracted peptides were analyzed by LC-MS/MS. In the analysis of MS-derived raw data using Maxquant, diGly (GlyGly) was selected as variable modification in order to detect ubiquitination events, not only on NCDN but also within the ubiquitin itself.

Finally, by comparing the intensity of diGly peptides corresponding to NCDN in both experimental conditions, the lysines that are being ubiquitinated can be inferred. Similarly, the comparison of ubiquitin diGly peptides could shed light on the ubiquitin chain linkages that are formed on NCDN.

First, we analysed the intensity of NCDN, ubiquitin and the rest of the proteins that were detected both in UBE3A WT- and LD-expressing samples. As expected, bearing in mind that NCDN-GFP was purified employing GFP-trap agarose beads, NCDN was the most abundant protein in both experimental conditions (**Figure 40A**). Interestingly, endogenous ubiquitin was the second most abundant protein detected, despite not being expected, but appeared less intense in the UBE3A LD condition than in the UBE3A WT sample (**Figure 40B**).

Second, we focused on the diGly peptides detected in NCDN. Based on our proteomics data, six lysines located in the N-terminal (K47 and K54) and central region (K214, K255, K266 and K371) of the protein were ubiquitinated (**Figure 41**). In order to determine whether UBE3A is responsible for ubiquitinating these specific sites on NCDN, we compared the intensity of diGly peptides recorded in WT and LD UBE3A samples, as UBE3A-dependent ubiquitination events should be compromised in UBE3A LD-expressing condition. As observed in **Figure 41**, the intensity of K54-, K214- and K266-containing diGly peptides were comparable in both conditions, indicating UBE3A did not modify such lysines. By contrast, we observed that the ubiquitination of K371 was reduced in the UBE3A LD sample. However, when checking the intensity of each of the replicas of each of the samples, we observed that K371 bearing diGly peptide was detected in a single UBE3A LD

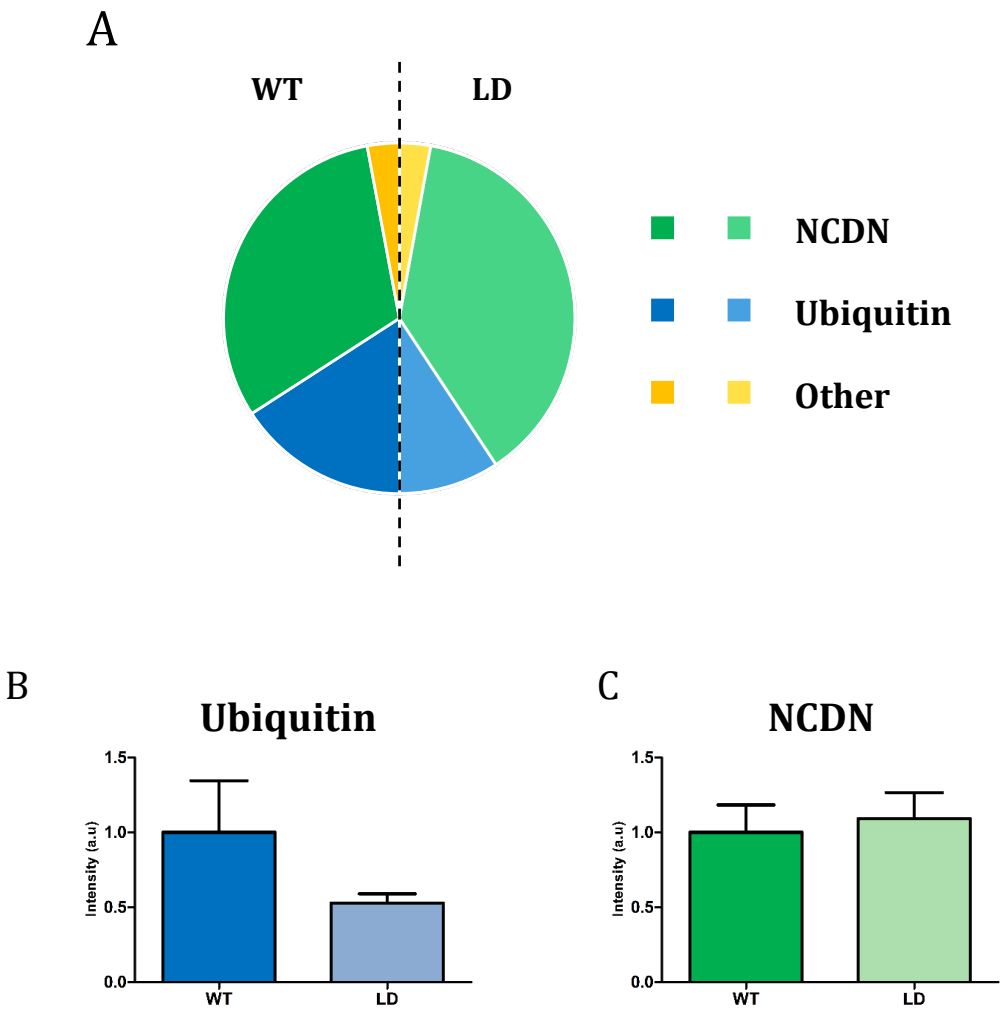

Figure 40. Distribution of the intensity of NCDN, Ubiquitin and the other identified proteins in the WT and LD samples. A) We performed a GFP stringent pulldown to enrich NCDN-GFP with its ubiquitinated forms. Samples were analysed through mass spectrometry to determine the formation of diGly peptides. The total intensities of each protein were added and the percentage of the total was calculated. Green: NCDN; Blue: Ubiquitin; Yellow: Other. B) Intensities of Ubiquitin of the three replicas for WT and LD conditions. (n=3; two-tailed p-value; error bars denote SEM). C) Intensities of NCDN of the three replicas for WT and LD conditions. (n=3; two-tailed p-value; error bars denote SEM).

replica, which displayed an intensity of $2.1x10^8$, similar to the intensity recorded in the distinct UBE3A WT replicas. Thus, we concluded that the reduction observed was not reliable. NCDN K255 containing diGly peptide was also more intense in the UBE3A WT condition, suggesting that UBE3A might be involved in its ubiquitination. Nevertheless, as the diGly peptide was only detected in 2 (2 WT and 0 LD UBE3A) out of the 6 replicas analysed, we decided not to consider it. Finally, and contrary to what we could expect, the K47-bearing diGly peptide was less intense in the UBE3A WT sample. However, the difference was not statistically significant.

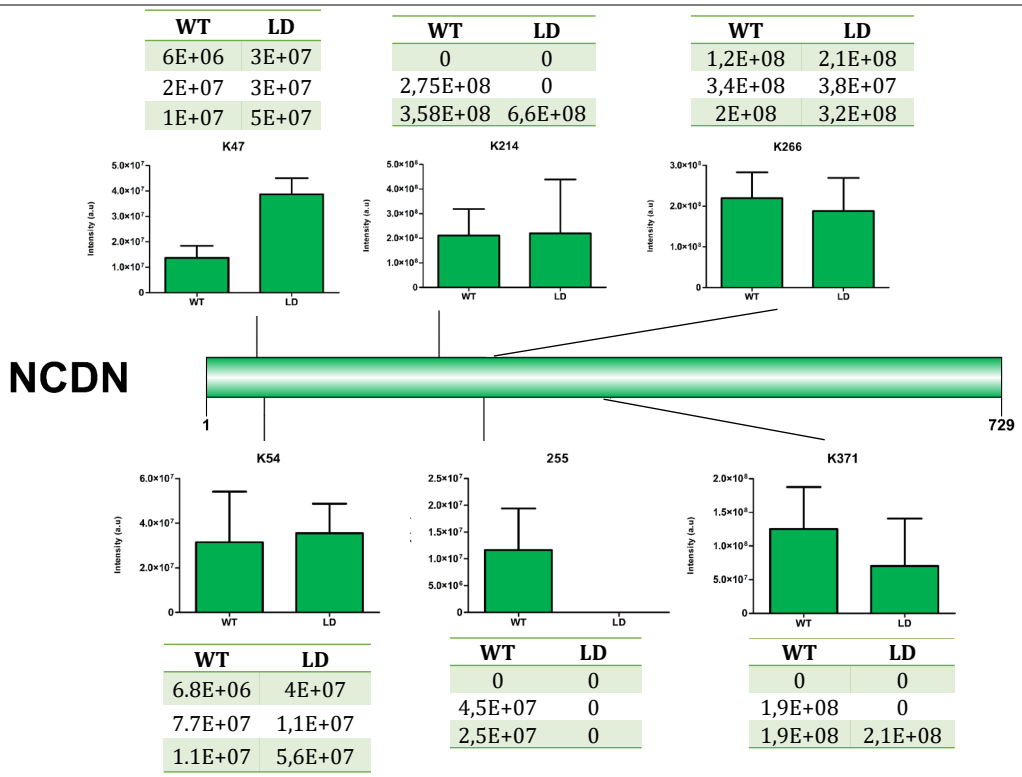

Figure 41. Differences in intensity of ubiquitination of NCDN's lysines 47, 54, 214, 255, 266 and 371. We performed a GFP stringent pulldown to enrich NCDN-GFP with its ubiquitinated forms. Samples were analysed through mass spectrometry to determine the formation of diGly peptides and study the levels of ubiquitination of the lysines in NCDN sequence. (n=3; p-value > 0.05; two-tailed p-value; error bars denote SEM). The tables above the bar graphs show the intensities determined in the MS analysis.

We also analysed the intensity of ubiquitin diGly peptides in order to infer ubiquitin chains formed on NCDN to try to validate our previous western blot results suggesting UBE3A forms K48 ubiquitin chains on NCDN (**Figure 42**). The intensity of diGly peptides containing K11, K33 and K29 was comparable in WT and LD UBE3A-expressing conditions, indicating UBE3A is not involved in their ubiquitination. As before, K6- and K27-containing ubiquitin diGly peptides were detected in only 2 (2 UBE3A WT samples) out of the 6 samples analysed and K63 only in 1 of the replicas, so we decided not to rely on these data (**Figure 42**). However, K48-linked ubiquitin chains were detected in all replicas but in one LD UBE3A condition. In line with our previous results, K48-bearing diGly peptide was more intense in WT UBE3A condition, suggesting UBE3A builds K48-type ubiquitin linkages in NCDN. Nevertheless, the difference measured by label-free quantitative mass spectrometry was not statistically significant.

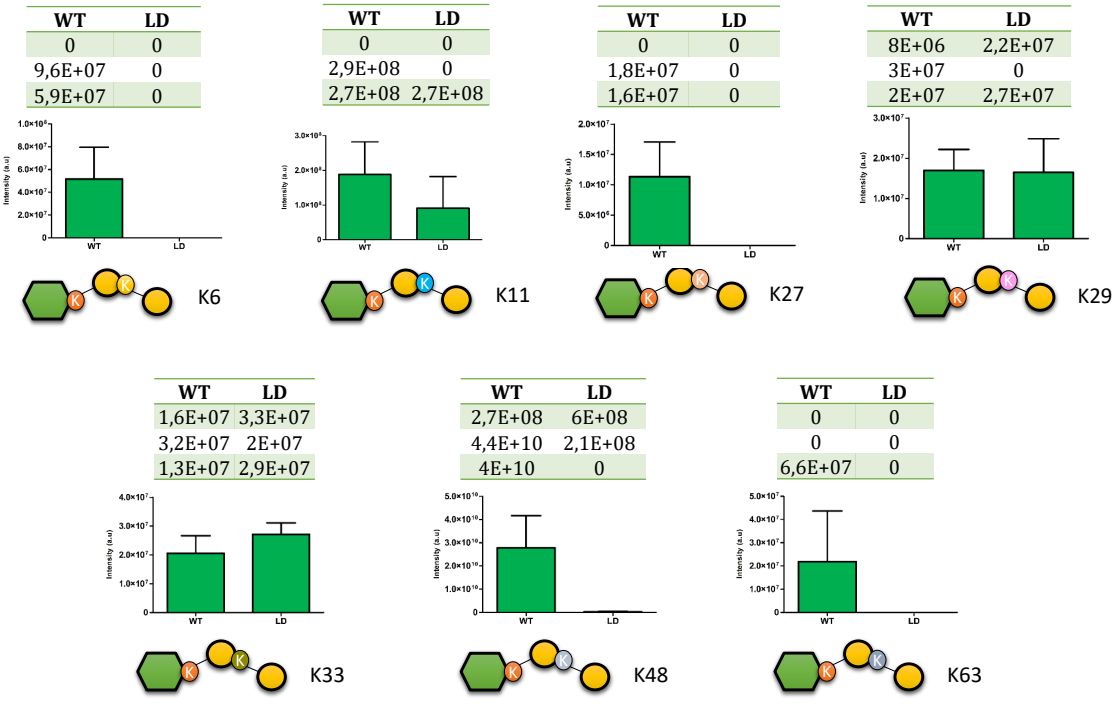

Figure 42. Differences in the intensity of ubiquitin chains. We performed a GFP stringent pulldown to enrich NCDN-GFP with its ubiquitinated forms. Samples were analysed through mass spectrometry to determine the formation of diGly peptides and to study the ubiquitin chains that were being formed on NCDN. (n=3; p-value > 0.05; two-tailed p-value; error bars denote SEM). The tables above the bar graphs show the intensities determined in the MS analysis.

Effect of UBE3A-dependent NCDN ubiquitination on CaMKIIa pT286

Our data described above suggest that UBE3A mediates K48-linked ubiquitination on NCDN. It is well known that NCDN negatively regulates CaMKIIa phosphorylation on T286 (Dateki et al. 2005). Therefore, we decided to test whether the ubiquitination status of NCDN could somehow affect CaMKIIa phosphorylation. To do so, we coexpressed in HEK 293T cells GFP-CaMKIIa, NCDN-GFP, UBE3A and HA-Ub WT or K48R that cannot form K48-linkages. Once we confirmed that all constructs were expressed correctly (**Figure 43A, input**), we enriched CaMKIIa by stringent GFP pulldown protocol from cells expressing WT ubiquitin and cells unable to form K48-type ubiquitin chains in which NCDN is less ubiquitinated. As shown in **Figures 43A and B**, total GFP-CaMKIIa levels, as well as pT286 CaMKIIa levels were comparable, suggesting that the ubiquitination status of NCDN does not affect the phosphorylation status of CaMKIIa.

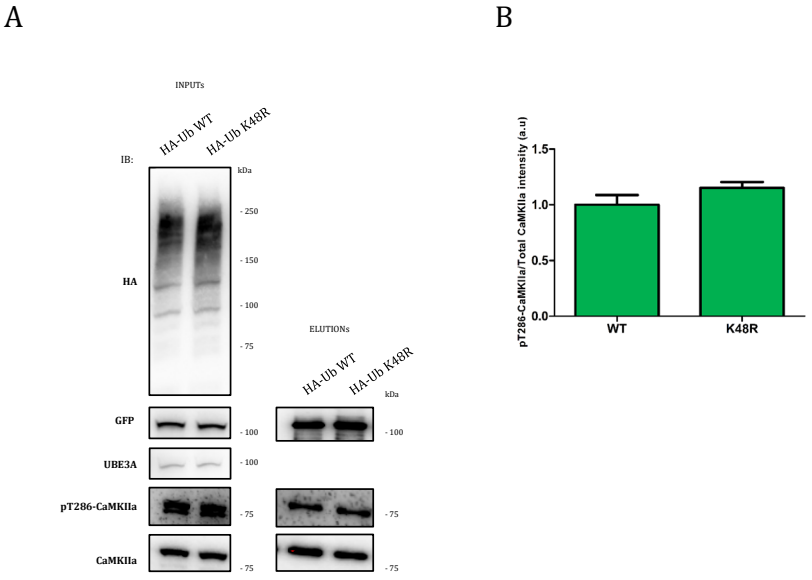

Figure 43. Formation of K48-linked chains on NCDN by UBE3A is not sufficient to alter CaMKIIa phosphorylation on T286. We coexpressed NCDN-GFP, GFP-CaMKIIa and UBE3A WT with either HA-Ub WT or K48R. NCDN-GFP and GFP-CaMKIIa were enriched through a GFP pulldown. A) Western blot of the input and the eluted fraction of the GFP pull down. In the inputs (left), the formed ubiquitin chains (smear) were detected with mouse anti-HA antibody. UBE3A expression was detected with anti-UBE3A. In the inputs and the elutions, NCDN-GFP expression was observed with mouse anti-GFP antibody and GFP-CaMKIIa and phosphorylated GFP-CaMKIIa expression was detected with anti-CaMKIIa and anti-phospho-CaMKII (T286), respectively. Apparently, no changes in NCDN-GFP, total GFP-CaMKIIa or phosphorylated GFP-CaMKIIa expression were detected in the inputs. B) Bar graph showing phosphoCaMKIIa (T286) normalised to the total levels of CaMKIIa. Intensity was normalised to the WT sample (n=3; p-value > 0.05; two-tailed p-value; error bars denote SEM).

Discussion

NCDN is a cytoplasmic protein that is mainly expressed in neuronal, chondral and bone tissues (Shinozaki et al. 1997; Ishizuka et al. 1999). Furthermore, it localises in the dendrite and somatic regions of neurons from the developing cerebellum, suggesting a role in dendrite outgrowth (Shinozaki et al. 1999). After

the induction of the LTP, the expression of NCDN is increased in the hippocampus (Shinozaki et al. 1997). NCDN is involved in hippocampal synaptic plasticity through the regulation of mGluR5 signalling at the dendritic spine (Hong Wang et al. 2009), and it associates with PKA at the postsynaptic density in hippocampal neurons (Ojha, Pal, and Bhattacharyya 2022). Mutations in NCDN are associated with neurodevelopmental delay, intellectual disability and epilepsy (Fatima et al. 2021). Thus, it was not surprising to identify NCDN as a putative substrate of UBE3A (Lectez et al. under revision).

As NCDN is a negative regulator of CaMKII activating phosphorylation of T286 through an alternative pathway for PP1 and PP2, which are the main phosphatases that dephosphorylate CaMKII (Dateki et al. 2005), we suggested that crosstalk between CaMKII, NCDN and UBE3A might be occurring.

Preliminary results of the interactome of CaMKIIa in rat cortical slices suggest that NCDN and CaMKIIa might be interacting. Nevertheless, we did not detect Ncdn as a CaMKII interactor in flies. The reason might be that fly neurochondrin is only expressed in the reproductive and in the muscle systems (Montana and Littleton 2006; Ajayi et al. 2022) while our $GAL4^{UAS}$ system used to uncover CaMKII binding proteins was expressed in fly eyes. On the contrary, rat NCDN's function is similar to the one carried out by human NCDN and it also localises to the neurons (Y. Xu et al. 2017).

In the experiments performed with HEK 293T cells, we have observed through coimmunoprecipitation followed by western blot detection that (i) CaMKIIa interacts with NCDN and UBE3A, (ii) UBE3A interacts with NCDN and (iii) the three

of them are pulled down together when coexpressed. However, it is uncertain to determine whether the three proteins interact through independent dimers or form a trimer. Indeed, according to our results, the amount of UBE3A precipitated is comparable in the experiments in which UBE3A is coexpressed only with NCDN and CaMKII but also when the three proteins are expressed together. Moreover, compared to the input levels, the eluted fraction of UBE3A is quite low, suggesting that the interaction with the other proteins is fast and transient. In the case of NCDN, it is what we expected as ligase-substrate interactions occur during a short lapse of time and these types of interactions are difficult to be detected by traditional PPI approaches (Qin et al. 2021).

Similarly, we could identify the interaction between CaMKIIa and UBE3A as a transient and weak one, and, therefore, we studied the possibility of CaMKIIa being a substrate of UBE3A. However, our results showed that this was not the case. To date, the only E3 ubiquitin ligase that has been associated with CaMKIIa is ITCH, which monoubiquitinates CaMKIIa as we have demonstrated in the 1st chapter of this thesis.

UBE3A-dependent ubiquitination can exert non-degradative functions including protein endocytosis (Sun et al. 2015; Avagliano Trezza et al. 2021). Nevertheless, UBE3A tends to form degrading K48-ubiquitin chains on its substrates (H. C. Kim and Huibregtse 2009). For instance, UBE3A-dependent PTP1 ubiquitination and degradation regulate PP2A phosphatase activity and dendritic spine morphology (J. Wang et al. 2019) whereas UBE3A ubiquitinates and targets p18 for proteasomal degradation to regulate mTOR activity and synaptic plasticity (Sun et al. 2018). In line with that, our MS results suggest that UBE3A forms K48

ubiquitin chains on NCDN. More interestingly, we revealed by western blot detection that NCDN levels are reduced as a consequence of UBE3A-dependent K48 ubiquitination.

To date, different studies have revealed seven lysines in the NCDN sequence (isoform 1) that might be ubiquitinated: K47, K61, K92, K272, K283, K412 and K483. However, no functional analysis has been performed as all studies are high throughput analyses focused on ubiquitination site detection (Udeshi et al. 2013; W. Kim et al. 2011; Akimov et al. 2018; Wagner et al. 2011; Povlsen et al. 2012). We have detected 6 ubiquitination sites on NCDN. Three of them are already known (K47, K255 (K272 in isoform 1) and K266 (K283 in isoform 1) but more interestingly, for the first time we demonstrate that K54, K.214and K371 on NCDN can be ubiquitinated. Ubiquitination on K47 showed higher intensities in the LD sample, the opposite effect we swould expect if this site was ubiquitinated by UBE3A. Quantitative data was not very conclusive as many replicas did not display an intensity value. However, a tendency was observedin the ubiquitination of K371, suggesting that this lysine might be ubiquitinated by UBE3A. Therefore, we think that repeating the experiment with more material would beneficial due to the number of missing values Additionally, future assays mutating the identified lysines on NCDN and testing whether ubiquitination by UBE3A is prevented or not should be performed. This kind of assay has already been performed by our group with positive results for the protein DDI1 (Elu et al. 2019).

Regarding CaMKIIa, we have not detected significant differences in CaMKIIa pT286 levels when we coexpressed NCDN with either HA-Ub K48R or HA-Ub WT. However, we believe that the employed system was not the most suitable one. In the

future, experiments should be performed in a more adequate environment, such as in neuronal cultures and instead of analysing overexpressed CaMKIIa, endogenous kinase should be analysed. Once determined the exact lysines of NCDN that are modified with ubiquitin by UBE3A, we could perform mutagenesis experiments on those lysines to generate NCDN constructs that cannot be ubiquitinated by this E3 ubiquitin ligase. By replacing the endogenous WT version of NCDN with any of these mutants in hippocampal primary cultures (Beaudoin et al. 2012), we should then be able to test whether NCDN ubiquitination by UBE3A affects endogenous CaMKIIa phosphorylation and, therefore, CaMKIIa activation.

CHAPTER IV

How to inactivate human ubiquitin E3 ligases by mutation

Abstract

E3 ubiquitin ligases are the ultimate enzymes involved in the transfer of ubiquitin to substrate proteins, a process that determines the fate of the modified protein. Numerous diseases are caused by defects in the ubiquitin-proteasome machinery, including when the activity of a given E3 ligase is hampered. Thus, inactivation of E3 ligases and the resulting effects at molecular or cellular level have been the focus of many studies during the last few years. For this purpose, site-specific mutation of key residues involved in either protein interaction, substrate recognition or ubiquitin transfer have been reported to successfully inactivate E3 ligases. Nevertheless, it is not always trivial to predict the mutation(s) that will block the catalytic activity of a ligase. Here we review over 250 site-specific inactivating mutations that have been carried out in 120 human E3 ubiquitin ligases. We foresee that the information gathered here will be helpful for the design of future experimental strategies.

Introduction

Ubiquitin is a 76-amino-acid protein, highly conserved among eukaryotic organisms (Zuin, Isasa, and Crosas 2014), used –through the ubiquitin-proteasome system- to regulate many cellular processes. Proteins are covalently modified on their Lys residues with ubiquitin via amide isopeptide linkages (Laney and Hochstrasser 1999). Frequently, ubiquitinated proteins are targeted for degradation through the proteasomal system on an ATP hydrolysis-dependent manner (Hershko and Ciechanover 1998; Komander and Rape 2012). But protein ubiquitination participates in a plethora of additional cellular responses including

regulation of gene expression, cell signalling, cell cycle, DNA repair and apoptosis (Pickart 2001; Gilberto and Peter 2017).

The ubiquitination reaction requires the coordinated action of three types of enzymes termed E1, E2 and E3. First, ubiquitin is activated with ATP in a process carried out by an activating E1 enzyme. Once ubiquitin is activated, it is transferred to the Cys on the active site of a conjugating E2 enzyme. Finally, ubiquitin is generally linked to a Lys of the target protein through an isopeptide bond, formed between the C-terminal carboxyl group of ubiquitin and the ε-amino group of the Lys. Substrate specificity in ubiquitination is attributed to E3 ligases, which are able to interact with both the ubiquitin-charged E2 and the substrates to be modified (Metzger et al. 2014). Like most post-translational modifications (PTMs), ubiquitination is reversible and deubiquitinating enzymes (DUBs) are responsible for hydrolysing the isopeptide bond between ubiquitin and substrate proteins or between ubiquitin molecules.

Proteins can be modified by ubiquitin in a wide range of manners. For instance, in addition to Lys, ubiquitin can be conjugated via a peptide bond to the N-terminal amino group of the substrates (Ciechanover and Ben-Saadon 2004), as well as to Cys or Ser/Thr residues by thio- or oxy-ester bonds, respectively (X. Wang, Herr, and Hansen 2012). Substrates can be mono-ubiquitinated, meaning modified in a single residue by only one ubiquitin. Multi-mono-ubiquitination occurs when several residues of a given protein are simultaneously modified with one ubiquitin each. Poly-ubiquitination occurs when the C-terminus of another ubiquitin associates to one of the seven Lys (Lys6, Lys11, Lys27, Lys29, Lys33, Lys48 and Lys63) or the N-terminal Met (Met1) on the previously added ubiquitin molecule.

Consequently, a ubiquitin chain is formed on the target protein. Depending on how ubiquitin residues are bound together, different ubiquitin chain architectures can be formed: (i) homogenous, if the Lys used throughout the chain is the same (*e.g.* Lys48-linked chains), (ii) heterogeneous, if they alternate (*e.g.* Lys48-Lys11-linked chains) and (iii) branched, if multiple Lys of the same ubiquitin are modified at the same time. Altogether, ubiquitin can generate a huge number of different types of modifications on any given protein (Komander and Rape 2012). Consequently, ubiquitin-mediated cellular responses will depend not only on the specific residues of the substrate that are modified but also on the topology of the ubiquitin chains that are formed.

Eukaryotic cells express hundreds of ubiquitin E3 ligases, which can operate in different cellular contexts, respond to numerous cellular signals, and process diverse protein substrates (Ning Zheng and Shabek 2017). Ubiquitin E3 ligases have been classically classified in two different groups, based on conserved structural domains and the mechanism by which ubiquitin is transferred: RING (really interesting new gene)-type E3s and HECT (homologous to the E6AP carboxyl terminus)-type E3s. Whereas RING E3 ligases directly transfer the ubiquitin from the E2-ubiquitin complex to the substrate (**Figure 1A** in the INTRODUCTION), HECT-type E3s transfer ubiquitin to their own catalytic Cys before linking it to the substrate (**Figure 1B** in the INTRODUCTION) (Deshaies and Joazeiro 2009). Additionally, a third group of E3s, that combines features from both RING- and HECT-type E3 families, has been established: the RING between RING (RBR) family (**Figure 1C** in the INTRODUCTION). RBR and RING E3s share RING binding domains,

but RBR family members have the ability to generate a thioester intermediate with ubiquitin, as HECT-type E3s do (Morreale and Walden 2016).

Typically, one E3 ligase is able to modify several substrates, as well as to bind different E2s. The same protein can, therefore, be ubiquitinated by different E2/E3 combinations, which will lead to different ubiquitination patterns (Metzger et al. 2014). Substrate recognition by HECT-type E3 ligases depends on protein-protein interactions that are mediated by specific motifs typically located in the N-terminal of the HECT domain (Scheffner and Kumar 2014). Substrate recognition by RING-type E3s is achieved either through regions of the E3 other than the RING domain, in the case of monomeric E3s, or through substrate recognition elements in other domains, in the case of multi-subunit RING E3s (Metzger et al. 2014). On the other hand, some studies have reported that substrate proteins have a short linear sequence, known as degron, important in the regulation of protein degradation rates. Not all degron are ubiquitin-dependent, but if they are, it appears that they facilitate the recognition of the substrate protein by the E3 ligase. Degrons can be modified by kinases and other enzymes. These modifications appear to be crucial for timing the interaction between E3 and substrate, even though they are not always necessary and many substrates of HECT-type E3s and CRLs are able to recognise their substrates in their native forms (Rotin and Kumar 2009; Kamadurai et al. 2009; Muńoz-Escobar et al. 2015; Kanelis, Rotin, and Forman-Kay 2001; Fukutomi et al. 2014). In order to increase the specificity towards their substrates, many E3 ligases, such as TRIMs, are able to form homo- and heterodimers and recognise multiple degrons located in the same substrate (Yang Li et al. 2014).

Moreover, the effect is summatory and a robust degron may have the same effect as two weak degrons (Welcker et al. 2013).

The role mediated by E3 ligases is so crucial, that their activity must be tightly controlled in order to ensure they solely act when necessary. Oligomerisation is one of the mechanisms that modulate the activity of HECT- and RING-type E3s. For instance, structural studies suggest that the trimeric arrangement of E6AP activates the ligase (Ronchi et al. 2014), whereas homodimerisation of the HECT domain of HUWE1 results in enzyme inactivity (Sander et al. 2017). RING-type E3s can act as independent enzymes, but most of them tend to form homo- or heterodimers, and even more complex multi-subunit assemblies in order to mediate ubiquitination (Metzger et al. 2014). For instance, RING E3 ligases cIAP, RNF4, BIRC7, IDOL, CHIP and Prp19 homodimerize, and RING domains of both units interact with E2 proteins. By contrast, RING-type E3 ligases BRCA1-BARD1, Mdm2-MdmX and RING1B-Bmi1 form heterodimers. While BRCA1 and Mdm2 have the ability to interact with E2 proteins, their partners do not. But they function as enhancers of ligase activity and interact with substrates (Brzovic et al. 2001; Cao, Tsukada, and Zhang 2005; Hengbin Wang et al. 2004; Joukov et al. 2001).

In this review we aim to provide a detailed description of mutations in ubiquitin E3 ligases, with the outlook that such detailed and structured catalogue of mutants will provide a pattern to be considered by future researchers when designing new mutations on their E3 ligases.

Mutations on RING-type E3 ligases

RING-type E3s are conserved from yeast to human. It is estimated that the human genome encodes above 600 different RING-type E3s. The RING domain was first characterised by Freemont and colleagues (Freemont, Hanson, and Trowsdale 1991). The canonical sequence for this 40-60 amino acid long domain is Cys-X_2-Cys-$X_{(9-39)}$-Cys-$X_{(1-3)}$-His-$X_{(2-3)}$-Cys-X_2-Cys-$X_{(4-48)}$-Cys-X_2-Cys. The conserved Cys residues (7 in total) and the single His are disposed in a "cross-brace" topology to coordinate two zinc ions and stabilise its structure (**Figure 2** in the INTRODUCTION) (Deshaies and Joazeiro 2009).

Initially, the role of RING domains was uncertain, although it was known they were involved in protein-protein interactions as well as in a wide range of cellular processes (Deshaies and Joazeiro 2009). However, it was not until 1997 that the function of RING domains was elucidated by Bailly and coworkers (Bailly et al. 1997). Moreover, in 1999, Joazeiro and coworkers observed that the adapter protein c-Cbl bears two domains that act coordinately to mediate ubiquitination and subsequent degradation of substrates. Whereas the SH2 domain of c-Cbl served to recognize specific substrates, the RING domain was necessary to recruit and activate an ubiquitin-conjugating E2 (Joazeiro et al. 1999). After that, a similar role was conferred to a number of RING domain-containing proteins (Lorick et al. 1999). At present, it is accepted that the RING domain present in all RING E3s associates and activates E2-Ub conjugates promoting the direct transfer of ubiquitin from the E2 to the target protein (**Figure 1A** in the INTRODUCTION).

The interaction between the RING domain of E3 ligases and E2s was first elucidated with the crystal structure of Cbl's RING domain bound to UbcH7 E2 (N Zheng et al. 2000). The combination of many structural studies allowed the characterization of the four residues of each protein that play a crucial role in the interaction, those are shown in green in **Figure 2** in the INTRODUCTION. Located between Cys residues C_1 and C_2 of the RING domain, a hydrophobic residue (Ile, Leu or Val) interacts with two Pro residues from the E2. Those two prolines are localised in one of the two loops that compose the accessible surface of the E2 enzyme. Additionally, another hydrophobic residue (typically Trp, His or Leu) from the E3 interacts with a Phe and a Pro present on the second loop of the E2. Simultaneously, this Pro interacts with a Pro of the E3 located between Cys residues C_6 and C_7. Which,in turn, is also connected to an Ala localised in the same loop of the E2. Finally, this same Ala of the E2 also interacts with a hydrophobic amino acid (typically Val, Phe or Ile) located straight after the Pro between C_6 and C_7 of the E3 (Deshaies and Joazeiro 2009).

More recently, structural studies focused on RING-type E3:E2-Ub complexes have revealed the mechanism by which this class of ubiquitin ligases facilitates Ub transfer to substrate proteins. The E2-Ub complex has a flexible topology with multiple inter-domain configurations that are altered upon E3 binding (Pruneda et al. 2011). More precisely, binding of RING E3 reduces the dynamics of E2-Ub and stabilizes in an ensemble of closed conformations. This modification facilitates the reactivity for substrate Lys that can perform the corresponding nucleophilic attack (Soss, Klevit, and Chazin 2013; Pruneda et al. 2012). Studies carried out on dimeric E3s such as RNF4 or BIRC7 also support the same mechanism by showing that a

positively charged residue (Arg or Lys) conserved in many RING E3s just straight after the last zinc-coordinating Cys supports the non-covalent interaction with the E2-Ub complex (Dou et al. 2012; Plechanovov et al. 2012).

As mentioned above, although some RING-type E3s act independently, they have the tendency to form homo- and heterodimers. Most RING-type E3s dimerise through their RING domain, such as RNF4 homodimers or MDM2/MDMX and BRAC1/BARD1 heterodimers (Liew et al. 2010; Linke et al. 2008; Brzovic et al. 2001). Nevertheless, there are exceptions. For instance, MARCH9 E3 ligase can form active dimers with RING-less variants (Hoer, Smith, and Lehner 2007), whereas viral RING-type E3s MIR1 and MIR2 are believed to homodimerise via their transmembrane domain (Lehner et al. 2005). The tripartite motif (TRIM) family members in metazoans contain an additional domain termed B-box. Like the above mentioned RING domain, the B-box domain is a zinc-binding domain. However, whereas the RING domain is essential for E2 binding and E3 ligase activity, it has recently been shown that the B-box domain is involved in chain assembly rate modulation (Lazzari et al. 2019). Similarly, the U-box domain is also related to the RING domain, but unlike the B-box, it can interact with E2s. Additionally, the U-box domain has no coordinating zinc, so in order to ensure the stability of the structure, zinc-binding residues present in RING are replaced by charged and polar residues (Vander Kooi et al. 2006; Aravind and Koonin 2000).

Inactivating RING-type E3s by mutating the zinc-coordinating residues

Since the coordination of the two atoms of zinc by the RING domain is crucial for E3 ligase activity, mutants that abolish such coordination have often been used

to create ligase-dead versions of those E3 enzymes. Mutation of any of the conserved Cys and His involved in zinc binding should compromise the E3 activity, and so have all been, individually or jointly, mutated for that purpose (**Figure 44**). The mutated residue of choice to prevent E3 ligase activity appears the first conserved Cys (C_1) of the RING domain, followed by the His (H), C_2, C_3 and C_4. To our knowledge, C_7 is the only key residue on the domain that has not been individually mutated for this purpose. However, it has been shown that simultaneous mutations on either C_1+C_7 or C_6+C_7 abolish the ligase activity of AMFR and some TRIM family members, respectively (Q. Wang et al. 2014; J. M. Lee et al. 2018; B. Liu et al. 2017). As shown in **Figure 44**, many E3 ligases have been inactivated by simultaneous mutations on C_1+C_2. Less frequently, additional double mutations and even the triple C_1+C_2+C_3 mutant have been efficiently applied to block the activity of distinct RING-type E3 ligases (**Figure 44**).

Zinc-coordinating Cys and His residues have been preferentially mutated into Ala in order to abolish the ubiquitin ligase activity of E3s (**Figure 44**). Nevertheless, in some cases, this type of substitution might be insufficient. In a recent research focused on studying TRIM27-dependent ubiquitination of UPS7, it was shown that a quadruple TRIM27 mutant, in which four zinc-coordinating residues of the RING domain (Cys16, Cys19, Cys31 and Cys33) were mutated into alanine, was still capable of ubiquitinating USP7. By contrast, the TRIM27 mutant, in which four zinc-binding residues of the B-box (Cys96, Cys99, His107 and Asp110) were simultaneously substituted by Ala, was incapable of ubiquitinating USP7 (not illustrated in **Figure 44**) (Zaman et al. 2013). Moreover, it should be taken into account that in some cases a dominant negative effect may be acquired by the

mutated E3 ligase. For example, CBL Cys381Ala mutant is not capable of ubiquitinating EGFR and thus, the subsequent desensitization of the receptor is abolished. However, CBL Cys381Ala mutant is still capable of interacting with EGFR, and consequently, competes with wild type CBL compromising CBL-mediated EGFR ubiquitination (Waterman et al. 1999). Similarly, the plant E3 ubiquitin ligase SINA1 mutant on the C_2 of the RING domain Cys47Ser mutant retains dimerisation and substrate binding ability but lacks ubiquitination activity (den Herder et al. 2012).

Despite less frequently, in a number of investigations, the Cys involved in zinc coordination have also been efficiently mutated into serine. Indeed, this type of point mutation that results on E3 ligase inactivation has served to uncover, among others, the role of MDM2, RNF8 and SIAH1 RING E3s in cell cycle regulation, DNA damage response and Wnt signalling, respectively (Tian et al. 2017; Tripathi and Smith 2017; Ji et al. 2017). Additionally, although there are fewer examples, it has been demonstrated that mutating the His into Glu, Tyr or Arg is sufficient to inactivate the ligase activity of MKRN1, RNF2 and RNF43 E3s, respectively (M. S. Lee et al. 2018; Xia et al. 2014; Loregger et al. 2015) (**Figure 44**). Similarly, it has been shown that mutating C_2 of RAD18 and CBL into Phe and Arg, respectively, as well as substituting C_3 of CNOT4 into Arg or C_6 of RAG1 into Tyr has an inhibitory effect (S. A. Williams et al. 2011; Javadi et al. 2013; Albert et al. 2002; Jones and Gellert 2003). It should be noted, however, that in search of structure-function relationships, the safest approach is to mutate into the smaller Ala residue (Fersht, 1999). Introducing larger residues might -in addition to preventing the coordination of the zinc- result in further distortions on the overall fold of the protein.

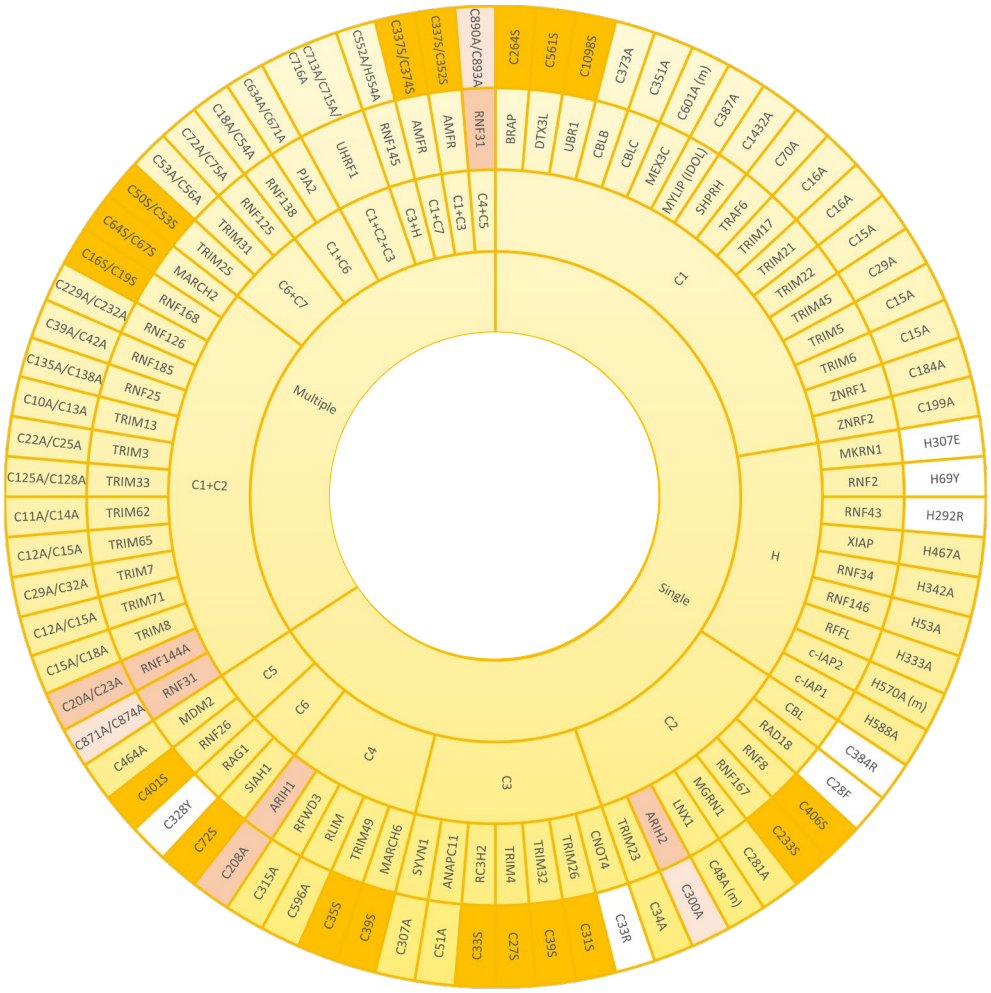

Figure 44. Mutations that alter zinc coordinating residues in RING domains. Wheel diagram showing the reported mutations in RING domains, classified first whether a unique (single) or various (multiple) residues were mutated simultaneously. Most of the inactive E3 enzymes have been obtained by mutating key residues into alanine (yellow). Lack of activity can also be acquired by mutations into serine (orange). Mutations into other residues have been also employed (white). Zinc coordinating residues of the first (pink) and the second (light pink) RING domains in RBR-type E3 ubiquitin ligases (pink) have also be modified in order to achieve inactivation. References to all the mutations shown in this figure are provided in **Table S1**.

Especially in the absence of the molecular structure, deciding the residues that should be mutated might not always be straightforward, but appropriate sequence alignments can provide sufficient insight. For instance, TRIM37 has two adjacent Cys residues (Cys36 and Cys37) that could correspond to the C_4 involved

in zinc coordination (Supplementary **Figure S3**). Therefore, to ensure the inactivation of the enzyme, both Cys were simultaneously mutated (Kallijärvi et al. 2005; W. Wang et al. 2017). Similarly, ZNRF4 has two His nearby (His329 and His332) and in principle, either of them could be involved in coordinating zinc atoms. Once again, both His were mutated in order to obtain a catalytically inactive form of the E3 (Bist et al. 2017). Based on metal-binding studies, MDM2 His457 was initially confirmed to be the conserved His involved in zinc-coordination (Lai et al. 1998). Nevertheless, His452 is also essential, as demonstrated in auto-ubiquitination assays of this E3 ligase, with both His residues being necessary (Fang et al. 2000). As it has been elucidated later on, and can be seen in the sequence alignment in **Figure 45B**, His452 actually takes the place of the conserved Cys C_3 in the zinc coordination.

Additionally, there are few E3s bearing RING domains in which a non-conserved amino acid plays an indirect but pivotal role in the coordination of the zinc atom, and therefore, can be mutated in order to disrupt the activity of the ligase. For example, Thr455, which was originally believed to be directly involved in the zinc-coordination based on an incorrect primary sequence alignment, has been reported to abolish -upon its mutation- MDM2-dependent p53 ubiquitination (Boddy, Freemont, and Borden 1994, Fang et al. 2000).

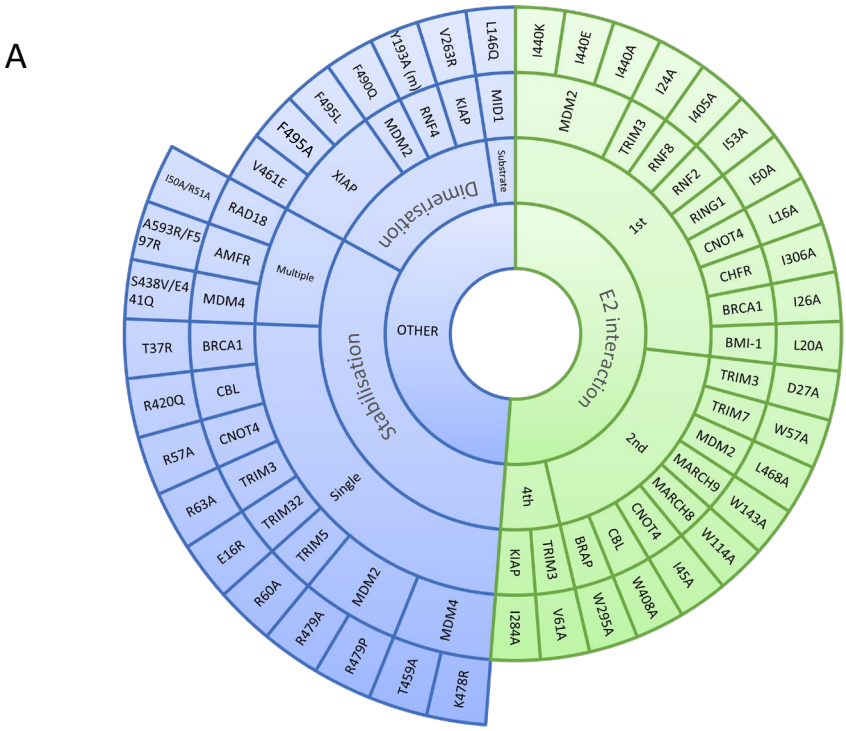

Figure 45. Mutations on RING- and RBR-type E3s that affect E2-interaction, domain stabilisation, protein dimerization or substrate recognition. A) In RING-type E3 ubiquitin ligases, inactivation can be obtained by abolishing the interaction with E2 ubiquitin-conjugating enzymes (green). This has mostly been achieved by mutating the conserved 1st (I/L) and 2nd (W/I/L) hydrophobic residues indicated in Figure 2. Other mutations affecting the stabilisation of key residues of the domain, dimerization or the interaction with a specific substrate also abolish the ligase activity (blue). For the stabilisation affecting muations, those have been classified

whether a unique (single) or various (multiple) residues were mutated simultaneously. References to all the mutations shown in this figure are provided in **Table S1**. B) Alignment of the RING domains of the RING-type E3 ligases involved in E2-interacting and stabilisation mutations within the RING domain. Conserved amino acids are highlighted in yellow and orange, respectively, for the Zn-coordinating Cys and His residues, and in green for the E2-interacting residues. The conserved positively charged residues at the end of the RING domain are highlighted in blue. Mutated E2-interacting residues are shown in bold and underlined. Mutated residues involved in stabilisation are shown in bold. Mutated residues involved in dimerisation are underlined and shadowed.

Inactivating RING-type E3s by mutating the E2-interacting residues

It has previously been described that RING E3s interact with E2-Ub conjugates via their RING domain to directly transfer the ubiquitin to the substrate protein. Therefore, disrupting the interaction between E2s and RING-type E3s has also been extensively used to block, or at least reduce ubiquitination mediated by RING E3s. All three key hydrophobic residues on E3s that mediate the interaction with E2s (shown in green in **Figure 2** in the INTRODUCTION) have been recurrently mutated to compromise the activity of the E3s. As shown in **Figure 45A**, numerous RING-type E3 ligases have been successfully inactivated by mutating the first Ile/Leu, the second Trp/Leu or the last Ile/Val into Ala. The first Ile/Leu has been mutated in BRCA1, BMI-1, CHFR, CNOT4, RING1, RNF2, RNF8 and TRIM3 (Alchanati et al. 2009; Eakin et al. 2007; J. M. Kim et al. 2010; Albert et al. 2002; Shen et al. 2018; S. Liu et al. 2018; Mallette et al. 2012; Raheja et al. 2014). The second Trp/Leu was mutated abolishing ligase activity in BRAP, CBL, MARCH8, MARCH9, MDM2 and TRIM7 (Hayes et al. 2012; Joazeiro et al. 1999; R. Chen et al. 2012; Fan and Wang 2017; Chakraborty et al. 2015; Tan et al. 2019). Finally, the last Ile/Val was

successfully mutated in KIAP and TRIM3 (Raheja et al. 2014; Dou et al. 2012). All these hydrophobic residues are conserved as seen in **Figure 45B**. However, to our knowledge, no one has mutated the E2-interacting Pro (located between C6 and C7) with the aim to disrupt the association with the E2 enzyme. Given the special properties of this cyclic amino acid, one certainly would have to be weary of additional conformational effects that could be caused by its mutation to Ala. Additionally, MDM2 mutant variants Ile440Glu and Ile440Lys prevent MDM2-dependent ubiquitination of p53, by disrupting the E2–ubiquitin binding by the E3 ligase without altering its RING domain structure (Nomura et al. 2017). This residue, however is barely conserved across the different RING domains.

However, other types of mutations have also been efficiently applied to disrupt the interaction between E2s and E3s. For instance, one of the few U-box-type E3s that has been mutated is CHIP, also known as STUB1, which was inactivated by substituting His260 into Glu (Seo et al. 2018). Likewise, the U-box domain-containing UBE4B E3 can be inactivated by mutating a Pro (Pro1140) that is conserved among U-box-type E3 ligases (Pro269 in CHIP) into Ala (not included in **Figure 45**) (X. Li et al. 2018; Okumura et al. 2004).

Inactivating RING-type E3s by disrupting substrate recognition, E3 dimerization and stability

Many RING-type E3 ligases possess a conserved positively charged residue (Arg or Lys) in the last position of the RING domain, which appears to be essential for the ubiquitination activity of the E3. Nevertheless, it is still controversial whether the effect of mutating this residue results from the impaired interaction with E2s or from destabilization of the RING domain (**Figure 45A**, included in stabilization)

(Dou et al. 2012; Albert et al. 2002; Linke et al. 2008; Raheja et al. 2014; Lienlaf et al. 2011; Nomura et al. 2017). But this uncertainty is not surprising given that mutations have been generated to substitute the positively charged residue by a very diverse choice of residues (mostly to Ala, but also to Glu, Pro and even Arg, as can be seen in **Figure 45A**. Future studies should preferably limit the mutations to substituting the positively charged residue by Ala.

As shown in **Figure 45A**, a number of other single point mutations, as well as multiple point mutations, have been generated along different positions of the RING domain to compromise protein stability and hence, E3 ligase activity, but no clear pattern can be predicted based on the studies reported so far. For example, the Tyr37Ala mutant in BRCA1 lack ligase activity and it was incapable of reversing γ-radiation hypersensitivity of BRCA1-null human breast cancer cells (Ruffner et al. 2001), and RAD18 Ile50Ala/Arg51Ala inactive mutant *allowed to study the formation of ternary complexes with RAD6A* (Masuda et al. 2012). In the last example, these two residues were selected because they were highly conserved among species.

RING-type E3s that act as dimers can also be inactivated by preventing their dimerization process. For instance, mutation of Val461Glu and Val263Arg within the RING domain diminishes oligomerisation and activity of XIAP and KIAP ligases, respectively (Nakatani et al. 2013; Poyurovsky et al. 2007)Dou et al. 2012). In other cases, however, the dimerization affecting residues are immediately after the RING domain (Supplementary **Figure S4**), as revealed for example by the mutation Phe490Gln in MDM2 (Poyurovsky et al. 2007). Another approach consists of inactivating oligomeric E3 ligases without affecting the oligomerisation process

itself. For example, RNF4 Val134Ala and Ile153Ala mutants can form dimers but are catalytically incapacitated (Liew et al. 2010). Similarly, other E3 ligase mutants have been shown to act in a dominant negative due to their homo-dimeric nature. For example, mutant Fbw7 has a dominant-negative effect when dimerising with wild-type Fbw7, being able to effectively bind their substrate MYC but not to ubiquitinate and degrade it (Welcker et al. 2013).

Several experiments have also been carried out mutating specific residues on E3 ligases that are critical for the interaction with a given substrate, such as Leu146Gln mutation on the B-box containing E3 MID1 that cannot associate, nor ubiquitinate its substrate PP2A alpha-2 (Du et al., 2013) (**Figure 45**).

Mutations on HECT type E3 ligases

The human HECT-type E3 family consists of 28 members that are divided into three different groups depending on their N-terminal domain architecture: (i) the *NEDD4 subfamily*, characterized by containing a C2 domain, a HECT domain and two to four WW domains, which bind to the PY motifs of target proteins (Kanelis, Rotin, and Forman-Kay 2001; Staub et al. 1996); (ii) the *HERC subfamily*, which integrates at least one regulator chromosome condensation 1 (RCC1)-like domain (RLDs) and a reduced HECT domain; and (iii) the *other HECT subfamily*, that embrace HECT-type E3s not fitting the above mentioned two subfamilies.

Despite those differences, all HECT-type E3s share a ~350 amino acid long HECT domain, that was first described in human papilloma virus E6 associated protein (E6AP, now more commonly referred to as Ube3a) (Huibregtse et al. 1995). In the HECT domain, a conserved Cys forms thioester-linked-intermediate

complexes with ubiquitin (**Figure 1B** in the INTRODUCTION), before being transferred and attached to the substrate through a transthiolation reaction. This conserved Cys is located in the C-terminal region of the HECT domain, while the E2 interacting site is localised in the N-terminal site (**Figure 1B** in the INTRODUCTION) (Rotin and Kumar 2009).

Inactivating HECT-type E3s

Given that an **active site Cys** is required for the formation of a thioester intermediate with ubiquitin, a typical approach is to mutate this specific Cys to generate ligase dead versions of HECT E3 ligases. As shown in Figure 5A, the majority of HECT-type E3 ligases have been inactivated by replacing this catalytic Cys by Ala. This approach has served to unveil, among others, the involvement of HERC3 in immune response (Hochrainer et al. 2015), the role of NEDD4L in EnaC receptor recycling (Zhou, Patel, and Snyder 2007), and the contribution of SMURF1 to Axin degradation (Fei et al. 2013).

Less frequently, some ligase dead HECT-type E3s have been generated by substitution of the active Cys into Ser (Figure 5A). It has been reported that when the catalytic Cys of an E3 is mutated into Ser, the residue is still capable of binding through an oxyester bond with ubiquitin, but incapable to transfer it to substrates, which might result in a dominant-negative effect. In ubiquitination assays employing this type of ligase dead E3s, a stable monoubiquitinated version of the E3 has been detected (S. Y. Lee et al. 2014). This approach has allowed, among other things to discover many substrates of distinct HECT-type E3 ligases. For instance, it was found that wild type version of HACE1 could ubiquitinate and target for degradation the small GTPase Rac1, but the Cys876Ser ligase dead version of the E3

ligase could not (Torrino et al. 2011). Similarly, HERC2 C4762S and HUWE C4341S mutants failed to ubiquitinate their substrates BRCA1 and N-Myc, respectively (Wu et al. 2010, Zhao et al. 2008). The sequence alignment for all the HECT domain E3 ligases illustrated in **Figure 46A** is shown around the catalytically active Cys in **Figure 46B**.

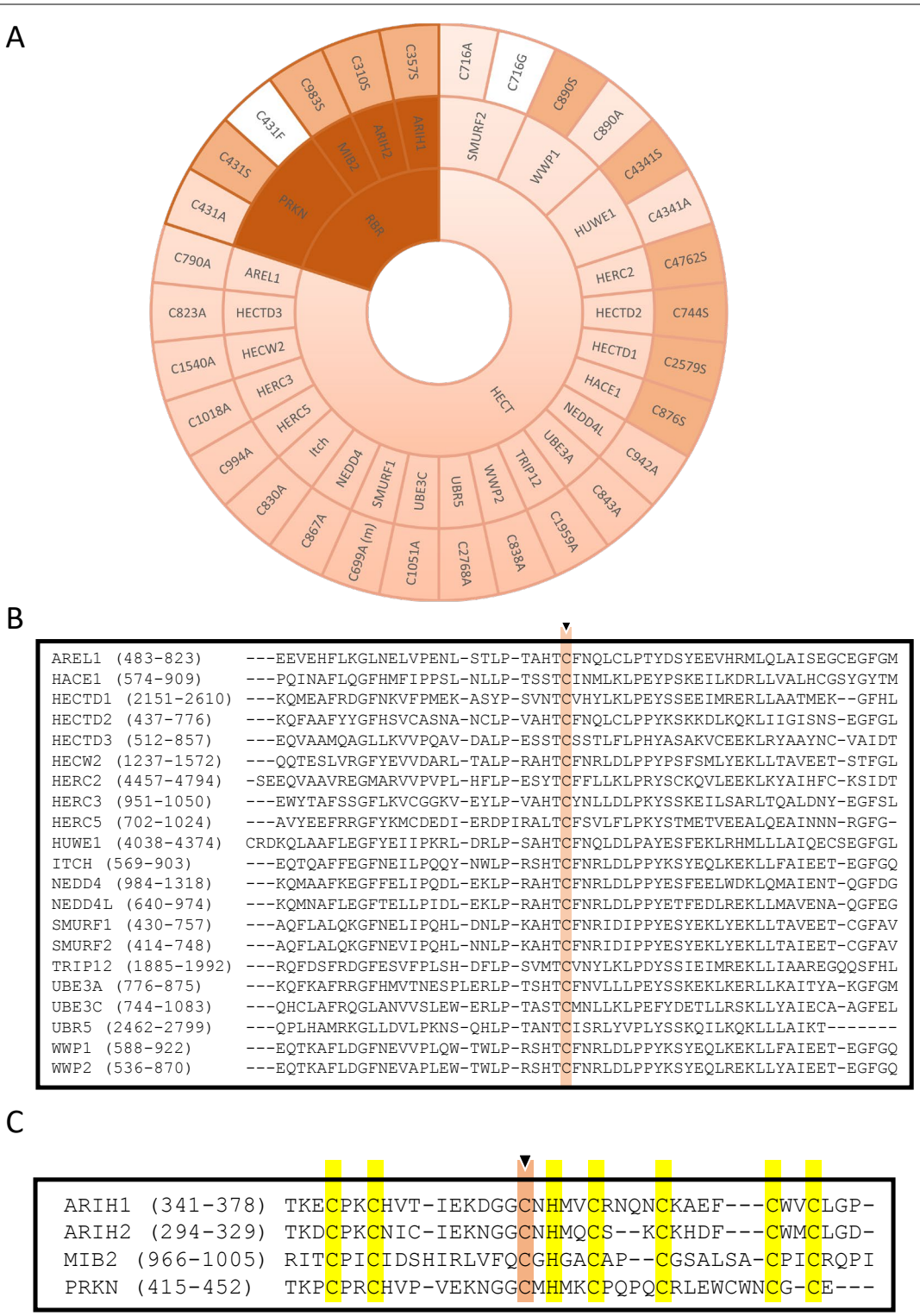

Figure 46. Inactivation of HECT- and RBR-type E3 ligases by mutation of the catalytic cysteine. A) Mutation of the catalytic cysteine into an alanine (light pink), a serine (pink) or another residue (white) abolishes transference of ubiquitin onto the substrate. Inactivation of the catalytic cysteine of RBR-type E3 ubiquitin ligases is obtained by mutation of the third conserved

cysteine in the second RING domain. (m) indicates that this mutation has been done in the mice homologue of the protein. References to all the mutations shown in this figure are provided in **Table S1**. B) Alignment of the HECT domains of the HECT-type E3 ligases. The conserved catalytic cysteine is highlighted in pink. C) Alignment of the RING2 domains of the RBR-type E3 ligases. Conserved zinc-coordinating cysteines and histidine on the second RING domain of mutated RBR E3 ligases are highlighted in yellow and the mutated catalytic cysteine is highlighted in pink.

Mutations on RBR type E3 ligases

RBR family members contain two RING domains (RING1 and RING2) that are separated by an in-between-RING (IBR) zinc-binding domain. Morett and Bork first characterised these domains in 1999 in a sequence profile-based characterisation (Morett and Bork 1999). In the process of confirming reports that UbcH7 could also interact with RBR E3s, they discovered that these RBR E3s act as RING/HECT hybrids. The first RING domain serves as the E2 binding platform, while the C_3 of the second RING serves as the active site that mediates ubiquitination similarly to HECT E3 ligases. (Wenzel et al. 2011) (**Figure 1C** from the INTRODUCTION and **Figure 46C**).

Inactivating RBR-type E3s

As it happens with HECT-type E3, the mutation of the catalytic Cys in the RING2 of RBR E3s results in the inactivation of these enzymes. However, unlike in HECT-type E3 ligases, in RBR E3s the active Cys has been mostly substituted by Ser, and less by Ala (**Figure 46A**). For example, C983S substitution in MIB2 resulted in ligase inactivation, and therefore, prevented ubiquitination of its substrate TANK-binding kinase 1 (Ye et al., 2014). Similarly, mutating the active Cys of ARIH2 (also called TRIAD1) into Ser or Ala completely abolished autoubiquitination of the RBR-

type E3 ligase. Parkison disease has been shown to develop in patients carrying a Cys431Phe mutation at the catalytic Cys of the RBR-type E3 ligase PRKN; those mutants have also been characterized in the lab (Sarraf et al. 2013), in addition to the more common substitutions to Ser and Ala (J. Liu et al. 2017; Xin et al. 2018).

In order to generate ligase dead versions of RBR-type E3s, it has been also shown to be plausible to preserve the active Cys, and instead mutate the zinc-coordinating residues in either of the two RING domains, substituting by Ala one or several of those key residues. For instance, ARIH1 and RNF144A have been successfully inactivated by modifying their RING1 domain (**Figure 44**, dark pink). Whereas mutating C4 of ARIH1 (Cys208) was sufficient to inhibit the ligase, Cys20 and Cys23 (C1+C2) were simultaneously modified to block the catalytic activity of the RBR-type E3 RNF144A (von Stechow et al. 2015; Ho et al. 2014). On the contrary, ARIH2 and RNF31 have been inactivated by mutating their RING2 domain zinc-coordinating Cys residues (Figure 3, light pink). Cells expressing an ARIH1 mutant in which the C2 of the RING2 domain was mutated into Ala (ARIH2 Cys300Ala mutant) was no longer able to ubiquitinate NLRPL3 (Kawashima et al. 2017). Similarly, Smit and coworkers generated various ligase dead versions of RNF31 by mutating simultaneously Cys871and C874 (C1+C2) or Cys890and Cys892 (C4+C5) of the RING2 domain (Smit et al. 2012).

Conclusions

Mutations on E3 ligases have been associated with a number of diseases, including neurological disorders (George et al. 2018; Osinalde et al. 2019). Thus, understanding their mechanism of action, as well as identifying which substrates

are regulated by each E3 at different developmental stages and cell types, will provide invaluable knowledge that might contribute to develop therapeutic strategies to treat these diseases. Generation of E3 ligase dead mutants can certainly provide crucial information for this purpose. While the use of gene silencing techniques might be more appropriate to study the phenotypes derived from the loss of function of E3 ligases, the overexpression of ligase death versions can provide information about (i) the E2 enzymes they work with, (ii) substrate recognition domains and (iii) existing mechanism that regulate their activity. Additionally, a number of biochemical experiments do benefit from comparing the ectopic expression of wild type active E3 ligases with their mutated inactive variants.

As evident from all the examples shown in this review, there are multiple options to disrupt the activity of an E3 ligase. As illustrated by the sequence alignment in **Figure 45B**, the first necessary step is to identify which are the key residues in our ligase of interest. This is an essential step to ensure that any mutagenesis performed has a higher chance of success in disrupting the E3 ligase activity. For example, not all cysteine residues within a RING domain are involved in zinc coordination, as can be seen in the sequence alignment of Mdm2 in **Figure 45B**. When this cysteine of the Mdm2 RING domain was mutated (Kostic et al. 2006) the zinc coordination was maintained and no disruption to the ubiquitination activity of Mdm2 was detectable.

It is worth mentioning that mutating key residues involved either in the coordination of the zinc ions, dimerisation, proteins stabilization or E2 interaction might not always be sufficient to abolish the catalytic activity of the E3 ligase. The resulting mutation replacing the original residue that is substituted can actually be

determinant in order to have a functional effect. For instance, mutating Phe495 of XIAP into either Ala, Tyr or Trp completely prevents E3 ligase autoubiquitination. However, XIAP Phe495Leu mutants appear to be functionally wild-type like (Nakatani et al. 2013); but might not be that surprising given the partial hydrophobic similarity between those two amino acids.

As illustrated within this review, so far one of the most frequent approaches for RING E3 ligases has been to mutate the residues involved in the zinc coordination (Cys and His residues, shaded in yellow and orange respectively in **Figure 45B**). Eliminating the zinc coordination on the RING domain is well known to severely disrupt the ubiquitination activity of those E3 ligases. However, this breakdown of the global structural integrity of the RING construct might lead to a severe effect in the folding and expression levels of the E3 ligase (Chasapis et al. 2010). Therefore, for certain experiments might be more effective to generate less disruptive point mutations. For example, the mutation of the hydrophobic residues (Ile, Leu, Trp, Val, shaded in green in **Figure 45B**) that mediate the interaction with the E2 conjugating enzyme, as demonstrated for a number of RING E3 ligases. To our knowledge this approach has not yet been employed for the E2-interacting RING domain of RBR E3 ligases, but it should indeed be an interesting experiment to perform.

Another approach that has been used as well is to eliminate by mutagenesis the positive charge of the Lys or Arg residue located straight after the last zinc-coordinating Cys of the RING domain. It is yet unclear however whether the effect caused by this mutation is on the interaction with E2s or from destabilization of the RING domain.

Mutations on the active Cys of HECT- and RBR-type E3 ligases are very straight forward, as they generate, without further effect to the structure and stability of the E3, ligase-dead versions of these enzymes. Those are of good value to be used as the best control in experiments overexpressing the wild type ligase, for example, to identify substrates in an unbiased manner. Additionally, if mutating the active site Cys to Ser, the formation of an oxyester to ubiquitin can be used with the aim to obtain a dominant-negative version of the ligase; the E3 will recruit the E2 and the substrate but the ubiquitination reaction cannot proceed since the ubiquitin cannot be released once it has conjugated to the E3.

To investigate the regulation of a specific protein by a particular HECT or RBR E3, however, it might be more suitable to mutate the ligase at the substrate recognition motif. Moreover, in some cases, as is the case of some RING E3s, the inactivation of E3 enzymes is not achieved by a single point mutation, even though such residue is defined as a key amino acid involved in substrate recognition. Hence, in such situations, several residues must be simultaneously mutated in order to disrupt the E3 ligase function. The generation and usage of E3 mutants have revealed unexpected and important lessons about the complexity of this family of enzymes. Nevertheless, a complete understanding of E3 ligases still requires more research, in which the generation of novel E3 ligase mutants will undoubtedly be decisive.

CONCLUSIONS

Conclusions

From the results obtained in this thesis, the following conclusions may be drawn:

1. The DUB MYSM1 controls indirectly CaMKIIa ubiquitination in HEK 293T cells. Active MYSM1 triggers CaMKIIa ubiquitination and inactive MYSM1 leads to less ubiquitination of CaMKIIa.
2. The ubiquitin E3 ligase ITCH induces CaMKIIa monoubiquitination in HEK 293T cells.
3. When CaMKIIa is ubiquitinated it is less active, as phosphorylation at T286 is significantly reduced.
4. The human protein SART3 interacts with CaMKIIa more efficiently than with CaMKIIb, while ARS2 interacts with both CaMKIIa and CaMKIIb. The expression of the redox-active cofactor of the 26 S proteasome TXNL1 induces CaMKIIa and CaMKIIb degradation.
5. The Sumo E3 ligase RanBP2 does not induce CaMKIIa sumoylation.
6. CaMKII interacts with NCDN and UBE3A. CaMKIIa interaction with UBE3A is independent from NCDN availability.
7. UBE3A is not the ubiquitin E3 ligase responsible for CaMKIIa ubiquitination.
8. UBE3A promotes the formation of K48-ubiquitin chains on NCDN and triggers NCDN degradation.

9. Mutating key residues involved either in the coordination of the zinc ions, dimerisation, proteins stabilization or E2 interaction might not always be sufficient to abolish the catalytic activity of the E3 ligase.
10. The resulting mutation replacing the original residue that is substituted can actually be determinant in order to have a functional effect.
11. The most frequent approaches for RING E3 ligases has been to mutate the residues involved in the zinc coordination.
12. Mutations on the active Cys of HECT- and RBR-type E3 ligases are very straight forward, as they generate, without further effect to the structure and stability of the E3, ligase-dead versions of these enzymes.

REFERENCES

Abbasi, Sanna, and Caroline Schild-Poulter. 2021. "Identification of Ku70 Domain-Specific Interactors Using BioID2." *Cells* 10 (3): 1–24. https://doi.org/10.3390/CELLS10030646.

Ajayi, Peter T., Prasanna Katti, Yingfan Zhang, T. Bradley Willingham, Ye Sun, Christopher K.E. Bleck, and Brian Glancy. 2022. "Regulation of the Evolutionarily Conserved Muscle Myofibrillar Matrix by Cell Type Dependent and Independent Mechanisms." *Nature Communications 2022 13:1* 13 (1): 1–12. https://doi.org/10.1038/s41467-022-30401-9.

Akimov, Vyacheslav, Inigo Barrio-Hernandez, Sten V.F. Hansen, Philip Hallenborg, Anna Kathrine Pedersen, Dorte B. Bekker-Jensen, Michele Puglia, et al. 2018. "UbiSite Approach for Comprehensive Mapping of Lysine and N-Terminal Ubiquitination Sites." *Nature Structural & Molecular Biology* 25 (7): 631–40. https://doi.org/10.1038/S41594-018-0084-Y.

Akita, Tenpei, Kazushi Aoto, Mitsuhiro Kato, Masaaki Shiina, Hiroki Mutoh, Mitsuko Nakashima, Ichiro Kuki, et al. 2018. "De Novo Variants in CAMK2A and CAMK2B Cause Neurodevelopmental Disorders." *Annals of Clinical and Translational Neurology* 5 (3): 280–96. https://doi.org/10.1002/ACN3.528.

Akutsu, Masato, Ivan Dikic, and Anja Bremm. 2016. "Ubiquitin Chain Diversity at a Glance." *Journal of Cell Science*. https://doi.org/10.1242/jcs.183954.

Albert, Thomas K, Hiroyuki Hanzawa, Yvonne I A Legtenberg, Marjolein J de Ruwe, Fiona A J van den Heuvel, Martine A Collart, Rolf Boelens, and H Th Marc Timmers. 2002. "Identification of a Ubiquitin-Protein Ligase Subunit within the CCR4-NOT Transcription Repressor Complex." *The EMBO Journal* 21 (3): 355–64. https://doi.org/10.1093/emboj/21.3.355.

Alchanati, Iris, Carmit Teicher, Galit Cohen, Vivian Shemesh, Haim M. Barr, Philippe Nakache, Danny Ben-Avraham, et al. 2009. "The E3 Ubiquitin-Ligase Bmi1/Ring1A Controls the Proteasomal Degradation of Top2α Cleavage Complex - A Potentially New Drug Target." *PLoS ONE*. https://doi.org/10.1371/journal.pone.0008104.

Anczurowski, Mark, Kenji Sugata, Yukiko Matsunaga, Yuki Yamashita, Chung Hsi Wang, Tingxi Guo, Kenji Murata, et al. 2019. "Chaperones of the Class I Peptide-Loading Complex Facilitate the Constitutive Presentation of Endogenous Antigens on HLA-DP84GGPM87." *Journal of Autoimmunity* 102 (August): 114–25. https://doi.org/10.1016/j.jaut.2019.04.023.

Andersen, Katrine M., Louise Madsen, S. øoren Prag, Anders H. Johnsen, Colin A. Semple, Klavs B. Hendil, and Rasmus Hartmann-Petersen. 2009. "Thioredoxin Txnl1/TRP32 Is a Redox-Active Cofactor of the 26 S Proteasome." *The Journal of Biological Chemistry* 284 (22): 15246–54. https://doi.org/10.1074/JBC.M900016200.

Andersen, R. 2005. "Calcium/Calmodulin-Dependent Protein Kinase II Alters Structural Plasticity and Cytoskeletal Dynamics in Drosophila." *Journal of Neuroscience* 25 (39): 8878–88. https://doi.org/10.1523/JNEUROSCI.2005-05.2005.

Anderson, Kathryn V., Gerd Jürgens, and Christiane Nüsslein-Volhard. 1985. "Establishment of Dorsal-Ventral Polarity in the Drosophila Embryo: Genetic Studies on the Role of the Toll Gene Product." *Cell* 42 (3): 779–89. https://doi.org/10.1016/0092-8674(85)90274-0.

Angers, Annie, Antoine R Ramjaun, and Peter S McPherson. 2004. "The HECT Domain Ligase Itch

Ubiquitinates Endophilin and Localizes to the Trans-Golgi Network and Endosomal System." *The Journal of Biological Chemistry* 279 (12): 11471–79. https://doi.org/10.1074/jbc.M309934200.

Antonin, Wolfram, Rosemarie Ungricht, and Ulrike Kutay. 2011. "Traversing the NPC along the Pore Membrane - Targeting of Membrane Proteins to the INM." *Nucleus* 2 (2): 87–91. https://doi.org/10.4161/nucl.2.2.14637.

Aravind, L, and E V Koonin. 2000. "The U Box Is a Modified RING Finger - a Common Domain in Ubiquitination." *Current Biology* 10 (4): R132-4. https://doi.org/10.1016/S0960-9822(00)00398-5.

Avagliano Trezza, Rossella, A. Mattijs Punt, Edwin Mientjes, Marlene van den Berg, F. Isabella Zampeta, Ilona J. de Graaf, Yana van der Weegen, Jeroen A.A. Demmers, Ype Elgersma, and Ben Distel. 2021. "Mono-Ubiquitination of Rabphilin 3A by UBE3A Serves a Non-Degradative Function." *Scientific Reports 2021 11:1* 11 (1): 1–14. https://doi.org/10.1038/s41598-021-82319-9.

Avagliano Trezza, Rossella, Monica Sonzogni, Stijn N.V. Bossuyt, F. Isabella Zampeta, A. Mattijs Punt, Marlene van den Berg, Diana C. Rotaru, et al. 2019. "Loss of Nuclear UBE3A Causes Electrophysiological and Behavioral Deficits in Mice and Is Associated with Angelman Syndrome." *Nature Neuroscience 2019 22:8* 22 (8): 1235–47. https://doi.org/10.1038/s41593-019-0425-0.

Bailly, V, S Lauder, S Prakash, and L Prakash. 1997. "Yeast DNA Repair Proteins Rad6 and Rad18 Form a Heterodimer That Has Ubiquitin Conjugating, DNA Binding, and ATP Hydrolytic Activities." *The Journal of Biological Chemistry* 272 (37): 23360–65. https://doi.org/10.1074/jbc.272.37.23360.

Bajrami, Emirjeta, and Mirko Spiroski. 2016. "Genomic Imprinting." *Open Access Macedonian Journal of Medical Sciences*. Open Access Macedonian Journal of Medical Sciences. https://doi.org/10.3889/oamjms.2016.028.

Barroso-Gomila, Orhi, Fredrik Trulsson, Veronica Muratore, Iñigo Canosa, Laura Merino-Cacho, Ana Rosa Cortazar, Coralia Pérez, et al. 2021. "Identification of Proximal SUMO-Dependent Interactors Using SUMO-ID." *Nature Communications* 12 (1). https://doi.org/10.1038/S41467-021-26807-6.

Baucum, Anthony J., Brian C. Shonesy, Kristie L. Rose, and Roger J. Colbran. 2015. "Quantitative Proteomics Analysis of CaMKII Phosphorylation and the CaMKII Interactome in the Mouse Forebrain." *ACS Chemical Neuroscience* 6 (4): 615–31. https://doi.org/10.1021/cn500337u.

Baudry, Michel, Eniko Kramar, Xiaobo Xu, Homera Zadran, Stephanie Moreno, Gary Lynch, Christine Gall, and Xiaoning Bi. 2012. "Ampakines Promote Spine Actin Polymerization, Long-Term Potentiation, and Learning in a Mouse Model of Angelman Syndrome." *Neurobiology of Disease* 47 (2): 210–15. https://doi.org/10.1016/j.nbd.2012.04.002.

Beaudoin, Gerard M.J., Seung Hye Lee, Dipika Singh, Yang Yuan, Yu Gie Ng, Louis F. Reichardt, and Jyothi Arikkath. 2012. "Culturing Pyramidal Neurons from the Early Postnatal Mouse Hippocampus and Cortex." *Nature Protocols* 7 (9): 1741–54.

https://doi.org/10.1038/NPROT.2012.099.

Becker, Janina, Sina V. Barysch, Samir Karaca, Claudia Dittner, He Hsuan Hsiao, Mauricio Berriel Diaz, Stephan Herzig, Henning Urlaub, and Frauke Melchior. 2013. "Detecting Endogenous SUMO Targets in Mammalian Cells and Tissues." *Nature Structural & Molecular Biology* 20 (4): 525–31. https://doi.org/10.1038/NSMB.2526.

Bhatnagar, Sanchita, Claude Gazin, Lynn Chamberlain, Jianhong Ou, Xiaochun Zhu, Jogender S Tushir, Ching-Man Virbasius, et al. 2014. "TRIM37 Is a New Histone H2A Ubiquitin Ligase and Breast Cancer Oncoprotein." *Nature* 516 (7529): 116–20. https://doi.org/10.1038/nature13955.

Bingol, Baris, Chi Fong Wang, David Arnott, Dongmei Cheng, Junmin Peng, and Morgan Sheng. 2010. "Autophosphorylated CaMKIIα Acts as a Scaffold to Recruit Proteasomes to Dendritic Spines." *Cell* 140 (4): 567–78. https://doi.org/10.1016/j.cell.2010.01.024.

Bird, Lynne M. 2014. "Angelman Syndrome: Review of Clinical and Molecular Aspects." *Application of Clinical Genetics*. Dove Medical Press Ltd. https://doi.org/10.2147/TACG.S57386.

Bist, Pradeep, Wan Shoo Cheong, Aylwin Ng, Neha Dikshit, Bae-Hoon Kim, Niyas Kudukkil Pulloor, Hanif Javanmard Khameneh, et al. 2017. "E3 Ubiquitin Ligase ZNRF4 Negatively Regulates NOD2 Signalling and Induces Tolerance to MDP." *Nature Communications* 8: 15865. https://doi.org/10.1038/ncomms15865.

Boddy, Michael N., Paul S. Freemont, and Katherine L B Borden. 1994. "The P53-Associated Protein MDM2 Contains a Newly Characterized Zinc-Binding Domain Called the RING Finger." *Trends in Biochemical Sciences* 19 (5): 198–99. https://doi.org/10.1016/0968-0004(94)90020-5.

Boutet, Stéphane C., Marie Hélène Disatnik, Lauren S. Chan, Kevin Iori, and Thomas A. Rando. 2007. "Regulation of Pax3 by Proteasomal Degradation of Monoubiquitinated Protein in Skeletal Muscle Progenitors." *Cell* 130 (2): 349–62. https://doi.org/10.1016/J.CELL.2007.05.044.

Brand, A. H., and N. Perrimon. 1993. "Targeted Gene Expression as a Means of Altering Cell Fates and Generating Dominant Phenotypes." *Development* 118 (2): 401–15.

Branon, Tess C, Justin A Bosch, Ariana D Sanchez, Namrata D Udeshi, Tanya Svinkina, Steven A Carr, Jessica L Feldman, Norbert Perrimon, and Alice Y Ting. 2018. "Efficient Proximity Labeling in Living Cells and Organisms with TurboID." *Nature Biotechnology* 36 (9). https://doi.org/10.1038/nbt.4201.

Braun, Pascal, and Anne Claude Gingras. 2012. "History of Protein-Protein Interactions: From Egg-White to Complex Networks." *Proteomics*. https://doi.org/10.1002/pmic.201100563.

Bridges, Calvin B., and Thomas Hunt Morgan. 1916. *Sex-Linked Inheritance in Drosophila, by T. H. Morgan and C. B. Bridges. Sex-Linked Inheritance in Drosophila, by T. H. Morgan and C. B. Bridges.* Washington,: Carnegie Institution of Washington,. https://doi.org/10.5962/bhl.title.22854.

Brocke, L., M. Srinivasan, and H. Schulman. 1995. "Developmental and Regional Expression of Multifunctional Ca2+/Calmodulin-Dependent Protein Kinase Isoforms in Rat Brain." *Journal of Neuroscience* 15 (10): 6797–6808. https://doi.org/10.1523/JNEUROSCI.15-10-06797.1995.

Brzovic, P S, P Rajagopal, D W Hoyt, M C King, and R E Klevit. 2001. "Structure of a BRCA1-BARD1 Heterodimeric RING-RING Complex." *Nature Structural Biology* 8 (10): 833–37. https://doi.org/10.1038/nsb1001-833.

Buiting, Karin, Charles Williams, and Bernhard Horsthemke. 2016. "Angelman Syndrome — Insights into a Rare Neurogenetic Disorder." *Nature Reviews Neurology* 12 (10): 584–93. https://doi.org/10.1038/nrneurol.2016.133.

Burke, James M., and Christopher S. Sullivan. 2017. "DUSP11–An RNA Phosphatase That Regulates Host and Viral Non-Coding RNAs in Mammalian Cells." *RNA Biology*. https://doi.org/10.1080/15476286.2017.1306169.

Butler, M. G., and T. Thompson. 2000. "Prader-Willi Syndrome Clinical and Genetic Findings." *Endocrinologist*.

Caforio, Matteo, Cristina Sorino, Stefano Iacovelli, Maurizio Fanciulli, Franco Locatelli, and Valentina Folgiero. 2018. "Recent Advances in Searching C-Myc Transcriptional Cofactors during Tumorigenesis." *Journal of Experimental and Clinical Cancer Research* 37 (1). https://doi.org/10.1186/S13046-018-0912-2.

Cao, Ru, Yu Ichi Tsukada, and Yi Zhang. 2005. "Role of Bmi-1 and Ring1A in H2A Ubiquitylation and Hox Gene Silencing." *Molecular Cell* 20 (6): 845–54. https://doi.org/10.1016/j.molcel.2005.12.002.

Capili, Allan D., and Christopher D. Lima. 2007. "Taking It Step by Step: Mechanistic Insights from Structural Studies of Ubiquitin/Ubiquitin-like Protein Modification Pathways." *Current Opinion in Structural Biology* 17 (6): 726–35. https://doi.org/10.1016/J.SBI.2007.08.018.

Carnesecchi, Julie, Gianluca Sigismondo, Katrin Domsch, Clara Eva Paula Baader, Mahmoud Reza Rafiee, Jeroen Krijgsveld, and Ingrid Lohmann. 2020. "Multi-Level and Lineage-Specific Interactomes of the Hox Transcription Factor Ubx Contribute to Its Functional Specificity." *Nature Communications* 11 (1). https://doi.org/10.1038/S41467-020-15223-X.

Castermans, D., V. Wilquet, E. Parthoens, C. Huysmans, J. Steyaert, L. Swinnen, J. P. Fryns, W. Van De Ven, and K. Devriendt. 2003. "The Neurobeachin Gene Is Disrupted by a Translocation in a Patient with Idiopathic Autism." *Journal of Medical Genetics* 40 (5): 352–56. https://doi.org/10.1136/JMG.40.5.352.

Castermans, Dries, Karolien Volders, An Crepel, Liesbeth Backx, Rita de Vos, Kathleen Freson, Sandra Meulemans, et al. 2010. "SCAMP5, NBEA and AMISYN: Three Candidate Genes for Autism Involved in Secretion of Large Dense-Core Vesicles." *Human Molecular Genetics* 19 (7): 1368–78. https://doi.org/10.1093/HMG/DDQ013.

Chakraborty, Atanu, Markus E Diefenbacher, Anastasia Mylona, Olivier Kassel, and Axel Behrens. 2015. "The E3 Ubiquitin Ligase Trim7 Mediates C-Jun/AP-1 Activation by Ras Signalling." *Nature Communications* 6: 6782. https://doi.org/10.1038/ncomms7782.

Chasapis, Christos T., Ariadni K. Loutsidou, Malvina G. Orkoula, and Georgios A. Spyroulias. 2010. "Zinc Binding Properties of Engineered Ring Finger Domain of Arkadia E3 Ubiquitin Ligase." *Bioinorganic Chemistry and Applications* 2010. https://doi.org/10.1155/2010/323152.

Cheerathodi, Mujeeb R., and David G. Meckes. 2020. "BioID Combined with Mass Spectrometry to Study Herpesvirus Protein-Protein Interaction Networks." *Methods in Molecular Biology (Clifton, N.J.)* 2060: 327–41. https://doi.org/10.1007/978-1-4939-9814-2_19.

Chen, Ling Chih, Yung Lin Hsieh, Grace Y.T. Tan, Tai Yun Kuo, Yu Chi Chou, Pang Hung Hsu, and Wendy W. Hwang-Verslues. 2021. "Differential Effects of SUMO1 and SUMO2 on Circadian Protein PER2 Stability and Function." *Scientific Reports 2021 11:1* 11 (1): 1–13. https://doi.org/10.1038/s41598-021-93933-y.

Chen, Rui, Mi Li, Yu Zhang, Qian Zhou, and Hong-bing Shu. 2012. "The E3 Ubiquitin Ligase MARCH8 Negatively Regulates IL-1 β -Induced NF- κ B Activation by Targeting the IL1RAP Coreceptor for Ubiquitination and Degradation" 109 (35): 14128–33. https://doi.org/10.1073/pnas.1205246109.

Chia, Poh Hui, Franklin Lei Zhong, Shinsuke Niwa, Carine Bonnard, Kagistia Hana Utami, Ruizhu Zeng, Hane Lee, et al. 2018. "A Homozygous Loss-of-Function CAMK2A Mutation Causes Growth Delay, Frequent Seizures and Severe Intellectual Disability." *ELife* 7 (May). https://doi.org/10.7554/ELIFE.32451.

Cho, Kelvin F., Tess C. Branon, Sanjana Rajeev, Tanya Svinkina, Namrata D. Udeshi, Themis Thoudam, Chulhwan Kwak, et al. 2020. "Split-TurboID Enables Contact-Dependent Proximity Labeling in Cells." *Proceedings of the National Academy of Sciences of the United States of America* 117 (22): 12143. https://doi.org/10.1073/PNAS.1919528117/-/DCSUPPLEMENTAL.

Chou, Ching Chieh, Yi Zhang, Mfon E. Umoh, Spencer W. Vaughan, Ileana Lorenzini, Feilin Liu, Melissa Sayegh, et al. 2018. "TDP-43 Pathology Disrupts Nuclear Pore Complexes and Nucleocytoplasmic Transport in ALS/FTD." *Nature Neuroscience* 21 (2): 228–39. https://doi.org/10.1038/S41593-017-0047-3.

Ciechanover, Aaron, and Ronen Ben-Saadon. 2004. "N-Terminal Ubiquitination: More Protein Substrates Join In." *Trends in Cell Biology* 14 (3): 103–6. http://www.ncbi.nlm.nih.gov/pubmed/15055197.

Comartin, David, Gagan D. Gupta, Eden Fussner, Étienne Coyaud, Monica Hasegan, Marco Archinti, Sally W.T. Cheung, et al. 2013. "CEP120 and SPICE1 Cooperate with CPAP in Centriole Elongation." *Current Biology : CB* 23 (14): 1360–66. https://doi.org/10.1016/J.CUB.2013.06.002.

Cook, Sarah G., Nicole L. Rumian, and K. Ulrich Bayer. 2022. "CaMKII T286 Phosphorylation Has Distinct Essential Functions in Three Forms of Long-Term Plasticity." *The Journal of Biological Chemistry* 298 (9). https://doi.org/10.1016/J.JBC.2022.102299.

Coultrap, Steven J., Isabelle Buard, Jaqueline R. Kulbe, Mark L. Dell'Acqua, and K. Ulrich Bayer. 2010. "CaMKII Autonomy Is Substrate-Dependent and Further Stimulated by Ca2+/Calmodulin." *The Journal of Biological Chemistry* 285 (23): 17930–37. https://doi.org/10.1074/JBC.M109.069351.

Couzens, Amber L., James D.R. Knight, Michelle J. Kean, Guoci Teo, Alexander Weiss, Wade H. Dunham, Zhen Yuan Lin, et al. 2013. "Protein Interaction Network of the Mammalian Hippo Pathway Reveals Mechanisms of Kinase-Phosphatase Interactions." *Science Signaling* 6 (302).

https://doi.org/10.1126/SCISIGNAL.2004712.

Coyaud, Etienne, Monika Mis, Estelle M.N. Laurent, Wade H. Dunham, Amber L. Couzens, Melanie Robitaille, Anne Claude Gingras, Stephane Angers, and Brian Raught. 2015. "BioID-Based Identification of Skp Cullin F-Box (SCF)β-TrCP1/2 E3 Ligase Substrates." *Molecular & Cellular Proteomics : MCP* 14 (7): 1781–95. https://doi.org/10.1074/MCP.M114.045658.

Cui, Yan, Susann Groth, Scott Troutman, Annemarie Carlstedt, Tobias Sperka, Lars Björn Riecken, Joseph L. Kissil, Hongchuan Jin, and Helen Morrison. 2019. "The NF2 Tumor Suppressor Merlin Interacts with Ras and RasGAP, Which May Modulate Ras Signaling." *Oncogene* 38 (36): 6370–81. https://doi.org/10.1038/S41388-019-0883-6.

Dagli, A., K. Buiting, and C. A. Williams. 2012. "Molecular and Clinical Aspects of Angelman Syndrome." *Molecular Syndromology* 2 (3–5): 100–112. https://doi.org/10.1159/000328837.

Dateki, Minori, Takuro Horii, Yoshitoshi Kasuya, Reiko Mochizuki, Yasumitsu Nagao, Junji Ishida, Fumihiro Sugiyama, et al. 2005. "Neurochondrin Negatively Regulates CaMKII Phosphorylation, and Nervous System-Specific Gene Disruption Results in Epileptic Seizure." *The Journal of Biological Chemistry* 280 (21): 20503–8. https://doi.org/10.1074/JBC.M414033200.

Deane, Caitlin. 2018. "PUP up the Volume." *Nature Chemical Biology 2018 14:10* 14 (10): 903–903. https://doi.org/10.1038/s41589-018-0138-9.

Deshaies, Raymond J., and Claudio A.P. Joazeiro. 2009. "RING Domain E3 Ubiquitin Ligases." *Annual Review of Biochemistry* 78 (1): 399–434. https://doi.org/10.1146/annurev.biochem.78.101807.093809.

Deshpande, Prasannakumar, Dani Flinkman, Ye Hong, Elena Goltseva, Valentina Siino, Lihua Sun, Sirkku Peltonen, et al. 2020. "Protein Synthesis Is Suppressed in Sporadic and Familial Parkinson's Disease by LRRK2." *FASEB Journal : Official Publication of the Federation of American Societies for Experimental Biology* 34 (11): 14217–33. https://doi.org/10.1096/FJ.202001046R.

Deshpande, Tarangini, Toshimitsu Takagi, Luning Hao, Stephen Buratowski, and Harry Charbonneau. 1999. "Human PIR1 of the Protein-Tyrosine Phosphatase Superfamily Has RNA 5′-Triphosphatase and Diphosphatase Activities *." *Journal of Biological Chemistry* 274 (23): 16590–94. https://doi.org/10.1074/JBC.274.23.16590.

Diamandis, E. P., and T. K. Christopoulos. 1991. "The Biotin-(Strept)Avidin System: Principles and Applications in Biotechnology." *Clinical Chemistry* 37 (5): 625–36. https://doi.org/10.1093/CLINCHEM/37.5.625.

Díaz-Alonso, Javier, and Roger A. Nicoll. 2021. "AMPA Receptor Trafficking and LTP: Carboxy-Termini, Amino-Termini and TARPs." *Neuropharmacology* 197 (October): 108710. https://doi.org/10.1016/J.NEUROPHARM.2021.108710.

Dindot, Scott V., Barbara A. Antalffy, Meenakshi B. Bhattacharjee, and Arthur L. Beaudet. 2008. "The Angelman Syndrome Ubiquitin Ligase Localizes to the Synapse and Nucleus, and Maternal Deficiency Results in Abnormal Dendritic Spine Morphology." *Human Molecular Genetics* 17 (1): 111–18. https://doi.org/10.1093/hmg/ddm288.

Dou, Hao, Lori Buetow, Gary J Sibbet, Kenneth Cameron, and Danny T Huang. 2012. "BIRC7-E2 Ubiquitin Conjugate Structure Reveals the Mechanism of Ubiquitin Transfer by a RING Dimer." *Nature Structural & Molecular Biology* 19 (9): 876–83. https://doi.org/10.1038/nsmb.2379.

Dumont, Audrey Ann, Lauralyne Dumont, Jonathan Berthiaume, and Mannix Auger-Messier. 2019. "P38α MAPK Proximity Assay Reveals a Regulatory Mechanism of Alternative Splicing in Cardiomyocytes." *Biochimica et Biophysica Acta. Molecular Cell Research* 1866 (12). https://doi.org/10.1016/J.BBAMCR.2019.118557.

Eakin, Catherine M, Michael J Maccoss, Gregory L Finney, and Rachel E Klevit. 2007. "Estrogen Receptor Alpha Is a Putative Substrate for the BRCA1 Ubiquitin Ligase." *Proceedings of the National Academy of Sciences of the United States of America* 104 (14): 5794–99. https://doi.org/10.1073/pnas.0610887104.

Elgersma, Ype, Nikolai B. Fedorov, Sami Ikonen, Esther S. Choi, Minetta Elgersma, Ofelia M. Carvalho, Karl Peter Giese, and Alcino J. Silva. 2002. "Inhibitory Autophosphorylation of CaMKII Controls PSD Association, Plasticity, and Learning." *Neuron*. https://doi.org/10.1016/S0896-6273(02)01007-3.

Elgersma, Ype, J. David Sweatt, and K. Peter Giese. 2004. "Mouse Genetic Approaches to Investigating Calcium/Calmodulin-Dependent Protein Kinase II Function in Plasticity and Cognition." *The Journal of Neuroscience* 24 (39): 8410. https://doi.org/10.1523/JNEUROSCI.3622-04.2004.

Elu, Nagore, Nerea Osinalde, Javier Beaskoetxea, Juanma Ramirez, Benoit Lectez, Kerman Aloria, Jose Antonio Rodriguez, Jesus M. Arizmendi, and Ugo Mayor. 2019. "Detailed Dissection of UBE3A-Mediated DDI1 Ubiquitination." *Frontiers in Physiology* 10 (MAY). https://doi.org/10.3389/FPHYS.2019.00534.

Fan, Chuandong, and Xinjiang Wang. 2017. "Mdm2 Splice Isoforms Regulate the P53 / Mdm2 / Mdm4 Regulatory Circuit via RING Domain-Mediated Ubiquitination of P53 and Mdm4." *Cell Cycle* 16 (7): 660–64. https://doi.org/10.1080/15384101.2017.1288327.

Fang, S, J P Jensen, R L Ludwig, K H Vousden, and A M Weissman. 2000. "Mdm2 Is a RING Finger-Dependent Ubiquitin Protein Ligase for Itself and P53." *The Journal of Biological Chemistry* 275 (12): 8945–51. https://doi.org/10.1074/jbc.275.12.8945.

Fatima, Ambrin, Jan Hoeber, Jens Schuster, Eriko Koshimizu, Carolina Maya-Gonzalez, Boris Keren, Cyril Mignot, et al. 2021. "Monoallelic and Bi-Allelic Variants in NCDN Cause Neurodevelopmental Delay, Intellectual Disability, and Epilepsy." *American Journal of Human Genetics* 108 (4): 739–48. https://doi.org/10.1016/J.AJHG.2021.02.015.

Fei, Cong, Zhenfei Li, Chen Li, Yuelei Chen, Zhangcheng Chen, Xiaoli He, Li Mao, Xin Wang, Rong Zeng, and Lin Li. 2013. "Smurf1-Mediated Lys29-Linked Nonproteolytic Polyubiquitination of Axin Negatively Regulates Wnt/β-Catenin Signaling." *Molecular and Cellular Biology* 33 (20): 4095–4105. https://doi.org/10.1128/MCB.00418-13.

Felberbaum-Corti, M, E Morel, V Cavalli, F Vilbois, and J Gruenberg. 2007. "The Redox Sensor TXNL1 Plays a Regulatory Role in Fluid Phase Endocytosis." *PLoS ONE* 2 (11): 1144. https://doi.org/10.1371/journal.pone.0001144.

Feng, Wei, Canzhao Liu, Simone Spinozzi, Li Wang, Sylvia M. Evans, and Ju Chen. 2020. "Identifying the Cardiac Dyad Proteome In Vivo by a BioID2 Knock-In Strategy." *Circulation*. NLM (Medline). https://doi.org/10.1161/CIRCULATIONAHA.119.043434.

Fersht, Alan, Michelle Russel Julet, and John Britch. 1997. *Structure and Mechanicsm in Protein Science - A. Fersht (W H Freeman, 1999)*. Vol. 13409.

Flotho, Annette, and Frauke Melchior. 2013. "Sumoylation: A Regulatory Protein Modification in Health and Disease." *Http://Dx.Doi.Org/10.1146/Annurev-Biochem-061909-093311* 82 (June): 357–85. https://doi.org/10.1146/ANNUREV-BIOCHEM-061909-093311.

Franco, Maribel, Nicholas T. Seyfried, Andrea H. Brand, Junmin Peng, and Ugo Mayor. 2011. "A Novel Strategy to Isolate Ubiquitin Conjugates Reveals Wide Role for Ubiquitination during Neural Development." *Molecular & Cellular Proteomics* 10 (5): M110.002188. https://doi.org/10.1074/mcp.M110.002188.

Freeman, Marc R., and Johnna Doherty. 2006. "Glial Cell Biology in Drosophila and Vertebrates." *Trends in Neurosciences*. Elsevier Current Trends. https://doi.org/10.1016/j.tins.2005.12.002.

Freemont, P S, I M Hanson, and J Trowsdale. 1991. "A Novel Cysteine-Rich Sequence Motif." *Cell* 64 (3): 483–84. https://doi.org/10.1016/0092-8674(91)90229-r.

Fukunaga, Kohji, Dominique Muller, and Eishichi Miyamoto. 1995. "Increased Phosphorylation of Ca2+/Calmodulin-Dependent Protein Kinase II and Its Endogenous Substrates in the Induction of Long Term Potentiation (∗)." *Journal of Biological Chemistry* 270 (11): 6119–24. https://doi.org/10.1074/JBC.270.11.6119.

Fukutomi, Toshiaki, Kenji Takagi, Tsunehiro Mizushima, Noriaki Ohuchi, and Masayuki Yamamoto. 2014. "Kinetic, Thermodynamic, and Structural Characterizations of the Association between Nrf2-DLGex Degron and Keap1." *Molecular and Cellular Biology* 34 (5): 832–46. https://doi.org/10.1128/MCB.01191-13.

Gaertner, Tara R., Steven J. Kolodziej, Dan Wang, Ryuji Kobayashi, John M. Koomen, James K. Stoops, and M. Neal Waxham. 2004. "Comparative Analyses of the Three-Dimensional Structures and Enzymatic Properties of α, β, γ, and δ Isoforms of Ca2+-Calmodulin-Dependent Protein Kinase II *." *Journal of Biological Chemistry* 279 (13): 12484–94. https://doi.org/10.1074/JBC.M313597200.

Gao, Guanghua, Jason G. Williams, and Sharon L. Campbell. 2004. "Protein-Protein Interaction Analysis by Nuclear Magnetic Resonance Spectroscopy." *Methods in Molecular Biology (Clifton, N.J.)* 261: 79–92. https://doi.org/10.1385/1-59259-762-9:079.

Garcia, Yenni A., Erick F. Velasquez, Lucy W. Gao, Ankur A. Gholkar, Kevin M. Clutario, Keith Cheung, Taylor Williams-Hamilton, Julian P. Whitelegge, and Jorge Z. Torres. 2021. "Mapping Proximity Associations of Core Spindle Assembly Checkpoint Proteins." *Journal of Proteome Research* 20 (7): 3414–27. https://doi.org/10.1021/ACS.JPROTEOME.0C00941.

George, Arlene J., Yarely C. Hoffiz, Antoinette J. Charles, Ying Zhu, and Angela M. Mabb. 2018. "A Comprehensive Atlas of E3 Ubiquitin Ligase Mutations in Neurological Disorders." *Frontiers in Genetics*. Frontiers Media S.A. https://doi.org/10.3389/fgene.2018.00029.

Ghabrial, Amin, Stefan Luschnig, Mark M. Metzstein, and Mark A. Krasnow. 2003. " Branching Morphogenesis of the Drosophila Tracheal System ." *Annual Review of Cell and Developmental Biology* 19 (1): 623–47. https://doi.org/10.1146/annurev.cellbio.19.031403.160043.

Giese, Karl Peter, Nikolai B. Fedorov, Robert K. Filipkowski, and Alcino J. Silva. 1998. "Autophosphorylation at Thr286 of the Alpha Calcium-Calmodulin Kinase II in LTP and Learning." *Science (New York, N.Y.)* 279 (5352): 870–73. https://doi.org/10.1126/SCIENCE.279.5352.870.

Gilberto, Samuel, and Matthias Peter. 2017. "Dynamic Ubiquitin Signaling in Cell Cycle Regulation." *The Journal of Cell Biology* 216 (8): 2259–71. https://doi.org/10.1083/jcb.201703170.

Gonzalez-Lozano, M. A., F. Koopmans, P. F. Sullivan, J. Protze, G. Krause, M. Verhage, K. W. Li, F. Liu, and A. B. Smit. 2020. "Stitching the Synapse: Cross-Linking Mass Spectrometry into Resolving Synaptic Protein Interactions." *Science Advances* 6 (8): 5783. https://doi.org/10.1126/SCIADV.AAX5783.

Grainger, Stephanie, Nicole Nguyen, Jenna Richter, Jordan Setayesh, Brianna Lonquich, Chet Huan Oon, Jacob M. Wozniak, et al. 2019. "EGFR Is Required for Wnt9a–Fzd9b Signalling Specificity in Haematopoietic Stem Cells." *Nature Cell Biology 2019 21:6* 21 (6): 721–30. https://doi.org/10.1038/s41556-019-0330-5.

Green, Douglas R., and Beth Levine. 2014. "To Be or Not to Be? How Selective Autophagy and Cell Death Govern Cell Fate." *Cell*. https://doi.org/10.1016/j.cell.2014.02.049.

Green, Eric M., Curtis F. Barrett, Geert Bultynck, Steven M. Shamah, and Ricardo E. Dolmetsch. 2007. "The Tumor Suppressor EIF3e Mediates Calcium-Dependent Internalization of the L-Type Calcium Channel CaV1.2." *Neuron* 55 (4): 615–32. https://doi.org/10.1016/J.NEURON.2007.07.024.

Griffith, Leslie C., Lynne M. Verselis, Kay Marie Aitken, Charalambos P. Kyriacou, Waleed Danho, and Ralph J. Greenspan. 1993. "Inhibition of Calcium/Calmodulin-Dependent Protein Kinase in Drosophila Disrupts Behavioral Plasticity." *Neuron* 10 (3): 501–9. https://doi.org/10.1016/0896-6273(93)90337-Q.

Groen, Ewout J.N., and Thomas H. Gillingwater. 2015. "UBA1: At the Crossroads of Ubiquitin Homeostasis and Neurodegeneration." *Trends in Molecular Medicine* 21 (10): 622–32. https://doi.org/10.1016/J.MOLMED.2015.08.003.

Guedouari, Hala, Yasmine Ould Amer, Nicolas Pichaud, and Etienne Hebert-Chatelain. 2021. "Characterization of the Interactome of C-Src within the Mitochondrial Matrix by Proximity-Dependent Biotin Identification." *Mitochondrion* 57 (March): 257–69. https://doi.org/10.1016/J.MITO.2020.12.012.

Guo, Dehuang, Manyu Li, Yan Zhang, Ping Yang, Sarah Eckenrode, Diane Hopkins, Weipeng Zheng, et al. 2004. "A Functional Variant of SUMO4, a New I Kappa B Alpha Modifier, Is Associated with Type 1 Diabetes." *Nature Genetics* 36 (8): 837–41. https://doi.org/10.1038/NG1391.

Han, Ke Jun, Daniel Foster, Edward W. Harhaj, Monika Dzieciatkowska, Kirk Hansen, and Chang Wei Liu. 2016. "Monoubiquitination of Survival Motor Neuron Regulates Its Cellular Localization

and Cajal Body Integrity." *Human Molecular Genetics* 25 (7): 1392. https://doi.org/10.1093/HMG/DDW021.

Han, Yisu, Tess Caroline Branon, Jeffrey D. Martell, Daniela Boassa, David Shechner, Mark H. Ellisman, and Alice Ting. 2019. "Directed Evolution of Split APEX2 Peroxidase." *ACS Chemical Biology* 14 (4): 619–35. https://doi.org/10.1021/ACSCHEMBIO.8B00919.

Hansen, Fynn M., Maria C. Tanzer, Franziska Brüning, Isabell Bludau, Che Stafford, Brenda A. Schulman, Maria S. Robles, Ozge Karayel, and Matthias Mann. 2021. "Data-Independent Acquisition Method for Ubiquitinome Analysis Reveals Regulation of Circadian Biology." *Nature Communications 2021 12:1* 12 (1): 1–13. https://doi.org/10.1038/s41467-020-20509-1.

Hartwell, Leland, Leroy E. Hood, Janice A. Fischer, and Michael L. Goldberg. 2003. *Genetics: From Genes to Genomes*. *Journal of the National Medical Association*. Vol. 95.

Hay, Bruce A., Tanya Wolff, and Gerald M. Rubin. 1994. "Expression of Baculovirus P35 Prevents Cell Death in Drosophila." *Development* 120 (8): 2121–29.

Hayes, Sebastian D., Han Liu, Ewan MacDonald, Christopher M. Sanderson, Judy M. Coulson, Michael J. Clague, and Sylvie Urbé. 2012. "Direct and Indirect Control of Mitogen-Activated Protein Kinase Pathway-Associated Components, BRAP/IMP E3 Ubiquitin Ligase and CRAF/RAF1 Kinase, by the Deubiquitylating Enzyme USP15." *Journal of Biological Chemistry* 287 (51): 43007–18. https://doi.org/10.1074/jbc.M112.386938.

Herder, Griet den, Satoko Yoshida, Meritxell Antolín-Llovera, Martina K. Ried, and Martin Parniskea. 2012. "Lotus Japonicus E3 Ligase SEVEN IN ABSENTIA4 Destabilizes the Symbiosis Receptor-like Kinase SYMRK and Negatively Regulates Rhizobial Infection." *Plant Cell* 24 (4): 1691–1707. https://doi.org/10.1105/tpc.110.082248.

Hershko, Avram, and Aaron Ciechanover. 1998. "The Ubiquitin System." *Annu. Rev. Biochem* 67: 425–79. https://doi.org/10.1146/annurev.biochem.67.1.425.

Ho, Shiuh-Rong, Christina S Mahanic, Yu-Ju Lee, and Weei-Chin Lin. 2014. "RNF144A, an E3 Ubiquitin Ligase for DNA-PKcs, Promotes Apoptosis during DNA Damage." *Proceedings of the National Academy of Sciences of the United States of America* 111 (26): E2646-55. https://doi.org/10.1073/pnas.1323107111.

Hochrainer, Karin, Nadja Pejanovic, Victoria A Olaseun, Sheng Zhang, Costantino Iadecola, and Josef Anrather. 2015. "The Ubiquitin Ligase HERC3 Attenuates NF-KB-Dependent Transcription Independently of Its Enzymatic Activity by Delivering the RelA Subunit for Degradation." *Nucleic Acids Research* 43 (20): 9889–9904. https://doi.org/10.1093/nar/gkv1064.

Hoer, Simon, Lorraine Smith, and Paul J Lehner. 2007. "MARCH-IX Mediates Ubiquitination and Downregulation of ICAM-1." *FEBS Letters* 581 (1): 45–51. https://doi.org/10.1016/j.febslet.2006.11.075.

Hu, Shuang, Jing Ouyang, Guoxing Zheng, Yingsi Lu, Qingqing Zhu, Bo Wang, Liping Ye, and Chengming Zhu. 2022. "Identification of Mutant P53-Specific Proteins Interaction Network Using TurboID-Based Proximity Labeling." *Biochemical and Biophysical Research Communications* 615 (July). https://doi.org/10.1016/J.BBRC.2022.05.046.

Huang, Da Wei, Brad T. Sherman, and Richard A. Lempicki. 2009. "Bioinformatics Enrichment Tools: Paths toward the Comprehensive Functional Analysis of Large Gene Lists." *Nucleic Acids Research* 37 (1): 1. https://doi.org/10.1093/NAR/GKN923.

Huang, Da Wei, Brad T Sherman, and Richard A Lempicki. 2008. "Systematic and Integrative Analysis of Large Gene Lists Using DAVID Bioinformatics Resources." *Nature Protocols 2009 4:1* 4 (1): 44–57. https://doi.org/10.1038/nprot.2008.211.

Hudmon, Andy, and Howard Schulman. 2002. "Neuronal CA2+/Calmodulin-Dependent Protein Kinase II: The Role of Structure and Autoregulation in Cellular Function." *Annual Review of Biochemistry* 71: 473–510. https://doi.org/10.1146/ANNUREV.BIOCHEM.71.110601.135410.

Huibregtse, J M, M Scheffner, S Beaudenon, and P M Howley. 1995. "A Family of Proteins Structurally and Functionally Related to the E6-AP Ubiquitin-Protein Ligase." *Proceedings of the National Academy of Sciences of the United States of America* 92 (11): 5249. http://www.ncbi.nlm.nih.gov/pubmed/7761480.

Hulsen, Tim, Jacob de Vlieg, and Wynand Alkema. 2008. "BioVenn - A Web Application for the Comparison and Visualization of Biological Lists Using Area-Proportional Venn Diagrams." *BMC Genomics* 9 (1): 488. https://doi.org/10.1186/1471-2164-9-488.

Hunter, Tony. 2007. "The Age of Crosstalk: Phosphorylation, Ubiquitination, and Beyond." *Molecular Cell* 28 (5): 730–38. https://doi.org/10.1016/J.MOLCEL.2007.11.019.

Ishizuka, Yasuyuki, Reiko Mochizuki, Kazuyuki Yanai, Miki Takatsuka, Takeshi Nonomura, Shumpei Niida, Hisashi Horiguchi, Norihiko Maeda, and Akiyoshi Fukamizu. 1999. "Induction of Hydroxyapatite Resorptive Activity in Bone Marrow Cell Populations Resistant to Bafilomycin A1 by a Factor with Restricted Expression to Bone and Brain, Neurochondrin." *Biochimica et Biophysica Acta (BBA) - Molecular Cell Research* 1450 (1): 92–98. https://doi.org/10.1016/S0167-4889(99)00039-7.

Ito, Takashi, Tomoko Chiba, Ritsuko Ozawa, Mikio Yoshida, Masahira Hattori, and Yoshiyuki Sakaki. 2001. "A Comprehensive Two-Hybrid Analysis to Explore the Yeast Protein Interactome." *Proceedings of the National Academy of Sciences of the United States of America* 98 (8): 4569–74. https://doi.org/10.1073/PNAS.061034498.

Jarome, Timothy J., Nicole C. Ferrara, Janine L. Kwapis, and Fred J. Helmstetter. 2016. "CaMKII Regulates Proteasome Phosphorylation and Activity and Promotes Memory Destabilization Following Retrieval." *Neurobiology of Learning and Memory* 128: 103–9. https://doi.org/10.1016/j.nlm.2016.01.001.

Javadi, Mojib, Terri D. Richmond, Kai Huang, and Dwayne L. Barber. 2013. "CBL Linker Region and RING Finger Mutations Lead to Enhanced Granulocyte-Macrophage Colony-Stimulating Factor (GM-CSF) Signaling via Elevated Levels of JAK2 and LYN." *Journal of Biological Chemistry* 288 (27): 19459–70. https://doi.org/10.1074/jbc.M113.475087.

Ji, Lei, Bo Jiang, Xiaomo Jiang, Olga Charlat, Amy Chen, Craig Mickanin, Andreas Bauer, Wenqing Xu, Xiaoxue Yan, and Feng Cong. 2017. "The SIAH E3 Ubiquitin Ligases Promote Wnt/β-Catenin Signaling through Mediating Wnt-Induced Axin Degradation." *Genes & Development* 31 (9): 904–15. https://doi.org/10.1101/gad.300053.117.

Jiang, Xiao Xia, Quan Nguyen, Yu Chia Chou, Tao Wang, Vijayalakshmi Nandakumar, Peter Yates, Lindsey Jones, et al. 2011. "Control of B Cell Development by the Histone H2A Deubiquitinase MYSM1." *Immunity* 35 (6): 883–96. https://doi.org/10.1016/J.IMMUNI.2011.11.010.

Joazeiro, C A, S S Wing, H Huang, J D Leverson, T Hunter, and Y C Liu. 1999. "The Tyrosine Kinase Negative Regulator C-Cbl as a RING-Type, E2-Dependent Ubiquitin-Protein Ligase." *Science* 286 (5438): 309–12. https://doi.org/10.1126/science.286.5438.309.

Jones, Jessica M, and Martin Gellert. 2003. "Autoubiquitylation of the V(D)J Recombinase Protein RAG1." *Proceedings of the National Academy of Sciences of the United States of America* 100 (26): 15446–51. https://doi.org/10.1073/pnas.2637012100.

Joukov, Vladimir, Junjie Chen, Edward A. Fox, Jeremy B.A. Green, and David M. Livingston. 2001. "Functional Communication between Endogenous BRCA1 and Its Partner, BARD1, during Xenopus Laevis Development." *Proceedings of the National Academy of Sciences of the United States of America* 98 (21): 12078–83. https://doi.org/10.1073/pnas.211427098.

Kaiser, Stephen E., Brigit E. Riley, Thomas A. Shaler, R. Sean Trevino, Christopher H. Becker, Howard Schulman, and Ron R. Kopito. 2011. "Protein Standard Absolute Quantification (PSAQ) Method for the Measurement of Cellular Ubiquitin Pools." *Nature Methods* 8 (8): 691–96. https://doi.org/10.1038/NMETH.1649.

Kallijärvi, Jukka, Ulla Lahtinen, Riikka Hämäläinen, Marita Lipsanen-Nyman, Jorma J Palvimo, and Anna-Elina Lehesjoki. 2005. "TRIM37 Defective in Mulibrey Nanism Is a Novel RING Finger Ubiquitin E3 Ligase." *Experimental Cell Research* 308 (1): 146–55. https://doi.org/10.1016/j.yexcr.2005.04.001.

Kamadurai, Hari B, Judith Souphron, Daniel C Scott, David M Duda, Darcie J Miller, Daniel Stringer, Robert C Piper, and Brenda a Schulman. 2009. "Insights into Ubiquitin Transfer Cascades from a Structure of a UbcH5B Approximately Ubiquitin-HECT(NEDD4L) Complex." *Molecular Cell* 36 (6): 1095–1102. https://doi.org/10.1016/j.molcel.2009.11.010.

Kanelis, Voula, Daniela Rotin, and Julie D. Forman-Kay. 2001. "Solution Structure of a Nedd4 WW Domain-ENaC Peptide Complex." *Nature Structural Biology* 8 (5): 407–12. https://doi.org/10.1038/87562.

Kawashima, Akira, Tadayoshi Karasawa, Kenji Tago, Hiroaki Kimura, Ryo Kamata, Fumitake Usui-Kawanishi, Sachiko Watanabe, et al. 2017. "ARIH2 Ubiquitinates NLRP3 and Negatively Regulates NLRP3 Inflammasome Activation in Macrophages." *Journal of Immunology (Baltimore, Md. : 1950)* 199 (10): 3614–22. https://doi.org/10.4049/jimmunol.1700184.

Kerscher, Oliver, Rachael Felberbaum, and Mark Hochstrasser. 2006. "Modification of Proteins by Ubiquitin and Ubiquitin-like Proteins." *Annual Review of Cell and Developmental Biology* 22: 159–80. https://doi.org/10.1146/ANNUREV.CELLBIO.22.010605.093503.

Kim, D. I., S. C. Jensen, K. A. Noble, B. KC, K. H. Roux, K. Motamedchaboki, and K. J. Roux. 2016. "An Improved Smaller Biotin Ligase for BioID Proximity Labeling." *Molecular Biology of the Cell* 27 (8): 1188–96. https://doi.org/10.1091/mbc.E15-12-0844.

Kim, Dae In, K. C. Birendra, Wenhong Zhu, Khatereh Motamedchaboki, Valérie Doye, and Kyle J. Roux.

2014. “Probing Nuclear Pore Complex Architecture with Proximity-Dependent Biotinylation.” *Proceedings of the National Academy of Sciences of the United States of America* 111 (24). https://doi.org/10.1073/PNAS.1406459111.

Kim, Dong Hyun, Sanghoon Kwon, Sangwon Byun, Zhen Xiao, Sean Park, Shwu Yuan Wu, Cheng Ming Chiang, Byron Kemper, and Jongsook Kim Kemper. 2016. “Critical Role of RanBP2-Mediated SUMOylation of Small Heterodimer Partner in Maintaining Bile Acid Homeostasis.” *Nature Communications* 7 (July). https://doi.org/10.1038/NCOMMS12179.

Kim, Hyung Cheol, and Jon M. Huibregtse. 2009. “Polyubiquitination by HECT E3s and the Determinants of Chain Type Specificity.” *Molecular and Cellular Biology* 29 (12): 3307–18. https://doi.org/10.1128/MCB.00240-09.

Kim, Joo Mi, Eun Nae Cho, Young Eun Kwon, Sung Jun Bae, Myungjin Kim, and Jae Hong Seol. 2010. “CHFR Functions as a Ubiquitin Ligase for HLTF to Regulate Its Stability and Functions.” *Biochemical and Biophysical Research Communications* 395 (4): 515–20. https://doi.org/10.1016/j.bbrc.2010.04.052.

Kim, Woong, Eric J. Bennett, Edward L. Huttlin, Ailan Guo, Jing Li, Anthony Possemato, Mathew E. Sowa, et al. 2011. “Systematic and Quantitative Assessment of the Ubiquitin-Modified Proteome.” *Molecular Cell* 44 (2): 325–40. https://doi.org/10.1016/J.MOLCEL.2011.08.025.

Kishino, Tatsuya, Marc Lalande, and Joseph Wagstaff. 1997. “UBE3A/E6-AP Mutations Cause Angelman Syndrome.” *Nature Genetics* 15 (1): 70–73. https://doi.org/10.1038/ng0197-70.

Koh, Young Ho, Evgenya Popova, Ulrich Thomas, Leslie C. Griffith, and Vivian Budnik. 1999. “Regulation of DLG Localization at Synapses by CaMKII-Dependent Phosphorylation.” *Cell* 98 (3): 353–63. https://doi.org/10.1016/S0092-8674(00)81964-9.

Komander, David, and Michael Rape. 2012. “The Ubiquitin Code.” *Annual Review of Biochemistry* 81 (1): 203–29. https://doi.org/10.1146/annurev-biochem-060310-170328.

Komata, Yosuke, Shoma Tsubota, Kazuma Sakamoto, Shinya Ikematsu, and Kenji Kadomatsu. 2021. “Screening of Novel Midkine Binding Protein by BioID2-Based Proximity Labeling.” *Nagoya Journal of Medical Science* 83 (3): 495–508. https://doi.org/10.18999/NAGJMS.83.3.495.

Kooi, Craig W. Vander, Melanie D. Ohi, Joshua A. Rosenberg, Michael L. Oldham, Marcia E. Newcomer, Kathleen L. Gould, and Walter J. Chazin. 2006. “The Prp19 U-Box Crystal Structure Suggests a Common Dimeric Architecture for a Class of Oligomeric E3 Ubiquitin Ligases.” *Biochemistry* 45 (1): 121–30. https://doi.org/10.1021/bi051787e.

Kostic, Milka, Theresia Matt, Maria A. Martinez-Yamout, H. Jane Dyson, and Peter E. Wright. 2006. “Solution Structure of the Hdm2 C2H2C4 RING, a Domain Critical for Ubiquitination of P53.” *Journal of Molecular Biology* 363 (2): 433–50. https://doi.org/10.1016/j.jmb.2006.08.027.

Küry, Sébastien, Geeske M. van Woerden, Thomas Besnard, Martina Proietti Onori, Xénia Latypova, Meghan C. Towne, Megan T. Cho, et al. 2017. “De Novo Mutations in Protein Kinase Genes CAMK2A and CAMK2B Cause Intellectual Disability.” *American Journal of Human Genetics* 101 (5): 768–88. https://doi.org/10.1016/J.AJHG.2017.10.003.

Kwak, Chulhwan, Sanghee Shin, Jong Seok Park, Minkyo Jung, Truong Thi My Nhung, Myeong Gyun Kang, Chaiheon Lee, et al. 2020. "Contact-ID, a Tool for Profiling Organelle Contact Sites, Reveals Regulatory Proteins of Mitochondrial-Associated Membrane Formation." *Proceedings of the National Academy of Sciences of the United States of America* 117 (22). https://doi.org/10.1073/PNAS.1916584117/-/DCSUPPLEMENTAL.

Lai, Z, D A Freedman, A J Levine, and G L McLendon. 1998. "Metal and RNA Binding Properties of the Hdm2 RING Finger Domain." *Biochemistry* 37 (48): 17005–15. http://www.ncbi.nlm.nih.gov/pubmed/9882094.

Lambert-Smith, Isabella A., Darren N. Saunders, and Justin J. Yerbury. 2020. "The Pivotal Role of Ubiquitin-Activating Enzyme E1 (UBA1) in Neuronal Health and Neurodegeneration." *The International Journal of Biochemistry & Cell Biology* 123 (June). https://doi.org/10.1016/J.BIOCEL.2020.105746.

Landry, Natalie M., Sunil G. Rattan, Krista L. Filomeno, Thomas W. Meier, Simon C. Meier, Sarah J. Foran, Claire F. Meier, et al. 2021. "SKI Activates the Hippo Pathway via LIMD1 to Inhibit Cardiac Fibroblast Activation." *Basic Research in Cardiology* 116 (1). https://doi.org/10.1007/S00395-021-00865-9.

Laney, Jeffrey D., and Mark Hochstrasser. 1999. "Substrate Targeting in the Ubiquitin System." *Cell 97 (4): 427-430*. https://doi.org/10.1016/S0092-8674(00)80752-7.

Lauks, Juliane, Patricia Klemmer, Fatima Farzana, Ramesh Karupothula, Robbert Zalm, Nancy E. Cooke, Ka Wan Li, August B. Smit, Ruud Toonen, and Matthijs Verhage. 2012. "Synapse Associated Protein 102 (SAP102) Binds the C-Terminal Part of the Scaffolding Protein Neurobeachin." *PloS One* 7 (6). https://doi.org/10.1371/JOURNAL.PONE.0039420.

Lazzari, Elisa, Medhat El-Halawany, Matteo De March, Floriana Valentino, Francesco Cantatore, Chiara Migliore, Silvia Onesti, and Germana Meroni. 2019. "Analysis of the Zn-Binding Domains of TRIM32, the E3 Ubiquitin Ligase Mutated in Limb Girdle Muscular Dystrophy 2H." *Cells* 8 (3): 254. https://doi.org/10.3390/cells8030254.

Lectez, Benoît, Rebekka Migotti, So Young Lee, Juanma Ramirez, Naiara Beraza, Bill Mansfield, James D. Sutherland, Maria L. Martinez-Chantar, Gunnar Dittmar, and Ugo Mayor. 2014. "Ubiquitin Profiling in Liver Using a Transgenic Mouse with Biotinylated Ubiquitin." *Journal of Proteome Research* 13 (6): 3016–26. https://doi.org/10.1021/pr5001913.

Lee, Boyoung, Eunyoung Bang, Won Suk Yang, Afshin Paydar, Go Eun Ha, Sujin Kim, Jong Hyun Kim, et al. 2018. "The Possible Role of Neurobeachin in Extinction of Contextual Fear Memory." *Scientific Reports* 8 (1). https://doi.org/10.1038/S41598-018-30589-1.

Lee, Jae Min, Sun Sil Choi, Yo Han Lee, Keon Woo Khim, Sora Yoon, Byung-Gyu Kim, Dougu Nam, Pann-Ghill Suh, Kyungjae Myung, and Jang Hyun Choi. 2018. "The E3 Ubiquitin Ligase TRIM25 Regulates Adipocyte Differentiation via Proteasome-Mediated Degradation of PPARγ." *Experimental & Molecular Medicine* 50 (10): 135. https://doi.org/10.1038/s12276-018-0162-6.

Lee, Min Sik, Hyun Ji Han, Su Yeon Han, Il Young Kim, Sehyun Chae, Choong Sil Lee, Sung Eun Kim, et al. 2018. "Loss of the E3 Ubiquitin Ligase MKRN1 Represses Diet-Induced Metabolic Syndrome

through AMPK Activation." *Nature Communications* 9 (1): 3404. https://doi.org/10.1038/s41467-018-05721-4.

Lee, So Young, Juanma Ramirez, Maribel Franco, Benoît Lectez, Monika Gonzalez, Rosa Barrio, and Ugo Mayor. 2014. "Ube3a, the E3 Ubiquitin Ligase Causing Angelman Syndrome and Linked to Autism, Regulates Protein Homeostasis through the Proteasomal Shuttle Rpn10." *Cellular and Molecular Life Sciences* 71 (14): 2747–58. https://doi.org/10.1007/s00018-013-1526-7.

Lehner, Paul J, Simon Hoer, Roger Dodd, and Lidia M Duncan. 2005. "Downregulation of Cell Surface Receptors by the K3 Family of Viral and Cellular Ubiquitin E3 Ligases." *Immunological Reviews* 207: 112–25. https://doi.org/10.1111/j.0105-2896.2005.00314.x.

Leidecker, Orsolya, Ivan Matic, Bidesh Mahata, Emmanuelle Pion, and Dimitris P. Xirodimas. 2012. "The Ubiquitin E1 Enzyme Ube1 Mediates NEDD8 Activation under Diverse Stress Conditions." *Cell Cycle (Georgetown, Tex.)* 11 (6): 1142–50. https://doi.org/10.4161/CC.11.6.19559.

Li, Haiwen, Li Xu, Yandi Gao, Yuanbojiao Zuo, Zuocheng Yang, Lingling Zhao, Zhiheng Chen, Shuliang Guo, and Renzhi Han. 2021. "BVES Is a Novel Interactor of ANO5 and Regulates Myoblast Differentiation." *Cell & Bioscience* 11 (1). https://doi.org/10.1186/S13578-021-00735-W.

Li, Wentian, Jan Freudenberg, Young Ju Suh, and Yaning Yang. 2014. "Using Volcano Plots and Regularized-Chi Statistics in Genetic Association Studies." *Computational Biology and Chemistry* 48 (February): 77–83. https://doi.org/10.1016/j.compbiolchem.2013.02.003.

Li, Xinchun, Li Zhong, Zhuo Wang, Huiming Chen, Dan Liao, Ruhua Zhang, Hongyu Zhang, and Tiebang Kang. 2018. "Phosphorylation of IRS4 by CK1γ2 Promotes Its Degradation by CHIP through the Ubiquitin/Lysosome Pathway." *Theranostics* 8 (13): 3643–53. https://doi.org/10.7150/thno.26021.

Li, Yang, Han Wu, Wei Wu, Wei Zhuo, Weixiao Liu, Yixiao Zhang, Minzhang Cheng, et al. 2014. "Structural Insights into the TRIM Family of Ubiquitin E3 Ligases." *Cell Research*. Nature Publishing Group. https://doi.org/10.1038/cr.2014.46.

Li, Yunfei, Shengde Liu, Lili Cao, Yujie Luo, Hongqiang Du, Siji Li, Zeming Zhang, et al. 2021. "CBRPP: A New RNA-Centric Method to Study RNA–protein Interactions." *RNA Biology* 18 (11): 1608. https://doi.org/10.1080/15476286.2021.1873620.

Liani, Esti, Allon Eyal, Eyal Avraham, Revital Shemer, Raymonde Szargel, Daniela Berg, Antje Bornemann, et al. 2004. "Ubiquitylation of Synphilin-1 and Alpha-Synuclein by SIAH and Its Presence in Cellular Inclusions and Lewy Bodies Imply a Role in Parkinson's Disease." *Proceedings of the National Academy of Sciences of the United States of America* 101 (15): 5500–5505. https://doi.org/10.1073/PNAS.0401081101.

Lienlaf, M., F. Hayashi, F. Di Nunzio, N. Tochio, T. Kigawa, S. Yokoyama, and F. Diaz-Griffero. 2011. "Contribution of E3-Ubiquitin Ligase Activity to HIV-1 Restriction by TRIM5αrh: Structure of the RING Domain of TRIM5." *Journal of Virology* 85 (17): 8725–37. https://doi.org/10.1128/jvi.00497-11.

Liew, Chu Wai, Huaiyu Sun, Tony Hunter, and Catherine L Day. 2010. "RING Domain Dimerization Is Essential for RNF4 Function." *The Biochemical Journal* 431 (1): 23–29.

https://doi.org/10.1042/BJ20100957.

Linke, K, P D Mace, C A Smith, D L Vaux, J Silke, and C L Day. 2008. "Structure of the MDM2/MDMX RING Domain Heterodimer Reveals Dimerization Is Required for Their Ubiquitylation in Trans." *Cell Death and Differentiation* 15 (5): 841–48. https://doi.org/10.1038/sj.cdd.4402309.

Lisman, J. E. 1985. "A Mechanism for Memory Storage Insensitive to Molecular Turnover: A Bistable Autophosphorylating Kinase." *Proceedings of the National Academy of Sciences of the United States of America* 82 (9): 3055–57. https://doi.org/10.1073/PNAS.82.9.3055.

Liu, Bingyu, Meng Zhang, Honglei Chu, Honghai Zhang, Haifeng Wu, Guanhua Song, Peng Wang, et al. 2017. "The Ubiquitin E3 Ligase TRIM31 Promotes Aggregation and Activation of the Signaling Adaptor MAVS through Lys63-Linked Polyubiquitination." *Nature Immunology* 18 (2): 214–24. https://doi.org/10.1038/ni.3641.

Liu, Hsiu Yu, and Cathie M. Pfleger. 2013. "Mutation in E1, the Ubiquitin Activating Enzyme, Reduces Drosophila Lifespan and Results in Motor Impairment." *PloS One* 8 (1). https://doi.org/10.1371/JOURNAL.PONE.0032835.

Liu, Juan, Cen Zhang, Yuhan Zhao, Xuetian Yue, Hao Wu, Shan Huang, James Chen, et al. 2017. "Parkin Targets HIF-1α for Ubiquitination and Degradation to Inhibit Breast Tumor Progression." *Nature Communications* 8 (1): 1823. https://doi.org/10.1038/s41467-017-01947-w.

Liu, Qiang, Jun Zheng, Weiping Sun, Yinbo Huo, Liye Zhang, Piliang Hao, Haopeng Wang, and Min Zhuang. 2018. "A Proximity-Tagging System to Identify Membrane Protein–protein Interactions." *Nature Methods*. https://doi.org/10.1038/s41592-018-0100-5.

Liu, Shuo, Minghong Jiang, Wendie Wang, Wei Liu, Xiaoqi Song, Zhongfei Ma, Shikun Zhang, Lun Liu, Yin Liu, and Xuetao Cao. 2018. "Nuclear RNF2 Inhibits Interferon Function by Promoting K33-Linked STAT1 Disassociation from DNA." *Nature Immunology* 19 (1): 41–52. https://doi.org/10.1038/s41590-017-0003-0.

Lohr, Naomi J., Jean P. Molleston, Kevin A. Strauss, Wilfredo Torres-Martinez, Eric A. Sherman, Robert H. Squires, Nicholas L. Rider, et al. 2010. "Human ITCH E3 Ubiquitin Ligase Deficiency Causes Syndromic Multisystem Autoimmune Disease." *American Journal of Human Genetics* 86 (3): 447–53. https://doi.org/10.1016/J.AJHG.2010.01.028.

Long, Xiaomeng, and Leslie C. Griffith. 2000. "Identification and Characterization of a SUMO-1 Conjugation System That Modifies Neuronal Calcium/Calmodulin-Dependent Protein Kinase II in Drosophila Melanogaster." *The Journal of Biological Chemistry* 275 (52): 40765–76. https://doi.org/10.1074/JBC.M003949200.

Loregger, Anke, Martina Grandl, Raquel Mejías-Luque, Michael Allgäuer, Kathrin Degenhart, Verena Haselmann, Christina Oikonomou, et al. 2015. "The E3 Ligase RNF43 Inhibits Wnt Signaling Downstream of Mutated β-Catenin by Sequestering TCF4 to the Nuclear Membrane." *Science Signaling* 8 (393): 1–13. https://doi.org/10.1126/scisignal.aac6757.

Lorick, K L, J P Jensen, S Fang, A M Ong, S Hatakeyama, and A M Weissman. 1999. "RING Fingers Mediate Ubiquitin-Conjugating Enzyme (E2)-Dependent Ubiquitination." *Proceedings of the National Academy of Sciences of the United States of America* 96 (20): 11364–69.

https://doi.org/10.1073/pnas.96.20.11364.

Lou, L. L., S. J. Lloyd, and H. Schulman. 1986. "Activation of the Multifunctional Ca2+/Calmodulin-Dependent Protein Kinase by Autophosphorylation: ATP Modulates Production of an Autonomous Enzyme." *Proceedings of the National Academy of Sciences of the United States of America* 83 (24): 9497. https://doi.org/10.1073/PNAS.83.24.9497.

Lv, Binna, Lele Fan, Shidong Li, and Manhong Sun. 2022. "Screening and Characterisation of Proteins Interacting with the Mitogen-Activated Protein Kinase Crmapk in the Fungus Clonostachys Chloroleuca." *Scientific Reports* 12 (1). https://doi.org/10.1038/S41598-022-13899-3.

MacBeath, Gavin, and Stuart L. Schreiber. 2000. "Printing Proteins as Microarrays for High-Throughput Function Determination." *Science (New York, N.Y.)* 289 (5485): 1760–63. https://doi.org/10.1126/SCIENCE.289.5485.1760.

Machitani, Mitsuhiro, Ichiro Taniguchi, and Mutsuhito Ohno. 2020. "ARS2 Regulates Nuclear Paraspeckle Formation through 3=-End Processing and Stability of NEAT1 Long Noncoding RNA." https://doi.org/10.1128/MCB.00269-19.

Mair, Andrea, Shou Ling Xu, Tess C. Branon, Alice Y. Ting, and Dominique C. Bergmann. 2019. "Proximity Labeling of Protein Complexes and Cell-Type-Specific Organellar Proteomes in Arabidopsis Enabled by TurboID." *ELife* 8 (September). https://doi.org/10.7554/ELIFE.47864.

Malinow, Roberto. 2003. "AMPA Receptor Trafficking and Long-Term Potentiation." *Philosophical Transactions of the Royal Society B: Biological Sciences* 358 (1432): 707. https://doi.org/10.1098/RSTB.2002.1233.

Mallette, Frédérick A, Francesca Mattiroli, Gaofeng Cui, Leah C Young, Michael J Hendzel, Georges Mer, Titia K Sixma, and Stéphane Richard. 2012. "RNF8- and RNF168-Dependent Degradation of KDM4A/JMJD2A Triggers 53BP1 Recruitment to DNA Damage Sites." *The EMBO Journal* 31 (8): 1865–78. https://doi.org/10.1038/emboj.2012.47.

Margolis, Seth S., Gabrielle L. Sell, Mark A. Zbinden, and Lynne M. Bird. 2015. "Angelman Syndrome." *Neurotherapeutics*. https://doi.org/10.1007/s13311-015-0361-y.

Martell, Jeffrey D., Thomas J. Deerinck, Yasemin Sancak, Thomas L. Poulos, Vamsi K. Mootha, Gina E. Sosinsky, Mark H. Ellisman, and Alice Y. Ting. 2012. "Engineered Ascorbate Peroxidase as a Genetically Encoded Reporter for Electron Microscopy." *Nature Biotechnology*. https://doi.org/10.1038/nbt.2375.

Martell, Jeffrey D., Masahito Yamagata, Thomas J. Deerinck, Sébastien Phan, Carolyn G. Kwa, Mark H. Ellisman, Joshua R. Sanes, and Alice Y. Ting. 2016. "A Split Horseradish Peroxidase for the Detection of Intercellular Protein-Protein Interactions and Sensitive Visualization of Synapses." *Nature Biotechnology* 34 (7): 774–80. https://doi.org/10.1038/NBT.3563.

Martínez-Noël, Gustavo, Katja Luck, Simone Kühnle, Alice Desbuleux, Patricia Szajner, Jeffrey T. Galligan, Diana Rodriguez, et al. 2018. "Network Analysis of UBE3A/E6AP-Associated Proteins Provides Connections to Several Distinct Cellular Processes." *Journal of Molecular Biology* 430 (7): 1024–50. https://doi.org/10.1016/j.jmb.2018.01.021.

Martinez, Aitor, Benoit Lectez, Juanma Ramirez, Oliver Popp, James D. Sutherland, Sylvie Urbé, Gunnar Dittmar, Michael J. Clague, and Ugo Mayor. 2017. "Quantitative Proteomic Analysis of Parkin Substrates in Drosophila Neurons." *Molecular Neurodegeneration* 12 (1): 29. https://doi.org/10.1186/s13024-017-0170-3.

Maruyama, Takeshi, Toshihiro Araki, Yosuke Kawarazaki, Isao Naguro, Susanne Heynen, Pedro Aza-Blanc, Ze'ev Ronai, Atsushi Matsuzawa, and Hidenori Ichijo. 2014. "Roquin-2 Promotes Ubiquitin-Mediated Degradation of ASK1 to Regulate Stress Responses." *Science Signaling* 7 (309): ra8. https://doi.org/10.1126/scisignal.2004822.

Masuda, Yuji, Miki Suzuki, Hidehiko Kawai, Fumio Suzuki, and Kenji Kamiya. 2012. "Asymmetric Nature of Two Subunits of RAD18, a RING-Type Ubiquitin Ligase E3, in the Human RAD6A-RAD18 Ternary Complex." *Nucleic Acids Research* 40 (3): 1065–76. https://doi.org/10.1093/nar/gkr805.

Matsuda, Shinji, Wataru Kakegawa, Timotheus Budisantoso, Toshihiro Nomura, Kazuhisa Kohda, and Michisuke Yuzaki. 2013. "Stargazin Regulates AMPA Receptor Trafficking through Adaptor Protein Complexes during Long-Term Depression." *Nature Communications* 4. https://doi.org/10.1038/NCOMMS3759.

Matsuura, Toshinobu, James S. Sutcliffe, Ping Fang, Robert Jan Galjaard, Yong Hui Jiang, Claudia S. Benton, Johanna M. Rommens, and Arthur L. Beaudet. 1997. "De Novo Truncating Mutations in E6-Ap Ubiquitin-Protein Ligase Gene (UBE3A) in Angelman Syndrome." *Nature Genetics* 15 (1): 74–77. https://doi.org/10.1038/ng0197-74.

Matz, A., S. J. Lee, N. Schwedhelm-Domeyer, D. Zanini, A. Holubowska, M. Kannan, M. Farnworth, O. Jahn, M. C. Göpfert, and J. Stegmüller. 2015. "Regulation of Neuronal Survival and Morphology by the E3 Ubiquitin Ligase RNF157." *Cell Death and Differentiation* 22 (4): 626–42. https://doi.org/10.1038/CDD.2014.163.

Mazina, Marina Yu, Rustam H. Ziganshin, Mikhail D. Magnitov, Anton K. Golovnin, and Nadezhda E. Vorobyeva. 2020. "Proximity-Dependent Biotin Labelling Reveals CP190 as an EcR/Usp Molecular Partner." *Scientific Reports* 10 (1): 4793. https://doi.org/10.1038/s41598-020-61514-0.

Metzger, Meredith B, Jonathan N Pruneda, Rachel E Klevit, and Allan M Weissman. 2014. "RING-Type E3 Ligases: Master Manipulators of E2 Ubiquitin-Conjugating Enzymes and Ubiquitination." *Biochimica et Biophysica Acta* 1843 (1): 47–60. https://doi.org/10.1016/j.bbamcr.2013.05.026.

Micallef, Luana, and Peter Rodgers. 2014. "EulerAPE: Drawing Area-Proportional 3-Venn Diagrams Using Ellipses." Edited by Hans A. Kestler. *PLoS ONE* 9 (7): e101717. https://doi.org/10.1371/journal.pone.0101717.

Michnick, Stephen W., Po Hien Ear, Christian Landry, Mohan K. Malleshaiah, and Vincent Messier. 2011. "Protein-Fragment Complementation Assays for Large-Scale Analysis, Functional Dissection and Dynamic Studies of Protein-Protein Interactions in Living Cells." *Methods in Molecular Biology (Clifton, N.J.)* 756: 395–425. https://doi.org/10.1007/978-1-61779-160-4_25.

Miller, Stephen G., and Mary B. Kennedy. 1986. "Regulation of Brain Type II Ca2+/Calmodulin-Dependent Protein Kinase by Autophosphorylation: A Ca2+-Triggered Molecular Switch." *Cell* 44 (6): 861–70. https://doi.org/10.1016/0092-8674(86)90008-5.

Mimnaugh, Edward G., Hou Yu Chen, James R. Davie, Julio E. Cells, and Len Neckers. 1997. "Rapid Deubiquitination of Nucleosomal Histones in Human Tumor Cells Caused by Proteasome Inhibitors and Stress Response Inducers: Effects on Replication, Transcription, Translation, and the Cellular Stress Response." *Biochemistry* 36 (47): 14418–29. https://doi.org/10.1021/BI970998J.

Monastirioti, Maria. 1999. "Biogenic Amine Systems in the Fruit Fly Drosophila Melanogaster." *Microscopy Research and Technique* 45 (2): 106–21. https://doi.org/10.1002/(SICI)1097-0029(19990415)45:2<106::AID-JEMT5>3.0.CO;2-3.

Montana, Enrico S., and J. Troy Littleton. 2006. "Expression Profiling of a Hypercontraction-Induced Myopathy in Drosophila Suggests a Compensatory Cytoskeletal Remodeling Response." *Journal of Biological Chemistry* 281 (12): 8100–8109. https://doi.org/10.1074/jbc.M512468200.

Morett, Enrique, and Peer Bork. 1999. "A Novel Transactivation Domain in Parkin." *Trends in Biochemical Sciences* 24 (6): 229–31. https://doi.org/10.1016/S0968-0004(99)01381-X.

Morgan, T. H. 1910. "Sex Limited Inheritance in Drosophila." *Science* 32 (812): 120–22. https://doi.org/10.1126/science.32.812.120.

Morreale, Francesca Ester, and Helen Walden. 2016. "Types of Ubiquitin Ligases." *Cell* 165 (1): 248–248.e1. https://doi.org/10.1016/j.cell.2016.03.003.

Morris, Joanna R., and Ellen Solomon. 2004. "BRCA1: BARD1 Induces the Formation of Conjugated Ubiquitin Structures, Dependent on K6 of Ubiquitin, in Cells during DNA Replication and Repair." *Human Molecular Genetics* 13 (8): 807–17. https://doi.org/10.1093/hmg/ddh095.

Mulhern, Maureen S., Constance Stumpel, Nicholas Stong, Han G. Brunner, Louise Bier, Natalie Lippa, James Riviello, et al. 2018. "NBEA: Developmental Disease Gene with Early Generalized Epilepsy Phenotypes." *Annals of Neurology* 84 (5): 788–95. https://doi.org/10.1002/ANA.25350.

Muńoz-Escobar, Juliana, Edna Matta-Camacho, Guennadi Kozlov, and Kalle Gehring. 2015. "The MLLE Domain of the Ubiquitin Ligase UBR5 Binds to Its Catalytic Domain to Regulate Substrate Binding." *Journal of Biological Chemistry* 290 (37): 22841–50. https://doi.org/10.1074/jbc.M115.672246.

Munter, Sofie De, Janina Görnemann, Rita Derua, Bart Lesage, Junbin Qian, Ewald Heroes, Etienne Waelkens, Aleyde Van Eynde, Monique Beullens, and Mathieu Bollen. 2017. "Split-BioID: A Proximity Biotinylation Assay for Dimerization-Dependent Protein Interactions." *FEBS Letters* 591 (2): 415–24. https://doi.org/10.1002/1873-3468.12548.

Nair, Ramya, Juliane Lauks, SangYong Jung, Nancy E. Cooke, Heidi de Wit, Nils Brose, Manfred W. Kilimann, Matthijs Verhage, and JeongSeop Rhee. 2013. "Neurobeachin Regulates Neurotransmitter Receptor Trafficking to Synapses." *Journal of Cell Biology* 200 (1): 61–80. https://doi.org/10.1083/jcb.201207113.

Nakatani, Yoshio, Torsten Kleffmann, Katrin Linke, Stephen M Condon, Mark G Hinds, and Catherine L Day. 2013. "Regulation of Ubiquitin Transfer by XIAP, a Dimeric RING E3 Ligase." *The Biochemical Journal* 450 (3): 629–38. https://doi.org/10.1042/BJ20121702.

Nandakumar, Vijayalakshmi, Yuchia Chou, Linda Zang, Xue F. Huang, and Si Yi Chen. 2013. "Epigenetic Control of Natural Killer Cell Maturation by Histone H2A Deubiquitinase, MYSM1." *Proceedings of the National Academy of Sciences of the United States of America* 110 (41). https://doi.org/10.1073/PNAS.1308888110.

Nessel, Timothy, John M. Beck, Shima Rayatpisheh, Yasaman Jami-Alahmadi, James A. Wohlschlegel, Daniel E. Goldberg, and Josh R. Beck. 2020. "EXP1 Is Required for Organisation of EXP2 in the Intraerythrocytic Malaria Parasite Vacuole." *Cellular Microbiology*, May. https://doi.org/10.1111/cmi.13168.

Nguyen, Thanh My Thi, Junhyung Kim, Thi Tram Doan, Min Woo Lee, and Mihye Lee. 2020. "APEX Proximity Labeling as a Versatile Tool for Biological Research." *Biochemistry* 59 (3): 260–69. https://doi.org/10.1021/ACS.BIOCHEM.9B00791/ASSET/IMAGES/MEDIUM/BI9B00791_0001.GIF.

Nomura, Koji, Marta Klejnot, Dominika Kowalczyk, Andreas K. Hock, Gary J. Sibbet, Karen H. Vousden, and Danny T. Huang. 2017. "Structural Analysis of MDM2 RING Separates Degradation from Regulation of P53 Transcription Activity." *Nature Structural and Molecular Biology* 24 (7): 578–87. https://doi.org/10.1038/nsmb.3414.

Nuytens, Kim, Ilse Gantois, Pieter Stijnen, Emilia Iscru, Annelies Laeremans, Lutgarde Serneels, Lien Van Eylen, et al. 2013. "Haploinsufficiency of the Autism Candidate Gene Neurobeachin Induces Autism-like Behaviors and Affects Cellular and Molecular Processes of Synaptic Plasticity in Mice." *Neurobiology of Disease* 51 (March): 144–51. https://doi.org/10.1016/J.NBD.2012.11.004.

Nuytens, Kim, Krizia Tuand, Michela Di Michele, Kurt Boonen, Etienne Waelkens, Kathleen Freson, and John Wm Creemers. 2013. "Platelets of Mice Heterozygous for Neurobeachin, a Candidate Gene for Autism Spectrum Disorder, Display Protein Changes Related to Aberrant Protein Kinase A Activity." *Molecular Autism* 4 (1). https://doi.org/10.1186/2040-2392-4-43.

O'Callaghan, Christopher A., Michael F. Byford, Jessica R. Wyer, Benjamin E. Willcox, Bent K. Jakobsen, Andrew J. McMichael, and John I. Bell. 1999. "BirA Enzyme: Production and Application in the Study of Membrane Receptor-Ligand Interactions by Site-Specific Biotinylation." *Analytical Biochemistry* 266 (1): 9–15. https://doi.org/10.1006/abio.1998.2930.

O'Connell, Mitchell R., Roland Gamsjaeger, and Joel P. Mackay. 2009. "The Structural Analysis of Protein-Protein Interactions by NMR Spectroscopy." *Proteomics* 9 (23): 5224–32. https://doi.org/10.1002/PMIC.200900303.

Ohsako, S, Y Nishida, H Ryo, and T Yamauchi. 1993. "Molecular Characterization and Expression of the Drosophila Ca2+/Calmodulin-Dependent Protein Kinase II Gene. Identification of Four Forms of the Enzyme Generated from a Single Gene by Alternative Splicing." *The Journal of Biological Chemistry* 268 (3): 2052–62. http://www.ncbi.nlm.nih.gov/pubmed/8380587.

Ojha, Prachi, Subhajit Pal, and Samarjit Bhattacharyya. 2022. "Regulation of Metabotropic Glutamate

Receptor Internalization and Synaptic AMPA Receptor Endocytosis by the Postsynaptic Protein Norbin." *The Journal of Neuroscience : The Official Journal of the Society for Neuroscience* 42 (5): 731–48. https://doi.org/10.1523/JNEUROSCI.1037-21.2021.

Okamoto, K.-I., R. Narayanan, S. H. Lee, K. Murata, and Y. Hayashi. 2007. "The Role of CaMKII as an F-Actin-Bundling Protein Crucial for Maintenance of Dendritic Spine Structure." *Proceedings of the National Academy of Sciences*. https://doi.org/10.1073/pnas.0701656104.

Okumura, Fumihiko, Shigetsugu Hatakeyama, Masaki Matsumoto, Takumi Kamura, and Keiichi I Nakayama. 2004. "Functional Regulation of FEZ1 by the U-Box-Type Ubiquitin Ligase E4B Contributes to Neuritogenesis." *The Journal of Biological Chemistry* 279 (51): 53533–43. https://doi.org/10.1074/jbc.M402916200.

Osinalde, Nerea, Anna Duarri, Juanma Ramirez, Rosa Barrio, Guiomar Perez de Nanclares, and Ugo Mayor. 2019. "Impaired Proteostasis in Rare Neurological Diseases." *Seminars in Cell and Developmental Biology* 93: 164–77. https://doi.org/10.1016/j.semcdb.2018.10.007.

Owerbach, David, Eileen M. McKay, Edward T.H. Yeh, Kenneth H. Gabbay, and Kurt M. Bohren. 2005. "A Proline-90 Residue Unique to SUMO-4 Prevents Maturation and Sumoylation." *Biochemical and Biophysical Research Communications* 337 (2): 517–20. https://doi.org/10.1016/J.BBRC.2005.09.090.

Paek, Jaeho, Marian Kalocsay, Dean P. Staus, Laura Wingler, Roberta Pascolutti, Joao A. Paulo, Steven P. Gygi, and Andrew C. Kruse. 2017. "Multidimensional Tracking of GPCR Signaling via Peroxidase-Catalyzed Proximity Labeling." *Cell* 169 (2): 338–349.e11. https://doi.org/10.1016/J.CELL.2017.03.028.

Pasqual, Giulia, Aleksey Chudnovskiy, Jeroen M.J. Tas, Marianna Agudelo, Lawrence D. Schweitzer, Ang Cui, Nir Hacohen, and Gabriel D. Victora. 2018. "Monitoring T Cell-Dendritic Cell Interactions in Vivo by Intercellular Enzymatic Labelling." *Nature*. https://doi.org/10.1038/nature25442.

Patterson, Kate I., Tilman Brummer, Philippa M. O'Brien, and Roger J. Daly. 2009. "Dual-Specificity Phosphatases: Critical Regulators with Diverse Cellular Targets." *Biochemical Journal* 418 (3): 475–89. https://doi.org/10.1042/BJ20082234.

Pavlopoulos, Elias, Pierre Trifilieff, Vivien Chevaleyre, Luana Fioriti, Sakellarios Zairis, Andrew Pagano, Gaël Malleret, and Eric R. Kandel. 2011. "Neuralized1 Activates CPEB3: A Function for Nonproteolytic Ubiquitin in Synaptic Plasticity and Memory Storage." *Cell* 147 (6): 1369–83. https://doi.org/10.1016/J.CELL.2011.09.056.

Peng, Junmin, Daniel Schwartz, Joshua E. Elias, Carson C. Thoreen, Dongmei Cheng, Gerald Marsischky, Jeroen Roelofs, Daniel Finley, and Steven P. Gygi. 2003. "A Proteomics Approach to Understanding Protein Ubiquitination." *Nature Biotechnology* 21 (8): 921–26. https://doi.org/10.1038/NBT849.

Phelan, James D., Ryan M. Young, Daniel E. Webster, Sandrine Roulland, George W. Wright, Monica Kasbekar, Arthur L. Shaffer, et al. 2018. "A Multiprotein Supercomplex Controlling Oncogenic Signalling in Lymphoma." *Nature* 560 (7718): 387–91. https://doi.org/10.1038/S41586-018-0290-0.

Pichler, Andrea, Andreas Gast, Jacob S. Seeler, Anne Dejean, and Frauke Melchior. 2002. "The Nucleoporin RanBP2 Has SUMO1 E3 Ligase Activity." *Cell* 108 (1): 109–20. https://doi.org/10.1016/S0092-8674(01)00633-X.

Pickart, Cecile M. 2001. "Mechanisms Underlying Ubiquitination." *Annual Review of Biochemistry* 70 (1): 503–33. https://doi.org/10.1146/annurev.biochem.70.1.503.

Pickart, Cecile M., and Michael J. Eddins. 2004. "Ubiquitin: Structures, Functions, Mechanisms." *Biochimica et Biophysica Acta - Molecular Cell Research*. https://doi.org/10.1016/j.bbamcr.2004.09.019.

Pitre, Sylvain, Md Alamgir, James R. Green, Michel Dumontier, Frank Dehne, and Ashkan Golshani. 2008. "Computational Methods for Predicting Protein-Protein Interactions." *Advances in Biochemical Engineering/Biotechnology* 110: 247–67. https://doi.org/10.1007/10_2007_089.

Pitzen, Valentin, Sophia Sander, Otto Baumann, Ralph Gräf, and Irene Meyer. 2021. "Cep192, a Novel Missing Link between the Centrosomal Core and Corona in Dictyostelium Amoebae." *Cells* 10 (9): 2384. https://doi.org/10.3390/CELLS10092384/S1.

Plechanovov, Anna, Ellis G. Jaffray, Michael H. Tatham, James H. Naismith, and Ronald T. Hay. 2012. "Structure of a RING E3 Ligase and Ubiquitin-Loaded E2 Primed for Catalysis." *Nature* 489 (7414): 115–20. https://doi.org/10.1038/nature11376.

Poncer, Jean Christophe, Jose a Esteban, and Roberto Malinow. 2002. "Multiple Mechanisms for the Potentiation of AMPA Receptor-Mediated Transmission by Alpha-Ca2+/Calmodulin-Dependent Protein Kinase II." *The Journal of Neuroscience : The Official Journal of the Society for Neuroscience* 22 (11): 4406–11. https://doi.org/20026449.

Povlsen, Lou K., Petra Beli, Sebastian A. Wagner, Sara L. Poulsen, Kathrine B. Sylvestersen, Jon W. Poulsen, Michael L. Nielsen, Simon Bekker-Jensen, Niels Mailand, and Chunaram Choudhary. 2012. "Systems-Wide Analysis of Ubiquitylation Dynamics Reveals a Key Role for PAF15 Ubiquitylation in DNA-Damage Bypass." *Nature Cell Biology* 14 (10): 1089–98. https://doi.org/10.1038/NCB2579.

Poyurovsky, Masha V., Christina Priest, Alex Kentsis, Katherine L.B. Borden, Zhen Qiang Pan, Nikola Pavletich, and Carol Prives. 2007. "The Mdm2 RING Domain C-Terminus Is Required for Supramolecular Assembly and Ubiquitin Ligase Activity." *EMBO Journal* 26 (1): 90–101. https://doi.org/10.1038/sj.emboj.7601465.

Prikas, Emmanuel, Anne Poljak, and Arne Ittner. 2020. "Mapping P38α Mitogen-Activated Protein Kinase Signalling by Proximity-Dependent Labelling." *Protein Science*, March. https://doi.org/10.1002/pro.3854.

Pruneda, Jonathan N., Peter J. Littlefield, Sarah E. Soss, Kyle A. Nordquist, Walter J. Chazin, Peter S. Brzovic, and Rachel E. Klevit. 2012. "Structure of an E3:E2~Ub Complex Reveals an Allosteric Mechanism Shared among RING/U-Box Ligases." *Molecular Cell* 47 (6): 933–42. https://doi.org/10.1016/j.molcel.2012.07.001.

Pruneda, Jonathan N., Kate E. Stoll, Laura J. Bolton, Peter S. Brzovic, and Rachel E. Klevit. 2011. "Ubiquitin in Motion: Structural Studies of the Ubiquitin-Conjugating Enzyme~Ubiquitin

Conjugate." *Biochemistry* 50 (10): 1624–33. https://doi.org/10.1021/bi101913m.

Qin, Wei, Kelvin F. Cho, Peter E. Cavanagh, and Alice Y. Ting. 2021. "Deciphering Molecular Interactions by Proximity Labeling." *Nature Methods 2021 18:2* 18 (2): 133–43. https://doi.org/10.1038/s41592-020-01010-5.

Raheja, Radhika, Yuhui Liu, Ellen Hukkelhoven, Nancy Yeh, and Andrew Koff. 2014. "The Ability of TRIM3 to Induce Growth Arrest Depends on RING-Dependent E3 Ligase Activity." *Biochemical Journal* 458 (3): 537–45. https://doi.org/10.1042/BJ20131288.

Rajan, Akhila, Benjamin E. Housden, Frederik Wirtz-Peitz, Laura Holderbaum, and Norbert Perrimon. 2017. "A Mechanism Coupling Systemic Energy Sensing to Adipokine Secretion." *Developmental Cell* 43 (1): 83–98.e6. https://doi.org/10.1016/J.DEVCEL.2017.09.007.

Ramirez, Juanma, Nagore Elu, Aitor Martinez, Benoit Lectez, and Ugo Mayor. 2017. "In Vivo Strategies to Isolate and Characterize the Neuronal Ubiquitinated Proteome." In *Current Proteomic Approaches Applied to Brain Function*, edited by Enrique Santamaría and Joaquín Fernández-Irigoyen, 179–89. New York, NY: Springer New York. https://doi.org/10.1007/978-1-4939-7119-0_11.

Ramirez, Juanma, Benoit Lectez, Nerea Osinalde, Monika Sivá, Nagore Elu, Kerman Aloria, Michaela Procházková, et al. 2018. "Quantitative Proteomics Reveals Neuronal Ubiquitination of Rngo/Ddi1 and Several Proteasomal Subunits by Ube3a, Accounting for the Complexity of Angelman Syndrome." *Human Molecular Genetics* 27 (11): 1955–71. http://dx.doi.org/10.1093/hmg/ddy103.

Ramirez, Juanma, Mingwei Min, Rosa Barrio, Catherine Lindon, and Ugo Mayor. 2016. "Isolation of Ubiquitinated Proteins to High Purity from In Vivo Samples." *Methods in Molecular Biology (Clifton, N.J.)* 1449 (September): 193–202. https://doi.org/10.1007/978-1-4939-3756-1_10.

Rao, V. Srinivasa, K. Srinivas, G. N. Sujini, and G. N. Sunand Kumar. 2014. "Protein-Protein Interaction Detection: Methods and Analysis." *International Journal of Proteomics* 2014 (February): 1–12. https://doi.org/10.1155/2014/147648.

Rhein, Cosima, Christiane Mühle, Bernd Lenz, Tanja Richter-Schmidinger, Georgios Kogias, Fernando Boix, Anbarasu Lourdusamy, et al. 2020. "Association of a CAMK2A Genetic Variant with Logical Memory Performance and Hippocampal Volume in the Elderly." *Brain Research Bulletin* 161 (August): 13–20. https://doi.org/10.1016/J.BRAINRESBULL.2020.05.001.

Rigaut, G., A. Shevchenko, B. Rutz, M. Wilm, M. Mann, and B. Seraphin. 1999. "A Generic Protein Purification Method for Protein Complex Characterization and Proteome Exploration." *Nature Biotechnology* 17 (10): 1030–32. https://doi.org/10.1038/13732.

Ritterhoff, Tobias, Hrishikesh Das, Götz Hofhaus, Rasmus R Schröder, Annette Flotho, and Frauke Melchior. 2016. "ARTICLE The RanBP2/RanGAP1*SUMO1/Ubc9 SUMO E3 Ligase Is a Disassembly Machine for Crm1-Dependent Nuclear Export Complexes." *Nature Communications* 7. https://doi.org/10.1038/ncomms11482.

Roberts, G. C. K. (Gordon Carl Kenmure). 1993. "NMR of Macromolecules : A Practical Approach," 399.

Roboti, Peristera, Craig Lawless, and Stephen High. 2022. "Mitochondrial Antiviral-Signalling Protein Is a Client of the BAG6 Protein Quality Control Complex." *Journal of Cell Science* 135 (9). https://doi.org/10.1242/JCS.259596.

Robzyk, Kenneth, Judith Recht, and Mary Ann Osley. 2000. "Rad6-Dependent Ubiquitination of Histone H2B in Yeast." *Science (New York, N.Y.)* 287 (5452): 501–4. https://doi.org/10.1126/SCIENCE.287.5452.501.

Rohila, Jai S., Mei Chen, Ronald Cerny, and Michael E. Fromm. 2004. "Improved Tandem Affinity Purification Tag and Methods for Isolation of Protein Heterocomplexes from Plants." *The Plant Journal : For Cell and Molecular Biology* 38 (1): 172–81. https://doi.org/10.1111/J.1365-313X.2004.02031.X.

Ronchi, Virginia P, Jennifer M Klein, Daniel J Edwards, and Arthur L Haas. 2014. "The Active Form of E6-Associated Protein (E6AP)/UBE3A Ubiquitin Ligase Is an Oligomer." *The Journal of Biological Chemistry* 289 (2): 1033–48. https://doi.org/10.1074/jbc.M113.517805.

Rosenfeld, Jill A., Rui Xiao, Mir Reza Bekheirnia, Farah Kanani, Michael J. Parker, Mary K. Koenig, Arie van Haeringen, et al. 2021. "Heterozygous Variants in SPTBN1 Cause Intellectual Disability and Autism." *American Journal of Medical Genetics. Part A* 185 (7): 2037–45. https://doi.org/10.1002/AJMG.A.62201.

Rosenthal, Shimon M., Tvisha Misra, Hala Abdouni, Tess C. Branon, Alice Y. Ting, Ian C. Scott, and Anne Claude Gingras. 2021. "A Toolbox for Efficient Proximity-Dependent Biotinylation in Zebrafish Embryos." *Molecular & Cellular Proteomics : MCP* 20. https://doi.org/10.1016/J.MCPRO.2021.100128.

Rotin, Daniela, and Sharad Kumar. 2009. "Physiological Functions of the HECT Family of Ubiquitin Ligases." *Nature Reviews Molecular Cell Biology* 10 (6): 398–409. https://doi.org/10.1038/nrm2690.

Roux, Kyle J., Dae In Kim, Manfred Raida, and Brian Burke. 2012. "A Promiscuous Biotin Ligase Fusion Protein Identifies Proximal and Interacting Proteins in Mammalian Cells." *Journal of Cell Biology* 196 (6): 801–10. https://doi.org/10.1083/jcb.201112098.

Ruffner, H, C A Joazeiro, D Hemmati, T Hunter, and I M Verma. 2001. "Cancer-Predisposing Mutations within the RING Domain of BRCA1: Loss of Ubiquitin Protein Ligase Activity and Protection from Radiation Hypersensitivity." *Proceedings of the National Academy of Sciences of the United States of America* 98 (9): 5134–39. https://doi.org/10.1073/pnas.081068398.

Saitoh, Tsunao, and James H. Schwartz. 1985. "Phosphorylation-Dependent Subcellular Translocation of a Ca2+/Calmodulin-Dependent Protein Kinase Produces an Autonomous Enzyme in Aplysia Neurons." *The Journal of Cell Biology* 100 (3): 835–42. https://doi.org/10.1083/JCB.100.3.835.

Sakin, Volkan, Sebastian M. Richter, He Hsuan Hsiao, Henning Urlaub, and Frauke Melchior. 2015. "Sumoylation of the GTPase Ran by the RanBP2 SUMO E3 Ligase Complex." *The Journal of Biological Chemistry* 290 (39): 23589. https://doi.org/10.1074/JBC.M115.660118.

Sakurai, Takeshi. 2012. "The Role of NrCAM in Neural Development and Disorders--beyond a Simple

Glue in the Brain." *Molecular and Cellular Neurosciences* 49 (3): 351–63. https://doi.org/10.1016/J.MCN.2011.12.002.

Sander, Bodo, Wenshan Xu, Martin Eilers, Nikita Popov, and Sonja Lorenz. 2017. "A Conformational Switch Regulates the Ubiquitin Ligase HUWE1." *ELife* 6. https://doi.org/10.7554/eLife.21036.

Sarraf, Shireen A., Malavika Raman, Virginia Guarani-Pereira, Mathew E. Sowa, Edward L. Huttlin, Steven P. Gygi, and J. Wade Harper. 2013. "Landscape of the PARKIN-Dependent Ubiquitylome in Response to Mitochondrial Depolarization." *Nature* 496 (7445): 372–76. https://doi.org/10.1038/nature12043.

Scheffner, Martin, and Sharad Kumar. 2014. "Mammalian HECT Ubiquitin-Protein Ligases: Biological and Pathophysiological Aspects." *Biochimica et Biophysica Acta* 1843 (1): 61–74. https://doi.org/10.1016/j.bbamcr.2013.03.024.

Schopp, Isabel Myriam, Cinthia Claudia Amaya Ramirez, Jerneja Debeljak, Elisa Kreibich, Merle Skribbe, Klemens Wild, and Julien Béthune. 2017. "Split-BioID a Conditional Proteomics Approach to Monitor the Composition of Spatiotemporally Defined Protein Complexes." *Nature Communications 2017 8:1* 8 (1): 1–14. https://doi.org/10.1038/ncomms15690.

Seo, Jae Ho, Ekta Agarwal, Kelly G. Bryant, M. Cecilia Caino, Eui Tae Kim, Andrew V. Kossenkov, Hsin Yao Tang, et al. 2018. "Syntaphilin Ubiquitination Regulates Mitochondrial Dynamics and Tumor Cell Movements." *Cancer Research* 78 (15): 4215–28. https://doi.org/10.1158/0008-5472.CAN-18-0595.

Shamloula, Hoda K., Mkajiuna P. Mbogho, Angel C. Pimentel, Zosia M.A. Chrzanowska-Lightowlers, Vanneta Hyatt, Hideyuki Okano, and Tadmiri R. Venkatesh. 2002. "Rugose (Rg), a Drosophila A Kinase Anchor Protein, Is Required for Retinal Pattern Formation and Interacts Genetically with Multiple Signaling Pathways." *Genetics* 161 (2): 693–710. https://doi.org/10.1093/GENETICS/161.2.693.

Shen, Jiajia, Pengyu Li, Xuejing Shao, Yang Yang, Xiujun Liu, Min Feng, Qiang Yu, Ronggui Hu, and Zhen Wang. 2018. "The E3 Ligase Ring1 Targets P53 for Degradation and Promotes Cancer Cell Proliferation and Survival." *Cancer Research* 78 (2): 359–71. https://doi.org/10.1158/0008-5472.CAN-17-1805.

Sherman, Emily J, Dylan C Mitchell, and Amanda L Garner. 2019. "The RNA-Binding Protein SART3 Promotes MiR-34a Biogenesis and G 1 Cell Cycle Arrest in Lung Cancer Cells." https://doi.org/10.1074/jbc.AC119.010419.

Shi, Yi, Ping Xu, and Jun Qin. 2011. "Ubiquitinated Proteome: Ready for Global?" *Molecular & Cellular Proteomics : MCP* 10 (5). https://doi.org/10.1074/MCP.R110.006882.

Shinoda, Natsuki, Nozomi Hanawa, Takahiro Chihara, Akiko Koto, and Masayuki Miura. 2019. "Dronc-Independent Basal Executioner Caspase Activity Sustains Drosophila Imaginal Tissue Growth." *Proceedings of the National Academy of Sciences of the United States of America* 116 (41): 20539–44. https://doi.org/10.1073/PNAS.1904647116.

Shinozaki, Kohki, Hideaki Kume, Hiroko Kuzume, Kunihiko Obata, and Kei Maruyama. 1999. "Norbin, a Neurite-Outgrowth-Related Protein, Is a Cytosolic Protein Localized in the Somatodendritic

Region of Neurons and Distributed Prominently in Dendritic Outgrowth in Purkinje Cells." *Molecular Brain Research* 71 (2): 364–68. https://doi.org/10.1016/S0169-328X(99)00181-3.

Shinozaki, Kohki, Kei Maruyama, Hideaki Kume, Hiroko Kuzume, and Kunihiko Obata. 1997. "A Novel Brain Gene, Norbin, Induced by Treatment of Tetraethylammonium in Rat Hippocampal Slice and Accompanied with Neurite-Outgrowth in Neuro 2a Cells." *Biochemical and Biophysical Research Communications* 240 (3): 766–71. https://doi.org/10.1006/BBRC.1997.7660.

Shkel, Olha, Yevheniia Kharkivska, Yun Kyung Kim, and Jun Seok Lee. 2022. "Proximity Labeling Techniques: A Multi-Omics Toolbox." *Chemistry, an Asian Journal* 17 (2). https://doi.org/10.1002/ASIA.202101240.

Simpson, Julie H. 2009. "Chapter 3 Mapping and Manipulating Neural Circuits in the Fly Brain." *Advances in Genetics* 65 (January): 79–143. https://doi.org/10.1016/S0065-2660(09)65003-3.

Sirois, Carissa L., Judy E. Bloom, James J. Fink, Dea Gorka, Steffen Keller, Noelle D. Germain, Eric S. Levine, and Stormy J. Chamberlain. 2020. "Abundance and Localization of Human UBE3A Protein Isoforms." *Human Molecular Genetics* 29 (18): 3021–31. https://doi.org/10.1093/HMG/DDAA191.

Sjödin, Simon, Gunnar Brinkmalm, Annika Öhrfelt, Lucilla Parnetti, Silvia Paciotti, Oskar Hansson, John Hardy, Kaj Blennow, Henrik Zetterberg, and Ann Brinkmalm. 2019. "Endo-Lysosomal Proteins and Ubiquitin CSF Concentrations in Alzheimer's and Parkinson's Disease." *Alzheimer's Research & Therapy* 11 (1). https://doi.org/10.1186/S13195-019-0533-9.

Smit, Judith J, Davide Monteferrario, Sylvie M Noordermeer, Willem J Van, Bert A Van Der Reijden, and Titia K Sixma. 2012. "The E3 Ligase HOIP Specifies Linear Ubiquitin Chain Assembly through Its RING-IBR-RING Domain and the Unique LDD Extension." *The EMBO Journal* 31 (19): 3833–44. https://doi.org/10.1038/emboj.2012.217.

Soss, Sarah E., Rachel E. Klevit, and Walter J. Chazin. 2013. "Activation of UbcH5c~Ub Is the Result of a Shift in Interdomain Motions of the Conjugate Bound to U-Box E3 Ligase E4B." *Biochemistry* 52 (17): 2991–99. https://doi.org/10.1021/bi3015949.

Srinivasan, Mallika, Carl F. Edman, and Howard Schulman. 1994. "Alternative Splicing Introduces a Nuclear Localization Signal That Targets Multifunctional CaM Kinase to the Nucleus." *Journal of Cell Biology* 126 (4): 839–52. https://doi.org/10.1083/JCB.126.4.839.

Staub, O, S Dho, P Henry, J Correa, T Ishikawa, J McGlade, and D Rotin. 1996. "WW Domains of Nedd4 Bind to the Proline-Rich PY Motifs in the Epithelial Na+ Channel Deleted in Liddle's Syndrome." *The EMBO Journal* 15 (10): 2371–80.

Stechow, Louise von, Dimitris Typas, Jordi Carreras Puigvert, Laurens Oort, Ramakrishnaiah Siddappa, Alex Pines, Harry Vrieling, Bob van de Water, Leon H. F. Mullenders, and Erik H. J. Danen. 2015. "The E3 Ubiquitin Ligase ARIH1 Protects against Genotoxic Stress by Initiating a 4EHP-Mediated MRNA Translation Arrest." *Molecular and Cellular Biology* 35 (7): 1254–68. https://doi.org/10.1128/mcb.01152-14.

Strack, S., A. J. Robison, M. A. Bass, and R. J. Colbran. 2000. "Association of Calcium/Calmodulin-

Dependent Kinase II with Developmentally Regulated Splice Variants of the Postsynaptic Density Protein Densin-180." *The Journal of Biological Chemistry* 275 (33): 25061–64. https://doi.org/10.1074/JBC.C000319200.

Sun, Jiandong, Yan Liu, Yousheng Jia, Xiaoning Hao, Wei ju Lin, Jennifer Tran, Gary Lynch, Michel Baudry, and Xiaoning Bi. 2018. "UBE3A-Mediated P18/LAMTOR1 Ubiquitination and Degradation Regulate MTORC1 Activity and Synaptic Plasticity." *ELife* 7: 1–31. https://doi.org/10.7554/eLife.37993.

Sun, Jiandong, Guoqi Zhu, Yan Liu, Steve Standley, Angela Ji, Rashmi Tunuguntla, Yubin Wang, et al. 2015. "UBE3A Regulates Synaptic Plasticity and Learning and Memory by Controlling SK2 Channel Endocytosis." *Cell Reports* 12 (3): 449–61. https://doi.org/10.1016/j.celrep.2015.06.023.

Szklarczyk, Damian, Annika L. Gable, David Lyon, Alexander Junge, Stefan Wyder, Jaime Huerta-Cepas, Milan Simonovic, et al. 2019. "STRING V11: Protein-Protein Association Networks with Increased Coverage, Supporting Functional Discovery in Genome-Wide Experimental Datasets." *Nucleic Acids Research* 47 (D1): D607–13. https://doi.org/10.1093/nar/gky1131.

Talamillo, Ana, Orhi Barroso-Gomila, Immacolata Giordano, Leiore Ajuria, Marco Grillo, Ugo Mayor, and Rosa Barrio. 2020. "The Role of SUMOylation during Development." *Biochemical Society Transactions* 48 (2): 463–78. https://doi.org/10.1042/BST20190390.

Tan, Cyrus, Eamon F X Byrne, Casey Ah-Cann, Melissa J Call, and Matthew E Call. 2019. "A Serine in the First Transmembrane Domain of the Human E3 Ubiquitin Ligase MARCH9 Is Critical for Down-Regulation of Its Protein Substrates." *The Journal of Biological Chemistry* 294 (7): 2470–85. https://doi.org/10.1074/jbc.RA118.004836.

Teplova, Anastasia D., Marina V. Serebryakova, Raisa A. Galiullina, Nina V. Chichkova, and Andrey B. Vartapetian. 2021. "Identification of Phytaspase Interactors via the Proximity-Dependent Biotin-Based Identification Approach." *International Journal of Molecular Sciences* 22 (23). https://doi.org/10.3390/IJMS222313123.

Thompson, Luke W., Kim D. Morrison, Sally L. Shirran, Ewout J.N. Groen, Thomas H. Gillingwater, Catherine H. Botting, and Judith E. Sleeman. 2018. "Neurochondrin Interacts with the SMN Protein Suggesting a Novel Mechanism for Spinal Muscular Atrophy Pathology." *Journal of Cell Science* 131 (8). https://doi.org/10.1242/JCS.211482.

Tian, Hui, Nicole R. Tackmann, Aiwen Jin, Junnian Zheng, and Yanping Zhang. 2017. "Inactivation of the MDM2 RING Domain Enhances P53 Transcriptional Activity in Mice." *Journal of Biological Chemistry* 292 (52): 21614–22. https://doi.org/10.1074/jbc.RA117.000122.

Tomaić, V., and L. Banks. 2015. "Angelman Syndrome-Associated Ubiquitin Ligase UBE3A/E6AP Mutants Interfere with the Proteolytic Activity of the Proteasome." *Cell Death & Disease* 6 (1). https://doi.org/10.1038/CDDIS.2014.572.

Tomita, Susumu, Valentin Stein, Tim J. Stocker, Roger A. Nicoll, and David S. Bredt. 2005. "Bidirectional Synaptic Plasticity Regulated by Phosphorylation of Stargazin-like TARPs." *Neuron* 45 (2): 269–77. https://doi.org/10.1016/j.neuron.2005.01.009.

Torrino, Stéphanie, Orane Visvikis, Anne Doye, Laurent Boyer, Caroline Stefani, Patrick Munro, Jacques Bertoglio, Gérard Gacon, Amel Mettouchi, and Emmanuel Lemichez. 2011. "The E3 Ubiquitin-Ligase HACE1 Catalyzes the Ubiquitylation of Active Rac1." *Developmental Cell* 21 (5): 959–65. https://doi.org/10.1016/j.devcel.2011.08.015.

Tripathi, Ekta, and Susan Smith. 2017. "Cell Cycle-regulated Ubiquitination of Tankyrase 1 by RNF8 and ABRO1/BRCC36 Controls the Timing of Sister Telomere Resolution." *The EMBO Journal* 36 (4): 503–19. https://doi.org/10.15252/embj.201695135.

Tyanova, Stefka, Tikira Temu, Pavel Sinitcyn, Arthur Carlson, Marco Y. Hein, Tamar Geiger, Matthias Mann, and Jürgen Cox. 2016. "The Perseus Computational Platform for Comprehensive Analysis of (Prote)Omics Data." *Nature Methods*. https://doi.org/10.1038/nmeth.3901.

Udeshi, Namrata D., Tanya Svinkina, Philipp Mertins, Eric Kuhn, D. R. Mani, Jana W. Qiao, and Steven A. Carr. 2013. "Refined Preparation and Use of Anti-Diglycine Remnant (K-ε-GG) Antibody Enables Routine Quantification of 10,000s of Ubiquitination Sites in Single Proteomics Experiments." *Molecular & Cellular Proteomics : MCP* 12 (3): 825–31. https://doi.org/10.1074/MCP.O112.027094.

Uetz, Peter, Loic Glot, Gerard Cagney, Traci A. Mansfield, Richard S. Judson, James R. Knight, Daniel Lockshon, et al. 2000. "A Comprehensive Analysis of Protein–protein Interactions in Saccharomyces Cerevisiae." *Nature 2000 403:6770* 403 (6770): 623–27. https://doi.org/10.1038/35001009.

Uezu, Akiyoshi, Daniel J. Kanak, Tyler W.A. Bradshaw, Erik J. Soderblom, Christina M. Catavero, Alain C. Burette, Richard J. Weinberg, and Scott H. Soderling. 2016. "Identification of an Elaborate Complex Mediating Postsynaptic Inhibition." *Science (New York, N.Y.)* 353 (6304): 1123–29. https://doi.org/10.1126/SCIENCE.AAG0821.

Ungricht, Rosemarie, Michael Klann, Peter Horvath, and Ulrike Kutay. 2015. "Diffusion and Retention Are Major Determinants of Protein Targeting to the Inner Nuclear Membrane." *Journal of Cell Biology* 209 (5): 687–704. https://doi.org/10.1083/jcb.201409127.

Volders, Karolien, Sabrina Scholz, Jan R. Slabbaert, Anja C. Nagel, Patrik Verstreken, John W.M. Creemers, Patrick Callaerts, and Martin Schwärzel. 2012. "Drosophila Rugose Is a Functional Homolog of Mammalian Neurobeachin and Affects Synaptic Architecture, Brain Morphology, and Associative Learning." *The Journal of Neuroscience : The Official Journal of the Society for Neuroscience* 32 (43): 15193–204. https://doi.org/10.1523/JNEUROSCI.6424-11.2012.

Wagner, Sebastian A., Petra Beli, Brian T. Weinert, Michael L. Nielsen, Jürgen Cox, Matthias Mann, and Chunaram Choudhary. 2011. "A Proteome-Wide, Quantitative Survey of in Vivo Ubiquitylation Sites Reveals Widespread Regulatory Roles." *Molecular & Cellular Proteomics : MCP* 10 (10): M111.013284. https://doi.org/10.1074/MCP.M111.013284.

Wal, Lennart van der, Karel Bezstarosti, Karen A. Sap, Dick H.W. Dekkers, Erikjan Rijkers, Edwin Mientjes, Ype Elgersma, and Jeroen A.A. Demmers. 2018. "Improvement of Ubiquitylation Site Detection by Orbitrap Mass Spectrometry." *Journal of Proteomics* 172 (February): 49–56. https://doi.org/10.1016/J.JPROT.2017.10.014.

Wang, Hejia Henry, and Andrew Tsourkas. 2019. "Site-Specific C-Terminal Labeling of Recombinant

Proteins with Proximity-Based Sortase-Mediated Ligation (PBSL)." *Methods in Molecular Biology* 2012: 15–28. https://doi.org/10.1007/978-1-4939-9546-2_2.

Wang, Hengbin, Liangjun Wang, Hediye Erdjument-Bromage, Miguel Vidal, Paul Tempst, Richard S Jones, and Yi Zhang. 2004. "Role of Histone H2A Ubiquitination in Polycomb Silencing." *Nature* 431 (7010): 873–78. https://doi.org/10.1038/nature02985.

Wang, Hong, Linda Westin, Yi Nong, Shari Birnbaum, Jacob Bendor, Hjalmar Brismar, Eric Nestler, Anita Aperia, Marc Flajolet, and Paul Greengard. 2009. "Norbin Is an Endogenous Regulator of Metabotropic Glutamate Receptor 5 Signaling." *Science (New York, N.Y.)* 326 (5959): 1554–57. https://doi.org/10.1126/SCIENCE.1178496.

Wang, Jie, Sen Sen Lou, Tingting Wang, Rong Jie Wu, Guangying Li, Miao Zhao, Bin Lu, et al. 2019. "UBE3A-Mediated PTPA Ubiquitination and Degradation Regulate PP2A Activity and Dendritic Spine Morphology." *Proceedings of the National Academy of Sciences of the United States of America* 116 (25): 12500–505. https://doi.org/10.1073/PNAS.1820131116.

Wang, Qiang, Xing Liu, Ye Cui, Yijun Tang, Wei Chen, Senlin Li, Huansha Yu, Youdong Pan, and Chen Wang. 2014. "The E3 Ubiquitin Ligase AMFR and INSIG1 Bridge the Activation of TBK1 Kinase by Modifying the Adaptor STING." *Immunity* 41 (6): 919–33. https://doi.org/10.1016/j.immuni.2014.11.011.

Wang, Tao, Vijayalakshmi Nandakumar, Xiao Xia Jiang, Lindsey Jones, An Gang Yang, Xue F. Huang, and Si Yi Chen. 2013. "The Control of Hematopoietic Stem Cell Maintenance, Self-Renewal, and Differentiation by Mysm1-Mediated Epigenetic Regulation." *Blood* 122 (16): 2812–22. https://doi.org/10.1182/BLOOD-2013-03-489641.

Wang, Wei, Zhi-Jie Xia, Jean-Claude Farré, and Suresh Subramani. 2017. "TRIM37, a Novel E3 Ligase for PEX5-Mediated Peroxisomal Matrix Protein Import." *The Journal of Cell Biology* 216 (9): 2843–58. https://doi.org/10.1083/jcb.201611170.

Wang, Xiaoli, Roger A. Herr, and Ted H. Hansen. 2012. "Ubiquitination of Substrates by Esterification." *Traffic 13 (1): 19-24*. https://doi.org/10.1111/j.1600-0854.2011.01269.x.

Waterman, Hadassa, Gil Levkowitz, Iris Alroy, and Yosef Yarden. 1999. "The RING Finger of C-Cbl Mediates Desensitization of the Epidermal Growth Factor Receptor." *Journal of Biological Chemistry* 274 (32): 22151–54. https://doi.org/10.1074/jbc.274.32.22151.

Wech, I., and Anj C. Nagel. 2005. "Mutations in Rugose Promote Cell Type-Specific Apoptosis in the Drosophila Eye." *Cell Death and Differentiation* 12 (2): 145–52. https://doi.org/10.1038/SJ.CDD.4401538.

Weeber, Edwin J, Yong-Hui Jiang, Ype Elgersma, Andrew W Varga, Yarimar Carrasquillo, Sarah E Brown, Jill M Christian, et al. 2003. "Derangements of Hippocampal Calcium/Calmodulin-Dependent Protein Kinase II in a Mouse Model for Angelman Mental Retardation Syndrome." *The Journal of Neuroscience : The Official Journal of the Society for Neuroscience* 23 (7): 2634–44. https://doi.org/23/7/2634 [pii].

Welcker, Markus, Elizabeth A. Larimore, Jherek Swanger, Maria T. Bengoechea-Alonso, Jonathan E. Grim, Johan Ericsson, Ning Zheng, and Bruce E. Clurman. 2013. "Fbw7 Dimerization Determines

the Specificity and Robustness of Substrate Degradation." *Genes and Development* 27 (23): 2531–36. https://doi.org/10.1101/gad.229195.113.

Wenzel, Dawn M, Alexei Lissounov, Peter S Brzovic, and Rachel E Klevit. 2011. "UBCH7 Reactivity Profile Reveals Parkin and HHARI to Be RING/HECT Hybrids." *Nature* 474 (7349): 105–8. https://doi.org/10.1038/nature09966.

Williams, Charles A., Daniel J. Driscoll, and Aditi I. Dagli. 2010. "Clinical and Genetic Aspects of Angelman Syndrome." *Genetics in Medicine*. https://doi.org/10.1097/GIM.0b013e3181def138.

Williams, Stacy A., Simonne Longerich, Patrick Sung, Cyrus Vaziri, and Gary M. Kupfer. 2011. "The E3 Ubiquitin Ligase RAD18 Regulates Ubiquitylation and Chromatin Loading of FANCD2 and FANCI." *Blood* 117 (19): 5078–87. https://doi.org/10.1182/blood-2010-10-311761.

Wise, Alexandria, Luis Tenezaca, Robert W. Fernandez, Emma Schatoff, Julian Flores, Atsushi Ueda, Xiaotian Zhong, Chun Fang Wu, Anne F. Simon, and Tadmiri Venkatesh. 2015. "Drosophila Mutants of the Autism Candidate Gene Neurobeachin (Rugose) Exhibit Neuro-Developmental Disorders, Aberrant Synaptic Properties, Altered Locomotion, and Impaired Adult Social Behavior and Activity Patterns." *Journal of Neurogenetics* 29 (2–3): 135–43. https://doi.org/10.3109/01677063.2015.1064916.

Woerden, Geeske M. Van, Karen D. Harris, Mohammad Reza Hojjati, Richard M. Gustin, Shenfeng Qiu, Rogerio De Avila Freire, Yong Hui Jiang, Ype Elgersma, and Edwin J. Weeber. 2007. "Rescue of Neurological Deficits in a Mouse Model for Angelman Syndrome by Reduction of ACaMKII Inhibitory Phosphorylation." *Nature Neuroscience* 10 (3): 280–82. https://doi.org/10.1038/nn1845.

Wu, Gang Y., and Hollis T. Cline. 1998. "Stabilization of Dendritic Arbor Structure in Vivo by CaMKII." *Science* 279 (5348): 222–26. https://doi.org/10.1126/science.279.5348.222.

Wu, Wenwen, Ko Sato, Ayaka Koike, Hiroyuki Nishikawa, Hirotaka Koizumi, Ashok R Venkitaraman, and Tomohiko Ohta. 2010. "HERC2 Is an E3 Ligase That Targets BRCA1 for Degradation." *Cancer Research* 70 (15): 6384–92. https://doi.org/10.1158/0008-5472.CAN-10-1304.

Xia, Pengyan, Shuo Wang, Guanling Huang, Ying Du, Pingping Zhu, Man Li, and Zusen Fan. 2014. "RNF2 Is Recruited by WASH to Ubiquitinate AMBRA1 Leading to Downregulation of Autophagy." *Nature Publishing Group* 24 (8): 943–58. https://doi.org/10.1038/cr.2014.85.

Xin, Di, Haiyan Gu, Enping Liu, and Qinmiao Sun. 2018. "Parkin Negatively Regulates the Antiviral Signaling Pathway by Targeting TRAF3 for Degradation." *Journal of Biological Chemistry* 293 (31): 11996–10. https://doi.org/10.1074/jbc.RA117.001201.

Xu, Guoqiang, Jeremy S. Paige, and Samie R. Jaffrey. 2010. "Global Analysis of Lysine Ubiquitination by Ubiquitin Remnant Immunoaffinity Profiling." *Nature Biotechnology* 28 (8): 868–73. https://doi.org/10.1038/NBT.1654.

Xu, Yali, Zengyou Li, Li Yao, Xingping Zhang, Dan Gan, Manchun Jiang, Na Wang, Guojun Chen, and Xuefeng Wang. 2017. "Altered Norbin Expression in Patients with Epilepsy and a Rat Model." *Scientific Reports* 7 (1). https://doi.org/10.1038/S41598-017-13248-9.

Yanagida, Mitsuaki. 2002. "Functional Proteomics; Current Achievements." *Journal of Chromatography B: Analytical Technologies in the Biomedical and Life Sciences*. https://doi.org/10.1016/S1570-0232(02)00074-0.

Yang, Eungyeong, and Howard Schulman. 1999. "Structural Examination of Autoregulation of Multifunctional Calcium/Calmodulin-Dependent Protein Kinase II." *Journal of Biological Chemistry* 274 (37): 26199–208. https://doi.org/10.1074/jbc.274.37.26199.

Yang, Jun, Yan Liu, Bing Wang, Hongzhen Lan, Ying Liu, Fei Chen, Ju Zhang, and Jian Luo. 2017. "Sumoylation in P27kip1 via RanBP2 Promotes Cancer Cell Growth in Cholangiocarcinoma Cell Line QBC939." *BMC Molecular Biology* 18 (1). https://doi.org/10.1186/S12867-017-0100-5.

Yang, Qinsong, Xinyue Wu, Yuhao Gao, Junbei Ni, Jinjin Li, Ziqi Pei, Songling Bai, and Yuanwen Teng. 2022. "PpyABF3 Recruits the COMPASS-like Complex to Regulate Bud Dormancy Maintenance via Integrating ABA Signaling and GA Catabolism." *The New Phytologist*, September. https://doi.org/10.1111/NPH.18508.

Yasuda, Hiroki, Alison L. Barth, David Stellwagen, and Robert C. Malenka. 2003. "A Developmental Switch in the Signaling Cascades for LTP Induction." *Nature Neuroscience* 6 (1): 15–16. https://doi.org/10.1038/NN985.

Yu, Jia Tian, Ye Liu, Ping Dong, Run En Cheng, Shao Xi Ke, Kai Qin Chen, Jing Jing Wang, Zhong Shan Shen, Qiong Yao Tang, and Zhe Zhang. 2019. "Up-Regulation of Antioxidative Proteins TRX1, TXNL1 and TXNRD1 in the Cortex of PTZ Kindling Seizure Model Mice." *PloS One* 14 (1). https://doi.org/10.1371/JOURNAL.PONE.0210670.

Yu, Yang, Celia Andreu-Agullo, Bing Fang Liu, Luendreo Barboza, Miklos Toth, and Eric C. Lai. 2020. "Regulation of Embryonic and Adult Neurogenesis by Ars2." *Development (Cambridge, England)* 147 (2). https://doi.org/10.1242/DEV.180018.

Zaman, Md Mahabub-Uz, Teruaki Nomura, Tsuyoshi Takagi, Tomoo Okamura, Wanzhu Jin, Toshie Shinagawa, Yasunori Tanaka, and Shunsuke Ishii. 2013. "Ubiquitination-Deubiquitination by the TRIM27-USP7 Complex Regulates TNF-α-Induced Apoptosis." *Molecular and Cellular Biology* 33 (24): 4971–84. https://doi.org/10.1128/MCB.00465-13.

Zampeta, F Isabella, Monica Sonzogni, Eva Niggl, Bas Lendemeijer, Hilde Smeenk, Femke M S De Vrij, Steven A Kushner, Ben Distel, and Ype Elgersma. 2020. "Conserved UBE3A Subcellular Distribution between Human and Mice Is Facilitated by Non-Homologous Isoforms." *Human Molecular Genetics* 29 (18): 3032–43. https://doi.org/10.1093/hmg/ddaa194.

Zhang, Bo, Yuanbing Zhang, and Ji-Long Liu. 2019. "TurboID-Mediated Proximity Labelling of Cytoophidium Proteome in Drosophila." *BioRxiv*, November, 848283. https://doi.org/10.1101/848283.

Zhang, Bo, Yuanbing Zhang, and Ji Long Liu. 2021. "Highly Effective Proximate Labeling in Drosophila." *G3 (Bethesda, Md.)* 11 (5). https://doi.org/10.1093/G3JOURNAL/JKAB077.

Zhang, Lian, Timo Kirschstein, Britta Sommersberg, Malte Merkens, Denise Manahan-Vaughan, Ype Elgersma, and Heinz Beck. 2005. "Hippocampal Synaptic Metaplasticity Requires Inhibitory Autophosphorylation of Ca2+/Calmodulin-Dependent Kinase II." *Journal of Neuroscience* 25

(33): 7697–7707. https://doi.org/10.1523/JNEUROSCI.2086-05.2005.

Zhang, Xuemei, Zihan Cheng, Wenjing Yao, Yuan Gao, Gaofeng Fan, Qing Guo, Boru Zhou, and Tingbo Jiang. 2022. "Overexpression of PagERF072 from Poplar Improves Salt Tolerance." *International Journal of Molecular Sciences* 23 (18): 10707. https://doi.org/10.3390/IJMS231810707.

Zhang, Y.-P., N. Holbro, and T. G. Oertner. 2008. "Optical Induction of Plasticity at Single Synapses Reveals Input-Specific Accumulation of CaMKII." *Proceedings of the National Academy of Sciences* 105 (33): 12039–44. https://doi.org/10.1073/pnas.0802940105.

Zhang, Yongliang, Gaoyuan Song, Neeraj K. Lal, Ugrappa Nagalakshmi, Yuanyuan Li, Wenjie Zheng, Pin jui Huang, et al. 2019. "TurboID-Based Proximity Labeling Reveals That UBR7 Is a Regulator of N NLR Immune Receptor-Mediated Immunity." *Nature Communications* 10 (1). https://doi.org/10.1038/S41467-019-11202-Z.

Zheng, Li, Mitesh Nagar, Aaron J. Maurais, Daniel J. Slade, Sangram S. Parelkar, Scott A. Coonrod, Eranthie Weerapana, and Paul R. Thompson. 2019. "Calcium Regulates the Nuclear Localization of Protein Arginine Deiminase 2." *Biochemistry* 58 (27): 3042–56. https://doi.org/10.1021/acs.biochem.9b00225.

Zheng, N, P Wang, P D Jeffrey, and N P Pavletich. 2000. "Structure of a C-Cbl-UbcH7 Complex: RING Domain Function in Ubiquitin-Protein Ligases." *Cell* 102 (4): 533–39. https://doi.org/10.1016/s0092-8674(00)00057-x.

Zheng, Ning, and Nitzan Shabek. 2017. "Ubiquitin Ligases : Structure , Function , and Regulation." *Annual Review of Biochemistry* 86: 129–57. https://doi.org/10.1042/BCJ20160028.

Zhou, Ruifeng, Saumil V Patel, and Peter M Snyder. 2007. "Nedd4-2 Catalyzes Ubiquitination and Degradation of Cell Surface ENaC." *Journal of Biological Chemistry* 282 (28): 20207–12. https://doi.org/10.1074/jbc.M611329200.

Zuin, Alice, Marta Isasa, and Bernat Crosas. 2014. "Ubiquitin Signaling: Extreme Conservation as a Source of Diversity." *Cells* 3 (3): 690–701. https://doi.org/10.3390/cells3030690.

SUPPLEMENTARY MATERIAL

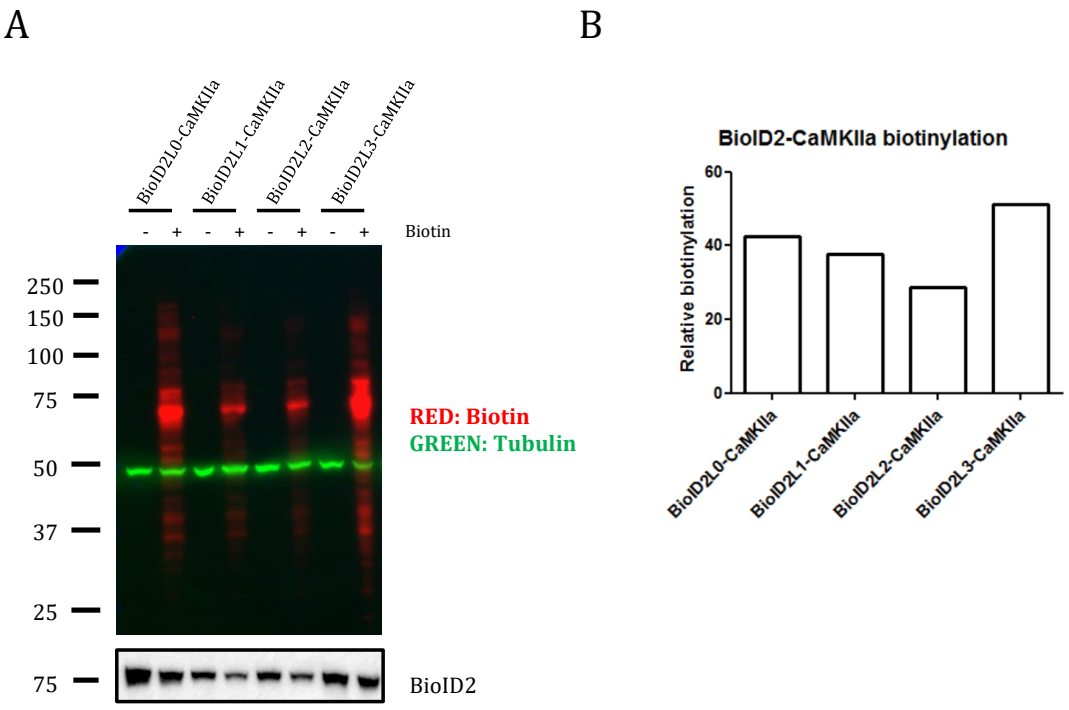

Figure S1. A linker between BioID2 and bait allows an efficient biotinylation. Western blot showing the biotinylation (red) of BioID2 fused to the bait (Camk2a) through the four linkers. Histogram in which relative biotinylation of the constructs is reflected Expression does not significantly change within constructs. Tubulin was analysed as control (red).

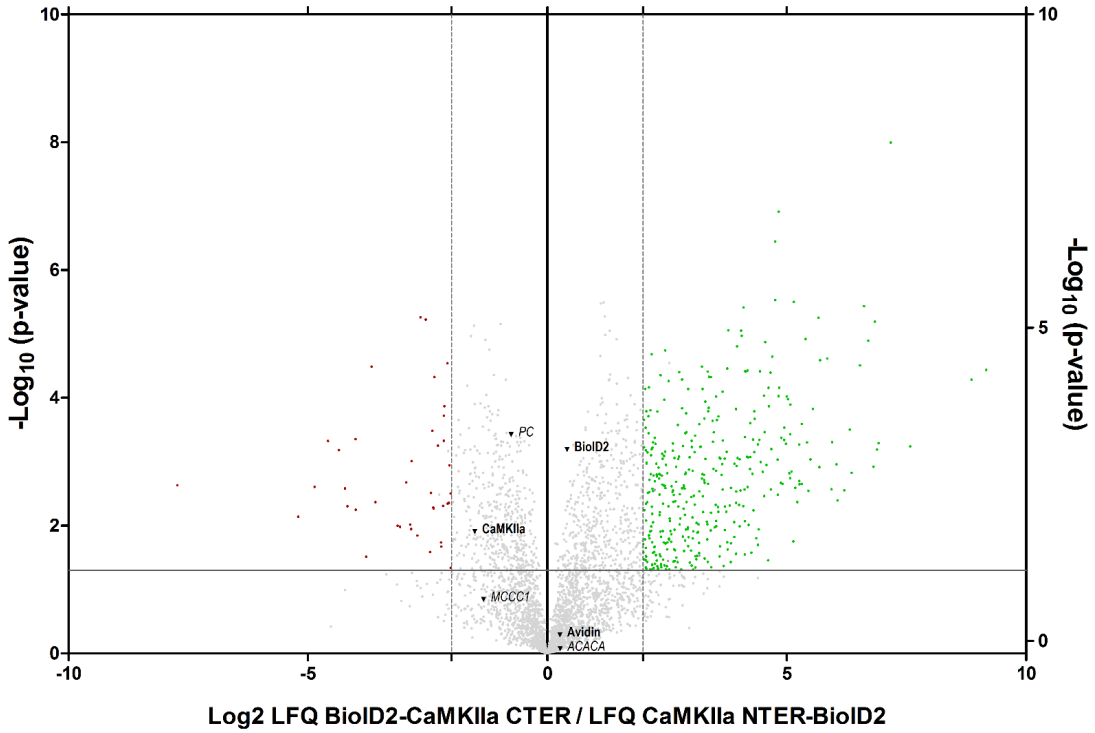

Figure S2. Validation of CTER and NTER interactors. A volcano plot in which the Log_{10} of the p-value is represented against fold change between samples. BioID2, avidin and endogenously biotinylated carboxylases (PC: Pyruvate carboxylase, ACACA: Acetyl-CoA Carboxylase) that are considered as controls are also highlighted. Proteins on the right square are more enriched in the CTER-CaMKIIa expressing sample in respect to the NTER-CaMKIIa expressing sample. Only proteins displaying a LFQ fold change bigger than 4 with a P-value smaller than 0.05 were considered as candidate binding proteins. Putative N-terminal CaMKII interactors are shown with a red circle and c-terminal interactors with a red circle.

Figure S3. Alignment of the RING domains of the RING-type E3 ligases TRIM37 and ZNRF4.

Conserved Zn-coordinating amino acids are highlighted in yellow (Cys) and orange (His). Mutated residues are shown in bold and underlined.

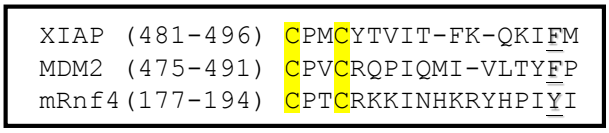

Figure S4. Alignment of the regions involved in dimerization of the RING-type E3 ligases XIAP, MDM2 and mouse RNF4. Mutated dimerization-involved residues are underlined and shadowed. Last 2 zinc-coordinating Cys of the RING domain are highlighted in yellow.

Table S1. **Inactivation of E3 ubiquitin ligases by mutation**. The residues of the domain are specified in brackets. (m) indicates that the mutations were performed in the mouse version of the protein. E2: an E2-interacting residue was mutated. Zn: one of the seven cysteines or the histidine that coordinated the atoms of Zn was mutated. Catalytic cysteine: the catalytic cysteine of the HECT domain was mutated. *specifies that the catalytic cysteine is from the RING2 domain in RBR-type E3 ligases. On each reference it is specified the substrate that was analysed.

Protein name	Uniprot Ref (human)	E3 type	Reference	Mutation	Type of mutation	Substrate
AMFR	Q9UKV5	**Ring (341-379)**	(W. Liu, Shang, and Li 2014)	A593R/F597R	**E2**	
			(Q. Wang et al. 2014)	C337S/C352S; C337S/C374S (m)	**Zn**	STING
			(Ying et al. 2009)	C341G	**Zn**	SOD1; Ataxin-3
ANAPC11	Q9NYG5	**Ring (34-77)**	(Gmachl et al. 2000)	C51A	**Zn**	Securin; cyclin B
AREL1	O15033	**HECT (483-823)**	(J. Bin Kim et al. 2013)	C790A	**Catalytic cysteine**	SMAC; HtrA2; ARTS
ARIH1	Q9Y4X5	**Ring 1 (186-236) IBR (256-317) Ring 2 (344-375)**	(Ardley et al. 2001)	C208A	**Zn**	
			(Duda et al. 2013)	F430A; E431A; E503A	**OTHER**	
			(Kelsall et al. 2013)	C357S	**Catalytic cysteine***	
			(Scott et al. 2016)	C357S	**Catalytic cysteine***	CRL substrates
			(von Stechow et al. 2015)	C208A	**Zn**	4EHP
			(Wenzel et al. 2011)	C357S	**Catalytic cysteine***	
ARIH2	O95376	**Ring 1 (139-188) IBR (208-270) Ring 2 (297-326)**	(Kawashima et al. 2017)	C300A; H158A	**Zn**	NLRP3
			(Kelsall et al. 2013)	C310S	**Catalytic cysteine***	
			(Marteijn et al. 2007)	H158A	**Zn**	¬Gf1
c-IAP1	Q13490	**Ring (571-606)**	(Blankenship et al. 2009)	H588A	**Zn**	Auto
			(Conze et al. 2005)	H582A (m)	**Zn**	c-IAP2
			(Li X, Yang Y, and Ashwell JD. 2002)	H588A	**Zn**	TRAF2

			(L. Xu et al. 2007)	H588A	**Zn**	MAD1
			(Y. Zhao et al. 2007)	H588A	**Zn**	ASK1
c-IAP2	Q13489	**Ring (557-592)**	(Conze et al. 2005)	H570A (m)	**Zn**	Auto
			(Conze, Zhao, and Ashwell 2010)	H570A (m)	**Zn**	
			(Giardino Torchia et al. 2015)	H570A (m)	**Zn**	
KIAP	Q96CA5	**Ring (252-286)**	(Dou et al. 2012)	I284A	**E2**	
				R286A	**OTHER**	
				F296H	**OTHER**	
				V263R	**OTHER**	
BMI-1	P35226	**Ring (18-57)**	(Alchanati et al. 2009)	L20A	**E2**	
BRAP	Q7Z569	**Ring (264-304)**	(Hayes et al. 2012)	W295A	**E2**	Auto; USP15
			(Shoji et al. 2017)	C264S	**Zn**	
BRCA1	P38398	**Ring (24-65)**	(Eakin et al. 2007)	I26A	**E2**	ERα
				C61G; C64G	**Zn**	ERα
			(Fabbro and Henderson 2008)	C61G	**Zn**	
				C61G	**Zn**	
			(Morris and Solomon 2004)	C61G	**Zn**	
			(Nelson and Holt 2010)	C61G	**Zn**	
			(Nishikawa et al. 2004)	C61G	**Zn**	
			(Ruffner et al. 2001)	C61G; C64G; C39Y; C24R	**Zn**	
				T37R	**OTHER**	
			(Sankaran et al. 2006)	I26A	**E2**	
			(Stewart et al. 2017)	L63A; K65A	**OTHER**	
				I26A	**E2**	
				C61G	**Zn**	

CBL	P22681	**Ring (381-420)**	(Bulut et al. 2013)	ΔY368; ΔY371	**OTHER**	PI3K
			(Duyvestyn et al. 2014)	C379A (m)	**Zn**	
			J(Javadi et al. 2013)	C384R	**Zn**	
				Y371H	**OTHER**	
			(Joazeiro et al. 1999)	W408A	**E2**	RPTKs
				C381A	**Zn**	RPTKs
			(Levkowitz et al. 1999)	C381A	**Zn**	EGFR
			(Lv et al. 2017)	C381A	**Zn**	JAK2
			(Miura-Shimura et al. 2003)	Y700F	**OTHER**	Vav
			(Molero et al. 2006)	C379A	**Zn**	
			(Oshikawa et al. 2011)	R420Q	**OTHER**	Flt3-ITD
			(Rathinam et al. 2010)	C379A	**Zn**	
			(Taylor et al. 2015)	C379A	**Zn**	FLT3
			(Thien, Walker, and Langdon 2001)	W408A; C381A; ΔC381; H398A; ΔH398	**Zn**	EGFR
				Y371F; ΔY368; ΔY371	**OTHER**	EGFR
			(Thien et al. 2005)	C381A	**Zn**	
			(Waterman et al. 1999)	C381A	**Zn**	EGFR
			(Xiong et al. 2011)	C381A	**Zn**	CSF-1R
CBLB	Q13191	**Ring (373-412)**	(Bachmaier et al. 2007)	C373A	**Zn**	
			(Ettenberg et al. 2001)	C373A	**Zn**	
			(Oksvold et al. 2008)	C373A	**Zn**	
			(Oshikawa et al. 2011)	C373A	**Zn**	Flt3-ITD
			(Rathinam et al. 2010)	C373A	**Zn**	
CBLC	Q9ULV8	**Ring (351-390)**	(M. Kim et al. 2004)	C351A	**Zn**	SRC

CHFR	Q96EP1	**Ring (304-343)**	(J. M. Kim et al. 2010)	I306A	**E2**	HLTF
CNOT4	O95628	**Ring (14-57)**	(Albert et al. 2002)	C17A; C33R	**Zn**	
				L16A; I45A	**E2**	
				R57A	**OTHER**	
DTX3L	Q8TDB6	**Ring (561-600)**	(Holleman and Marchese 2014)	C561A/C596A/C599A	**Zn**	CXCR4
			(Yong Zhang et al. 2015)	C561S; C564S	**Zn**	H2BJ
HACE1	Q8IYU2	**HECT (574-909)**	(Anglesio et al. 2004)	C876S	**Catalytic cysteine**	
			(Hollstein et al. 2015)	C876S	**Catalytic cysteine**	
			(Palicharla and Maddika 2015)	C876S	**Catalytic cysteine**	YB-1
			(Torrino et al. 2011)	C876S	**Catalytic cysteine**	Rac1
HECTD1	Q9ULT8	**HECT(2151-2610)**	(Sarkar and Zohn 2012)	C2579G	**Catalytic cysteine**	Hsp90
			(Sugrue et al. 2019)	C2579G	**Catalytic cysteine**	RARA
			(Tran et al. 2013)	C2579G	**Catalytic cysteine**	APC
HECTD2	Q5U5R9	**HECT (437-776)**	(Coon et al. 2015)	C744S	**Catalytic cysteine**	PIAS1
HECTD3	Q5T447	**HECT (512-857)**	(Y. Li et al. 2013)	C823A	**Catalytic cysteine**	Caspase-8
			(F. Li et al. 2018)	C823A	**Catalytic cysteine**	TRAF3
			(J. Yu et al. 2008)	C539A	**Catalytic cysteine**	TARA
HECW2	Q9P2P5	**HECT (1237-1572)**	(K. Choi et al. 2016)	C1540A	**Catalytic cysteine**	AMOTL1
			(Krishnamoorthy, Khanna, and Parnaik 2018)	C1540A	**Catalytic cysteine**	PCNA; lamin B1
HERC2	O95714	**HECT (4457-4794)**	(Chan et al. 2014)	C4762S	**Catalytic cysteine**	USP33
			(Kühnle et al. 2011)	C4762S	**Catalytic cysteine**	
			(Wu et al. 2010)	C4762S	**Catalytic cysteine**	BRCA1
HERC3	Q15034	**HECT (951-1050)**	(Cruz et al. 2001)	C1018A	**Catalytic cysteine**	
			(Hochrainer et al. 2015)	C1018A	**Catalytic cysteine**	RelA
HERC5		**HECT (702-1024)**	(Kroismayr et al. 2004)	C994A	**Catalytic cysteine**	

	Q9UII4		(Shi et al. 2010)	C994A	**Catalytic cysteine**	IRF3
			(Wong et al. 2006)	C994A	**Catalytic cysteine**	
HUWE1	Q7Z6Z7	**HECT (4038-4374)**	(Y.-F. Cheng, Tong, and Edge 2016)	C4341A	**Catalytic cysteine**	Atoh1
			(de Groot et al. 2014)	C4341A	**Catalytic cysteine**	Dvl
			(Forget et al. 2014)	C4341A	**Catalytic cysteine**	Atoh1
			(Kurokawa et al. 2013)	C4341A	**Catalytic cysteine**	Mcl-1; PP5
			(Xiaozhen Wang et al. 2014)	C4341A	**Catalytic cysteine**	BRCA1
			(X. Zhao et al. 2008)	C4341S	**Catalytic cysteine**	N-Myc
Itch	Q96J02	**HECT (569-903)**	(Angers, Ramjaun, and McPherson 2004)	C830A	**Catalytic cysteine**	Endophilin A1
			(Chmura et al. 2017)	C830A	**Catalytic cysteine**	vFLIP
			(Han et al. 2016)	C830A	**Catalytic cysteine**	VP40
			(Theivanthiran et al. 2015)	C830A	**Catalytic cysteine**	Tab1
LNX1	Q8TBB1	**Ring (41-79)**	(Lenihan, Saha, and Young 2017)	C48A (m)	**Zn**	PPFIA1; KLHL11; KIF7; ERC2
			(Nie et al. 2002)	C45A (m)	**Zn**	Numb
			(Wolting et al. 2011)	C45A (m)	**Zn**	Numb
MARCH2	Q9P0N8	**RING (56-116)**	(J. Cheng and Guggino 2013)	C64S/C67S	**Zn**	CFTR
MARCH5	Q9NX47	**Ring (6-75)**	(Z. Chen et al. 2017)	H43W; C65S; C68S	**Zn**	FUNDC1
			(Karbowski, Neutzner, and Youle 2007)	H43W; C65S; C68S	**Zn**	Drn1
			(Y. Y. Park et al. 2010)	H43W	**Zn**	Mfn1
			(Yoo et al. 2015)	H43W	**Zn**	MAVS
MARCH6	O60337	**Ring (1-62)**	(Zattas et al. 2016)	C9A; C39S	**Zn**	
MARCH8	Q5T0T0	**Ring (72-133)**	(R. Chen et al. 2012)	W114A	**E2**	IL1RAP
MARCH9	Q86YJ5	**Ring (102-162)**	(Hör et al. 2009)	W143A	**E2**	FcγRIIb; SLAM
			(Tan et al. 2019)	W143A	**E2**	HLA-A2
MDM2	Q00987	**Ring (438-479)**	(Bonacci et al. 2017)	C462A	**Zn**	NUB1

			(Boyd, Tsai, and Jacks 2000)	C464A	**Zn**	p53
			(Brenkman et al. 2008)	C464A	**Zn**	FOXO4
			(C. Fan and Wang 2017)	L468A	**E2**	p53
			(Fang et al. 2000)	C464A; C461S; C478S; C475G; H452A; H457S; T455A	**Zn**	p53
			(Geyer, Yu, and Maki 2000)	C464A	**Zn**	p53
			(Gopinathan et al. 2009)	C464A	**Zn**	PPARα
			(He et al. 2013)	C464A	**Zn**	
			(Honda and Yasuda 2000)	C464A; C441A; C449A; C461A; C475A; C478A; C439A	**Zn**	Auto; p53
			(Honda, Tanaka, and Yasuda 1997)	C464A	**Zn**	p53
			(Inuzuka et al. 2010)	C464A	**Zn**	
			(Kannemeier, Liao, and Sun 2007)	C436L; H455S; C459S; C473G	**E2**	p53
			(Kawai, Wiederschain, and Yuan 2003)	C464A	**Zn**	p53
			(Kubbutat et al. 1999)	C464A	**Zn**	p53
			(Linke et al. 2008)	L468A; I440A; P476A	**E2**	Auto; Mdm4
				R479A	**OTHER**	Auto; Mdm4
			(Nomura et al. 2017)	I440E,K	**E2**	p53
				R479P	**OTHER**	p53
			(Pettersson et al. 2009)	C464A	**Zn**	IRF-2
			(Poyurovsky et al. 2007)	F490Q	**OTHER**	
			(Tian et al. 2017)	C462A	**Zn**	p53
			(Uchida et al. 2005)	C438A	**Zn**	pRb
			(Wawrzynow et al. 2009)	C464A; C478S	**Zn**	p53
MDM4	O15151	**Ring (437-478)**	(Egorova and Sheng 2014)	T459A; K478R; S438V/E441Q; T459A/H462T; R453/K478R	**E2**	Auto
MEX3C	Q5U5Q3	**Ring (608-648)**	(Kuniyoshi et al. 2014)	C601A (m)	**Zn**	RIG-I
MGRN1	O60291	**Ring (278-317)**	(Benvegnù, Wahle, and Dotti 2017)	C278A; C281A	**Zn**	APP

			(Gunn et al. 2013)	C278A; C281A	**Zn**	TSG101
			(Jiao et al. 2009)	C278A; C281A	**Zn**	TSG101
MIB2	Q96AX9	**Ring 1 (890-925) Ring 2 (969-1002)**	(Ye et al. 2014)	C983S	**Catalytic cysteine***	MAVS
MID1	O15344	**Ring (10-60) B-BOX1 (115-165) B-BOX2 (172-212)**	(H. Du et al. 2013)	L146Q	**OTHER**	α4
MKRN1	Q9UHC7	**Ring (281-335)**	(J. H. Kim et al. 2005)	H307E	**Zn**	hTERT
			(Ko et al. 2010)	H307E	**Zn**	WNVCp
			(E. Lee et al. 2009)	H307E	**Zn**	p53; p21
			(M. S. Lee et al. 2018)	H307E	**Zn**	AMPK
MUL1	Q969V5	**Ring (302-340)**	(Zemirli et al. 2014)	C339A	**Zn**	
MYLIP (IDOL)	Q8WY64	**Ring (387-422)**	(J. Gao et al. 2017)	C387A	**Zn**	ApoER2
			(Hong et al. 2010)	C387A	**Zn**	VLDLR; ApoER2
			(Sorrentino et al. 2011)	C387A	**Zn**	LDLR
			(Zelcer et al. 2009)	C387A	**Zn**	LDLR
NEDD4	P46934	**HECT (984-1318)**	(Q. Lin et al. 2017)	C867A	**Catalytic cysteine**	SQSTM1
			(F. Song et al. 2013)	C967S	**Catalytic cysteine**	THO
			(Sugeno et al. 2014)	C867A	**Catalytic cysteine**	α-Synuclein
			(Xinjiang Wang et al. 2008)	C967S	**Catalytic cysteine**	PTEN
			(Zeng et al. 2014)	C867A	**Catalytic cysteine**	PTEN
NEDD4L	Q96PU5	**HECT (640-974)**	(Albesa et al. 2011)	C801S	**Catalytic cysteine**	hERG1
			(Arroyo et al. 2011)	C822S (m)	**Catalytic cysteine**	NCC
			(Debonneville et al. 2001)	C962A	**Catalytic cysteine**	ENaC
			(Ding et al. 2013)	C821A	**Catalytic cysteine**	Dvl2
			(S. Gao et al. 2009)	C962A	**Catalytic cysteine**	Smad2; Smad3
			(Y. H. Kim et al. 2018)	C942A (m)	**Catalytic cysteine**	CRTC3
			(Palmada et al. 2004)	C938S	**Catalytic cysteine**	NaPi Iib

			(D. Xu et al. 2016)	C821A	**Catalytic cysteine**	hOAT1
			(R. Zhou, Patel, and Snyder 2007)	C821A	**Catalytic cysteine**	Auto
				C821A	**Catalytic cysteine**	α-,β-, γENaC
PJA2	O43164	**Ring (634-675)**	(Faust et al. 2017)	C634A/C671A	**Zn**	Tat
PRKN	O60260	**Ring 0 (141-225) Ring 1 (238-293) Ring 2 (418-449)**	(Aguileta et al. 2015)	C431F	**Catalytic cysteine***	
			(Ahmed et al. 2011)	G430D; T415N	**OTHER**	Arrestin-3
			(Bendikov-Bar et al. 2014)	T240R	**OTHER**	Gcase; PARIS; ARTS
			(D. Chen et al. 2010)	C431F	**Catalytic cysteine***	Bcl-2
				K161N; T240R; P437L	**OTHER**	Bcl-2
			(Fiesel et al. 2015)	C431S	**Catalytic cysteine***	
			(Joch et al. 2007)	C431F	**Catalytic cysteine***	PICK1
			(Johnson et al. 2012)	R275W; W453X	**OTHER**	Bax
			(Juan Liu et al. 2017)	C431A	**Catalytic cysteine***	HIF-1
			(Matteucci et al. 2018)	G430D	**OTHER**	MICU1
			(McWilliams et al. 2018)	C431S	**Catalytic cysteine***	
			(Moore et al. 2008)	T240R	**OTHER**	Hsp70
			(Riley et al. 2013)	C431S, A	**Catalytic cysteine***	
			(Sarraf et al. 2013)	C431F	**Catalytic cysteine***	
			(P. Song et al. 2016)	C431S	**Catalytic cysteine***	Rab7
			(Y. Wang et al. 2018)	K151E	**OTHER**	RIPK1
			(Wauer et al. 2015)	K151E	**OTHER**	
			(Xin et al. 2018)	C431S	**Catalytic cysteine***	TRAF3
RAD18	Q9NS91	**Ring (25-64)**	(J. Huang et al. 2009)	C28F	**Zn**	
			(Masuda et al. 2012)	I50A/R51A	**E2**	
			(Tateishi et al. 2000)	C28F	**Zn**	

			(Williams et al. 2011)	C28F	**Zn**	FANCD2
RAG1	P15918	**(Ring 293-332)**	(Jones and Gellert 2003)	C328Y	**Zn**	Auto
RC3H2	Q9HBD1	**Ring (14-54)**	(Maruyama et al. 2014)	C33S	**Zn**	ASK1
RFFL	Q8WZ73	**Ring (316-351)**	(Sakai et al. 2019)	C316A/C319A; H333A	**Zn**	Rab11 effectors
RFWD3	Q6PCD5	**Ring (287-331)**	(Feeney et al. 2017)	C315A	**Zn**	
Ring1	Q06587	**Ring (48-88)**	(Shen et al. 2018)	I50A	**E2**	p53
RLIM	Q9NVW2	**Ring (570-611)**	(R. Gao, Wang, et al. 2016)	C596A	**Zn**	c-Myc
RNF125	Q96EQ8	**Ring (37-76)**	(Jia et al. 2017)	C72A/C75A	**Zn**	TRIM14
			(L. Yang et al. 2015)	C72A/C75A	**Zn**	p53
RNF126	Q9BV68	**Ring (229-270)**	(Benini et al. 2017)	C229A/C232A	**Zn**	Frataxin
RNF138	Q8WVD3	**Ring (18-58)**	(W. Kim et al. 2018)	C18A/C54A	**Zn**	rpS3
RNF144A	P50876	**Ring 1 (20-70) IBR (91-156) Ring 2 atypical (185-214)**	(Ye Zhang et al. 2017)	C20A/C23A	**Zn**	PARP1
			(Ho et al. 2014)	C20A/C23A	**Zn**	DNA-PKcs
RNF145	Q96MT1	**Ring (537-575)**	(Jiang et al. 2018)	C537A	**Zn**	HMGCR
			(Menzies et al. 2018)	C552A/H554A	**Zn**	HMGCR
RNF146	Q9NTX7	**Ring (37-75)**	(Callow et al. 2011)	H53A	**Zn**	Axin; Tankyrase
RNF152	Q8N8N0	**Ring (12-55)**	(Deng et al. 2015)	4C-->S	**Zn**	RagA GTPase
RNF167	Q9H6Y7	**Ring (230-272)**	(Deshar et al. 2016)	C233S	**Zn**	Arl8B
RNF168	Q8IYW5	**Ring (16-55)**	(Pinato et al. 2009)	C16S/C19S	**Zn**	H2A; H2AX
RNF185	Q96GF1	**Ring (39-80)**	(El Khouri et al. 2013)	C39A/C42A	**Zn**	CFTR
RNF2	Q99496	**Ring (51-91)**	(S. Liu et al. 2018)	I53A	**E2**	H2A
			(Xia et al. 2014)	H69Y	**Zn**	AMBRA1
RNF220	Q6PDX6	**Ring (513-553)**	(Ma et al. 2014)	W539R	**E2**	Sin3B
RNF25	Q96BH1	**Ring (134-203)**	(R. Gao, Ma, et al. 2016)	C135A/C138A	**Zn**	
RNF26	Q9BY78	**Ring (378-425)**	(Qin et al. 2014)	C395S; C399S; C401S	**Zn**	STING

RNF31	Q96EP0	**Ring 1 (699-749)IBR (779-841) Ring 2 (871-901)**	(Smit et al. 2012)	C871A/C874A; C890A/C893A; C885A/H887A; C898A/C901A; C719A; C885A/H887A; C885S	**Zn**	
			(Zhu et al. 2018)	C871A/C874A; C890A/C893A; C885A/H887A; C898A/C901A; C719A; C885A/H887A; C885S	**Zn**	FOXP3
RNF34	Q969K3	**Ring (325-360)**	(H. Jin et al. 2014)	H342A	**Zn**	$GABA_ARs$
			(Wei et al. 2018)	C656A (d)	**Zn**	PGC-1
			(R. Zhang et al. 2014)	H342A	**Zn**	NOD-1
RNF4	P78317	**Ring (132-177)**	(Liew et al. 2010)	M149A; D141A; V161A; V134E; S155E R181A; Y193A (m)	**OTHER**	
RNF40	O75150	**Ring (948-987)**	(Foglizzo, Middleton, and Day 2016)	Y999A	**OTHER**	
RNF43	Q68DV7	**Ring (272-313)**	(Loregger et al. 2015)	H292R	**Zn**	TCF4
RNF8	O76064	**Ring (403-441)**	(Lu et al. 2012)	C403S	**Zn**	Nsb1
			(Mailand et al. 2007)	C403S	**Zn**	H2A; H2AX
			(Mallette et al. 2012)	I405A	**E2**	JMJD2A
			(Rai et al. 2011)	C406S	**Zn**	TPP1
			(Tripathi and Smith 2017)	C403S	**Zn**	TNKS1
SHPRH	Q149N8	**Ring (1432-1479)**	(Motegi et al. 2006)	C1432A	**Zn**	PCNA
SIAH1	Q8IUQ4	**Ring (41-76)**	(Grishina et al. 2012)	C44S	**Zn**	CBP/p300
			(Ji et al. 2017)	C41S/C44S (m)	**Zn**	Axin 1
			(Se-yong Kim et al. 2009)	C41S/C44S (m)	**Zn**	HIPK2
			(S. Lee et al. 2015)	C44S	**Zn**	p34
			(M. Liu et al. 2012)	C75S	**Zn**	ELL2
			(Pietschmann et al. 2012)	C72S	**Zn**	PML-RARα
			(Y. Zhou et al. 2008)	C41S/C44S (m)	**Zn**	TRB3
SIAH2	O43255	**Ring (80-115)**	(Habelhah et al. 2002)	H99A/C102A (m)	**Zn**	TRAF2
SMURF1	Q9HCE7	**HECT (420-757)**	(Fei et al. 2013)	C699A (m)	**Catalytic cysteine**	Axin
			(Shan Li et al. 2010)	C699A (m)	**Catalytic cysteine**	TRAF4
			(Tajima et al. 2003)	I612A/L614A (m)	**OTHER**	Smad7

			(H.-R. Wang et al. 2006)	C699A (m)	**Catalytic cysteine**	
			(Xiangchun Wang et al. 2013)	C710A	**Catalytic cysteine**	TRAF4
			(M. Zhao et al. 2003)	C710A	**Catalytic cysteine**	Smad1; Cbfa1
SMURF2	Q9HAU4	**HECT (414-748)**	(Borroni et al. 2018)	C716G	**Catalytic cysteine**	Lamin A
			(J. X. Du et al. 2011)	C716A	**Catalytic cysteine**	KLF5
			(Jeong et al. 2014)	C716G	**Catalytic cysteine**	YY1
			(C. Jin et al. 2009)	C716G	**Catalytic cysteine**	
			(Sewoon Kim and Jho 2010)	C716G	**Catalytic cysteine**	Axin
			(Pan et al. 2014)	C716A	**Catalytic cysteine**	MAVS
			(Shukla et al. 2014)	C716A	**Catalytic cysteine**	KRAS
STUB1	Q9UNE7	**U-BOX (226-300)**	(M. Fan, Park, and Nephew 2005)	H260Q	**E2**	Erα
			(J.-H. Kim et al. 2017)	H260Q	**E2**	PPARγ
			(X. Li et al. 2018)	H260Q	**E2**	IRS4
				P269A	**E2**	IRS4
			(Seo et al. 2018)	H260Q	**E2**	SNPH
			(Shimamoto et al. 2013)	H260Q	**E2**	
				P269A	**E2**	
SYVN1	Q86TM6	**Ring (291-330)**	(Tanabe et al. 2012)	C307A	**Zn**	RER1
TRAF6	Q9Y4K3	**Ring (70-109)**	(Y. B. Choi and Harhaj 2014)	C70A	**Zn**	Mcl-1
			(Funakoshi-Tago et al. 2009)	C70A	**Zn**	
			(Ning et al. 2008)	C70A	**Zn**	IRF7
			(W. L. Yang et al. 2009)	C70A	**Zn**	Akt
			(Jiazhen Zhang et al. 2017)	C70A	**Zn**	
				L74H	**E2**	
TRIM11	Q96F44		(L. Chen et al. 2018)	C16A/C19A	**Zn**	

		Ring (16-57) B-BOX (87-128)	(T. Liu et al. 2016)	C53A7 C56A	**Zn**	AIM2
TRIM13	O60858	**Ring (10-58) B-BOX (89-131)**	(B. Huang et al. 2018)	C10A/C13A	**Zn**	Nur77
TRIM17	Q9Y577	**Ring (16-66) B-BOX (94-135)**	(Lassot et al. 2010)	C16A	**Zn**	
TRIM21	P19474	**Ring (16-55) B-BOX (92-123)**	(Wada and Kamitani 2006)	C16A	**Zn**	p62
TRIM22	Q8IYM9	**Ring (15-60) B-BOX (92-133)**	(Duan et al. 2008)	C15A	**Zn**	Auto
TRIM23	P36406	**Ring (31-76) B-BOX (122-168)**	(Arimoto et al. 2010)	C34A	**Zn**	NEMO
			(Sparrer et al. 2017)	C34A	**Zn**	
TRIM25	Q14258	**Ring (13-54)**	(J. M. Lee et al. 2018)	C50S/C53S	**Zn**	PPARγ
TRIM26	Q12899	**Ring (16-57) B-BOX (97-138)**	(Ran et al. 2016)	C31S	**Zn**	
TRIM27	P14373	**Ring (16-57) B-BOX (96-127)**	(Zaman et al. 2013)	C96A/C99A/H107A/D110A	**Zn**	USP7
			(Zurek et al. 2012)	C16A/C31A	**Zn**	NOD2
TRIM3	O75382	**Ring (22-63) B-BOX (110-151)**	(Hung et al. 2010)	C22A/C25A	**Zn**	GKAP/SAPAP1
			(Raheja et al. 2014)	C22A/C25A	**Zn**	p21
				I24A; L26A; D27A; V61A; R63A	**E2**	p21
TRIM31	Q9BZY9	**Ring (16-57) B-BOX (90-131)**	(B. Liu et al. 2017)	C53A/C56A	**Zn**	MAVS
			(H. Song et al. 2016)	C16A/C36A	**Zn**	NLRP3
TRIM32	Q13049	**Ring (20-65) B-BOX (103-133)**	(Fu et al. 2015)	C39S	**Zn**	PB1
			(Koliopoulos et al. 2016)	E16R	**OTHER**	
			(Ryu et al. 2011)	C23A	**Zn**	XIAP
			(Jing Zhang et al. 2012)	C39S	**Zn**	STING
TRIM33	Q9UPN9	**Ring (125-154) B-BOX1 (212-259) B-BOX2 (271-312)**	(Xue et al. 2015)	C125A/C128A	**Zn**	β-catenin
TRIM37	O94972	**Ring (15-55) B-BOX (90-132)**	(Bhatnagar et al. 2014)	C18R	**Zn**	H2A
			(Kallijärvi et al. 2005)	C35S/C36S	**Zn**	
			(W. Wang et al. 2017)	C35S/C36S; C18R	**Zn**	PEX5

TRIM4	Q9C037	**Ring (12-53) B-BOX (82-123)**	(J. Yan et al. 2014)	C27S	**Zn**	RIG-1
TRIM45	Q9H8W5	**Ring (29-98) B-BOX1 (130-176) B-BOX2 (186-227)**	(Jindong Zhang et al. 2017)	C29A	**Zn**	p53
TRIM49	P0CI25	**Ring (15-56) B-BOX (88-129)**	(Guimarães and Gomes 2018)	C35S	**Zn**	
TRIM5	Q9C035	**Ring (15-59) B-BOX (90-132)**	(Lienlaf et al. 2011)	R60A	**E2**	Auto
			(Yamauchi et al. 2008)	C15A	**Zn**	
			(Yudina et al. 2015)	Y63E; I77R	**OTHER**	
TRIM50	Q86XT4	**Ring (16-57) B-BOX (84-125)**	(Fusco et al. 2012)	C52X (m)	**Zn**	
TRIM6	Q9C030	**Ring (15-60) B-BOX (92-133)**	(Bharaj et al. 2017)	C15A	**Zn**	VP35
TRIM62	Q9BVG3	**Ring (11-54) B-BOX (88-128)**	(Zhifang Cao et al. 2015)	C11A/C14A	**Zn**	CARD9
			(F. Huang et al. 2013)	C11A	**Zn**	
TRIM65	Q6PJ69	**Ring (12-51) B-BOX (90-137)**	(Shitao Li et al. 2014)	C12A/C15A	**Zn**	TNRC6
TRIM7	Q9C029	**Ring (29-82) B-BOX (125-166)**	(Chakraborty et al. 2015)	C29A/C32A	**Zn**	RACO-1
				W57A	**E2**	RACO-1
TRIM71	Q2Q1W2	**Ring (12-95) B-BOX 1 (194-241) B-BOX2 (273-314)**	(Yin et al. 2016)	C12A/C15A	**Zn**	Lin28B
TRIM8	Q9BZR9	**Ring (15-56) B-BOX1 (92-132) B-BOX2 (140-182)**	(F.-J. Yan et al. 2017)	C15A/C18A	**Zn**	TAK1
TRIP12	Q14669	**HECT (1885-1992)**	(Hanoun et al. 2014)	C1959A	**Catalytic cysteine**	PTF1a
			(Y. Park, Yoon, and Yoon 2009)	C1972S	**Catalytic cysteine**	
UBE3A	Q05086	**HECT (776-875)**	(Chhabra et al. 2017)	C843A	**Catalytic cysteine**	G-CSFR
			(Harlalka et al. 2013)	C820A	**Catalytic cysteine**	
			(Kumar, Talis, and Howley 1999)	C833A	**Catalytic cysteine**	HHR23
			(S. Y. Lee et al. 2014)	C941S (d)	**Catalytic cysteine**	Rpn10
			(Mortensen et al. 2015)	C820A	**Catalytic cysteine**	
			(Munakata et al. 2007)	C840A	**Catalytic cysteine**	pRb
			(Pal et al. 2013)	C843A	**Catalytic cysteine**	C/EBPα
			(Y. Yang et al. 2007)	C833A	**Catalytic cysteine**	TH1

UBE3C	Q15386	**HECT (744-1083)**	(Chu et al. 2013)	C1051A	**Catalytic cysteine**	
			(Y. Yu and Hayward 2010)	C1051A	**Catalytic cysteine**	IRF3; IRF7
UBE4B	O95155	**U-BOX (1227-1300)**	(Okumura et al. 2004)	P1140A (m)	**OTHER**	FEZ1
UBR1	Q8IWV7	**Ring (1098-1201)**	(Sasaki et al. 2006)	C1098S	**Zn**	c-FOS
UBR5	O95071	**HECT (2462-2799)**	(T. Zhang et al. 2014)	C2768A	**Catalytic cysteine**	ATMIN
UHRF1	Q96T88	**Ring (724-763)**	(Nishiyama et al. 2013)	C713A/C715A/C716A (m)	**Zn**	H3
			(H. Zhang et al. 2016)	H754A	**Zn**	RIF-1
WWP1	Q9H0M0	**HECT (588-922)**	(Han et al. 2017)	C890A	**Catalytic cysteine**	VP40
			(Heidecker et al. 2007)	C890S	**Catalytic cysteine**	Gag
			(Laine and Ronai 2007)	C883A	**Catalytic cysteine**	p53
			(L. Lin et al. 2016)	C886S (m)	**Catalytic cysteine**	Htt (160Q)
			(Zaarour et al. 2012)	C890A	**Catalytic cysteine**	Ezrin
			(Z. Zhou, Liu, and Chen 2012)	C890A	**Catalytic cysteine**	
WWP2	O00308	**HECT (536-870)**	(Jung et al. 2014)	C838A	**Catalytic cysteine**	Notch3
			(Luo et al. 2014)	C838A	**Catalytic cysteine**	SRG3
			(Nakamura et al. 2011)	C838A	**Catalytic cysteine**	Sox9
			(H. M. Xu et al. 2004)	C838A	**Catalytic cysteine**	oct-04
XIAP	P98170	**Ring (450-485)**	(Zipeng Cao et al. 2013)	H467A	**Zn**	Cyclin D1
			(Jinyi Liu et al. 2012)	H467A	**Zn**	
			(Nakatani et al. 2013)	F495A; F495L; V461E	**OTHER**	
			(Q. Yang 2004)	H467A	**Zn**	Auto
ZNRF1	Q8ND25	**Ring (184-225)**	(Toshiyuki and Milbrandt 2003)	C184A	**Zn**	
ZNRF2	Q8NHG8	**Ring (199-240)**	(Toshiyuki and Milbrandt 2003)	C199A	**Zn**	
ZNRF4	Q8WWF5	**Ring (309-352)**	(Bist et al. 2017)	H329W/H332W	**Zn**	RIP2